

30th conference with international participation



BOOK OF EXTENDED ABSTRACTS

November 3 - 5, 2014

HOTEL HORIZONT, ŠPIČÁK
CZECH REPUBLIC



Central European Association
for Computational Mechanics



INVESTMENTS IN EDUCATION DEVELOPMENT

This action is realized by the project EXLIZ – CZ.1.07/2.3.00/30.0013, which is co-financed by the European Social Fund and the state budget of the Czech Republic.

BOOK OF EXTENDED ABSTRACTS

30th conference with international participation **Computational Mechanics 2014**

ISBN 978-80-261-0429-2

Published by

University of West Bohemia, Univerzitní 8, 306 14 Plzeň, Czech Republic, IC 49777513

Edited by

Vítězslav Adámek

Martin Zajíček

Alena Jonášová

Conference secretariat

Petra Pechmanová

Department of Mechanics

Faculty of Applied Sciences

University of West Bohemia

Univerzitní 8

306 14 Plzeň

Czech Republic

phone: +420 377 634 736

e-mail: vm@kme.zcu.cz

Copyright © 2014 University of West Bohemia, Plzeň, Czech Republic

PREFACE

The Book of Extended Abstracts contains 89 two-page abstracts of talks presented during the 30th conference **COMPUTATIONAL MECHANICS 2014** and the workshop **Modelling and Inverse Problems for Heterogeneous Media**, which were held at the Hotel Horizont in Špičák, Czech Republic on November 3 – 5, 2014. The annual conference and the workshop, which were attended by more than one hundred participants from the Czech Republic and Slovakia, were organised by the Department of Mechanics, Faculty of Applied Sciences of the University of West Bohemia under the auspices of

- Miroslav Lávička, the Dean of the Faculty of Applied Sciences,
- Jiří Struček, the Vice-President of the Pilsen Region for Education, Sport, Culture and Tourism,
- Czech Society for Mechanics,
- Czech National Committee of IFToMM,
- Central European Association for Computational Mechanics.

The main objective of this traditional conference is to bring together academicians, researchers and industrial partners interested in relevant disciplines of mechanics including

- solid mechanics,
- dynamics of mechanical systems,
- mechatronics and vibrations,
- reliability and durability of structures,
- fracture mechanics,
- mechanics in civil engineering,
- fluid mechanics and fluid-structure interaction,
- thermodynamics,
- biomechanics,
- heterogeneous media and multiscale problems,
- experimental methods in mechanics,

to create an opportunity for meeting, discussion and collaboration among the participants. As in the previous years, the three best papers presented at this conference were awarded the Czech Society for Mechanics Award for young researchers under 35 years of age.

To all conference participants, we offer the possibility to publish their peer-reviewed full papers in the international journal **Applied and Computational Mechanics**, which has been published by the University of West Bohemia since 2007 (see <http://www.kme.zcu.cz/acm/>).

We would like to express our gratitude to all the invited speakers for their significant contribution to the conference and the time and effort they put. Considerable acknowledgement belongs also to the members of the Organising Committee for their important work.

We strongly believe that all participants enjoyed the 30th anniversary of the conference Computational Mechanics and that they spent their time in the beautiful nature of the Šumava region in a meaningful way. Finally, we want to invite you all to come to the next conference CM2015.

Jan Vimmr

University of West Bohemia
Chairman of the Scientific
Committee

Vítězslav Adámek

University of West Bohemia
Chairman of the Conference
Organising Committee

Eduard Rohan

University of West Bohemia
Chairman of the Workshop
Organising Committee

SCIENTIFIC COMMITTEE

Chairman:

Jan Vimmr

University of West of West Bohemia, Faculty of Applied Sciences, Czech Republic

Members:

Miroslav Balda

Institute of Thermomechanics, Czech Academy of Sciences, Czech Republic

Jan Dupal

University of West of West Bohemia, Faculty of Applied Sciences, Czech Republic

Miroslav Holeček

University of West Bohemia, New Technologies Research Centre, Czech Republic

Jaromír Horáček

Institute Thermomechanics, Czech Academy of Sciences, Czech Republic

Jiří Křen

University of West Bohemia, Faculty of Applied Sciences, Czech Republic

Vladislav Laš

University of West Bohemia, Faculty of Applied Sciences, Czech Republic

Eduard Malenovský

Brno University of Technology, Faculty of Mechanical Engineering, Czech Republic

Milan Naď

Slovak University of Technology in Bratislava, Faculty of Materials Science and Technology in Trnava,
Slovak Republic

Miloslav Okrouhlík

Institute of Thermomechanics, Czech Academy of Sciences, Czech Republic

Pavel Polach

Research and Testing Institute Plzeň, Czech Republic

Josef Rosenberg

University of West Bohemia, Faculty of Applied Sciences, Czech Republic

Milan Růžička

Czech Technical University in Prague, Faculty of Mechanical Engineering, Czech Republic

Milan Sága

University of Žilina, Faculty of Mechanical Engineering, Slovak Republic

Eugeniusz Switonski

Silesian University of Technology, Faculty of Mechanical Engineering, Poland

Michael Valášek

Czech Technical University in Prague, Faculty of Mechanical Engineering, Czech Republic

Jaroslav Zapoměl

VŠB - Technical University of Ostrava, Faculty of Mechanical Engineering, Czech Republic

Vladimír Zeman

University of West Bohemia, Faculty of Applied Sciences, Czech Republic

Table of Contents

Conference Computational Mechanics 2014

Adamčík J., Šika Z., Beneš P., Svatoš P.: <i>Linear fiber-based additional measurements of position of serial angular robots</i>	1
Beneš P., Šika Z., Rázus M., Neoral M.: <i>Dynamic cloth model for motion planning simulations</i>	3
Blehta J., Soják R.: <i>Algorithm for chute motion control</i>	5
Bublík O., Jonášová A., Vimmr J.: <i>Comparison of explicit and implicit discontinuous Galerkin finite element methods for steady and unsteady flow problems</i>	7
Bulín R., Hajžman M.: <i>Usage of the particle swarm optimization in problems of mechanics</i>	9
Buzík J.: <i>Damage of the boiler collector caused by vibration</i>	11
Čečrdle J.: <i>Updating of aircraft dynamic model according results of ground vibration test</i>	13
Červená O., Balda M.: <i>Possibility of a rotor-stator contact assessment</i>	15
Čibera V.: <i>Three filaments model of sarcomere</i>	17
Dubina R., Eliáš J.: <i>Representation of crushing phenomenon in DEM model of railway ballast</i>	19
Dupal J., Zajíček M.: <i>Analytical periodic solution and stability assessment of Cardan's mechanism</i>	21
Dvořák V.: <i>Optimization of counter flow plate heat exchangers</i>	23
Dyk Š., Zeman V.: <i>Nonlinear vibration of beam-type components with inner impact interaction</i>	25
Eliáš J.: <i>Explanation of difference between sequentially linear solvers in damage mechanics</i>	27
Feistauer M., Hadrava M., Horáček J., Kosík A.: <i>DGM-ALE method for FSI problems</i>	29
Fišer M., Bublík O., Lobošský L., Vimmr J.: <i>Problems and solutions connected with the wet/dry interface in the mathematical model of the shallow water equations</i>	31
Had J., Růžička M.: <i>Damage analysis of hybrid composite cell structure</i>	33
Hamza J., Klečková J.: <i>Investigation of flow over non-vibrating and vibrating airfoil</i>	35

Havelková L., Svoboda Z., Hynčík L.: <i>Musculoskeletal computer model used for gait analysis of patients with total endoprosthesis</i>	37
Hála J., Luxa M., Bublík O., Prausová H., Vimmr J.: <i>Compressible viscous flow in minichannel - experiment and numerical studies</i>	39
Hora P., Pelikán D.: <i>Robust method for finding of dispersion curves in a thick plate problem</i>	41
Hračov S.: <i>Approximate eigen-solution of linear viscously damped system with vibration absorber</i>	43
Hruš T., Círk D.: <i>Estimating material properties of PU foam using genetic algorithms</i>	45
Chlud M., Joch L., Vašek M.: <i>Seismic response of piping systems with viscous dampers in nuclear power plants</i>	47
Janoušek J., Balda M., Chocholoušek M.: <i>Crack propagation under nonzero mean combined loading</i>	49
Kalinský M., Trubač J.: <i>Virtual simulation of traffic barrier</i>	51
Klesa J.: <i>Influence of noise reduction on the propeller performance</i>	53
Kolman R., Cho S., Červ J., Park K.: <i>Component-wise partitioned finite element method for wave propagation and dynamic contact problems</i>	55
Kolman R., Sorokin S., Bastl B., Kopačka J., Plešek J.: <i>Isogeometric analysis in free vibration problems</i>	57
Kořista M.: <i>Analytical solution of the film flow on the inner surface of the pipe driven by the flow of the wet steam</i>	59
Kotoul M.: <i>Fracture mechanics of composite materials – determination and representation of stress coefficient terms</i>	61
Kottner R., Bek L., Krystek J.: <i>Comparison of numerical simulation and experiment in case of bending test of composite rectangular tubes</i>	63
Král R., Náprstek J., Pospíšil S.: <i>An investigation of stochastic resonance using the Fokker-Planck equation and finite element method</i>	65
Křen J., Lobovský L., Vitáková K.: <i>Flow of non-Newtonian fluid</i>	67
Létal T.: <i>Algorithmization issues of flat end check method according to EN 13445-3</i>	69
Lobovský L., Hartlová J., Salášek M., Krystek J., Zemčík R., Křen J.: <i>Experimental investigation of deformations in human pelvis</i>	71
Lutovinov M., Papuga J., Ličková D.: <i>Database FinLiv – Focus on Manson-Coffin curves</i>	73
Makovička D., Makovička D.: <i>Dynamic response prediction of building loaded by traffic vibration, propagated through subsoil</i>	75
Malínek P.: <i>Direct dynamic response computation of an aircraft structure based on experimentally identified modal model</i>	77

Man V., Novák K., Polzer S., Burša J.: <i>Can Laplace law replace more sophisticated analyses of aortic aneurysms?</i>	79
Marek R., Plešek J., Hrubý Z., Parma S.: <i>FE implementation of directional distortional hardening model for metal plasticity</i>	81
Michálek T., Zelenka J.: <i>Modelling of flexi-coil springs with rubber-metal pads in a locomotive running gear</i>	83
Míkula J., Hutař P., Švečík M., Náhlík L.: <i>Crack propagation in welded polyolefin pipes</i>	85
Močilan M., Žmindák M.: <i>Thermo-mechanical finite element analysis of mould for piston casting</i>	87
Mráz L., Volech J., Šika Z., Valášek M.: <i>Model of robot with additional flexible deformation sensing for improved control</i>	89
Murín J., Hrabovský J., Kutíš V., Paulech J.: <i>Modelling and analysis of the 3D FGM beam structures</i>	91
Naď M., Rolník L.: <i>Modal analysis of beam structures reinforced by partially embedded reinforcing core.</i>	93
Náprstek J.: <i>Dynamic stability and post-critical behavior of aeroelastic systems</i>	95
Neusser Z., Vampola T., Valášek M.: <i>Stability limits of the pre-stressed lightweight material model</i>	97
Okrouhlík M.: <i>Fourier and dispersion</i>	99
Padovec Z., Sedláček R., Král M., Růžička M.: <i>Stress and strength analysis of flat samples manufactured from C/PPS pellets</i>	101
Parma S., Hrubý Z., Marek R., Plešek J.: <i>Identification of the directional distortional hardening model on the basis of hysteresis loop</i>	103
Parma S., Papuga J.: <i>Identifying parameters of Kohout-Věchet fatigue curve model</i>	105
Pečínka L., Švrček M.: <i>Parametric excitation on the fuel assembly TVSA-T</i>	107
Pecháč P., Sága M.: <i>Comparison study of algorithms based on fully stress design method for discrete optimization of truss, beam and thin shell finite elements</i>	109
Poduška J., Ševčík M., Kučera J., Hutař P., Sadílek J., Náhlík L.: <i>Residual stress distribution in polyolefin pipes</i>	111
Pokorný P., Náhlík L., Hutař P.: <i>Fatigue crack propagation in railway axles</i>	113
Polach P., Hajžman M., Šika Z., Svatoš P.: <i>Influence of the fibre stiffness model in a weight-fibre-pulley-drive mechanical system on the coincidence with the experimental measurement results</i>	115
Půst L., Pešek L., Radolfová A.: <i>Vibrations of blades couple connected by slip-stick dry friction.</i>	117

Rendlová Z.: <i>The influence of floating ring bearing parameters on turbocharger dynamic behavior</i>	119
Rudolf P., Kozák J.: <i>Computational modelling of cavitation in simple geometries, but complex flows</i>	121
Sháněl V., Ben Zineb T., Plešek J.: <i>Extended thermomechanical model for NiTi-based shape memory alloys with plasticity</i>	123
Slažanský M., Bursá J., Polzer S.: <i>Influence of gripping method in biaxial testing of soft biological tissues</i>	125
Smetanka L., Gerlici J., Pelagič Z.: <i>Numerical homogenization of fibres reinforced composite materials using representative volume</i>	127
Staňák P., Tadeu A., Sládek J., Sládek V.: <i>Elastic wave propagation in nonhomogeneous media: A solution using the 2.5D meshless MLPG approach in the frequency domain</i> . . .	129
Svatoš P., Šika Z.: <i>Model identification and control law optimization of fiber driven mechanism QuadroSphere</i>	131
Ševčík M., Hutař P., Arbeiter F., Pinter G., Náhlík L.: <i>Influence of soil loading on fracture behavior of multilayer polymer pipe</i>	133
Šmejkal J., Plánička F.: <i>Foundation for heavy machines</i>	135
Špička J., Hajžman M., Hynčík L.: <i>Multibody model of a human body</i>	137
Štegnerová K., Náhlík L., Hutař P.: <i>Crack initiation from sharp V-notch tip in the case of out of plane bended specimen</i>	139
Štemberk P., Záruba J., Řeháček S., Čítek D.: <i>String meters for testing of mechanical functionality of bridges</i>	141
Štastný M., Šejna M.: <i>Thermodynamic loss of condensation in steam turbine cascade</i> . . .	143
Voldřich J., Očenášek J.: <i>One-dimensional mathematical model of oil extraction process in a continuous screw press</i>	145
Volech J., Šika Z.: <i>Phenomenological and physical models of automotive shock absorbers</i> . .	147
Zábranský T.: <i>Principles of creation of structured grids for CFD simulations</i>	149
Zapoměl J., Dekýš V., Ferfecki P., Sapietová A.: <i>Vibration attenuation of a periodically loaded system supported by carbon composite bars</i>	151
Záruba J., Štemberk P., Čítek D.: <i>Experimental verification of fatigue state of bridge construction using string tensometric method</i>	153
Zeman V., Hlaváč Z., Dyk Š.: <i>Nonlinear vibration and modelling of fretting wear of the nuclear fuel rods</i>	155
Žák J., Kolář J.: <i>Simulation of an air jet weft pick</i>	157

Žmindač M., Kompiš V., Murčínková Z.: <i>Micro-mechanical analysis of fiber reinforced composites with large aspect ratio by meshless method</i>	159
--	-----

Workshop Modelling and Inverse Problems for Heterogeneous Media

Doškář M., Novák J.: <i>Towards RVE via Wang tilings</i>	163
Krutil J., Pochylý F., Fialová S.: <i>The additional effects of fluid in a thin gap with a heterogeneous environment</i>	165
Lukáš D., Bouchala J., Theuer M.: <i>Homogenization using boundary element methods</i>	167
Lukeš V., Rohan E., Jonášová A., Bublík O.: <i>Computational modeling of liver perfusion - towards a patient specific model</i>	169
Rohan E., Nguyen V., Naili S.: <i>A model of wave propagation in homogenized Biot medium with dual porosity</i>	171
Roubíček T.: <i>Modelling of various phase transformations in ferroic solids, in particular magnetic shape-memory materials</i>	173
Šedlbauer D.: <i>Hard packing for 3D Wang cubes generation</i>	175
Turjanicová J., Rohan E.: <i>Macroscopic modeling of electro-osmosis in the porous structure of a cortical bone tissue</i>	177
Vondřejc J., Zeman J., Marek I.: <i>FFT-based Galerkin method for homogenization of periodic media</i>	179

Conference
Computational Mechanics 2014

Linear fiber-based additional measurements of position of serial angular robots

J. Adamčík^a, Z. Šika^a, P. Beneš^a, P. Svatoš^a

^a Department of Mechanics, Biomechanics and Mechatronics, Faculty of Mechanical Engineering, Czech Technical University in Prague, Technická 4, 166 07 Praha, Czech Republic

The paper presents a new concept of additional measuring of position using the fiber system. The fiber system is placed on the shoulders of the kinematic pairs in order to reduce restriction of the motion and the manipulation space. The system is designed to measure redundantly the complete relative motion with 6 degrees of freedom (DOF) including arm deformations. The redundancy then provides the possibility of the self-calibration of the entire device.

The idea of the measuring system is similar to the principle presented in [1]. Unlike the cited paper, where the fibers are used as driving units, the presented idea applies the members as pure measuring elements. The essential difference is that the authors in [1] consider four fibers for controlling 3 DOF, i.e. with redundancy of degree one. The presented concept takes into account 6 DOF measured by 8 fibers, i.e. with redundancy of degree two.

The mounting points are placed on the two crosses turned by 45° for higher handling ability. The distances between the end points of the auxiliary crosses, measured as the length of each fiber vl_k ($k = 1 \dots 8$), then clearly determines the relative position of the arms of the identified kinematic pair (Fig. 1). Constant parameters of the system are the arm lengths (distance between the auxiliary arms centre and the joint), the length of each auxiliary arm and their orientation, expressed by the direction angles.

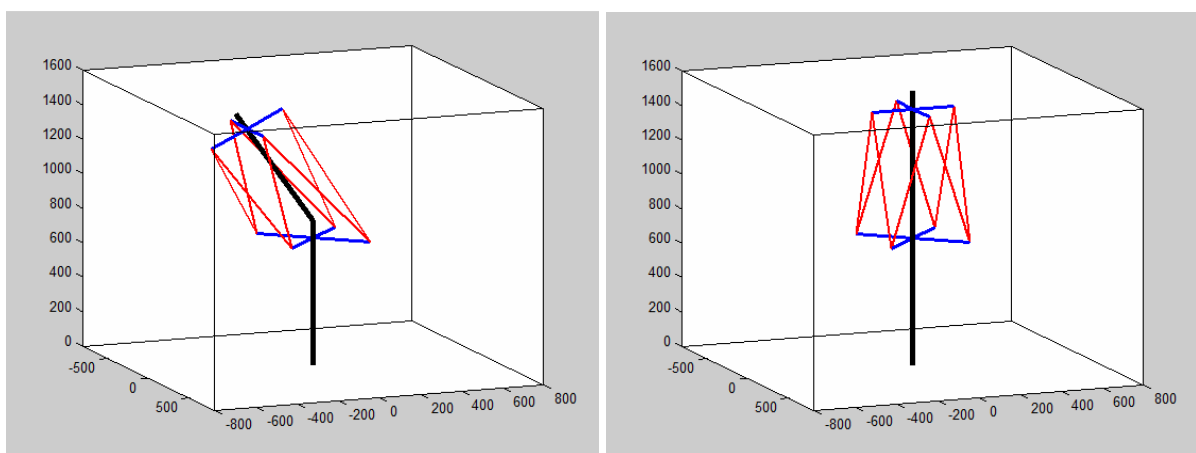


Fig. 1. The beam model of fiber measuring system in two different positions

The relative motion of the arms is then defined not only by the main motion of the kinematic pair, but also through the backlash and deformations. The first step of the synthesis was the setup of the inverse kinematic model [2]. The second step was the creation of the sensitivity model. The third important step of the work was the forward kinematic model,

simulating the real use of the system. This model determines the current position of the system and calculates the maximum localization error from the specified lengths of fibers (Table 1). The model also allows the choice of the considered accuracy of primary measuring (considered measurement accuracy of fiber was $5\mu\text{m}$). The optimization of the parameters has been realized based on the calibrability criterion [3], the example of the result is in the Fig. 2.

Table 1. The accuracy of the measuring system, determined by the simulation model

$\Delta\varphi_x$	$\Delta\varphi_y$	$\Delta\varphi_z$	$d\Delta x$	$d\Delta y$	$d\Delta z$
$3\div 5 \times 10^{-5}$ [rad]	$9\div 14 \times 10^{-6}$ [rad]	$2\div 5 \times 10^{-5}$ [rad]	$15\div 30 \times 10^{-3}$ [mm]	$8\div 13 \times 10^{-3}$ [mm]	$3\div 5 \times 10^{-3}$ [mm]

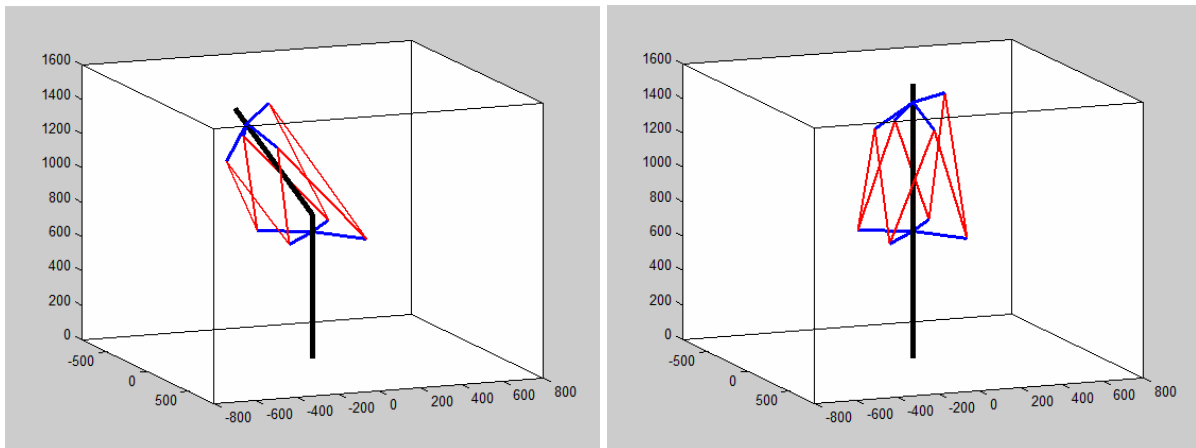


Fig. 2. The beam model of fiber measuring system after parameter optimization

Although the simulation only refers to the intended application with some range of individual drives, the determined accuracy at the level indicates the high potential of the measuring system. The ability to identify and quantify the deformation and backlash of individual kinematic pairs and the possibility of implementing them as a feedback could significantly affect not only the positional accuracy of the robot, but also the possibility of increasing the maximum permitted load without increasing the weight and massiveness of the structure.

Acknowledgements

The authors appreciate the kind support by the grant GA13-39057S “**Position Feedback Based Stiffness Increase of Robots by Redundant Measurement**” of the Czech Science Foundation and of the project SGS13/177/OHK2/3T/12 “**Mechatronics a adaptronics 2013**” of CTU in Prague.

References

- [1] Chen, Q., Chen, W., Yang G., Liu, R., An integrated Two-Level Self-Calibration Method for a cable-driven humanoid arm, IEEE Transactions on automation science and engineering 10 (2) (2013) 380–291.
- [2] Stejskal, V., Valášek, M., Kinematics and dynamics of machinery, Marcel Dekker, Inc., New York, 1996.
- [3] Šika, Z., Hamrle, V., Valášek, M., Beneš, P., Calibrability as additional design criterion of parallel kinematic machines, Mechanism and Machine Theory 50 (2012) 48–63.

Dynamic cloth model for motion planning simulations

P. Beneš^a, Z. Šika^a, M. Rázus^a, M. Neoral^b

^aDepartment of Mechanics, Biomechanics and Mechatronics, Faculty of Mechanical Engineering, Czech Technical University in Prague, Technická 4, 166 07 Praha 6, Czech Republic

^bDepartment of Cybernetics, Faculty of Electrical Engineering, Czech Technical University in Prague, Technická 2, 166 27 Praha 6, Czech Republic

Dynamic animation of cloth is today a common part of computer games, virtual reality animations or movies. However most of these models are focused only on a fancy visualisation. Many of them are even not based on cloth physical properties. In case we need a real-life simulation, e.g. for motion planning, it is not enough that it looks like real or sometimes maybe even better. We need a more accurate model that truly behaves as a real. The presented paper describes physical model of cloth based on a spring-mass-damper approach. The model is a part of EU-FP7 research project CloPeMa (Clothes perception and manipulation) [3]. The two handed CloPeMa robot will learn to manipulate, perceive and fold a variety of textiles. The presented model will be used for motion planning.

The basic structure of two considered simulation models is in the Fig. 1. The nodes of the structure represent uniformly distributed mass of the cloth. These nodes are connected to each other either by springs (Fig. 1a) or by kinematic constraints for defined constant length (Fig. 1b). In that case nodes represent spherical joints as well. The dissipative properties of the garment are modelled using shear dampers (red) and flexion dampers (green). Moreover there is a viscous damping applied on each node representing the interaction with air.

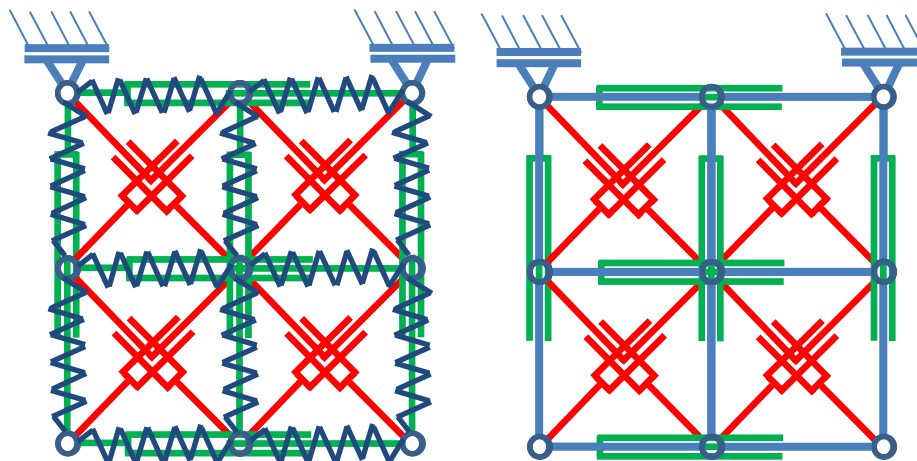


Fig. 1. Basic model structure: a) model with springs, b) model with kinematic constraints

The motion equations of the whole simulation can be formulated by many different methods. As the kinematic constraints are defined within the structure the Lagrange equations of mixed type were used and the numerical calculation was stabilized using Baumgarte's approach [2]. The motion of the grasping points is defined as kinematic excitation concerning that the motion of garment does not influence the robot dynamics.

The identification of the model parameters (stiffness of springs, damping ratios, air resistance...) is based on the experimental results. The robot manipulation with textile objects was captured by colour camera and the rangefinder sensor [1]. The maneuver that was used for parameter identification represents the flapping with the cloth. The upper edge of sheet-like cloth was hold by two robot grippers. Then robot arms moved forwards/backwards. The records were analysed and transformed to the time series of grid points coordinates. The goal of parameter identification was to minimize the difference between real garment grid coordinates and simulation model nodes coordinates (Fig. 2).

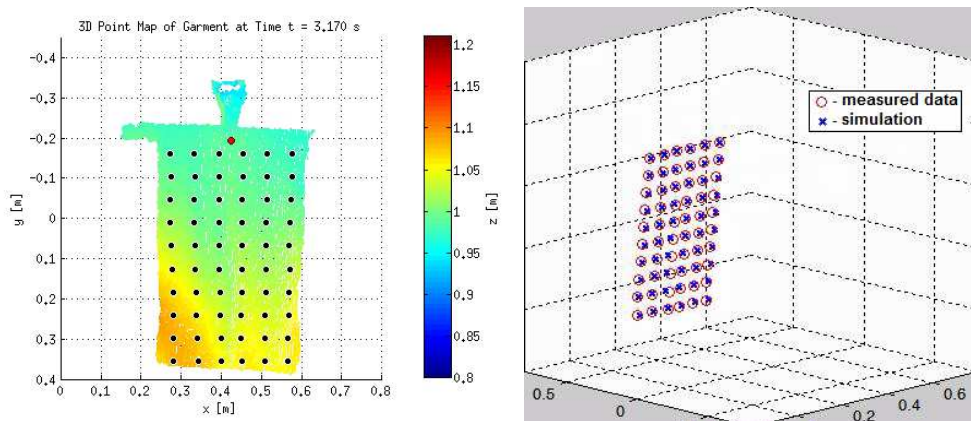


Fig. 2. Identification in $t = 3.17$ s: a) image processing, b) comparison of measured data and simulation

The problem of identification is that the rapid robot maneuver excites cloth in such a degree that some grid points are hidden behind other ones and cannot be captured by the rangefinder. On the other hand the identification from slow maneuvers results in wide variety of parameter values.

Finally both models were identified. The simulation model with constraints is very fast but its performance was less accurate compared to springs model. Especially when the movement of cloth is very fast and the free bottom edge flapping. This effect was well covered by the model with springs, however stiff springs mean high natural frequencies and therefore small integration steps and more time consuming calculation.

During manipulation and folding operations the cloth collides with other object such as robot arms or the working table. The other type of collision is the self-colliding of cloth. Naturally the cloth cannot penetrate itself or other rigid objects. Therefore the collision detection together with further improvements in parameter identification will be the next step in model development.

Acknowledgements

The work has been supported by the EC Research Project FP7-288553 CloPeMa.

References

- [1] Neoral, M., Extraction of features from moving garment (bachelor thesis), CTU in Prague, FEE – Dept. of Cybernetics, Prague 2014.
- [2] Rázus, M., Dynamic cloth model (bachelor thesis), CTU in Prague, FME – Dept. of Mechanics, Biomechanics and Mechatronics, Prague 2014.
- [3] CloPeMa – Clothes perception and manipulation, <http://clopema.eu>, Accessed: 2014-10-04.

Algorithm for chute motion control

J. Blekta^a, R. Soják^a

^a Faculty of Mechanical Engineering, Technical University of Liberec, Studentská 2, 460 01 Liberec, Czech Republic

In the surface mines belt conveyors are very important part of the transport chain. Conveyors transports coal or blasted rock (overburden). The length of conveyor line is from 5 to 10 kilometers. In the case of rocks transportation, overburden is transported to the opposite side of the mine, where it is put to the hole again. Conveyor line consists from several conveyor belts, usually of the 1 km length. The rock is poured from one belt to another. This causes a great wear of the belt [1]. The aim of this paper is to find a suitable way to reduce the kinetic energy of the falling mass. This would increase the life of conveyor belts.

Each belt conveyor consists of a driving and return station. The first one is responsible for driving the conveyor belt and it is positioned at the end of the belt (in the direction of material transportation). Another role of the driving station is to pour transported material to return station of the subsequent conveyor. This is done approximately from a height of 10 m. During pouring of the transported material the rocks fall down on the adjustable steel shield that directs material flow into the center of the outgoing belt. This causes uniform loading of the belt. Return and driving stations are shown in Fig. 1.

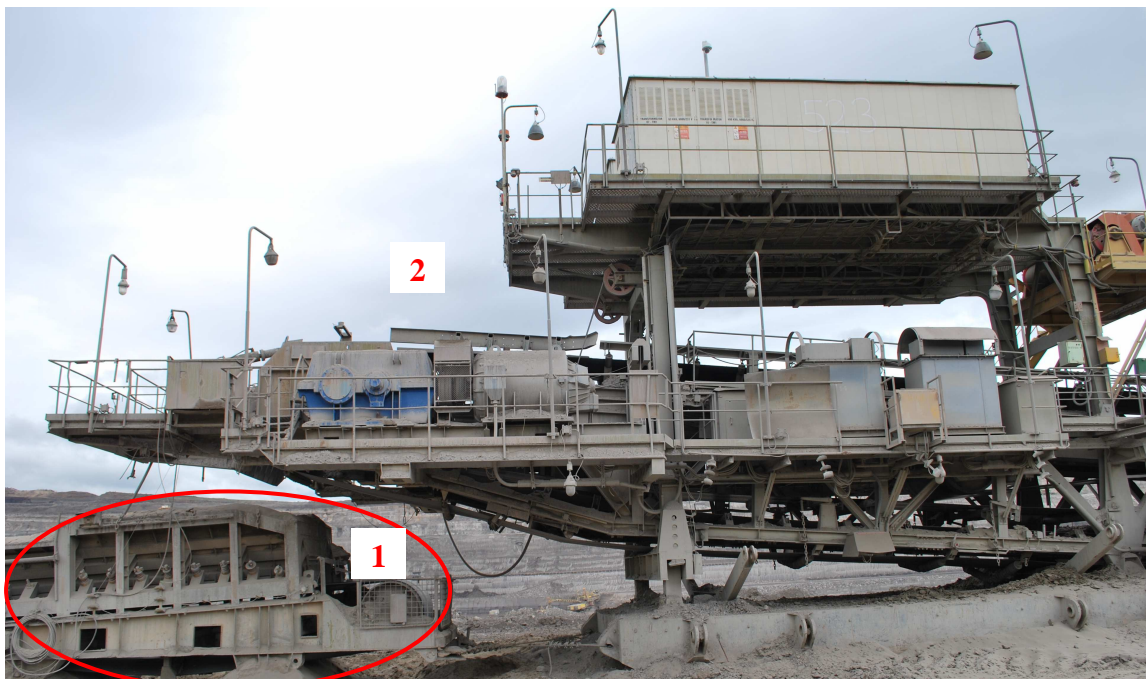


Fig. 1. Return (1) and driving (2) station

At the beginning of the project solution it was initially considered to reduce the drop height by constructional modification of the return or driving station. After a careful examination of the drawing and project documentation it has been stated, that distance

reduction between incoming and outgoing belt is not possible. For this reason, it was proposed a new solution of the steel chute insertion between incoming and outgoing belt. The advantage of this conception is a significant reduction of the impact energy of the falling material, the disadvantage is the danger of clogging of the hopper area, when the adhesive material is transported. Therefore, it was decided, that the chute must be extensible.

The chute movement control suitable algorithm was designed. In the base of hardness and the size of transported pieces of overburden this algorithm decide, when the chute would be slid out or slide back. The hardness of the transported material are identified by the extent of excitation of the shield eigenfrequencies. By impact of the hard material, eigenfrequencies are excited with much greater intensity than in the case of the soft adhesive material. This characteristic was supported by a lot of measurements in different weathers and with different types of transported materials. In Fig. 2 can be seen spectrograph of shield vibration. Independent axis is time, the another two quantities in the graph are the frequencies of the shield vibrations (dependent axis) and the intensity of shield vibrations (defined by color). Comparison of several spectrographs measured for different transported material shows dependence of shield vibrations intensity on the transported material hardness.

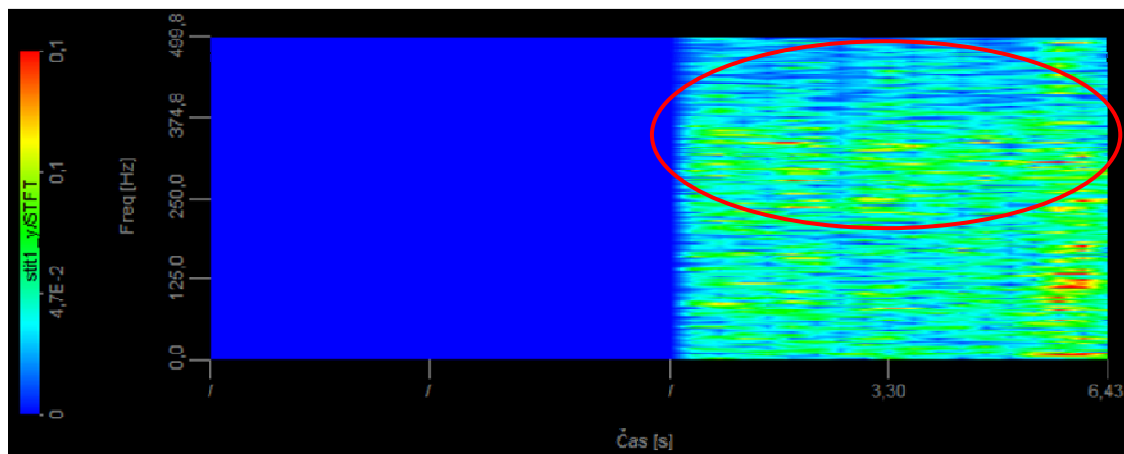


Fig. 2. Spectrogram of shield vibration (1 - field of the shield eigenfrequencies)

Real-time computer, installed on the driving station, assesses the intensity of the eigenfrequencies excitation. In the case of safe limit exceeding, it pass the information to slide chute out. This information is transmitted to the control station and the driver of bucket-wheel excavator decides to slide chute out or not.

Acknowledgements

This work has been supported by the research project FR-TI4/310 of the Ministry of Industry and Trade of the Czech Republic.

References

- [1] Bocko, P., Petříková, I., Kraus, V., Marvalová, B., Blekta, J., Skarolek, A. Increasing of working life of conveyor belts affected by shocks. *The International Journal of Transport and Logistics*, 25 (2012) 164-168.

Comparison of explicit and implicit discontinuous Galerkin finite element methods for steady and unsteady flow problems

O. Bublík^a, A. Jonášová^a, J. Vimmr^a

^a*European Centre of Excellence NTIS – New Technologies for Information Society, Faculty of Applied Sciences,
University of West Bohemia, Univerzitní 22, 306 14 Pilsen, Czech Republic*

In recent years, the discontinuous Galerkin (DG) finite element method [5] has become more popular for the solution of various flow problems [1, 4]. This popularity is mainly due to its ability to achieve high order of spatial accuracy, low artificial damping, robustness and stability. The main drawback of the method is the high number of unknowns, solution of which is connected with high computational demands. For this reason, the choice of an efficient time integration method is of crucial importance.

The purpose of the present work is to compare two basic classes of time integration methods in terms of CPU time usage and quality of results. First, the class of explicit time integration methods is considered. It is well known that their computational efficiency is directly affected by the maximal size of the global time step, which is restricted by the CFL condition of stability. This restriction becomes especially notable when the applied computational mesh consists of elements with large variations in size. Because of this, the explicit schemes are known to be computationally inefficient. To overcome this drawback in this work, we implement the local time stepping (LTS) method. As shown in [3], the use of LTS Runge-Kutta method can massively increase the computational performance of explicit schemes without any substantial modification of the algorithm. As a second class of methods, we consider the implicit time integration methods. Although this type of methods is able to overcome the restriction imposed on the size of the computational time step, their implementation is connected with several difficulties. Among them, it is possible to mention the need to solve a system of non-linear algebraic equations during every time iteration. The solution of this system is usually performed using the Newton method, where it is required to solve a system of linear equations repeatedly until convergence. The use of the Newton method is, however, connected with the disadvantage in the form of Jacobian matrix, whose exact expression is very difficult, especially in the case of the DG method. To overcome this problem, many authors use Jacobian free methods [2] based on the Krylov methods such as BICGSTAB and GMRES. On the other hand, the knowledge of the Jacobian matrix can be useful when building a preconditioner matrix. In this work, we employ the technique of the Jacobian free methods in order to numerically assemble the Jacobian matrix. This approach is independent of equations complexity and boundary conditions and as such allows to easily solve complex flow problems like the turbulent flow. The drawback of this approach lies in higher computational demands on Jacobian matrix assembly, which can be compensated with a parallel algorithm.

In this work, the computational performance of explicit and implicit methods is compared for several test cases. For example, Fig. 1 shows the solution of steady compressible inviscid and viscous laminar flow around the NACA 0012 airfoil computed by the implicit backward

Euler method with linear polynomial basis functions. The CPU times necessary for the steady state solution are shown in Fig. 2. On the basis of the steady flow simulations, it can be observed that the implicit method is computationally more efficient than the explicit LTS method. Other cases, especially unsteady flow simulations, will be presented at the conference.

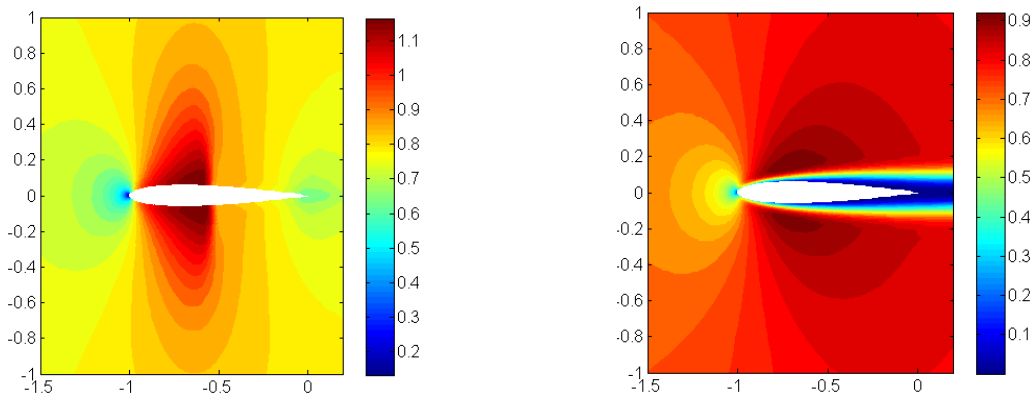


Fig. 1. Mach number isolines around the NACA 0012 airfoil: (left) inviscid flow ($M_\infty = 0.8$, $\alpha = 0$), (right) viscous flow ($M_\infty = 0.8$, $\alpha = 0$, $Re = 5000$)

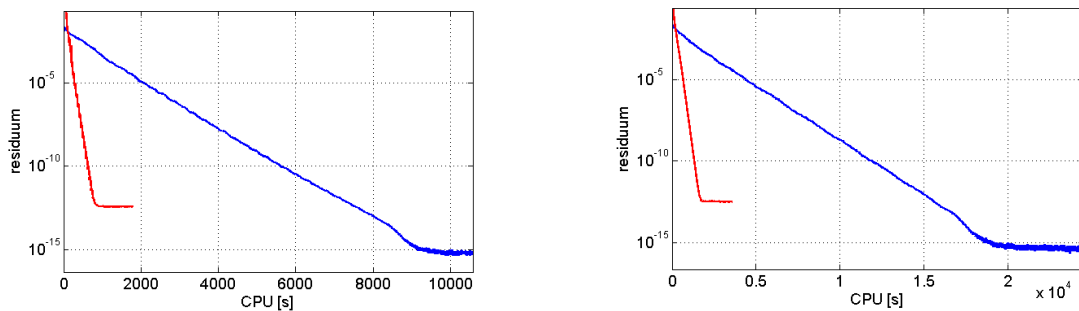


Fig. 2. Residuum as a function of CPU time for inviscid (left) and viscous (right) flows (the implicit method in red, the explicit LTS method in blue)

Acknowledgement

This work was supported by the project TE01020068 "Centre of research and experimental development of reliable energy production" of the technology Agency of the Czech Republic.

References

- [1] Bassi, F., Rebay, S., Mariotti, G., Pedinotti, S., Savini, M., A high-order accurate discontinuous finite element method for inviscid and viscous turbomachinery flows, Proc. of the 2nd European Conference on Turbomachinery, Fluid Dynamics and Thermodynamics, 1997, pp. 99-108.
- [2] Birken, P., Gassner, G., Haas, M., Munz, C.-D., Efficient time integration for discontinuous Galerkin method for the unsteady 3D Navier-Stokes equations, Proceedings of ECCOMAS 2012, Vienna, 2012, pp. 4334-4353.
- [3] Bublík, O., Vimmr, J., Jonášová, A., A local time step discontinuous Galerkin finite element method for the solution of Euler equations on unstructured meshes, Proceedings of the 27th conference Computational Mechanics 2011, Pilsen, 2011.
- [4] Cockburn, B., Shu, C.-W., The local discontinuous Galerkin method for time-dependent convection-diffusion systems, SIAM Journal on Numerical Analysis (35) (1998) 2440-2463.
- [5] Reed, W. H., Hill, T. R., Triangular mesh methods for the neutron transport equations. Los Alamos Scientific Laboratory Report LA-UR-73-479, 1973. (unpublished)

Usage of the particle swarm optimization in problems of mechanics

R. Bulín^a, M. Hajžman^a

^aFaculty of Applied Sciences, UWB in Pilsen, Univerzitní 22, 306 14 Plzeň, Czech Republic

Optimization process is a very important part in designing dynamic systems. Optimal parameters can make a system less noisy, decrease amplitudes of vibration, make a system cheaper etc., so they can be essential in a project realization. There are many approaches how to find optimal parameters [3]. Some methods are searching for local optimum only or require differentiable functions and that may be a drawback [2]. That is why methods of zero order are used, since they do not use derivations of an objective (or so called fitness) function in the optimization process. One of these methods is the method called Particle Swarm Optimization (PSO), which has the ability to find global optimum of objective (fitness) functions [1].

The basic PSO method was introduced by James Kennedy and Russel C. Eberhart in year 1995. It is based on a behaviour of animals (such as sheep, birds or fish) in a flock or a swarm. Each individual in a swarm cooperates with others to find areas, where can be enough food or something. All individuals in a swarm creates a social behaviour, which leads to finding optimum areas in a search space.

The PSO algorithm uses a *swarm* of size n_s , which is made by individual *particles* represented by vector $\mathbf{x}_i(t) = [x_{i1}, x_{i2}, \dots, x_{in}]$, where n is dimension of a search space, $i = 1, 2, \dots, n_s$ is index of a particle and t is discrete time step. The position of a particle is changing due to vector of *velocity* $\mathbf{v}_i(t) = [v_{i1}, v_{i2}, \dots, v_{in}]$ according to equation

$$\mathbf{x}_i(t + 1) = \mathbf{x}_i(t) + \mathbf{v}_i(t + 1). \quad (1)$$

The start position of particle $\mathbf{x}_i(0)$ in a search space is random and is generated by the uniform distribution. The initial velocity $\mathbf{v}_i(0)$ is set to zero vector.

Each particle has a memory, where its best position found during the searching process is stored. This position is called *personal best* or *pbest* and is represented by position vector $\mathbf{y}_i(t) = [y_{i1}, y_{i2}, \dots, y_{in}]$, which is calculated by

$$\mathbf{y}_i(t + 1) = \begin{cases} \mathbf{y}_i(t) & \text{for } f(\mathbf{x}_i(t + 1)) \geq f(\mathbf{y}_i(t)), \\ \mathbf{x}_i(t + 1) & \text{for } f(\mathbf{x}_i(t + 1)) < f(\mathbf{y}_i(t)), \end{cases} \quad (2)$$

where $f : \mathbb{R}^n \rightarrow \mathbb{R}$ is fitness function, which determines the quality of a particle position.

Particles can cooperate with others and they form *neighbourhoods*. Inside a neighbourhood the particles, which belong to this neighbourhood, share information about their *pbest* positions. The best position of all *pbest* positions in a neighbourhood is called *local best* or *lbest*. The velocity of a particle is based on the difference between the actual position and *pbest* and *lbest* positions. There are two basic versions of the algorithm, which differ in neighbourhood size

and structure. The first one is called *Global Best PSO* and the second one is called *Local Best PSO*.

The particle velocity is calculated by

$$v_{ij}(t+1) = v_{ij}(t) + c_1 r_{1j}(t)[y_{ij}(t) - x_{ij}(t)] + c_2 r_{2j}(t)[\hat{y}_{ij}(t) - x_{ij}(t)], \quad (3)$$

where $v_{ij}(t)$ is velocity of particle i in direction j ($j = 1, 2, \dots, n$) in time step t , c_1 and c_2 are positive coefficients which indicate how much is the particle attracted by its *pbest* position and *lbest* position, $r_{1j}(t)$ and $r_{2j}(t)$ are random values from $\langle 0, 1 \rangle$ generated by the uniform distribution, representing a stochastic element of the algorithm and \hat{y}_{ij} is the j -th component of vector $\hat{y}_i(t)$ which is the *lbest* position for particle i .

The basic version of PSO does not provide satisfactory convergence to an optimum. That is why some improvements were applied, such as a modification called *inertia weight*, a velocity improvement called *velocity clamping* and time dependent c_1 and c_2 coefficients. The goal of these modifications is to give particles appropriate ration between *exploration* and *exploitation* ability. The good exploration ability means, that the particles cover the whole search space during their life. This helps to find optimum areas in the search space, but the particles are unable to focus on a global optimum. On the other hand, exploitation ability represents the effort of particles to concentrate on a small area from the search space and find the best solution here. It is necessary to find an appropriate balance between these two abilities. In the first half of the optimization process the particles should have good exploration ability and than the exploitation ability.

The PSO algorithm was used in various benchmark problems from mechanics—the tuning of a dynamic vibration absorber model is presented the abstract. The model is shown in Fig. 1. The steady response before and after optimization using the PSO algorithm is shown in Fig. 2.

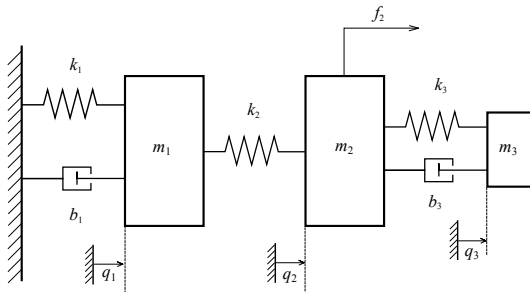


Fig. 1. Dynamic absorber of vibrations

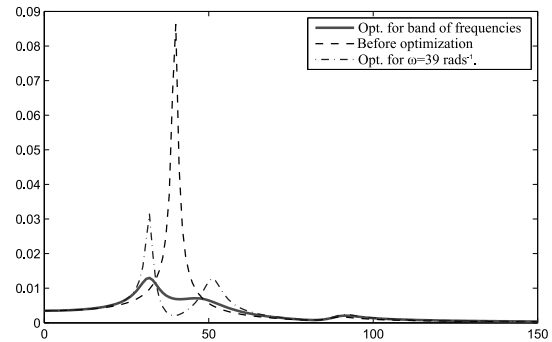


Fig. 2. Steady response q_2 before and after optimization with PSO algorithm

Acknowledgement

This work was supported by SGS-2013-036.

References

- [1] Engelbrecht, A. P., Fundamentals of computational swarm intelligence, John Wiley & Sons, Chichester, 2005.
- [2] Hajžman, M., OPTIMIZATION TOOLBOX for MATLAB – Practical application and examples with emphasis on dynamic optimization, University of West Bohemia, Plzeň, 2003. (in Czech)
- [3] Hlaváč, Z., Dynamic synthesis and optimization, University of West Bohemia, Plzeň, 1995. (in Czech)

Damage of the boiler collector caused by vibration

J. Buzík^a

^a *Institute of Process and Environmental Engineering UPEI-VUT, Faculty of Mechanical Engineering, Brno University of Technology, Technická 2, 616 69 Brno, Czech Republic*

This contribution is devoted to searching of the damage causes of the boiler collector. To date of 6/11/95 the boiler had exhausted life from 40 %. Operation of boiler is accompanied with periodically creation of crack between nozzles. This crack is created in hoop direction in the middle part of the collector. Collector serves to distribution steam about temperature 350 °C to tubes. Next, this steam is overheated by flue gases to temperature 486 °C. Flue gases are generated by burning heavy fuel oil, natural gas and tar mixture. Tubes leading from collector to boiler have U-tube bundle shape in boiler. In boiler space the tube bundle is insert to second space with natural draught. Space with collector and boiler space is separated by membrane wall. Tube bundle leads through this membrane wall.

The boiler collector was repaired in 2005. In this year occurred the exchange of the part of boiler between nozzles. This exchange was required because it occurred to crack of collector. Necessity of exchange of the part of collector was required more two times with same interval. This is reason to consider the creating crack in periodically from 4 to 5 years. This is reason to classify of fatigue like to high-cycle fatigue. Collector exchange is possible in summer and winter shutdown only. All these factors lead to economic-ecology reflection. This is necessity to design thorough preparation of boiler exchange in shutdown time.

When searching causes this damage was followed completely systematically. Firstly were created analysis (FEM – finite element method and CFD – computational fluid dynamics) who they can confirm static damage from irregular flow of steam distribution to the tube of tube bundle. This inequality can cause irregular thermal expansion and possible damage of collector, respectively the tubes. But, these analyses didn't confirm static respectively quazi-static causes of damage. In order to check most information about collector was created heat-hydraulic check calculation. This calculation obtained velocity of flue gas $v_{fg} = 0.6$ m/s, overall heat transfer coefficient of flue gas $\alpha_{fg} = 35.85$ W/(m².K) and steam $\alpha_s = 1124.06$ W/(m².K), Reynolds number of flue gas $Re_{fg} = 57242.95$, density flue gas $\rho_{fg} = 0.48$ kg/m³ and dynamic viscosity of flue gas $\eta_{fg} = 2.5e-5$ Pa.s. In next part was performed CFD analysis inside of boiler. The CFD analysis revealed the vortexes behind tubes. This information was important for next analyses. These vortexes are reason of tube vibration and can be main reason for tubes damage respectively collector. The values of frequency vortexes were calculated by method from publication: VDI Heat Atlas [3], TEMA [2] and Hewitt [1]. All calculation from these publications to confirm occurrence of vortex excitation in values higher then allowed value. The vortex vibration accompanied acoustic vibration. Vortexes excitation cannot be marked like main reason damage of collector in case large rigidities tubes and membrane wall respectively tube bundle support connections. In this case would occur to shear tensions on the tubes and membrane wall connections respectively on the tubes and tube bundle supports, but it did not take place. Assumption of low rigidities tube is crucial for next calculation.

For calculation of amplitudes vibration were used tube supports with 2DoF (two degrees of freedom) from moments in tube axis direction and in perpendicular direction to tube axis and perpendicular direction to flue gas flow. Tube supports have distance from 0.85 to 1 meter. The results from these analyses have value of vibration amplitude to 7 mm.

Next important part was classification and describe of vortexes behind tubes. These calculations were make in CFD with used UDF (user define function) for 6DoF (six degrees of freedom). These DoF limits computational model on 2DoF as described above. Next more important step at CFD analyses was choosing appropriate viscous model for well describe of vortex excitation. The best models were laminar, k-omega SST and k-epsilon Realizable. For next analyses were waived from initial value of velocity flue gas ($v_{fg} = 0.6$ m/s), dynamic viscosity of flue gas $\eta_{fg} = 2.5e-5$ Pa.s and density flue gas $\rho_{fg} = 0.48$ kg/m³. The main reason this step was checking behaviour these physical variables for flue gas (velocity, density and dynamic viscosity) on the forces of vortexes excitation. The results describe insignificant influence of dynamic viscosity and important influence of velocity, density and their combination. The results from CFD were pictures, graphs and value. On the pictures was describe geometry and flow of vortexes couple Kármán Vortex Street. On the graphs was described time dependence of lift and drag force, dependence of lift and drag force and reduced velocity to vortexes amplitude.

In last step was evaluated the vortexes excitation stress. The values of these stresses from vortexes excitation didn't exceed of allowed value. The values of these frequencies were in range from 7 to 20 Hz. From this information was determined high-cycles fatigue, wherein it occurred to exhaustion of life and plastic deformation collector between nozzles.

Every analysis confirmed presence and influence of the vortexes excitation on the boiler collector respectively tube bundle. Basically, vortexes excitations were main causes of damage of collector in above. The real model will have different results because his geometry has connection to Y-bifurcated tube. This geometry causes additions or subtraction wave on the tubes connection. The continuation of this contribution will be more accurate with the results on the real geometry model and evaluation of sample from damage geometry. Very elegant solution can be in insert specifically geometry for break of vortex excitation with preserving of heat performance of tube bundle.

Acknowledgements

The authors gratefully acknowledge financial support provided by Technology Agency of the Czech Republic within the research project No. TE02000236 "Waste-to-Energy (WtE) Competence Centre".

References

- [1] ANSYS® Academic Research, Release 14.5, Help System, Coupled Field Analysis Guide, ANSYS, Inc.
- [2] Buzík, J., Nováček, F., Lošák, P., CFD and FEA boiler collector analysis, In Proceedings of the 17th Conference on Process Integration, Modelling and Optimisation for Energy Saving and Pollution Reduction PRES 2014, CHEMICAL ENGINEERING TRANSACTIONS. Milan, Italy: Aidic Servizi S.r.l., 2014, pp. 847-852.
- [3] Hewitt, G., Heat exchanger design handbook, Begell House, New York, 1998.
- [4] TEMA, Standards of the tubular exchanger manufacturers association, 9th ed. Tubular Exchanger Manufacturers Association, New York, 2007.
- [5] VDI Heat Atlas 2nd ed., Deutschland, Springer, Berlin, 2010.

Updating of aircraft dynamic model according results of ground vibration test

J. Čečrdle^a

^a Aeronautical Research and Test Institute, a.s., Beranových 130, 199 05 Praha - Letňany, Czech Republic

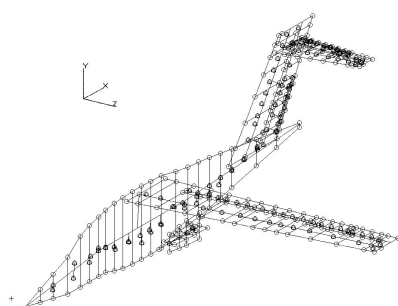


Fig. 1. FE model

Analytical models of aircraft structures that are used for flutter analyses must be validated by means of the ground vibration test (GVT) results. Airworthiness regulations include this demand, because the data based on a theoretical virtual model are not reliable enough. With regard to GVT results incorporation, there are two options of the flutter analysis: 1) direct usage of GVT results and, 2) updating of a structural model according GVT results. The former option is used mainly for general aviation aircraft. The advantage is a direct

relation to a real aircraft structure; however, flutter analyses are more or less limited to the tested structure. The latter option is used mainly for utility or commuter aircraft, for which the development and certification process is more complex. An analytical model is updated to match the GVT-based modal characteristics as closely as possible. Such an updated model allows to make parametrical studies or to include further modifications of structural parameters.

The procedure of an analytical model updating may be based on these two approaches: **1) Model updating by Bayesian least squares method**, where the objective function is defined as a distance between actual modal responses and target (GVT) modal responses. The solution is iterative, based on the matrix equation of the form:

$$\{P_u\} = \{P_o\} + [G]\{-\Delta R\}, \quad (1)$$

where $\{P_u\}$ is parameter vector after updating; $\{P_o\}$ is parameter vector before updating; $\{\Delta R\}$ is response change vector and $[G]$ is "gain matrix" computed according Bayesian estimation theory.

2) More general model optimization by gradient based methods. An example of the objective function expressing weighted squared minimization of relative error in modal frequencies, mode shapes expressed by the Modal Assurance criterion (MAC) and changes of design variables can be expressed as:

$$\min \left(\{\varepsilon_f\}^T [W_f] \{\varepsilon_f\} + \{W_{MAC}\}^T \{1 - [MAC]\} + \{\Delta P\}^T [W_p] \{\Delta P\} \right). \quad (2)$$

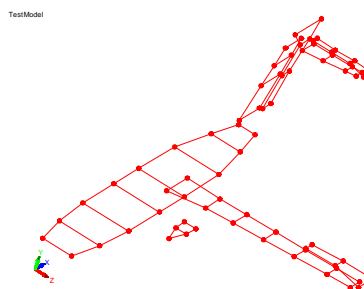


Fig. 2. Experimental points

Model updating of an aircraft structure model is very complex problem. The key issue is the appropriate selection of parameters and responses. It requires good knowledge regarding an updated structure, possible error sources and the appropriate strategy of updating. Methodology is demonstrated on a twin turboprop utility aircraft.

FE model is shown in Fig. 1. Grid of measurement points is adjusted and reduced as shown in Fig. 2. Before the main updating phase, the engine attachment is updated to match the node points of the measured engine vibration modes. Inertia characteristics of controls are also adjusted according mass measurements. Finally, overall inertia characteristics are updated according a prototype weighting. Stiffness parameters of tabs are usually updated according static stiffness measurement results.

The main updating includes the modes of main structural part vibrations (wing, fuselage, horizontal and vertical tail), engines and controls. Symmetric and antisymmetric models are updated separately, thus we obtain diverse parameter values for both models. Parameters available for updating include stiffness (vertical bending, in-plane bending, torsion) of beam elements modeling the main structural parts and controls, and stiffness of spring elements modeling engine attachments, control actuations and the structural part connections. Response parameters available for updating are modal frequencies and mode shapes, that are included using MAC criterion. First, modes of the main structural parts and engines are updated by means of beam global stiffness parameters. Next, the same modes are updated via local parameters. Finally, all the modes including controls are updated by means of local parameters. Updating should not include unnecessary modes. Optionally, further updating to a subset of modes contributing to the specific flutter instability may be performed.

As an example, updating of symmetric model is shown here. Comparison of initial and final pairing of modes is shown in Figs. 3 and 4. Fig. 3 shows the relative error in natural frequencies. The final errors are up to 1.5 %. Fig. 4 shows MAC values. The final ones increased or remained the same compare to the initial ones. To summarize, modal parameters after updating got much closer to the target GVT data. Updated model is now prepared for the usage in the final phase of flutter calculations.

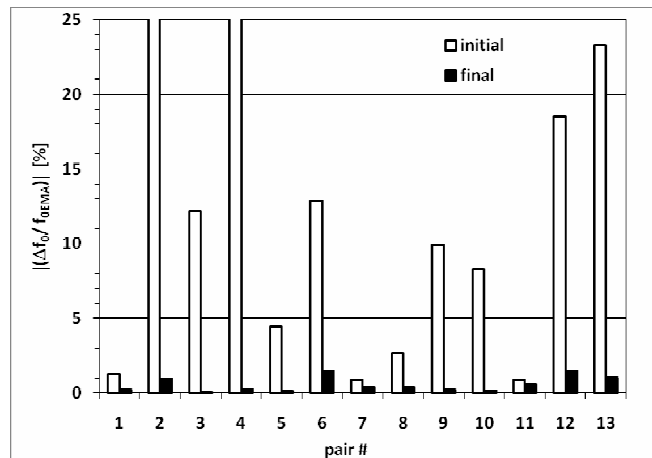


Fig. 3. Pairing of modes (frequency relative error)

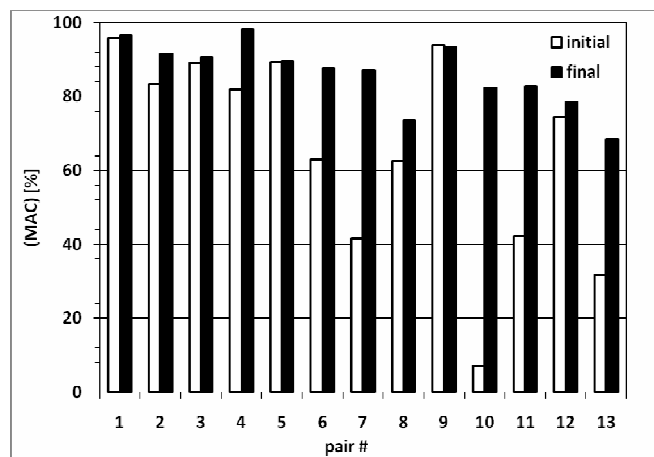


Fig. 4. Pairing of modes (MAC values)

References

- [1] Čečrdle, J., Maleček, J., Dynamic Tuning of Aircraft FE Models to Results of Modal Tests, Czech Aerospace Proceedings 1, 1998, pp. 14-24.

Possibility of a rotor-stator contact assessment

O. Červená^a, M. Balda^a

^aVýzkumný a zkušební ústav Plzeň s.r.o., Tylova 1581/46, 301 00 Plzeň, Czech Republic

High-speed rotors are endangered by contacts with stators when rotating. The contribution presents the analysis of conditions of this phenomenon initiation for high power turbosets. A contact between rotor and stator arises when a trajectory of vibrating rotor runs out of clearances at an arbitrary point along the rotor length. The limiting situation occurs when the rotor just touches stator surface at a critical place. This danger can be minimized by a suitable machine alignment. If the rotor flexure is smaller than a limiting one, the phenomenon might not occur. This can be found out of data measured at common places at low speed.

Limiting cases of rotor flexure or unbalance may be obtained by the application of programs for calculating rotor forced vibrations providing values of dynamic deviations along the rotor axis caused by its bend or unbalance. Should trajectory overcome a fleeting touch, a phenomenon denoted as rubbing was initiated. In that case, heat is generated by intensive friction, which may terminate in a permanent bend of the rotor due to introduced plastic deformation in the point of contact. This situation is out of abilities of linear computations of forced vibrations.

A mathematical model of a rotor (rotating at angular velocity ω) can be generally written in form [1, 2]

$$\mathbf{M}\ddot{\mathbf{q}}(t) + [\mathbf{B}(\omega) + \omega\mathbf{G}]\dot{\mathbf{q}}(t) + \mathbf{K}(\omega)\mathbf{q}(t) = \mathbf{f}(t, \omega), \quad (1)$$

where \mathbf{M} is mass matrix, \mathbf{B} is damping matrix, $\omega\mathbf{G}$ is a matrix of gyroscopic effects, \mathbf{K} is stiffness matrix, $\mathbf{f}(t, \omega)$ is general force excitation vector and $\mathbf{q}(t)$ is vector of generalized coordinates.

Since the force excitation from unbalance has harmonic waveform: $\mathbf{f}(t, \omega) = \mathbf{f}(\omega)e^{i\omega t}$, the dynamical response has harmonic waveform too, $\mathbf{q}(t, \omega) = \mathbf{q}(\omega)e^{i\omega t}$. After substituting all into (1), the unknown vector of complex deflections can be expressed as

$$\mathbf{q}(\omega) = \{-\omega^2\mathbf{M} + i\omega[\mathbf{B}(\omega) + \omega\mathbf{G}] + \mathbf{K}(\omega)\}^{-1} \mathbf{f}(\omega). \quad (2)$$

The centrifugal forces generated during rotation of the unbalanced shafts produce transverse vibrations of the rotor and its surroundings. It can be shown that the trajectory of the shaft center section in any transverse plane is an ellipse, which can be circular or degenerated in a line in extreme cases. It is created by composition of two harmonic processes of the same frequency in a transverse plane of two axes, vertical y and horizontal z , in complex form

$$\begin{aligned} q_y(t, \omega) &= \operatorname{Re}(y_o \exp(i\omega t)) = |y_o| \cos(\omega t + \varphi_y) \\ q_z(t, \omega) &= \operatorname{Re}(z_o \exp(i\omega t)) = |z_o| \cos(\omega t + \varphi_z) \end{aligned} \quad (3)$$

where y_o and z_o are complex amplitudes in time $t = 0$. The trajectory in plane yz is created by composition of vectors $q_y(t, \omega)$ and $q_z(t, \omega)$. The angular frequency of oscillation is ω , time t , and phase angles φ_y and φ_z of real harmonic functions $q_y(t) = \operatorname{Re}(y(t))$ and $q_z(t) = \operatorname{Re}(z(t))$.

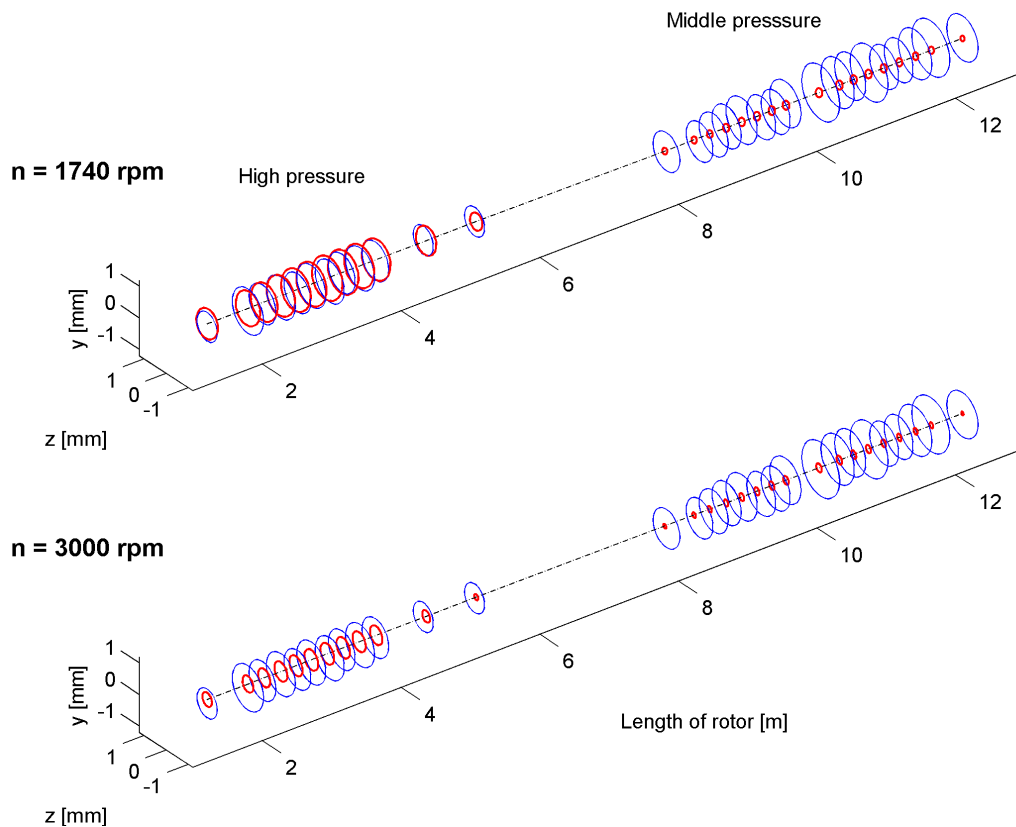


Fig. 1. The trajectories of the shaft center of unbalanced rotor and seal clearances

The trajectories of the shaft center of unbalanced rotor in critical and operational speeds are compared with clearances in seals along all length of the rotor in Fig. 1. Blue lines depict clearances in seals of high pressure and middle pressure parts of the rotor, and trajectories of shaft center are shown by red lines. It is obvious that the rotor trajectories overcome clearances in some seals of high pressure part of the rotor at critical speeds. Situation is complicated by the fact that seals used to be not well aligned as is seen from the middle pressure part of the rotor. In computations of dynamic responses of unbalanced rotor, it is possible to find out boundary values of rotor deformations, for which this does not occur.

The unbalance of the rotor can be caused by its thermal deflection coming from uneven temperature distribution in the cross sections of the rotor body after it stops. The problem of finding temperature distribution is very complicated because of vague knowledge of properties of surrounding media. However, the subject is studied, and it is expected that ways to its solution will be found in future.

Acknowledgements

The paper has been originated in the framework of institutional support for the long-time conception development of the research institution provided by Ministry of Industry and Trade of the Czech Republic.

References

- [1] Byrtus, M., Hajžman, M., Zeman, V., Dynamics of rotating systems, University of West Bohemia, Plzeň, 2010. (in Czech)
- [2] Slavík J., Stejskal V., Zeman V., Fundamentals of machine dynamics, Vydavatelství ČVUT, Praha, 1997. (in Czech)

Three filaments model of sarcomere

V. Čibera^a

^a Faculty of Applied Sciences, University of West Bohemia, Univerzitní 22, 306 14 Plzeň, Czech Republic

This contribution deals with a theoretical mathematical model of the elementary contractile mechanism in the skeletal and heart muscles, i.e. with unit named sarcomere. The most influential model of this phenomenon was already proposed in 1957 by A.F. Huxley in [3]. Nowadays, Huxley's model is considered as a classical model, which significantly contributed to the explanation of muscle contraction on molecular level. Huxley and his colleagues introduced the approach on the muscle contraction theory called cross-bridge theory. In this theory, there is a strong emphasis on the explanation of muscle contraction based namely on the interaction of two proteins. Both of the proteins form a shape of filaments, which are able to actively slide along each other. First protein, called myosin, serves as a molecular motor. Its pivotal property is that it can cyclically bind and unbind the second protein called actin. During every bind/unbind-action, actin is shifted by myosin in one direction, which is the main principle of contraction and force production of muscles.

During the past decades, mathematical models based on the cross-bridge theory sufficiently succeeded in the description of concentric and isometric contraction, where in the first case the muscle shortens and in the second case muscle produces force at constant length. Till nowadays, the most challenging part in cross-bridge theory remains the explanation of eccentric contraction, which is followed by the phenomena called force enhancement. In this case, muscle (sarcomere) is stretched by external load. After the stretch, the muscle produces more force than the cross-bridge theory is able to explain.

Following the latest experimental and theoretical results, the classical cross-bridge model was modified in this contribution in two ways as follows. Firstly, according to the results and proposals in [2], it seems like the third most abundant protein titin in sarcomere also plays an active role during contraction. According to [2], titin is also able to actively attach at actin filaments the way that affect namely eccentric contraction. The second crucial modification was the implementation of the non-linear elastic property of myosin as measured in [4].

After modifications, the classical cross-bridge model was changed to the form:

$$\begin{aligned}
 F_S &= F_{CB} + F_T, \\
 F_{CB} &= l \int_{-\infty}^{\infty} f_K(x)n(x,t)dx \\
 F_T &= k_T l_T \\
 \frac{\partial n(x,t)}{\partial t} - v(t) \frac{\partial n(x,t)}{\partial x} &= (1-n)f(x) - ng(x) \\
 \frac{dl}{dt} &= v(t) \\
 \frac{dl_T}{dt} &= -v(t)
 \end{aligned} \tag{1}$$

where F_s denotes sarcomere/half-sarcomere force, F_{CB} represents force achieved by cross-bridge cycling, l is the magnitude of the actin-myosin filaments overlap, $f_k(x)$ is the force-length relationship as measured in [4], where x is the length of single myosin cross-bridge, $n(x,t)$ is the distribution of the cross-bridges x -lengths. F_T is force produced by titin filaments, where k_T is the elasticity of the bunch of titins and l_T is its length. $v(t)$ expresses the velocity of contraction. $f(x)$ and $g(x)$ are specific rate functions describing kinetics of the cross-bridge cycling.

The modified cross-bridge model was used to simulate all kind of contraction, i.e. concentric, isometric and at last challenging eccentric contraction. Further, two special cases of contraction were simulated: sudden shortening of sarcomere - special case of concentric contraction and sudden stretch of sarcomere – special case of eccentric contraction. All of the results are comparable with the measured experimental data as available in literature. This leads to the conclusion that the role of the titin might be more important than originally thought in cross-bridge theory as proposed in [2]. As an example of the results, graphs depicting force production during eccentric contraction and sudden stretch are presented.

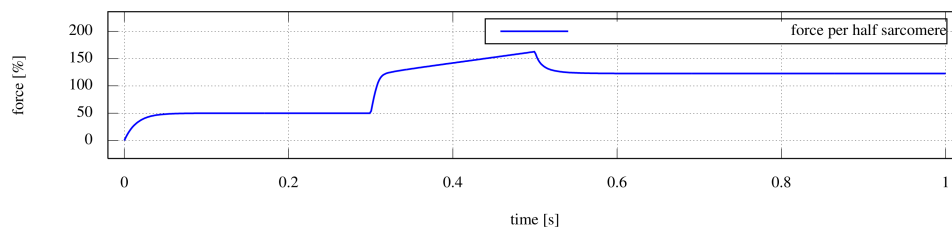


Fig. 1. Force during eccentric contraction of sarcomere

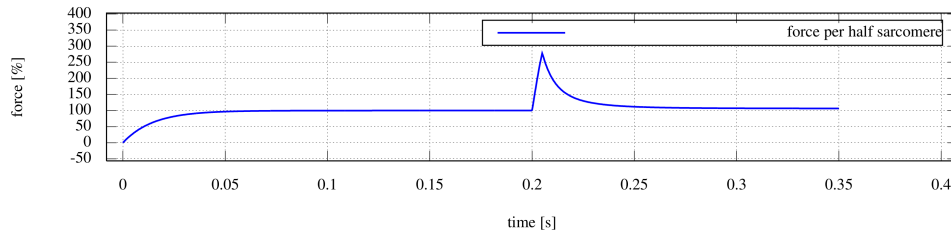


Fig. 2. Force during sudden stretch of sarcomere

Acknowledgements

The work has been supported by the grant project SGS-2013-026. Special thanks go to the group supervised by Dr. Walter Herzog at the University of Calgary, where the crucial part of presented contribution was accomplished.

References

- [1] DuVall, M., Gifford, J. L., Amrein M., Herzog, W., Altered mechanical properties of titin immunoglobulin domain 27 in presence of calcium, *European Biophysics Journal* 42 (2013) 301-307.
- [2] Herzog, W., Leonard, T., Joumaa, V., DuVall, M., Panchangam, A., The three filament model of skeletal muscle stability and force production, *Molecular and Cellular Biomechanics* 9 (2012) 175-191.
- [3] Huxley, A. F., Muscle structure and theories of contraction, *Prog Biophys Chem* 7 (1957) 255-318.
- [4] Kaya, M., Higuchi, H., Stiffness, working stroke, and force of single-myosin molecules in skeletal muscle: elucidation of these mechanical properties via nonlinear elasticity evaluation, *Cellular and Molecular Life Sciences* 70 (2013) 4275-4292.

Representation of crushing phenomenon in DEM model of railway ballast

R. Dubina^a, J. Eliáš^a

^a*Faculty of Civil Engineering, University of Technology, Veveří 331/95, 602 00 Brno, Czech Republic*

Representation of ballast behavior in Discrete Element Models (DEM) would not be complete without including crushing of grains. The grain crushing leads to degradation of the ballast in the railway. Therefore it is necessary to take the crushing into account. Two approaches have been developed in literature. The first one represents every grain as an assembly of smaller units with cohesive contacts between them. These cohesive contacts may break and many ruptures result in the separation of grain parts. This approach is relatively precise and universal, but it demands extreme computational resources. The other approach is exploited here. Every grain is modeled as one rigid body. In case which is presented here, grains are modeled as spheres. The crushing occurs when some equivalent stress in the grain σ_e [4], here determined as von Mises stress computed from fabric stress tensor, exceeds the material strength f_t

$$\sigma_e > f_t. \quad (1)$$

The fabric tensor [1] in the particle can be expressed as

$$\sigma_{ij} = \frac{1}{V} \sum_c l_i^{(c)} F_j^{(c)}, \quad (2)$$

when c runs over all contacts of the particle, $\mathbf{F}^{(c)}$ is a force acting at the c -th contact at position $\mathbf{l}^{(c)}$. Subsequently the stress vector is symmetrized by averaging opposite non-diagonal members. Principle stresses ($\sigma_I > \sigma_{II} > \sigma_{III}$) and their directions are found by eigenvalue analysis. The equivalent stress is obtained from the von Mises condition which is defined as

$$\sigma_e = \frac{\sqrt{(\sigma_I - \sigma_{II})^2 + (\sigma_{II} - \sigma_{III})^2 + (\sigma_I - \sigma_{III})^2}}{V_{\text{sphere}}}, \quad (3)$$

where $\sigma_I, \sigma_{II}, \sigma_{III}$ are principal stresses and V_{sphere} is the volume of the sphere. Then the average stress in the grain is compared to material strength f_t , which depends on the radius of the sphere

$$f_t = \frac{f_0}{r_{\text{sphere}}}, \quad (4)$$

where f_0 is reference strength and r_{sphere} is the radius of the sphere. For convenience some chosen minimal radius serves as lower limit for which the spheres can break. If all conditions are satisfied, the grain is then replaced by several smaller bodies, pieces [3, 5]. These pieces must often have the same shape as the original grain (typically spherical) and their assembly therefore cannot exactly create the shape of the original grain as shown in Fig. 1.

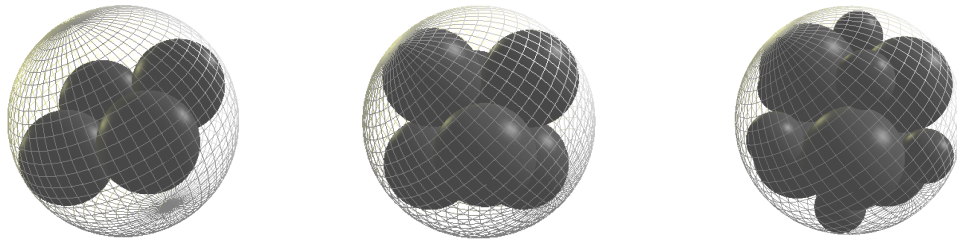


Fig. 1. The replacement subsidiaries of the parent – three variants with 4, 6 or 14 spheres

The orientation of new group of spheres is set in such a way that the direction of minimal principal stress is identical to the direction of the softest axis of the new configuration. From Fig. 1, it is apparent that a substantial part of the volume is lost. It can be the problem in such cases, when it occurs to the many crushing of the grains in the sample. In these cases the artificial deformation of the sample can significantly affect results. The resolution of this problem can be the approach presented in [2] when polyhedrons instead of spheres were implemented. In this case it does not occur to the volume loss. To preserve the mass law, a possibility to increase the density during splitting might be implemented.

The results depending on the size of minimum splittable radius, the variant differing in number of pieces of the replacement, the influence of density increase and the influence of other input parameters are investigated.

The major work is performed on oedometer test where all the above mentioned tests were performed. The goal is to find a reasonable value of material strength. The results show that in case of oedometer test the increase of the density does not play a significant role. It is probably caused by static character of the simulation. The other tests show that the splitting into 6 or 14 spheres gives similar results.

In future we are going to use a particle crushing in so-called box-test and in the simulation of cutting of railway.

Acknowledgement

This outcome has been achieved with the financial support under project No. FAST-J-14-2471. The support is gratefully acknowledged.

References

- [1] Bagi, K., Stress and strain in granular assemblies, Elsevier, 1996.
- [2] Eliáš, J., Simulation of railway ballast using crushable polyhedral particles, Powder Technology 264 (2014) 458-465.
- [3] Hossain, Z., Indraratna, B., Darve, F., Thakura, P. K., DEM analysis of angular ballast breakage under cyclic loading, Geomechanics and Geoengineering: International Journal 2 (3) (2007) 175-182.
- [4] Lobo-Guerrero, S., Vallejo, L.E., Discrete element method analysis of railtrack ballast degradation during cyclic loading, Granular Matter 8 (3-4) (2006) 195-204.
- [5] Tsoungui, O., Vallet, D., Charmet, J.C., Numerical model of crushing of grains inside two-dimensional granular materials, Powder Technology 105 (1-3) (1999) 190-198.

Analytical periodic solution and stability assessment of Cardan's mechanism

J. Dupal^a, M. Zajíček^a

^a Faculty of Applied Sciences, University of West Bohemia, Univerzitní 22, 306 14 Plzeň, Czech Republic

The Cardan shaft is used as a component of many mechanisms for the transmission of torque through angularly misaligned rotating shafts. Often we meet with its use, e.g., in automobile industry. The typical design of the Cardan shaft is composed of two Cardan's joints in series and mutually connected with a shaft that usually enables an axial dilatation, see Fig. 1. A major problem with the use of Cardan's joint is that it transforms a constant input speed to a periodically fluctuating one. This means that the dynamic system with these joints is parametrically excited. It introduces a number of specific resonance conditions or dynamic instability of the system. The main goal of analyzing such systems is assessment the (in)stability conditions as well as the amplitudes of the steady state motion.

In the present study, the simplified model for description of Cardan's mechanism depicted in Fig. 1 is considered under the assumption of a small angular misalignment δ . The governing equation of periodic motion can be then linearized under this assumption and after some adjustments it can be found in the form of the Mathieu equation

$$\ddot{\varphi} + 2D\Omega\dot{\varphi} + \Omega^2(1 \mp \varepsilon \cos 2\omega t)\varphi = \frac{M_1(t)}{I_1} + \frac{M_6(t)}{I_6}, \quad (1)$$

where φ is a relative angle between the members 1 and 6, D is a damping ratio, Ω is a natural frequency of a system without periodic stiffness, $\varepsilon = \delta^2/2$ is measure of stiffness modulation, I_1 and I_6 are moments of inertia and $M_1(t)$ and $M_6(t)$ are the periodic functions. After dimensionless transformation and some term rearrangements, Eq. (1) should be rewritten as

$$\varphi'' + 2D\varphi' + (1 \mp \varepsilon \cos 2\eta\tau)\varphi = \frac{1}{\Omega^2} \left(\frac{M_1(\tau)}{I_1} + \frac{M_6(\tau)}{I_6} \right). \quad (2)$$

The analytic periodic solution of Eq. (2) in a steady state can be found by means of a periodic Green's function and the Fredholm's integral equation with degenerated kernel, see [1]. As

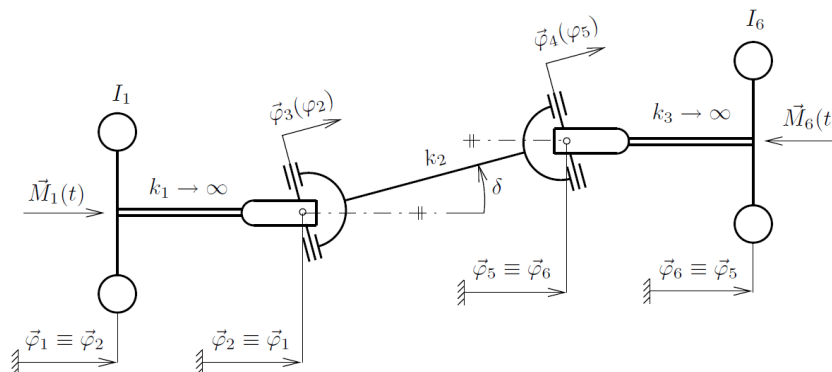


Fig. 1. Scheme of Cardan shaft

further shown in this paper, the existence of solution is closely related to investigation of the (in)stability borders. This problem leads to calculation of eigenvalues of a certain matrix described in detail, see [1]. The stability chart for undamped system is shown in Fig. 2 where $1/\eta = (\Omega/\omega)^2$. The correctness of borders is verified by using the Floquet theory [3].

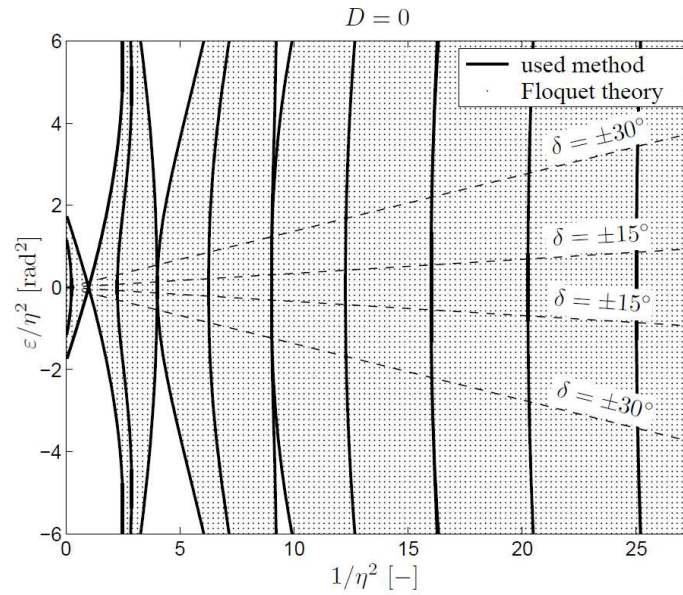


Fig. 2. Stable and instable regions, problem without damping

The response calculation in steady state is performed for Eq. (2) with right site in the form

$$\begin{aligned} \frac{1}{\Omega^2} \left(\frac{M_1(\tau)}{I_1} + \frac{M_6(\tau)}{I_6} \right) &= \frac{M_1}{k_2} \frac{I_1 I_6}{I_1 + I_6} \left\{ \frac{1}{I_1} + \frac{1}{I_6} [r_0 + r_1 \cos(\eta\tau + \phi) + r_2 \cos 2\eta\tau] \right\} \\ &= \frac{\varphi_m}{1 + \lambda_I} [\lambda_I + r_0 + r_1 \cos(\eta\tau + \phi) + r_2 \cos 2\eta\tau], \end{aligned} \quad (3)$$

where $M_1(t) = M_1 = \text{const.}$, $\varphi_m = M_1/k_2$ (k_2 is stiffness), $\lambda_I = I_6/I_1$. The numerical simulations with parameter settings $r_0 = 1$, $r_1 = 0.5$, $r_2 = 0.25$, $\phi = \pi/4$, $\lambda_I = 1$ and $\delta = \{15^\circ, 30^\circ\}$ were done. The oscillation results for the system in the stable region were validated by means of the Runge-Kutta integration method and very good agreements were observed. We can conclude that the use of presented solution is suitable to a linear system with periodically varying stiffness and excitation, see [2].

Acknowledgements

This work was supported by the European Regional Development Fund (ERDF), project "NTIS – New Technologies for the Information Society", European Centre of Excellence, CZ.1.05/1.1.00/02.0090 and by the project TE01020068 "Centre of research and experimental development of reliable energy production" of the Technology Agency of the Czech Republic.

References

- [1] Dupal, J., Zajíček, M., Analytical periodic solution and stability assessment of 1 DOF parametric systems with time varying stiffness, *Applied Mathematics and Computation* 243 (2014) 138–151.
- [2] Dupal, J., Zajíček, M., Analytical solution of the drive vibration with time varying parameters, *Proceedings of the ASME 2011 International Design Engineering Technical Conferences & Computers and Information in Engineering Conference*, Washington DC, USA, 2011, pp. 1365-1370.
- [3] Floquet, G., Sur les équations différentielles linéaires á coefficients périodiques, *Annales scientifiques de l' Ecole Normale Supérieure* 12 (1883) 47-88. (in French)

Optimization of counter flow plate heat exchangers

V. Dvořák^a

^a Faculty of Mechanical Engineering, TU of Liberec, Studentská 2, 461 17 Liberec, Czech Republic

The development of recuperative heat exchangers in recent years focused on increasing efficiency. Another challenge is the development of so-called enthalpy exchangers for simultaneous heat and moisture transport, i.e. transport of both sensible and latent heat, as presented by Vít et al. in work [6]. A lot of others researchers dealt with design and optimization of plate heat exchangers, for example Gut et al. [2]. Fewer scientists dealt with optimization of the shape of the heat exchange area, e.g. Kanaris et al. [4] investigated a plate heat exchanger with undulated surfaces or Han et al. in article [3] numerically investigated turbulent flow in chevron-type plate heat exchangers with sinusoidal-shaped corrugations using the SST $k-\omega$ turbulence model.

This work is motivated by the need to optimize heat transfer area of heat recovery heat exchangers which are assembled from plates. Plates are made of metal, paper or plastic and are shaped by press molding. Ridges, grooves or undulation are supposed to increase the heat transfer and also determine the plate pitch and carry the heat exchanger. By assembling the heat exchanger from plates, complicated and irregular narrow channels are created.

To optimize a heat exchanger, we have to create a model and a computational mesh and use computational fluid dynamic (CFD) software. Disadvantages of repeated generation of computational meshes are: It is slow, meshes made in different models are not similar and parameterization of the model is problematic. Further, even a small change of geometry requires going through the whole process of model creation and mesh generation again, as for example did Novosad in work [5]. Therefore, a new method for generation computational variants was developed and was presented by Dvorak in work [1].

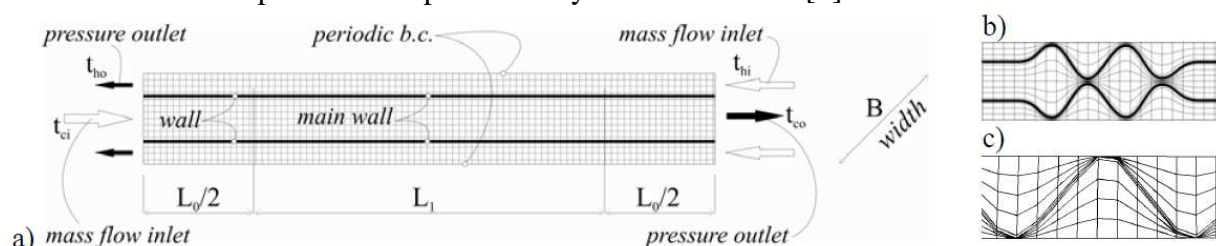


Fig. 1. Model of heat exchange surface of counter flow recuperative heat exchanger, a) – initial mesh, b) – deformed mesh, c) – detail of a mesh example

The method used in work [1] and this work is based on dynamic mesh method, provided by software Fluent, which allows control of movement of each node in the computational domain. First a simple but fully functional model with straight walls, see Fig. 1a, is created. In the subsequent step, the computational mesh is deformed using the user defined functions, see Fig. 1b. It is possible to change the spacing of the plates, to create undulations and also define the size of cells adjacent to the wall during the deformation.

Usually, we optimize for maximum efficiency for a given pressure drop, which if for various applications different, therefore a target function was designed in work [1] as

$$F = \eta - c_\eta \frac{|\Delta p - \Delta p_R|}{\Delta p_R}, \quad (1)$$

where η is efficiency, $c_\eta = 2$ [1] is penalization of the objective function for relative difference between actual pressure loss Δp [Pa] and required pressure loss Δp_R [Pa].

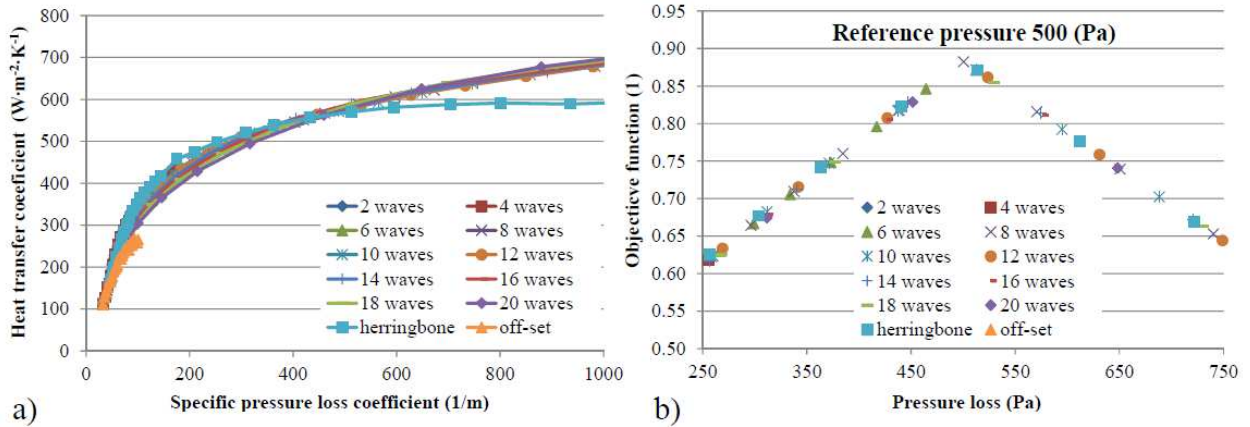


Fig. 2. Results for various topologies of heat transport surface: a) – dependence of heat transfer coefficient on specific pressure loss coefficient, b) – objective function for reference pressure 500 [Pa]

There are dependences of heat transfer coefficient [W·m⁻²·K⁻¹] on specific pressure loss [1/m] for ridges in herringbone pattern and for off-set pattern with intermitted ridges in Fig. 2a. There are also curves for ridges with various counts of waves there. It is obvious that for low pressure losses, the herringbone pattern is the most advantageous while waves are optimal for higher pressure losses. The results indicate that the topology of the off-set pattern is not suitable in any range of pressure losses.

An example of calculated values of objective function is in Fig. 2, where results are plotted for reference pressure 500 [Pa] according Eq. (1). The objective function, which is a linear combination of efficiency and pressure loss, creates roof-like curves which enable to identify the best variant for given pressure loss. Later, it will be possible to optimize the topology of plates of the heat exchangers.

Acknowledgements

Author gratefully acknowledges financial support by Czech Technological Agency under the project TACR TA01020313.

References

- [1] Dvořák, V., A method for optimization of counter flow plate heat exchanger, Proceedings of CSCC 2014: Advances in Information Science and Applications - Vol. I, Santorini Island, Greece, 2014, pp. 193-198.
- [2] Gut, J.A.W., Pinto, J.M., Modeling of plate heat exchangers with generalized configurations, International Journal of Heat and Mass Transfer 46 (2003) 2571-2585.
- [3] Han, W., Saleh, K., Aute, V., Ding, G., Hwang, Y., Radermacher, R., Numerical simulation and optimization of single-phase turbulent flow in chevron-type plate heat exchanger with sinusoidal corrugations, HVAC&R Research 17 (2011) 186-197.
- [4] Kanaris, A.G., Mouza, A.A., Paras, S.V., Optimal design of a plate heat exchanger with undulated surfaces, International Journal of Thermal Sciences 48 (2009) 1184-1195.
- [5] Novosád, J., Dvořák, V., Investigation of effect of oblique ridges on heat transfer in plate heat exchangers, Experimental Fluid Mechanics (2013) 510-514.
- [6] Vít, T., Novotný, P., Nguyen Vu, Dvořák, V., Testing method of materials for enthalpy wheels, Recent Advances in Energy, Environment, Economics and Technological Innovation (2013) 34-38.

Nonlinear vibration of beam-type components with inner impact interaction

Š. Dyk^a, V. Zeman^a

^aFaculty of Applied Sciences, UWB in Pilsen, Univerzitní 22, 306 14 Plzeň, Czech Republic

Presented investigation of strongly nonlinear phenomena between two 1D interacting continua is motivated by research of nonlinear vibration of fuel rod in nuclear fuel assembly. To describe nonlinear impact vibration of nuclear fuel rod (FR) in fuel assemblies (FA) of nuclear power plants (NPP) [2], a FR is considered as a system of two beam-type components – FR cladding (outer continuum, index *out*) and a column of fuel pellets (inner continuum, index *in*). The outer continuum is coupled with frame by several elastic couplings. Both of these subsystems are kinematically polyharmonically driven in lower ends by pressure pulsations of circulation pumps. Between these two subsystems, there is a clearance and impact between them can occur.

Generally, let us consider two one dimensional continua with circle cross-section (one inside the second). There is a little clearance between them and both continua are driven by kinematical excitation in their lower end. Both continua are supposed to satisfy Euler-Bernoulli theory for elastic beams and they are modelled using finite element method for 1D continua [1]. Vector of generalized coordinates of subsystems can be expressed in the form

$$\mathbf{q}^{(out)} = \begin{bmatrix} \mathbf{q}_L^{(out)} \\ \mathbf{q}_F^{(out)} \end{bmatrix}, \quad \mathbf{q}^{(in)} = \begin{bmatrix} \mathbf{q}_L^{(in)} \\ \mathbf{q}_F^{(in)} \end{bmatrix}, \quad (1)$$

where displacements of the lower node (index *L*) are integrated in subvectors $\mathbf{q}_L^{(out)}$ and $\mathbf{q}_L^{(in)}$ and the displacements of free subsystems nodes (index *F*) are integrated in subvectors $\mathbf{q}_F^{(out)} \in \mathbb{R}^{n_{out}}$ and $\mathbf{q}_F^{(in)} \in \mathbb{R}^{n_{in}}$. The vectors of nodal points displacements of FR beam subsystems have the form

$$\mathbf{q}_F^{(X)} = [\dots, \xi_i^{(X)}, \eta_i^{(X)}, \psi_i^{(X)}, \vartheta_i^{(X)}, \dots]^T, \quad X = in, out, \quad (2)$$

where $\xi_i^{(X)}, \eta_i^{(X)}$ are mutually perpendicular lateral displacements of the subsystem centres in nodal points *i*. Angular displacements $\psi_i^{(X)}, \vartheta_i^{(X)}$ express bending angles of cross-sections around lateral displacements. The mathematical models of the loosed undamped both subsystems in the decomposed block form corresponding to partitioned subvectors according to (1) can be written as

$$\begin{bmatrix} \mathbf{M}_L^{(out)} & \mathbf{M}_{L,F}^{(out)} \\ \mathbf{M}_{F,L}^{(out)} & \mathbf{M}_F^{(out)} \end{bmatrix} \begin{bmatrix} \ddot{\mathbf{q}}_L^{(out)} \\ \ddot{\mathbf{q}}_F^{(out)} \end{bmatrix} + \left(\begin{bmatrix} \mathbf{K}_L^{(out)} & \mathbf{K}_{L,F}^{(out)} \\ \mathbf{K}_{F,L}^{(out)} & \mathbf{K}_F^{(out)} \end{bmatrix} + \mathbf{K}_C \right) \begin{bmatrix} \mathbf{q}_L^{(out)} \\ \mathbf{q}_F^{(out)} \end{bmatrix} = \begin{bmatrix} \mathbf{f}_C^{(out)} \\ \mathbf{f}_{out,in}(\mathbf{q}_F^{(out)}, \mathbf{q}_F^{(in)}) \end{bmatrix}, \quad (3)$$

$$\begin{bmatrix} \mathbf{M}_L^{(in)} & \mathbf{M}_{L,F}^{(in)} \\ \mathbf{M}_{F,L}^{(in)} & \mathbf{M}_F^{(in)} \end{bmatrix} \begin{bmatrix} \ddot{\mathbf{q}}_L^{(in)} \\ \ddot{\mathbf{q}}_F^{(in)} \end{bmatrix} + \begin{bmatrix} \mathbf{K}_L^{(in)} & \mathbf{K}_{L,F}^{(in)} \\ \mathbf{K}_{F,L}^{(in)} & \mathbf{K}_F^{(in)} \end{bmatrix} \begin{bmatrix} \mathbf{q}_L^{(in)} \\ \mathbf{q}_F^{(in)} \end{bmatrix} = \begin{bmatrix} \mathbf{f}_C^{(in)} \\ \mathbf{f}_{in,out}(\mathbf{q}_F^{(out)}, \mathbf{q}_F^{(in)}) \end{bmatrix}, \quad (4)$$

where \mathbf{M} , \mathbf{K} corresponds to mass (stiffness) submatrices of the subsystems and matrix \mathbf{K}_C expresses influence of elastic supports. Subvectors $\mathbf{f}_{in,out}(\mathbf{q}_F^{(out)}, \mathbf{q}_F^{(in)})$ and $\mathbf{f}_{out,in}(\mathbf{q}_F^{(out)}, \mathbf{q}_F^{(in)})$ express nonlinear impact forces between both continua. The damping is supposed to be proportional ($\mathbf{B} = \alpha\mathbf{M} + \beta\mathbf{K}$, $\alpha, \beta \in \mathbb{R}^+$) and models of both FR subsystems can be written in the compact form as

$$\begin{bmatrix} \mathbf{M}_F^{(out)} & \mathbf{0} \\ \mathbf{0} & \mathbf{M}_F^{(in)} \end{bmatrix} \begin{bmatrix} \ddot{\mathbf{q}}_F^{(out)} \\ \ddot{\mathbf{q}}_F^{(in)} \end{bmatrix} + \begin{bmatrix} \mathbf{B}_F^{(out)} & \mathbf{0} \\ \mathbf{0} & \mathbf{B}_F^{(in)} \end{bmatrix} \begin{bmatrix} \dot{\mathbf{q}}_F^{(out)} \\ \dot{\mathbf{q}}_F^{(in)} \end{bmatrix} + \\ + \begin{bmatrix} (\mathbf{K}_F^{(out)} + \mathbf{K}_C) & \mathbf{0} \\ \mathbf{0} & \mathbf{K}_F^{(in)} \end{bmatrix} \begin{bmatrix} \mathbf{q}_F^{(out)} \\ \mathbf{q}_F^{(in)} \end{bmatrix} = \begin{bmatrix} \mathbf{f}_L^{(out)}(t) \\ \mathbf{f}_L^{(in)}(t) \end{bmatrix} + \begin{bmatrix} \mathbf{f}_{out,in}(\mathbf{q}_F^{(out)}, \mathbf{q}_F^{(in)}) \\ \mathbf{f}_{in,out}(\mathbf{q}_F^{(out)}, \mathbf{q}_F^{(in)}) \end{bmatrix}, \quad (5)$$

where subvectors $\mathbf{f}_L^{(X)}(t) = -\mathbf{M}_{F,L}^{(X)}\ddot{\mathbf{q}}_L^{(X)} - \mathbf{K}_{F,L}^{(X)}\mathbf{q}_L^{(X)}$, $X = in, out$, express the kinematic excitation by node L motion. The model (5) can be formally rewritten into standard matrix form for dynamical systems of second order

$$\mathbf{M}\ddot{\mathbf{q}}(t) + \mathbf{B}\dot{\mathbf{q}}(t) + \mathbf{K}\mathbf{q}(t) = \mathbf{f}_N(\mathbf{q}, t). \quad (6)$$

System represented by n nonlinear second order ODEs (6) can be rewritten into the form of $2n$ first order ODEs and solved using, e.g., Runge-Kutta method (ode45 in MATLAB). Such

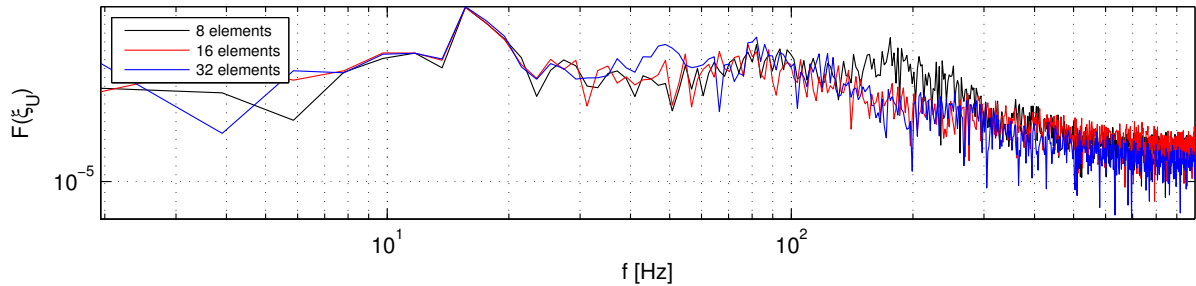


Fig. 1. Fourier spectra of time response ξ_U of the upper node for different discretization

a system was analyzed to describe influence of parameters to quality of vibration. In Fig. 1, the Fourier spectra of time behavior (response to kinematical excitation of lower node) of the upper node ξ_U for different discretization of continua are depicted. The analogical analysis was performed for several radial clearances δ . Obtained results show differences between impact behavior of such a system with different discretization and an influence of the clearance value.

Acknowledgements

The work was supported by the grant SGS-2013-36.

References

- [1] Byrtus, M., Hajžman, M., Zeman, V., Dynamics of rotating systems, University of West Bohemia, Plzeň, 2010. (in Czech)
- [2] Hlaváč, Z., Zeman, V., Vibration of nuclear fuel assemblies: Modelling, methods, application, LAP Lambert Academic Publishing, 2013.

Explanation of difference between sequentially linear solvers in damage mechanics

J. Eliáš^a

^a*Faculty of Civil Engineering, Brno University of Technology, Veveří 331/95, 602 00 Brno, Czech Republic*

The modelling of fracture in concrete structural components has been under investigation for several decades. Many efficient and robust material models are available today. Usually, a solution is obtained by applying load incrementally in a number of small steps in which an iterative algorithm is employed. The robustness of the chosen iterative scheme is of importance. Problems with the convergence of iterative methods in the case of bifurcations, snap-backs, sudden changes in constitutive law, etc., have led to the development of non-iterative methods.

Non-iterative methods can be applied in connection with damage-based saw-tooth constitutive laws composed of linear segments (which when extended pass through the origin of the stress-strain space) followed by immediate jumps to lower stiffness. The classical load-unload (*L-U*) solution method is usually used. This solution method was developed for lattices [5], but can be applied also in connection with finite element method [4].

The *L-U* solution scheme proceeds simply by releasing the whole load after every rupture event and then loading the system with reduced stiffness by a load increment that induces reference elemental stresses $\Delta\sigma_i$, where index i refers to individual elements. The load increment (and reference stress) is then scaled by factor λ to satisfy the following condition

$$f(\lambda\Delta\sigma_k) = 1 \quad \wedge \quad \forall h \neq k : f(\lambda\Delta\sigma_h) < 1, \quad (1)$$

where subscript k denotes the critical element and $f()$ is a stress-based failure criterion which indicates elemental failure when equal to one. The critical element is damaged or completely removed and a new stiffness matrix and corresponding reference stresses are evaluated for the next step. Multiplier λ is selected so that exactly one (critical) element breaks at each step.

Another method applicable to the saw-tooth type of constitutive law is the force-release (*F-R*) method developed to simulate brittle fracture in lattice models [3] and to improve the sequentially linear concept for non-proportional loading paths [2]. The *F-R* method resembles dynamic process of redistributing released stresses from damaged elements while the external load is kept unchanged. During the redistribution, the system evolves from static equilibrium state through disequilibrium states until the static equilibrium is reached again.

In contrast with the *L-U* method, the *F-R* algorithm does not unload to the origin after every rupture, but keeps the whole previously applied load acting. It starts from an equilibrium state (initially, the load-free structure) where elements are exposed to stresses σ_i . As with the *L-U* method, reference elemental stresses $\Delta\sigma_i$ caused by an external load increment are evaluated. Then, critical element k and load multiplier λ are found by satisfying the following condition

$$f(\sigma_k + \lambda\Delta\sigma_k) = 1 \quad \wedge \quad \forall h \neq k : f(\sigma_h + \lambda\Delta\sigma_h) < 1. \quad (2)$$

Critical element k is damaged. The change in the critical element stiffness gives rise to unbalanced forces in nodes connected to this element. Again, Eq. (2) is used but the reference stress $\Delta\sigma_i$ is now the stress in elements caused by these unbalanced forces only. If no element breaks during the redistribution, a new equilibrium state is found by adding all unbalanced forces to the system ($\lambda = 1$), else unbalanced forces are updated after every rupture.

It has been shown that $L-U$ and $F-R$ methods yield different results [3]. It is difficult to judge which method is better, especially for the proportional loading path. Both of the methods are rough approximations of a complex dynamic process. Therefore, the consideration of time scales allows some comparison between the methods.

The contribution shows that the $F-R$ method is suitable for processes where the redistribution is much faster than the reaction speed of the external load, whereas the $L-U$ method is good choice for systems with long redistribution times compared to the reaction time of the external load. Moreover, a *general* method that connects the $L-U$ and $F-R$ algorithm is developed. This method is essentially nothing else but the $F-R$ method extended to allow the modification of the external load during redistribution. Let us first define two reference stress variables, $\Delta\sigma^{(L)}$ and $\Delta\sigma^{(S)}$, where the former (with the superscript (L)) is induced by the external load increment and the latter (with superscript (S)) by unbalanced forces. The $F-R$ method is simply enhanced by combining the unbalanced force effect $\Delta\sigma^{(S)}$ with stress caused by modification of the external load $\omega\Delta\sigma^{(L)}$ during redistribution

$$\Delta\sigma = \Delta\sigma^{(S)} + \omega\Delta\sigma^{(L)}. \quad (3)$$

The factor ω determines the ratio between these two effects. High ω in absolute value means that the redistribution is relatively slow compared to the load changes ($L-U$ method) while ω close to zero means the redistribution velocity is high compared to the external load changes ($F-R$ method). The reference stress from Eq. (3) is plugged into Eq. (2) and we obtain final condition which is used to find the critical element and multiplier λ in the *general* method

$$f(\sigma_k + \lambda[\Delta\sigma_k^{(S)} + \omega\Delta\sigma_k^{(L)}]) = 1 \quad \wedge \quad \forall h \neq k : f(\sigma_h + \lambda[\Delta\sigma_h^{(S)} + \omega\Delta\sigma_h^{(L)}]) < 1. \quad (4)$$

The *general* algorithm can be used for indirect control of the simulation and also in connection with non-proportional loading paths. Details and examples can be found in [1].

Acknowledgements

This paper was elaborated with the financial support of the (i) European Union's "Operational Programme Research and Development for Innovations", No. CZ.1.05/2.1.00/03.0097, as an activity of the regional Centre AdMaS, and (ii) the Ministry of Education, Youth and Sports of the Czech Republic under Project No. LH12062.

References

- [1] Eliáš, J., Generalization of load-unload and force-release sequentially linear methods, International Journal of Damage Mechanics (2014), doi: 10.1177/1056789514531001. (in press)
- [2] Eliáš, J., Frantík, P., Vořechovský, M., Improved sequentially linear solution procedure, Engineering Fracture Mechanics 77 (12) (2010) 2263–2276.
- [3] Liu, J.X., El Sayed, T., On the load-unload (L-U) and force-release (F-R) algorithms for simulating brittle fracture processes via lattice models, International Journal of Damage Mechanics 1 (7) (2012) 960–988.
- [4] Rots, J.G., Invernizzi, S., Regularized sequentially linear saw-tooth softening model, International Journal for Numerical and Analytical Methods in Geomechanics 28 (7-8) (2004) 821–856.
- [5] van Mier, J.G.M., Concrete fracture: A multiscale approach, CRC Press, 2013.

DGM-ALE method for FSI problems

M. Feistauer^{a,b}, M. Hadrava^{a,b}, J. Horáček^b, A. Kosík^{a,b,c}

^aCharles University in Prague, Faculty of Mathematics and Physics, Sokolovská 83, 186 75 Prague 8, Czech Republic

^bInstitute of Thermomechanics, Czech Academy of Sciences, Dolejškova, 182 00 Prague 8, Czech Republic

^cUniversity of Dortmund, Department of Mathematics, Cauerstr. 11, Dortmund, Germany

One of subjects which plays an important role in science and technology is the mathematical simulation of fluid-structure interaction. It has applications in a number of areas as, for example, aerospace engineering (analysis of wing vibrations), mechanical engineering (analysis of vibrations of blades in turbomachines or vibrations of parts of cars), civil engineering (vibrations of various constructions as bridges, TV towers and cooling towers under the influence of a strong wind), but also medicine (simulation of blood flow in veins and heart or flow of air in vocal folds). Problems of fluid-structure interaction are rather complex, which causes that there is a lack of mathematical theoretical results. Particularly, in the case of compressible flow, not only mathematical theory is missing, but also the situation in numerical analysis is not satisfactory. It is caused by several obstacles, which have to be overcome: the dependence of the domain occupied by the fluid on time, shock waves and contact discontinuities in high-speed flows, acoustic effects and instabilities in low Mach number flows at incompressible limit, boundary layers and wakes for high Reynolds numbers and spurious oscillations in numerical solutions in the vicinity of discontinuities and large gradients (i.e., in internal and boundary layers).

The lecture will be concerned with the simulation of viscous compressible flow in time dependent domains with applications to the interaction of compressible flow and elastic structures. The motion of the boundary of the domain occupied by the fluid is taken into account with the aid of the ALE (Arbitrary Lagrangian-Eulerian) formulation of the compressible Navier-Stokes equations.

This system is discretized by the discontinuous Galerkin method (DGM) using piecewise polynomial discontinuous approximations. The time discretization is based on a semi-implicit linearized backward difference formula (BDF) or the time discontinuous Galerkin method. It is necessary to include a suitable local artificial viscosity in order to avoid spurious oscillations in the vicinity of internal and boundary layers. It appears that the developed method is accurate, efficient and robust with respect to the magnitude of the Mach number and the Reynolds number and allows the solution of complicated practical problems.

The compressible Navier-Stokes equations are coupled with equations describing the behaviour of elastic structures under the action of a moving gas. In [2], [3] and [4], the dynamic linear elasticity initial-boundary value problem is discretized by the conforming finite element method in space and by the Newmark method in time. Here we shall pay attention to the solution of the dynamic elasticity problem by the DGM applied to the time discretization. The discretization in time is carried out by the backward Euler (BE) difference or general backward difference formula (BDF) or DGM in time. We are concerned with linear elasticity model as well as nonlinear St. Venant-Kirchhoff model. Numerical experiments show that as a most

accurate technique the space-time DGM appears and gives equally accurate results in the case of the benchmark as in [5].

Finally, the developed methods for the solution of compressible flow in time-dependent domains and the dynamic elasticity are used for the simulation of the interaction of compressible flow with elastic structures. In the paper [1], the airfoil vibrations induced by compressible high-speed flow with shock waves is analyzed. In this case, the developed compressible solver is combined with ordinary differential equations describing the vertical displacement and rotation of the airfoil. Now our main attention is paid to the simulation of vibrations of human vocal folds induced by the airflow from lungs.

References

- [1] Česenek, J., Feistauer, M., Kosík, A., DGFEM for the analysis of airfoil vibrations induced by compressible flow, *Zeitschrift für Angewandte Mathematik und Mechanik* 93 (6-7) (2013) 387–402.
- [2] Česenek, J., Feistauer, M., Horáček, J., Kučera, V., Prokopová, J., Simulation of compressible viscous flow in time-dependent domains, *Applied Mathematics and Computation* 219 (2013) 7139–7150.
- [3] Feistauer, M., Hasnedlová-Prokopová, J., Horáček, J., Kosík, A., Kučera, V., DGFEM for dynamical systems describing interaction of compressible fluid and structures, *Journal of Computational and Applied Mathematics* 254 (2013) 17–30.
- [4] Hasnedlová, J., Feistauer, M., Horáček, J., Kosík, A., Kučera, V., Numerical simulation of fluid-structure interaction of compressible flow and elastic structure, *Computing* 95 (2013) 343-361.
- [5] Turek, S., Hron, J., Proposal for numerical benchmarking of fluid-structure interaction between an elastic object and laminar incompressible flow, In: Bungartz, H. J., Schäfer, M., (Eds.), *Fluid-Structure Interaction: Modelling, Simulation, Optimization*, Springer, Berlin, Netherlands, 2006, pp. 371–385.

Problems and solutions connected with the wet/dry interface in the mathematical model of the shallow water equations

M. Fišer^a, O. Bublík^a, L. Lobovský^a, J. Vimmr^a

^aEuropean Centre of Excellence NTIS – New Technologies for Information Society, Faculty of Applied Sciences, University of West Bohemia in Pilsen, Univerzitní 22, 306 14 Pilsen, Czech Republic

Shallow water equations are suitable for the modelling of the free surface flows when the horizontal scales of a liquid mass are much bigger than the vertical scale and vertical flows are negligible. Mathematical model of Shallow Water Equations (SWE) was described by Berre Saint-Venant in 1872 and one of its forms written in 1D is

$$\underbrace{\frac{\partial}{\partial t} \begin{bmatrix} h \\ hu \end{bmatrix}}_{\mathbf{W}} + \underbrace{\frac{\partial}{\partial x} \begin{bmatrix} hu \\ hu^2 + \frac{1}{2}gh^2 \end{bmatrix}}_{\mathbf{F}(\mathbf{W})} = \underbrace{\begin{bmatrix} 0 \\ -gh \frac{\partial B}{\partial x} \end{bmatrix}}_{\mathbf{S}_B} + \underbrace{\begin{bmatrix} 0 \\ -\tau_f \end{bmatrix}}_{\mathbf{S}_f}, \quad (1)$$

where $\mathbf{W}=[w_1, w_2]^T = [h, hu]^T$ is the vector of conservative variables represented by the water depth $h(x, t)$, and the flow velocity $u(x, t)$, $\mathbf{F}(\mathbf{W})$ is inviscid flux, g represents gravitational acceleration, \mathbf{S}_B is the bed slope source term, the function $B(x)$ describes irregularities of the bed, \mathbf{S}_f is the friction source term caused by the bed roughness and $\tau_f = g \frac{n^2}{\sqrt{h}} u|u|$ is the shear stress written in Manning's formulation [3], where n is Mannings bed roughness factor. This model is, in this study, discretised by the finite volume method.

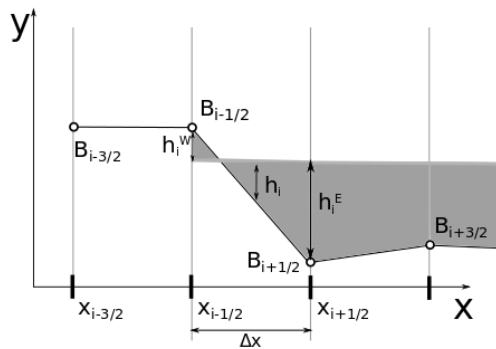


Fig. 1. Negative water depth h_i^W

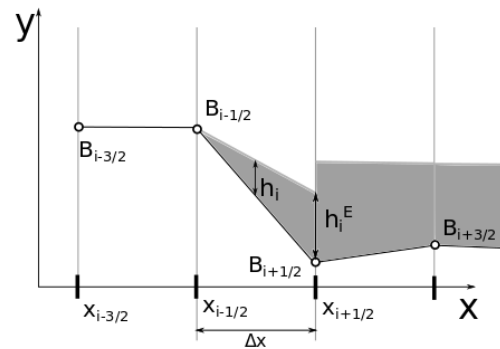


Fig. 2. Corrected water level with $h_i^W = 0$

However this method can lead to the negative water depth h_i^W at the finite volume edge as shown in Fig. 1. To deal with this problem Kurganov and Petrova [1] suggest replacing the constant water depth by the linear function at the wet/dry interface. This function is defined as follows

$$\text{if } h_i^W < 0 \quad \Rightarrow \quad \begin{cases} h_i^W = 0, \\ h_i^E = 2h_i + \frac{B_{i+\frac{1}{2}} - B_{i-\frac{1}{2}}}{2}. \end{cases} \quad (2)$$

New corrected water level is shown in Fig. 2. But the correction causes non-physical discontinuity at the point $x_{i+\frac{1}{2}}$ and scheme does not satisfy the 'C-property' condition. This condition is satisfied when for the initial conditions $u = 0$ and $h + B = \text{constant}$, the water remains still, i.e., when the bed slope source term approximation is equal to the numerical flux.

In [2] can be found the solution of this problem for the bed function approximated in the middle of the finite volume. For the case when the bed function is approximated at the edges of the finite volume, in this work is proposed a novel modification of the bed slope source term.

The flux across edge $x_{i-\frac{1}{2}}$ is considered to be zero. To satisfy the 'C-property' the numerical flux $\Phi_{i+\frac{1}{2}}$ across the edge $x_{i+\frac{1}{2}}$ must be equal to the bed slope source term approximated as $\mathbf{S}_{B_i} = [0, -gh\Delta B_i/\Delta x_i]^T$, where Δx_i is the cell width and ΔB_i is in [1] computed as $\Delta B_i = B_{i+\frac{1}{2}} - B_{i-\frac{1}{2}}$. In this work the component ΔB_i is chosen to be modified and the following equation is solved considering $h_i = (h_i^W + h_i^E)/2$

$$\Phi_{i+\frac{1}{2}} = \mathbf{S}_{B_i} \Rightarrow \begin{bmatrix} 0 \\ -gh_i \frac{\Delta B_i}{\Delta x_i} \end{bmatrix} = \begin{bmatrix} 0 \\ \frac{1}{2\Delta x} g(h_i^E)^2 \end{bmatrix} \Rightarrow \Delta B_i = -\frac{(h_i^E)^2}{h_i^W + h_i^E}. \quad (3)$$

The conditions for ΔB can be summarised as

$$\Delta B_i = \begin{cases} -\frac{(h_i^E)^2}{(h_i^W + h_i^E)} & \text{when } h_i^W < B_{i-\frac{1}{2}}, \\ \frac{(h_i^W)^2}{(h_i^W + h_i^E)} & \text{when } h_i^E < B_{i+\frac{1}{2}}, \\ B_{i+\frac{1}{2}} - B_{i-\frac{1}{2}} & \text{other cases.} \end{cases} \quad (4)$$

This proposed bed slope source term approximation satisfies the 'C-property' condition.

Another problem rises when a small water depth emerges in the computational area. The bed friction term becomes non-physically high because of the h in the denominator and friction term does not stop the flow, as expected, but turns the flow to the opposite direction. The solution of this problem is discussed in [3]. The second problem connected with the h in the denominator is the computation of the flow velocity computed as $u = \frac{w_1}{w_2} = \frac{hu}{h}$. The velocity can also become non-physically high. In [1] is suggested to compute the flow velocity as $u = \frac{\sqrt{2h(hu)}}{\sqrt{h^4 + \max(h^4, \epsilon_v)}}$, where ϵ_v is a small constant. This modification solves the problem with the high velocity but at the other hand causes non-physical behaviour at the front-face of the surge. One of the solution can be setting of zero velocity at the wet/dry interface as discussed in [4].

Acknowledgement

This study was supported by the project at the University of West Bohemia SGS-2013-036.

References

- [1] Kurganov, A., Petrova, G., A second-order well-balanced positivity preserving central-upwind scheme for the Saint-Venant system, *Communications in Mathematical Sciences* 5 (1) (2007) 133–160.
- [2] Fišer, M., Bublík, O., Lobovský, L., Vimmr, J., Modification of the central- upwind scheme providing C-property implemented on shallow water equations, *Proceedings of the 29th conference Computational Mechanics 2013*, Špičák, University of West Bohemia, 2013.
- [3] Liang, Q., Marche, F., Numerical resolution of well-balanced shallow water equations with complex source terms, *Advances in Water Resources* 32 (6) (2009) 873–884.
- [4] George, D.L., Numerical approximation of the nonlinear shallow water equations with topography and dry beds: A Godunov-type scheme, Master thesis, University of Washington, Washington, 2004.

Damage analysis of hybrid composite cell structure

J. Had^a, M. Růžička^a

^a Department of Mechanics, Biomechanics and Mechatronics, Faculty of Mechanical Engineering, Czech Technical University in Prague, Technická 4, 166 07 Praha 6, Czech Republic

A novel type of hybrid cell composite structure has been developed, experimentally investigated and used for many practical applications. The cell system can fill relatively thick parts of cross sections of beams with lower risk of shear stress damage and cracks between uniaxial oriented fibres. Typical macroscopic sub-cells in the cross section structure are formed by the stamping process of partially cured and axially-oriented high modulus carbon fibre bundles (“cores”, about 4-6 mm in the diameter), which are wrapped around by a thin layer of high strength fibres (“winding”, oriented in ± 45 or 89 degrees). This new material structure has its own specific stiffness properties and specific damage behavior and failure modes respectively, see Fig. 1.

Presented work is focused on analysis of static damage of composite cell structure, on its real progression and computational simulation.

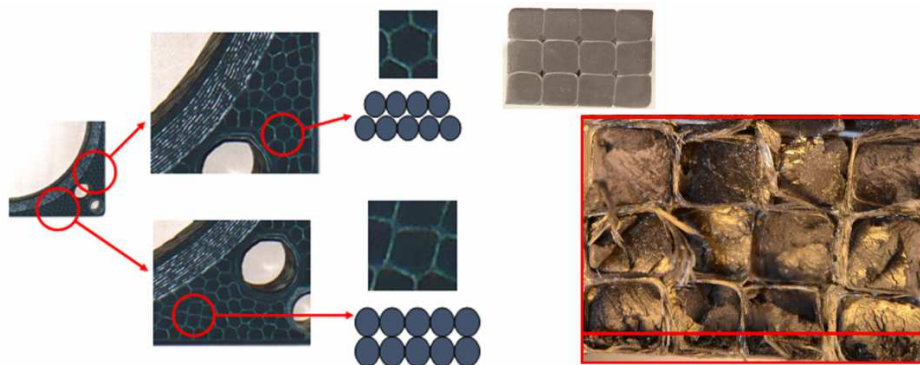


Fig. 1. Example of detail of spindle beam made from 3D cell structure and fracture area of bending sample

The main application of this structure is for thick-walled or nearly solid beams with maximum bending strength. Therefore experimental observations were focused on bending configuration and its relative loading states. Beam specimens were tested in four-point bending configuration. Loading state was measured with force and deflection sensors and with installed strain gauges. Progression of damage was measured with acoustic emission. Moreover, fractography analysis was performed on ruptured specimens.

Measurement of failure behaviour of building constituents were performed as well. Compressive tests in longitudinal and transversal direction were done on unidirectional composites made from ultra-high modulus fibre and from high-strength fibre. Measurement of shear failure behaviour was tested in standardized Iosipescu fixture.

It was stated important contribution of filling pure matrix area and interface layer to damage progression. Behaviour of material of matrix in tensile and compressive loading was measured. Two different tests were chosen to measure failure behaviour of interface layer, normal and shear failure.

Complex modelling of damage progression even in a few cells would demands of tremendous computational performance. In such limitation homogenization method was proposed to simulate of damage progression. Similarly as prediction of static stiffness (see [1]), hierarchy (meso-mechanical) approach is used. Modified Non-uniform Transformation Field Analysis (NTFA, see [1]) was proposed to simulate it. This method was developed originally for the composites with plastic matrix. The aim of the NTFA method is to account for the non-uniformity of the plastic strain field. The field of an-elastic strains is decomposed on a set of fields, called plastic modes.

Global damage progression of cell structure acts as quasi ductile material, despite of mostly brittle micro-behaviour of building parts themselves.

Presented solution of damage is based on formulation of damage modes instead of plastic modes. Specific type of damage of building parts (core, windings, matrix part and interface layers) is taken into account in this approach. Their damage behaviour in each damage mode was implemented. Generally, material model of damage modes consists of combination of plastic behaviour with subsequent degradation mechanism. Modified NTFA method was incorporated into FEM code.

Proposed modified method was verified in four-point bending test. The experimental specimens have a form beams with the rectangular cross-section 30x20 mm. Two different loading configurations were tested, bending of “long” and “short” beam. Length of the beam was 600mm with the force span of 200mm in the case of “long” beam; and 300mm and 160mm in the case of “short” beam respectively. Comparison simulated response of 4PB bending with the experimental data can be seen in Fig. 2.

Research of newly formed material structure was done. Capability of ductile type of failure of the cell structure was demonstrate despite to quasi brittle behavior of constituent. Damage progression was simulated using modified hierarchy homogenization method. Proposed modified NTFA method has been used different formulation of damage modes and specific material behavior of constituent.

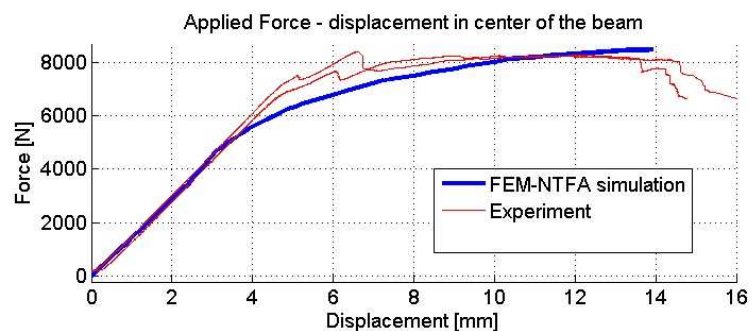


Fig. 2. Comparison of experimental data with simulated response for four point bending

Acknowledgements

The authors would like to thank the Ministry of Industry and Trade of the Czech Republic for supporting this research in the framework of project no. TA02010543. Support from the CompoTech Plus Company in manufacturing the composite specimens is also gratefully acknowledged.

References

- [1] Had, J., Růžička, M., Parametric study of a 3D composite structure, *Bulletin of Applied Mechanics* 8 (31) (2012) 1-5.
- [2] Michel, J.C., Suquet, P., Computational analysis of nonlinear composite structures using the nonuniform transformation field analysis, *Computer methods in applied mechanics and engineering* 193 (48) (2004) 5477-5502.

Investigation of flow over non-vibrating and vibrating airfoil

J. Hamza^{a,b}, J. Klečková^{a,c}

^a Research and Testing Institute Plzeň s.r.o., Tylova 1581/46, 301 00 Plzeň, Czech Republic

^b Faculty of Mechanical Engineering, University of West Bohemia, Univerzitní 22, 306 14 Plzeň, Czech Republic

^c Faculty of Applied Sciences, University of West Bohemia, Univerzitní 22, 306 14 Plzeň, Czech Republic

Aeroelasticity is a field of physics which studies movement of structure induced by fluid flow comprising effects of aerodynamic, elastic and inertia forces. Solving fluid - structure interaction is a complex problem consisting of many tasks such as fluid flow over a structure, deformation of loaded structure or remeshing of the computational domain. The main reason for solving these problems is to prevent a structure from unstable behaviour which could lead to irreversible damages. One of these instabilities is a self-excited vibration called flutter which can occur in many industrial applications such as aircraft, turbomachinery etc.

In our paper, the viscous fluid flow over the airfoil is investigated as a part of the solution of the project focused on flutter prediction and modeling of fluid-structure interaction. The two-dimensional computational model of NACA 0012 which was used for this study is a symmetrical profile with no camber and with a thickness of 12% of its chord length. In our case, the chord is 100 mm long so the airfoil maximum thickness is 12 mm. The computational domain was meshed by a C-type structured grid containing 330 000 cells using GridPro software. The low velocity fluid flow over a non-vibrating and vibrating airfoil was modelled using ANSYS Fluent software. Three turbulence models were consecutively used to solve the problem: 1-equation Spalart Allmaras model and 2-equation turbulent models SST k-omega and k-epsilon with enhanced wall treatment. Numerical simulations were first provided for a non-vibrating profile with different angles of attack.

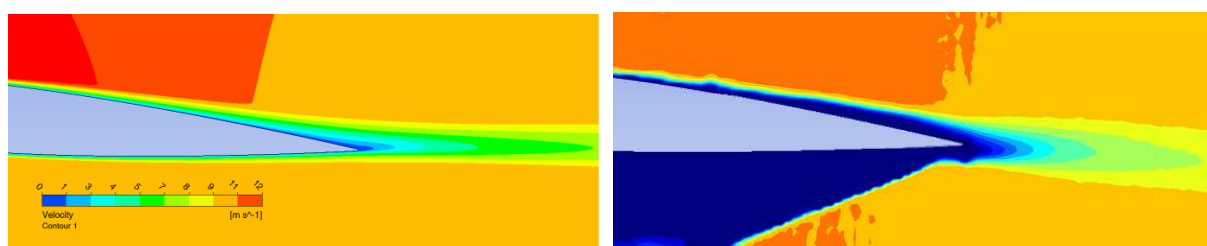


Fig. 1. Contours of velocity obtained by Fluent, using SST k-omega turbulence model (left) and experimental data gained by PIV technique (right), both for a 5° angle of attack

The results achieved by a numerical simulation accomplished by ANSYS Fluent software are compared with experimental data gained by the time-resolved PIV technique which is described in [2]-[4]. Fig. 1 shows velocity contours as a result of numerical simulation compared with experimental measurement, both for a five-degree angle of attack. The dark-blue field below the airfoil on the right figure is a shadow with no measured data.

In Fig. 2, the comparison of the velocity distribution along the vertical line placed in 40% (left) and 103% (right) of the airfoil chord is shown. Data for the left graph of the Fig. 2 were obtained for the case with a zero-degree angle of attack. The results of air flow simulation

achieved by a solver based on the discontinuous Galerkin finite element method with Wilcox k-omega turbulence model, described in [1], are added to this comparison. The second graph compares the velocity distribution along the vertical line placed 3 mm behind the profile trailing edge for the case with a five-degree angle of attack.

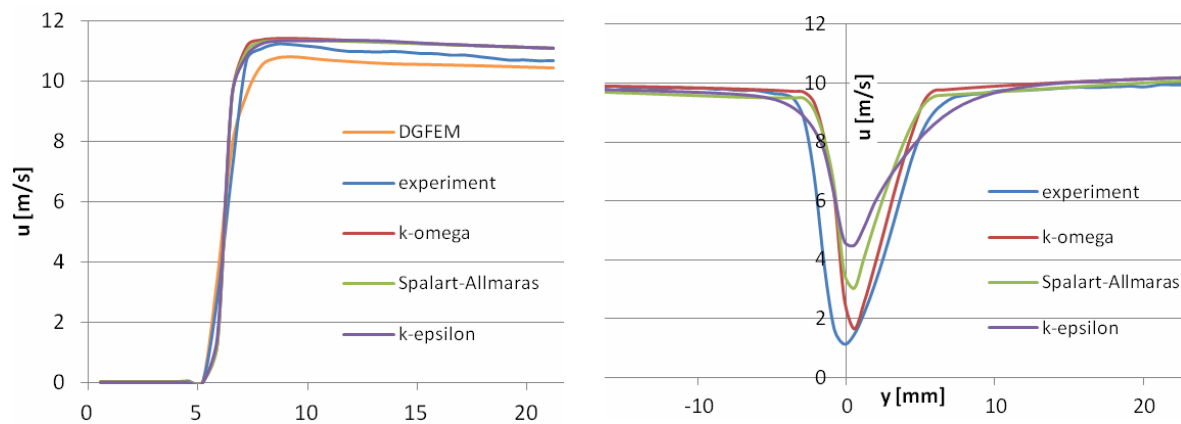


Fig. 2. Comparison of the u-velocity distribution along the vertical line placed in 40% (left) and 103% (right) of the airfoil chord for 0°(left) and 5°(right) angle of attack

As the next part of the research, the fluid flow over a vibrating airfoil was modelled as a rigid structure movement with prescribed displacement and rotation defined by a time-dependent function.

A comparison of the results of the air flow simulation over NACA profile obtained by ANSYS Fluent with data gained by experimental technique shows the best agreement for the k-omega turbulence model. The most significant discrepancy between the experimental and the computational results were apparent at the wake area behind the profile.

Acknowledgements

The work has been supported by the research project of Czech Ministry of Education, Youth and Sports No. MSM 4771868401.

References

- [1] Bublík, O., Vimmr, J., Jonášová, A., A parallel local time stepping discontinuous Galerkin method for the solution of flow problems, Proceedings of the 29th conference with international participation Computational Mechanics 2013, Špičák, Czech Republic, 2013, pp. 1-2.
- [2] Chládek, Š., Zolotarev, I., Uruba, V., Numerical simulation and experiments with the profile NACA 0012, Proceedings 18th international conference Engineering Mechanics 2012, Svratka, Czech Republic, 2012, pp. 132-133.
- [3] Uruba, V., Dynamics of flow around vibrating wing NACA 0012, Proceedings Interaction and Feedbacks 2012, Praha, Czech Republic, 2012, pp. 117-124.
- [4] Uruba, V., Flow around Vibrating Airfoil, ERCOFTAC SYMPOSIUM on Unsteady Separation in Fluid-Structure Interaction, Mykonos, Greece, 2013, pp. 247-258.

Musculoskeletal computer model used for gait analysis of patients with total endoprosthesis

L. Havelková^a, Z. Svoboda^b, L. Hynčík^a

^a *New Technologies – Research Centre, University of West Bohemia, Univerzitní 8, 306 14 Plzeň, Czech Republic*

^b *Faculty of Physical Culture, Palacký University Olomouc, Tř. Míru 115, 771 11 Olomouc, Czech Republic*

The number of patients with total hip endoprosthesis is still increasing. This problem often causes movement restriction and subsequently complication with integration into society. Thus some suitable modern treatments and rehabilitations are essential for their efficient help. The aim of work is to reconstruct the real recorded motions of orthopaedic patients and to perform mechanical analysis of human body. Obtained results provide to the doctors a comprehensive description of the mechanical behavior of lower extremities of orthopedic patients.

Five patients performed a 3D motion capture gait analysis of the lower extremity using Vicon system. Two time points were considered – pre-operative (t_0) and post-operative (t). Sixteen retro-reflective markers were used to record performing gait. The patients walked at self-selected speed. The ground reaction forces were recorded simultaneously using two force plates. Before the recording, the patients were asked to walk on the walkway three times in order to acquaint themselves with measurement and laboratory.

Obtained motion capture data were used to drive the computer musculoskeletal human body model available within the open repository of AnyBody Modeling System (AMS) [2]. The original model was adapted to the measurement and thus only lower extremity was separated and used. This three dimensional model is in general used to estimate the muscle and joint reaction forces, muscle activation, overload as well as fatigue. Model consists of all major bones, joints and muscles. Bones are modeled by rigid bodies defined by their mass, position in 3D space, rotational matrix and inertia. To get the more realistic visualization the segments are represented by real bone contours obtained from magnetic resonance imaging method. Bones are connected by mechanical joints corresponding to the real anatomy and physiology. The muscles are attached to the segments and split into several lines of action modeled by string elements. Trajectories of muscle lines are computed by via points or by obstacle wrapping method explained in literature [5]. AMS is based on the inverse dynamic analysis and an optimization algorithm for muscle recruitment. Whole model is described in [4] in more details. The anthropometrical parameters of presented subjects are necessary for motion reconstruction. The body proportions were measured respecting the anthropometrical standards [1].

Presented process is shown in schema, see Fig. 1. The hip reaction forces as well as muscle activity was calculated for both time points (t_0 , t). The results for time t_0 , t_1 and the data of healthy subjects were compared.

The model was validated before the use. Three healthy volunteer male subjects were invited to perform motion capture gait analysis. The same measurement chain as well as the

data processing with the same workflow as for the patient study was performed. The hip reaction forces were calculated using AMS and compared with Bergmann's dataset [3].

The purpose of this study was to compare the hip reaction forces and muscles forces of the patients before the total endoprosthesis, after this and the healthy subjects. Obtained results confirm the significant improvements of patients after the operation even few days after surgical intervention. The walking speeds in time t_0 and t were similar. The most serious problem in time t_0 is the asymmetrical loading of the whole human body. This problem was eliminated in time t . Moreover the direction of reaction forces generated in the hip joints was significantly changed to ensure the joint stability.

The obvious lack of this study is the use of only lower limbs instead of the whole body. Nevertheless the movement of the upper body (such as torso, head and upper extremities) significantly affects the lower body behavior. To improve the results the upper body should be also considered. Despite that, the model provides sufficient results and thus it could already contribute to faster diagnosis, optimize rehabilitations, help to prevent some diseases, etc.

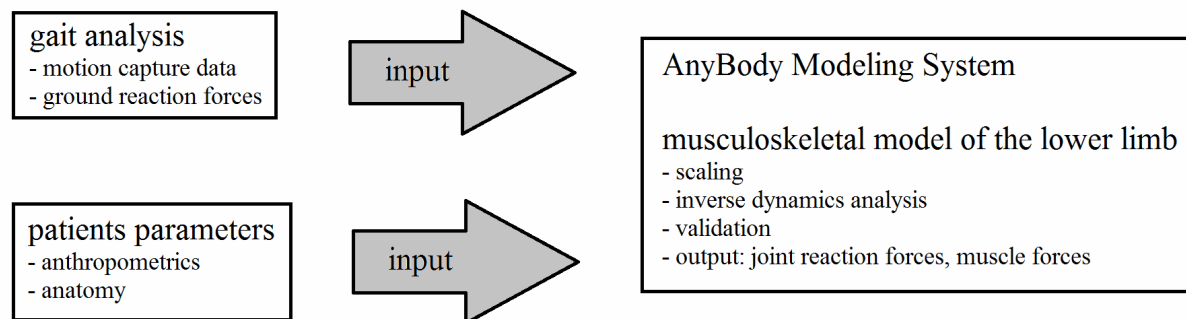


Fig. 1. The workflow – combination of experimental data with numerical simulation

Acknowledgements

This study was co-financed by the grant SGS-2013-26.

References

- [1] Anthropometry and Biomechanics, National Aeronautics and Space Administration, retrieved from: <https://msis.jsc.nasa.gov/sections/section03/htm>, 2008.
- [2] AnyBody Modeling System retrieved from: <http://www.anybodytech.com>.
- [3] Bergmann, G., Deuretzbacher, G., Heller, M., Graichen, F., Rohlmann, A., Strauss, J., & Duda, G.N., Hip contact forces and gait patterns from routine activities, *Journal of Biomechanics* 34 (2001) 859-871.
- [4] Damsgaard, M., Rasmussen, J., Christensen, S.T., Surma, E., & de Zee, M., Analysis of musculoskeletal systems in the AnyBody Modeling System, *Simulation Modelling Practice and Theory* 14 (2006) 1100-1111.
- [5] Garner, B.A., Pandy, M.G., The Obstacle-Set Methods for representing muscle paths in musculoskeletal models, *Computer Methods in Biomechanics and Biomedical Engineering* 3 (2000) 1-30.

Compressible viscous flow in minichannel – Experiment and numerical studies

J. Hála^a, M. Luxa^a, O. Bublík^b, H. Prausová^b, J. Vimmr^b

^a*Institute of Thermomechanics AS CR, v. v. i. Dolejškova 1402/5, 182 00 Praha 8, Czech Republic*

^b*New Technologies for the Information Society, Faculty of Applied Sciences, University of West Bohemia, Pilsen, Czech Republic*

The flow in channels with characteristic dimension of the order of millimetres is of high importance for determination of losses of the devices such as small turbines, screw-type compressors and for investigation of the tip leakage flow. Since most of the contemporary studies deal with the micro or nano flows, the purpose of this work is to provide a reliable experimental data and to explore the possibilities of the numerical simulations of the minichannel flow.

The experiments were carried out in the Aerodynamics Laboratory of the Institute of Thermomechanics AS CR, v.v.i. in Nový Knín. The laboratory is equipped with the wind tunnel of the indraft type and intermittent operation. For the purposes of minichannel flow examination, special measurement facility was designed and manufactured. The air enters the test section directly from the laboratory and flows through the minichannel formed by two parallel steel plates with polished surface (upper and lower walls) and by the side walls with glass windows. Then the air continues to the settling chamber, where the back pressure p_B is maintained.

Application of classical pressure probes as well as thermoanemometric probes is problematic since the dimension of the probes might be comparable to the height of the minichannel. Therefore, the pressure measurements were performed using only static pressure taps at the centreline of the top wall of the minichannel. The pressure in the settling chamber and the barometric pressure was also measured.

Another data were obtained using optical methods employing Mach-Zehnder type interferometer in infinite fringe set-up. This technique allows to capture the interferograms - images depicting the interference fringes that represents the lines with constant index of refraction of the medium. According to the Lorentz-Lorentz equation it is possible to relate the index of refraction to density of the medium and thus obtain the density field inside a minichannel [1].

Subsequently the compressible viscous fluid flow in the minichannel was modeled on a simplified 2D geometry, using both commercial software Fluent and an in-house code implemented in environment Matlab and programming language Java. Favre-averaged system of compressible Navier-Stokes equations is considered and in case of Fluent it is completed by the Menter's SST $k-\omega$ model and four equation SST Transition model. Using the in-house code, laminar, turbulent and transitional flow regime was examined. The discontinuous Galerkin finite element method is applied for spatial discretization of governing equations.

The experiments were performed for the channel of the height 2 mm, length and width 100 mm and various pressure ratios π (ratio of the back pressure to stagnation pressure at the inlet), however the pressure ratios π were chosen as small to obtain the choked flow conditions at an exit cross-sectional plane.

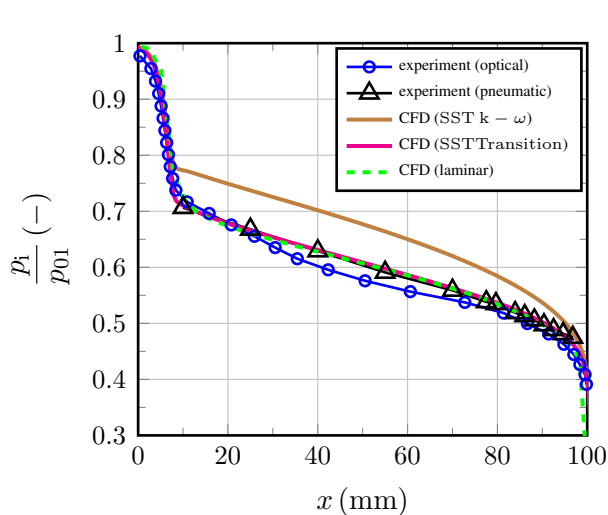


Fig. 1. Distribution of the pressure ratio $\frac{p_i}{p_{01}}$ obtained from optical and pneumatic methods compared to results of the numerical simulations

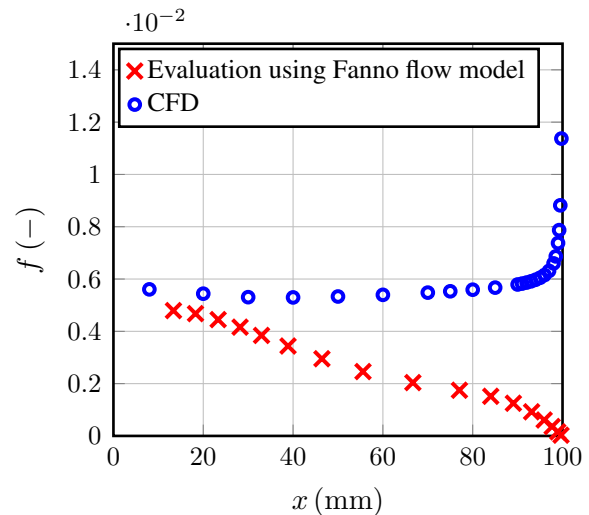


Fig. 2. Distribution of the friction factor f along the wall of the channel for $\pi = 0.188$

The distribution of the ratio of the static pressure to inlet stagnation pressure can be seen in the Fig. 1. It can be observed that results correspond well, however slight difference can be explained by the fact that for the evaluation of the pressure from the interferograms the assumption of the isentropic flow had to be made.

From the comparison of the experimental data to numerical simulation (Fig. 1), it is possible to observe that the laminar simulation gives satisfying results in case of interest in the pressure distribution along the channel axis. To properly simulate also the free outflow behind the minichannel the turbulence or transition model has to be used. Results obtained from simulation using SST transition model corresponds much better then the other one using SST $k-\omega$ model. It was later explored that the SST $k-\omega$ model caused premature development of the flow and thus different results in pressure distribution.

Another analysis was made in terms of friction factor distribution along the channel length. To evaluate the friction factor (skin friction) from experiments the Fanno flow model [2] and corresponding formula was used providing surprising result of decreasing friction factor with channel length. This result is in contrast to the results obtained from numerical simulation (Fig. 2). Also the interferograms and the fact that the density profile is uniformizing near the exit plane might indicate increased friction near the exit.

Acknowledgements

This work was supported by the Technology Agency of the Czech Republic under the grant No. TA03020277 and by the European Regional Development Fund (ERDF), project "NTIS - New Technologies for the Information Society", European Centre of Excellence, CZ.1.05/1.1.00/02.0090. Institutional support RVO:61388998 and student project SGS-2013-036 are also gratefully acknowledged.

References

- [1] Mokřý, M., Aerodynamic measurements using Mach-Zehnder interferometer, Scientific Report Z-239/67, Institute of Thermomechanics AS CR, v.v.i., Prague, 1967.
- [2] Shapiro, A.H., The dynamics and thermodynamics of compressible fluid flow, Vol. I., Ronald Press Co., New York, 1953.

Robust method for finding of dispersion curves in a thick plate problem

P. Hora^a, D. Pelikán^a

^a*Institute of Thermomechanics, Czech Academy of Sciences, Veleslavínova 11, 301 14 Plzeň, Czech Republic*

Waves propagation in thick plates is well solvable problem [2]. One of part of task solution is to find the waveform dispersion curves. This problem has been chosen for the first trial using interval arithmetic [3], because of its relative simplicity. In calculating the dispersion curves is needed to quantify the only trigonometric functions, hyperbolic functions, and square roots. All of these functions are already included in INTLAB [4] and therefore need not to be newly programmed.

The thick plate is defined as that it has a nonzero thickness d and endless remaining dimensions. To calculate the stress wave propagation in plates it is used the integration along the dispersion curves for thick plates. This dispersion relations is defined as

$$(\xi^2 - 2)^2 \tanh\left(kd\sqrt{1 - \xi^2}\right) - 4 \cdot \sqrt{1 - \xi^2} \sqrt{1 - \kappa\xi^2} \tanh\left(kd\sqrt{1 - \kappa\xi^2}\right) = 0,$$

where κ mean the ratio of the squares of the phase velocities for the plate's material. Due avoid computation in the complex domain, because of implementation in INTLAB, it was necessary to divide the dispersive depending equations according to the value of ξ . For each interval are the equations shown in Table 1. To quantify the equations and finding the waveform dispersion curves is used interval arithmetic.

Tab. 1. Dispersion equation
 $(\xi^2 - 2)^2 \cdot \alpha - 4 \cdot \beta \cdot x_1 x_2 = 0$

	$0 < \xi < 1$	$1 < \xi < \frac{1}{\sqrt{\kappa}}$	$\frac{1}{\sqrt{\kappa}} < \xi$
x_1	$\sqrt{1 - \xi^2}$	$\sqrt{\xi^2 - 1}$	$\sqrt{\xi^2 - 1}$
x_2	$\sqrt{1 - \kappa\xi^2}$	$\sqrt{1 - \kappa\xi^2}$	$\sqrt{\kappa\xi^2 - 1}$
α	$\sinh(kdx_1) \cosh(kdx_2)$	$\sin(kdx_1) \cosh(kdx_2)$	$\sin(kdx_1) \cos(kdx_2)$
β	$\cosh(kdx_1) \sinh(kdx_2)$	$\cos(kdx_1) \sinh(kdx_2)$	$-\cos(kdx_1) \sin(kdx_2)$

Interval arithmetic is an extension of arithmetic over real numbers, where for each real function $f(x_1, \dots, x_n)$, the interval function $F(X_1, \dots, X_n)$ is called an interval extension of the function f if for each intervals I_1, \dots, I_n function $F(I_1, \dots, I_n)$ returns interval I such that $\forall y_1 \in I_1 \dots \forall y_n \in I_n (f(y_1, \dots, y_n) \in I)$. For other applications it is particularly important the interval Newton method, according to which each continuously differentiable function f

each interval I must be $\forall a, x \in I, \exists \epsilon \in I(f(x) = f(a) + (x - a)f'(\epsilon))$. Specifically then, the function f continuously differentiable on the interval I has all the roots in I in interval $N_a = a - (F(a)/F'(I))$, where a is an arbitrary element of I and F, F' is an interval extension function of f, f' .

For quantification of interval arithmetic was used MATLAB's toolbox INTLAB, which are defined not only the basic functions for interval arithmetic, but their automatic differentiation too [1].

When trying to use the Newton method in INTLAB was needed to solve the problem by dividing intervals. INTLAB always returns the result $\langle -\infty, \infty \rangle$ for each I/J , where $0 \in J$. However, for this case, it was necessary defined alternative way of dividing, when the interval is divided into two portions, and finding roots thus diverges into two tasks. The actual calculation is solved in recursive steps. In a single step in the equation $N_a = a - (F(a)/F'(I))$ is substituted middle I per a , yielding a new interval $J = I \cap N_a$. This one is used in the next recursive step. The calculation continues until the result interval width falls under a predetermined accuracy.

Interval arithmetic provides a robust method for finding the roots of the dispersion equation. For relatively low speed, this method is not suitable to complete the calculation, it is however possible to use the first approach with low accuracy, or when using the Gaussian integration method.

Acknowledgement

The work was supported by the institutional support RVO:61388998.

References

- [1] Bücker, H.M., Corliss, G., Hovland, Naumann, U., Norris, B., Automatic differentiation: Applications, theory, and implementations, Lecture Notes in Computational Science and Engineering Vol. 50, Springer, New York, 2005.
- [2] Graff, K.F., Wave motion in elastic solids, Dover Publications, 1975.
- [3] Moore, R.E., Kearfott, R.B., Cloud, M.J., Introduction to interval analysis, Society for Industrial and Applied Mathematics, Philadelphia, 2009.
- [4] Rump, S.M., INTLAB - INTerval LABoratory, Kluwer Academic Publishers, 1999, pp. 77-104.

Approximate eigen-solution of linear viscously damped system with vibration absorber

S. Hračov^a

^a*Institute of Theoretical and Applied Mechanics AS CR, v.v.i., Prosecká 76, 19000, Prague, Czech Republic.*

Existing cantilever structures such as towers, chimneys or poles are often equipped with a damping device which suppresses undesired vibrations caused by wind load. The structure itself despite being constructed from different materials can be approximately considered as a linear classically (proportionally) damped system. It provides easier mathematical modeling and numerical calculation of modal properties and dynamic response. However, the installation of the vibration absorber into the structure could significantly change its dissipative properties and make the complete system non-proportionally damped. The eigen-solution is then more computationally intensive and can be time-consuming. In this paper an efficient approximative method for eigen-value calculation of such a type of systems is presented.

If the damping matrix of the linear viscously damped system representing the structure with absorber can be expressed as:

$$\mathbf{C} = \mathbf{C}_p + \mathbf{d} \cdot \mathbf{d}^T, \quad (1)$$

where matrix \mathbf{C}_p is the proportional part of damping matrix, while the product consisting of vector \mathbf{d} stands for the non-proportional part arising from the presence of the absorber, the eigen-values λ of the complete system are given, see [1], by solving the equation:

$$\frac{1}{\lambda} + \sum_{i=1}^n \frac{\tilde{d}_i^2}{\lambda^2 + \lambda \tilde{C}_{p_{i,i}} + \omega_i^2} = 0, \quad (2)$$

where n is a number of the eigen-modes of the complete system, \tilde{d}_i is given by product of transposed i -th eigen-mode and vector \mathbf{d} . Element $\tilde{C}_{p_{i,i}}$ is i -th diagonal element of modal damping matrix $\tilde{\mathbf{C}}_p$ calculated from matrix \mathbf{C}_p , ω_i is i -th undamped angular eigen-frequency of the structure with absorber. The solution of the j -th eigen-value λ_j can be sought in a form:

$$\lambda_j = \lambda_{0,j} + \Delta\lambda_j. \quad (3)$$

Symbol $\lambda_{0,j}$ stands for the known or easily obtained eigen-solution of the same system with, e.g., different damping properties of the absorber, while $\Delta\lambda_j$ represents its deviation from the exact solution λ_j . Inserting solution (3) into Eq. (2) and performing few mathematical operations lead to:

$$\prod_{i=1}^n (\alpha_{i,j} + \beta_{i,j} \Delta\lambda_j + \Delta\lambda_j^2) + (\lambda_{0,j} + \Delta\lambda_j) \sum_{l=1}^n \tilde{d}_l^2 \prod_{\substack{i=1 \\ i \neq l}}^n (\alpha_{i,j} + \beta_{i,j} \Delta\lambda_j + \Delta\lambda_j^2) = 0, \quad (4)$$

$$\alpha_{i,j} = \lambda_{0,j}^2 + \lambda_{0,j} \tilde{C}_{p_{i,i}} + \omega_i^2, \quad \beta_{i,j} = 2\lambda_{0,j} + \tilde{C}_{p_{i,i}}.$$

After expansion of Eq. (4) the numerically favorable simplification consisting in keeping only the first or the first two powers of $\Delta\lambda_j$ can be made. Then value $\Delta\lambda_j$ is easily calculated and subsequently the eigen-value λ_j can be determined.

In this paper the accuracy of suggested approach was analyzed for the numerical model of the existing tower with absorber modeled as one dof. The exactness of the calculated eigen-solution was investigated parametrically for a set of various damping ratios of the absorber ζ_d and constant proportional damping matrix of the structure (structural damping ratio $\zeta = 0.005$). The eigen-values of the classically damped system were chosen as the reference values λ_0 in Eq. (3). In Eq. (4) only the first eight eigen-modes of undamped structure with absorber were taken into account. The results were subsequently compared with the exact solution and with commonly used approach based on the neglecting of the off-diagonal elements of modal damping matrix, see Fig. 1.

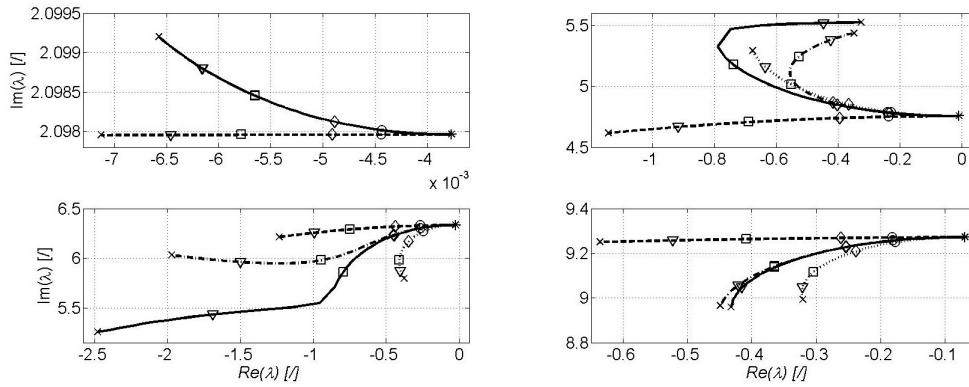


Fig. 1. The first four eigen-values λ_j as a function of damping ratio ζ_d (solid line – exact solution; dashed line – traditional approximate solution; dotted line – proposed solution with only the first power of $\Delta\lambda_j$; dash-dot line – solution with the first two powers of $\Delta\lambda_j$); (* - $\zeta_d = 0$; o - $\zeta_d = 0.1$; ◇ - $\zeta_{d,opt} = 0.17$; □ - $\zeta_d = 0.3$; ▽ - $\zeta_d = 0.4$; × - $\zeta_d = 0.5$)

The proposed method provided very good accuracy and higher precision in comparison with results of traditional approach especially for the first, the fourth and higher eigen-values. Dash-dot lines, i.e., solutions containing the first two powers of $\Delta\lambda_j$ are almost coincident with solid lines, i.e., exact solutions. On the other hand, the solution corresponding to the second and the third eigen-value which are the most influenced by the absorber and connected with its frequency tuning showed certain discrepancy. The sufficient accuracy below 10% was reached as expected only in a limited interval ($\zeta_d \in (0; 0,25)$) close to the proportional state. To gain higher precision author recommends to combine the proposed method with the step method. In this case the eigen-solution is calculated step-by-step with sufficiently small increment (step) $\Delta\zeta_d$ starting from the proportional or known state towards the desired value of ζ_d . After each step obtained eigen-values are used as initially values λ_0 in the next step of the solution.

Acknowledgements

The kind support of the Czech Science Foundation project No. 13-41574P and of the RVO 68378297 institutional support are gratefully acknowledged.

References

- [1] Gürgöze, M., Proportionally damped systems subjected to damping modifications by several viscous dampers, Journal of Sound and Vibration 255(2) (2002) 407-412.

Estimating material properties of PU foam using genetic algorithms

T. Hruš^a, D. Círk^a

^aFaculty of Mechanical Engineering, Technical University of Liberec, Studentská 2, 461 17 Liberec, Czech Republic

Polyurethane foam is an important material for example in car industry. By car seat design it is necessary to know foam material properties. Different material models were tried to describe the mechanical behavior of the foam [2, 3].

A new material model was developed on Department of elasticity and strength CTU Liberec few years ago [1]. The model is shown on Fig. 1. The model consist of three parallel combinations spring-damper with three more components. The friction force (the most left component in the picture) depends on the total force of three the spring-damper components. All components of the model are non-linear, so the total number of material constants of this model is 27.

For finding material properties of the model was genetic algorithm used with success.

Result from the experiment is a set of couples $[t_i, F_i^{exp}]$, which is compared with data $[t_i, F_i^{mod}]$ obtained from the model. The goal is to minimize the difference between the experimental and model data.

Fitness function of the genetic algorithm was set as a total difference between experimental and computational data and it was adapted for the possibility to compare different sets of input data (different magnitude, length, sampling):

$$FITNESS = \frac{\sum_{i=0}^N |F_i^{experiment} - F_i^{model}| \Delta t}{(t_N - t_0) F_{mean}^{experiment}},$$

where

$$F_{mean}^{experiment} = \frac{1}{N+1} \sum_{i=0}^N |F_i^{experiment}|.$$

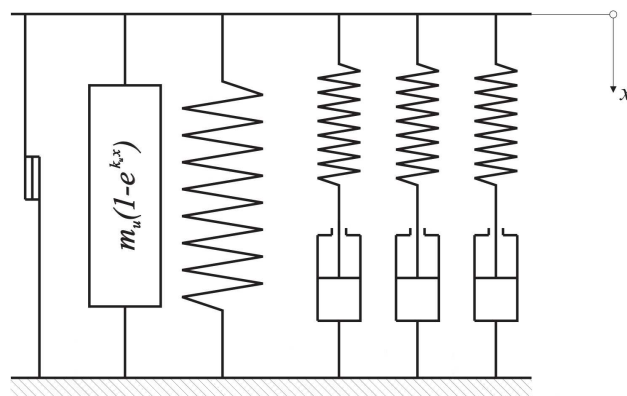


Fig. 1. PU foam material model

Estimating one set of model data takes (on a common PC) time of order 10^{-2} sec, because of necessity of solving three differential equations (each for one spring-damper pair). Genetic algorithm with 10^1 phenotypes and 10^2 generations takes approximately $10^1 - 10^2$ hours of core time. This number of phenotypes and generations is high enough to find an individual with good fitness (below 5%). A typical result for a complex signal is shown on Fig. 2.

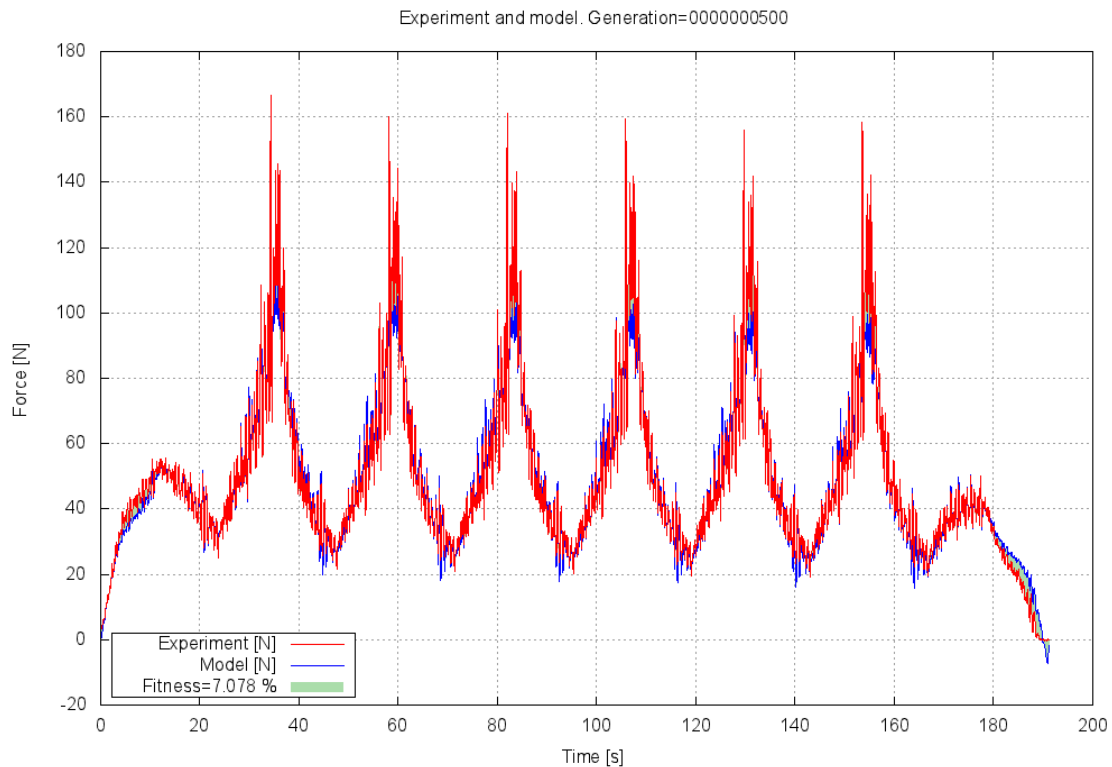


Fig. 2. A set of experimental data (red) and data from the model (blue). The green area (visible on the right side of the graph and in the “peaks”) between the lines corresponds with the fitness

By analysis of the data produced by genetic algorithms a large fraction (more than 5%) of duplications was found. Prevention of evaluation of duplications is a possible way to speed-up the program. Other possibility is a fast non-exact evaluation of the model and exact (and time consuming) evaluation only of promising candidates. Some of material constants is also possible to guess with good accuracy *before* the start of genetic algorithm.

Genetic algorithms are useful for finding material constants of our model of PU foam. The necessary time is long, but they are possibilities to speed up the process.

References

- [1] Cirkl, D., Hruš, T., Simulation model of polyurethane foam for uniaxial dynamical compression, ICOVP 2013, Druskinikai, Lithuania, 2013.
- [2] Ehlers, W., Markert, B., A macroscopic finite strain model for cellular polymers, International Journal of plasticity 19 (2003) 961-976. (www.elsevier.com/locate/ijplas)
- [3] Patten, W.N., Sha, S., Mo, C., A vibration model of open celled polyurethane foam automotive seat cushions, Journal of Sound and Vibrations 217(1) (1998) 145-161.

Seismic response of piping systems with viscous dampers in nuclear power plants

M. Chlud^a, L. Joch^a, M. Vašek^a

^a Institute of Applied Mechanics Brno, Ltd., Resslova 972/3, Veveří, 602 00, Czech Republic

Viscous dampers are widely used to ensure seismic resistance of pipelines and equipment in nuclear power plants. Damping characteristics of these dampers are nonlinearly frequency dependent [3] and thus causing complications in computational modeling of seismic response. Engineers commonly use two ways to deal with this nonlinearity:

The first option is to consider damper by means of “snubber”. This is essentially linear spring element that is active for dynamic load and does not resist static loads. Snubber behavior during seismic event is described by equivalent stiffness (sometimes called pseudostiffness). Equivalent stiffness could be defined by iterative calculations of piping natural frequencies and mode shapes taking into account seismic excitation. However in complicated structures such as the main circulation loop of nuclear power plant the iterative calculation is difficult and could bring significant inaccuracies. From the other hand, the benefit of such modeling is a possibility to apply commonly used linear response spectrum method for a solution.

The second option is to describe damping characteristics using suitable rheological model. The seismic response is then determined by direct integration of the equations of motion. The behavior of dampers is described exactly enough but the calculation and post-processing, especially nodal stresses time-histories, are time consuming.

The goal of this work was to find a methodology for more accurate determination of equivalent stiffness and its subsequent use as input parameter for seismic response calculation via response spectrum method with all benefits of such approach.

The procedure is as follows. First, specialized piping program (AutoPIPE) is used for the development of computational model. Next step is to determine static response of structure and its verification with experimental measurements, if possible. Using script in Python language a computational model is converted from AutoPIPE into general finite element model in ANSYS system. Four-parameter Maxwell rheological model is used to describe behavior of viscous dampers [1]. Seismic load is represented by synthetic accelerograms. Newmark algorithm of direct integration of the equation of motion is used to obtain seismic response (only reactions and displacements in nodes of interest are necessary). The equivalent stiffness is then gained from displacements and reactions as median value of their ratios. Received stiffness are subsequently transferred to AutoPIPE program where the seismic solution is performed using response spectra method. Finally dynamic response is combined with static response and stress assessment according standards is done.

The created methodology was applied in the seismic resistance calculation of the main circulation piping of nuclear power plants [2]. The computational model (Fig. 1 and Fig. 2) consists of a reactor pressure vessel, connecting pipelines, main circulation pump, steam generator, steam pipeline, feed water pipeline and emergency cooling pipeline.

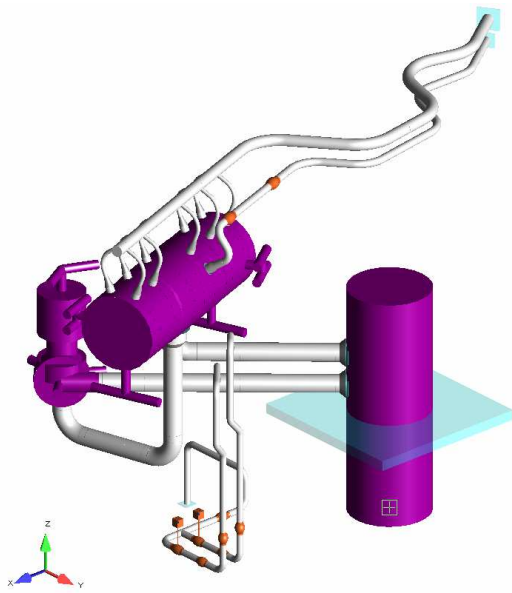


Fig. 1. Computational model in AutoPIPE

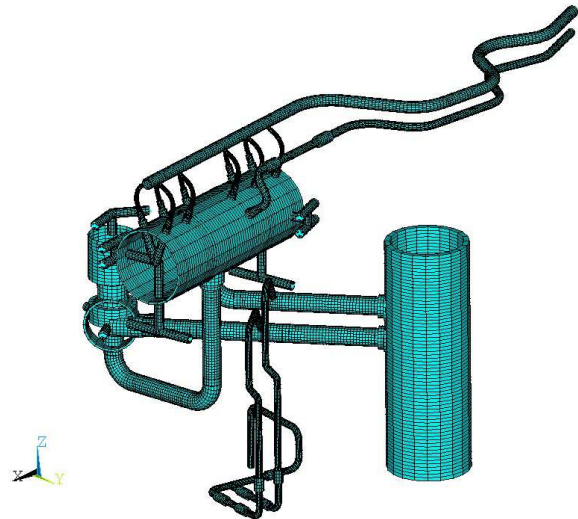


Fig. 2. Computational model in ANSYS

Circulation loop is damped by GERB VD-630/426-15 absorbers (12 dampers mounted on steam generator, 3 on main circulation pump and one on steam pipeline) and GERB VES-100/V40/H80 (2 dampers mounted on pump engine). Dampening capabilities of viscous dampers are illustrated in the following Table 1 via horizontal displacements of the centers of the steam generator and main circulation pumps. Table 1 also compares displacements computed from response spectra method and time-history analysis. You can see that the response spectra method provides slightly conservative results compared to direct integration of equation of motion.

Table 1. Horizontal displacement in points of interest

Point of interest	Without dampers response spectrum method		With dampers response spectrum method		With dampers time-history analysis	
	x [mm]	y [mm]	x [mm]	y [mm]	x [mm]	y [mm]
Steam generator centre	14,8	14,4	3,8	3,9	-3,1	-2,9
					3,2	2,8
Circulation pump centre	15,0	16,5	2,5	2,8	-2,1	-2,3
					1,8	1,8

This paper presented a methodology for determining the seismic response of complex piping systems with viscous dampers. The presented method is sufficiently precise and allows obtaining results in effective time.

References

- [1] Berkovsky, A., Vasilyev, P., Kireev, O., Different approaches for the modelling of high viscous dampers in piping dynamic analysis. Acceptable Limits for Simplifications, SMiRT 20-Division V, Paper 1833, Espoo, Finland, August 9-14, 2009.
- [2] Chlud, M., Strength, dilatation and seismic calculation of pipelines DPS 1.20R and 1.20G inside the hermetic zone with new GERB dampers at 20°C, ÚAM Brno, arch. no. 5031/12, Brno, 2012.
- [3] Kostarev, V., Viscoelastic dampers VD series specifications, NPP Edition, 2009, CKTI-VIBROSEISM Co. Ltd., TU 4192-001-20503039-01.

Crack propagation under nonzero mean combined loading

J. Janoušek^a, M. Balda^b, M. Chocholoušek^a

^a Research Centre Rez, Hlavní 130, 250 68 Husinec-Řež, Czech Republic

^b Research and Testing Institute Plzen, Tylova 1581/46, 301 00 Plzeň, Czech Republic

Proposed scientific research brings new knowledge about crack propagation during tests which were performed and presented in [1]. These tests were unique by combination of normal and shear mean stresses. The mean values in normal and shear components were proposed in the ratio 3:2 in agreement with the coefficient k_c which corresponds with ratio of fatigue limits in tension and torsion. Except for static pre-stresses in both stress components, the conception includes one dynamical normal component with sinusoidal 10 Hz loading. The specimens were tubular with 30 mm diameter, wall thickness 2 mm and a notch in the shape of one-sided transverse hole of diameter 3 mm positioned in the middle of the specimen. The specimens were made of structural low carbon steel ČSN 41 1523.1 after normalization annealing. The experiments were carried out on an electrohydraulic computer-controlled testing machine Inova ZUZ 200-1.

The locations, directions and growth rates of fatigue cracks have been explored on surface of transverse notch area in tested tubular specimens. The growth rate serves for determination of constants C and n in the Paris law for linear propagation and for possibility of residual lifetime assessment. A detection device enables optical tracking of crack end position changes in two orthogonal coordinate planes, and visual reading of position values from scales. Measured displacements should be recomputed on the specimen rounded surface. It implies that a final transverse coordinate is obtained as a product of tube radius and an angle, which comes as a difference from the former coordinate. The origin of coordinates coincides with the specimen longitudinal axis. The cracks usually grow in four quadrants under combined tension-compression and torsion loading. The dynamic components are always decisive for direction of fatigue crack propagation in the part subjected to a combination of static and dynamic components of stress [2]. The static components have an influence on growth rate, because in case of positive pre-stress crack front opens, and it affects the overall life [3]. Therefore in this conception cracks were always created in pairs.

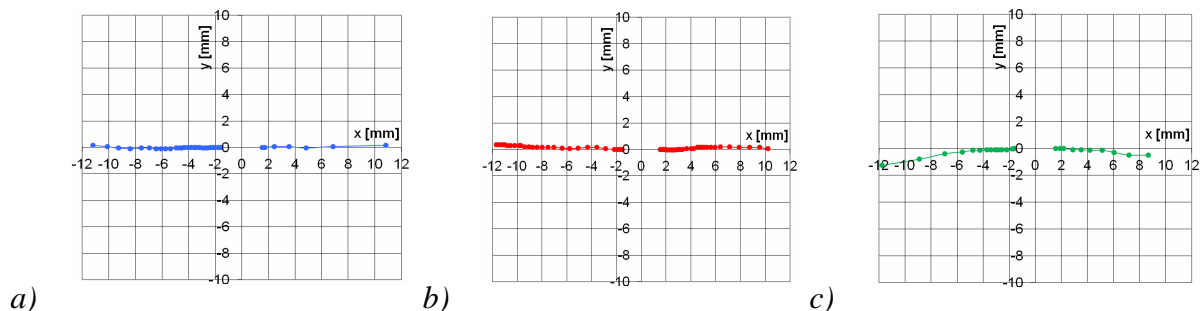


Fig. 1. Crack propagation in specimens which were loaded with combined pre-stresses $\sigma_m = 90$ MPa and $\tau_m = 60$ MPa and normal stress amplitudes a) 100 MPa, b) 110 MPa and c) 130 MPa

The experiments with stress mean values $\sigma_m = 90$ MPa and $\tau_m = 60$ MPa provided the level of fatigue limit $\sigma_{cm} = 90$ MPa from 5 specimens. The crack propagation monitoring was performed under normal stress amplitudes 100, 110 and 130 MPa. The results are indicated in Fig. 1. The differences were only in the growth rate corresponding to the loading intensity. The dependence of crack length on cycle number is displayed in fig. 2 where the black curves represent both cracks and red one their average.

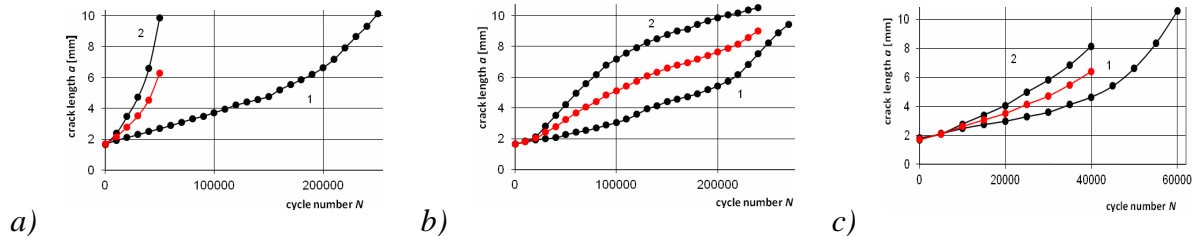


Fig. 2. Curve of fatigue crack development in specimens which were loaded with combined pre-stresses $\sigma_m = 90$ MPa and $\tau_m = 60$ MPa and normal stress amplitudes a) 100 MPa, b) 110 MPa and c) 130 MPa

Fig. 3 shows the dependences of the above crack growth rates on the range of stress intensity factor ΔK , and also the regression curves passing through all the plotted points. These functions correspond to the known Paris law. The average values were used for composition because every crack has an influence on damage of material.

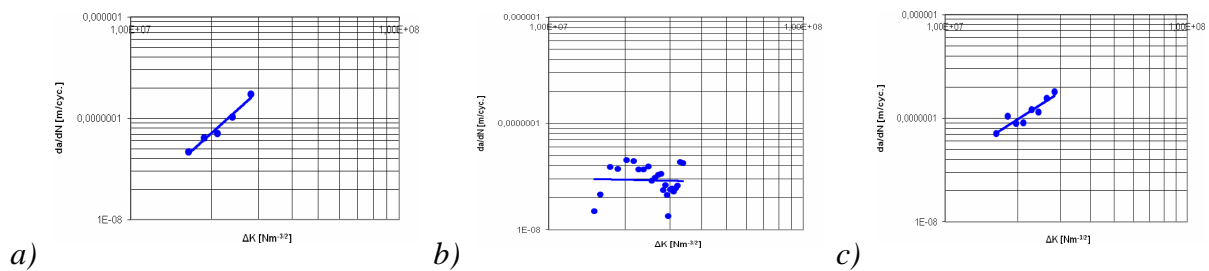


Fig. 3. Curve of fatigue crack growth in specimens which were loaded with combined pre-stresses $\sigma_m = 90$ MPa and $\tau_m = 60$ MPa and normal stress amplitudes a) 100 MPa, b) 110 MPa and c) 130 MPa

All three crack growth observations confirm that the static component has an influence on crack growth rate and as far as a direction of crack propagation is concerned, only character of dynamical components plays role.

Acknowledgements

This research work has been prepared with institutional support RVO: 61388998 of the Institute of Thermomechanics through the internal pilot project No. 904146 in 2012 and supported by the SUSEN Project CZ.1.05/2.1.00/03.0108 realized in the framework of the European Regional Development Fund (ERDF).

References

- [1] Janoušek, J., Balda, M., Chocholoušek, M., An influence of combined mean stresses on lifetime under high-cycle fatigue, Conference on experimental stress analysis, Mariánské lázně, 2014.
- [2] Balda, M., Svoboda, J., An influence of static load on fatigue life of parts under combined stress, Applied and Computational Mechanics 2 (1) (2008) 5-12.
- [3] Janoušek, J., Balda, M., Svoboda, J., The mean stress influence on lifetime under high-cycle fatigue combined loading, Applied and Computational Mechanics 7 (1) (2013) 31-38.

Virtual simulation of a traffic barrier

M. Kalinský, J. Trubač

TÜV SÜD Czech, Integral Testing and Support, Novodvorská 994/138, 142 21 Prague 4, Czech Republic

Nowadays road restraint systems are a common part of the infrastructure. It is an active safety component that is designed to prevent vehicle from leaving and to mitigate consequences of a crash on the crew. The number of people killed and injured on the roads in the Czech Republic is still high, despite the effort of experts and manufacturers of active and passive safety components.

A design of a traffic barrier is based on EN 1317 European regulation in the Czech Republic. This regulation exactly defines characteristics and requirements (e.g. theoretical values of impact forces) which have to be met. However, the real values of forces might be significantly higher (up to five times), which is mentioned in documents for overloaded construction design. Within the research of traffic barriers, some workplaces (eg. Aachen University, TNO Delft, Klokner Institute) have been engaging in a more accurate conception of the crash process, which is more meaningful and reliable than above mentioned theoretical impact force.

TÜV SÜD Automotive GmbH, mostly Passive Safety department deals with traffic barriers crash testing. This department has a testing track for a comprehensive range of crash tests and it represents the important institution for traffic barrier testing in Europe.

TÜV SÜD Czech by means of Computer aided services have been dealing with computer modelled crashes of vehicles to a traffic barrier and put these methods in place. For the simulation purposes, commercially available solver for nonlinear problems from ESI Group - Visual Environment is used. Numerical simulations of impacts as required by EN 1317 are performed. There are models of light passenger cars, buses and lorries in the company database. Computer aided services are currently one of the participants of Technology Agency of the Czech Republic (TA CR) project - *Využití spolehlivostních metod při výzkumu a ověřování inovativních silničních svodidel (Use of reliability methods in research and verification of innovative road barriers)*.

This project deals with the development and validation of the new innovative traffic barrier, which meets the requirements of the applicable regulations. The new traffic barrier has to not only be able to retain a bus on the road, but it also contains structural modifications aimed at safety and protection of motorcyclists during an accident. Structure with modified design better protects against dangerous contact with posts and anchoring elements which represent the greatest danger for motorcyclists.

One of the main objectives in TA CR project solution is a methodology development how to simulate a vehicle crash into the traffic barrier. Replacement of the real test by a numerical simulation has a great importance in the design of traffic barrier, its optimization and validation of so called modified traffic barrier as well. There is only slight difference between the original approved type and the prototype. The extent of these design modifications is exactly defined in EN 1317 regulation. Nowadays it is not possible to completely replace crash tests with simulations. Even so, the creation of this methodology is generally supported

by the traffic-engineering institutions. It is obvious that its use helps to reduce the total cost of development, the possibility of rapid tests repeatability, design modifications and thorough results research.

The basis of the success of the project is to prove the adequate conformity of theoretical calculations with real tests. At this stage, wide experience with crash tests of colleagues from TÜV SÜD Garching - Department of passive safety is applied.

Traffic barrier design

To ensure the correct behaviour of the newly designed road restraint system crash tests are performed, as an example is an impact of a heavy truck (38 tons), which hits the traffic barrier at the speed of 65 km/h, at the angle of 20°. The current level of FEM software allows to simulate highly detailed models and to analyze the relatively wide range of output data. The main disadvantage of simulations is how to achieve a reliable behaviour with the minimal amount of data. Therefore, it is necessary to perform number of real static and dynamic tests, such as tensile test or a hammer drop test of a steel post to describe the material behaviour and to perform its validation.

The impact itself is from the viewpoint of physics a combination of deformation characteristics of the traffic barrier and a vehicle. Due to computational demands, it is possible to simplify some parts, which means replacing components with simplified shape bodies. If this is the first simulation, this approach is possible, but not acceptable for a preparation of a real and predictive model. In this case, a virtual vehicle has to have a same response as a real one. This means that the model should contain not only a validated material model but also and a kinematic model of suspension, steering, etc.

Even though there is a trend in the current technical practice to include numerical simulations to the testing methods and therefore to minimize the number of physical tests, it can't be assumed that a new type of the traffic barrier will be approved only based on the results of computer simulations. Ideally, it is possible to reduce the number of the real tests to the only one – a homologation test.

Actually there is nothing which could perfectly replace physical tests, therefore virtual and physical tests will continue to supplement themselves in the near future.

References

- [1] ČSN EN 1317 – Road restraint systems, 2011.
- [2] Kalinský, M., Virtual testing of the road barriers, TÜV SÜD Journal Czech Republic, 1/2014.
- [3] Kalinský, M., Application of reliability methods in research and verification of innovative road safety barriers, Project Technical Report 2013, TÜV SÜD Czech, Prague, 2012.
- [4] Kubeš, J., Crash analysis of the road safety barrier with the passenger car, Diploma thesis, CTU Prague, Prague, 2013.

Influence of noise reduction on the propeller performance

J. Klesa

Faculty of Applied Sciences, University of West Bohemia, Univerzitni 22, 306 14 Plzeň, Czech Republic

Noise reduction of propellers is considered as a very important issue in aviation. Principal means for the noise reduction are decrease in blade tip Mach number, i.e., lower propeller diameter and RPM, and increase in number of blades. All these measures influence propeller performance and thus also efficiency. The main aim of this paper is to explain and correct some common misunderstandings about this subject.

According to the aeroacoustic theory of Gutin [3] propeller noise can be reduced by increasing of the number of propeller blades and by decreasing of the blade tip Mach number. This influence is investigated at the example of a propeller for the small transport propeller represented by Let L-410UVP with the engines M-601.

The propellers are designed for the maximum cruise speed conditions. The novel method for the aerodynamic design of a propeller [5] is applied. It is based on the blade element method and represents generalization of [2] for any number of propeller blades. Blade element method was verified on the comparison with the experimental data from [4]. Aerodynamic data of the airfoils from the ARA-D family [1] are used for aerodynamic design of the propeller.

Firstly the efficiency for 2, 3, 5, 10 and 20 blades is investigated for the propeller diameter from 1.5 to 3.0 meters. Results are presented in Fig. 1. Propeller RPM are set to 2 080 which is the nominal value for the M-601 engine.

The efficiency for the blade tip Mach number equals to 0.5, 0.7 and 0.9 is computed for the the propeller diameter from 1.5 to 3.0 metres. In this case, it is assumed that propeller RPM for each propeller diameter is set so that required value of blade tip Mach number is reached.

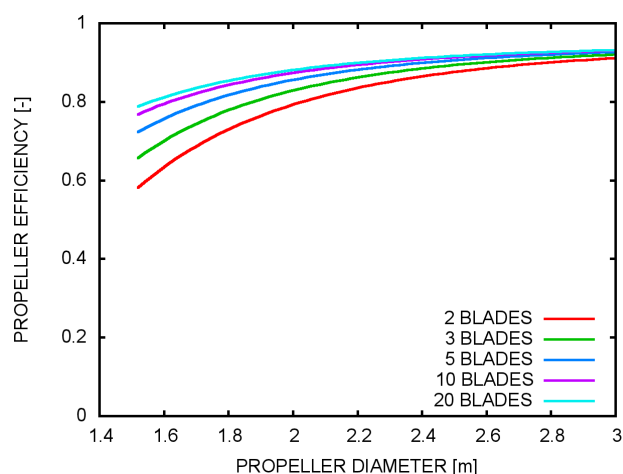


Fig. 1. Dependence of the propeller efficiency on the diameter and number of blades, engine with 2 080 RPM

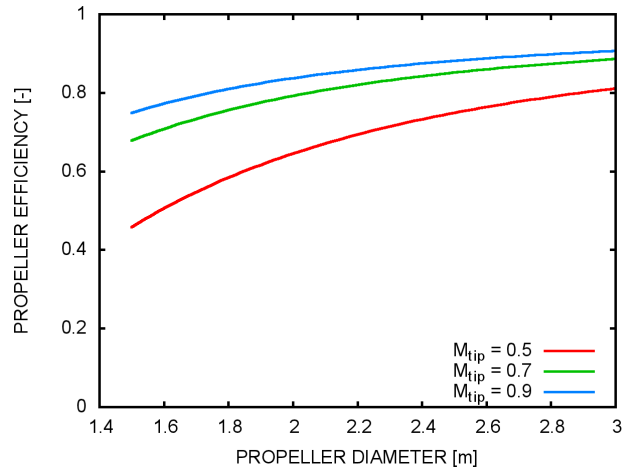


Fig. 2. Dependence of the propeller efficiency on blade tip Mach number for the propeller with 2 blades

This means that the engine gearbox must be modified according to this condition. Results are presented in Fig. 2.

Fig. 1 gives clear proof that increasing of the number of propeller blades has positive influence on efficiency. Influence of the number of blades becomes smaller for higher propeller diameter. This corrects common mistake which can be often found in the literature. For noise reduction it is also recommended to use as many blades as possible. Fig. 2 shows that noise reduction by the decrease of the blade tip Mach number has negative influence on the efficiency. In this case has noise reduction negative influence on the propeller efficiency, so as high blade tip Mach number as possible should be used so that noise regulations are fulfilled.

Acknowledgments

This work has been supported by the project EXLIZ CZ.1.07/2.3.00/30.0013, which is co-financed by the European Social Fund and the state budget of the Czech Republic.

References

- [1] Bocci, A.J., A new series of aerofoil sections suitable for aircraft propellers, *Aeronautical Quarterly* 28 (1977) 59-73.
- [2] Broz, V., Aerodynamic design of a highly efficient propeller blade, NASA-TT-F-11218, 1967.
- [3] Gutin, L., On the sound field of a rotating propeller, NACA-TM-1195, 1948.
- [4] Hartman, E.P., Biermann, D., The aerodynamic characteristics of six full-scale propellers having different airfoil sections, NACA Technical Report No. 650, Langley Memorial Aeronautical Laboratory, 1939.
- [5] Klesa, J., Optimal circulation distribution on propeller with the influence of viscosity, Proceedings of the 32nd AIAA Applied Aerodynamics Conference, Atlanta, 2014, AIAA Paper 2014-3132, doi: 10.2514/6.2014-3132.

Component-wise partitioned finite element method for wave propagation and dynamic contact problems

R. Kolman^a, S.S. Cho^b, J. Červ^a, K.C. Park^c

^aInstitute of Thermomechanics, v.v.i., Academy of Sciences of the Czech Republic, Dolejškova 5, Prague 8, Czech Republic

^bKorea Atomic Energy Research Institute, 999-111 Daedeok-Daero, Yuseong-gu, Daejeon, Republic of Korea

^cCenter for Aerospace Structures, University of Colorado at Boulder, Boulder, CO 80309 - 0429, Colorado, USA

An explicit time scheme for finite element computations of wave propagation problems in solids and contact problems is presented. The presented algorithm, with the component-wise partition of equations of motion to the longitudinal and shear parts, is designed to more precisely integrate wave propagation in accordance with their different propagation wave speeds [1, 4]. The scheme is a modification of the conventional central difference method in the connection with the pullback interpolation with the time step size satisfied the CFL limit for each element-by-element partition of equations of motion.

The suggested three-time step integrator is fully explicit with the diagonal mass matrix, of second-order accuracy, conditionally stable and exhibits minimal sensitivity behaviour on stable time step size. We present several numerical tests of wave propagation and dynamic contact problems to show accuracy and performance of the proposed method.

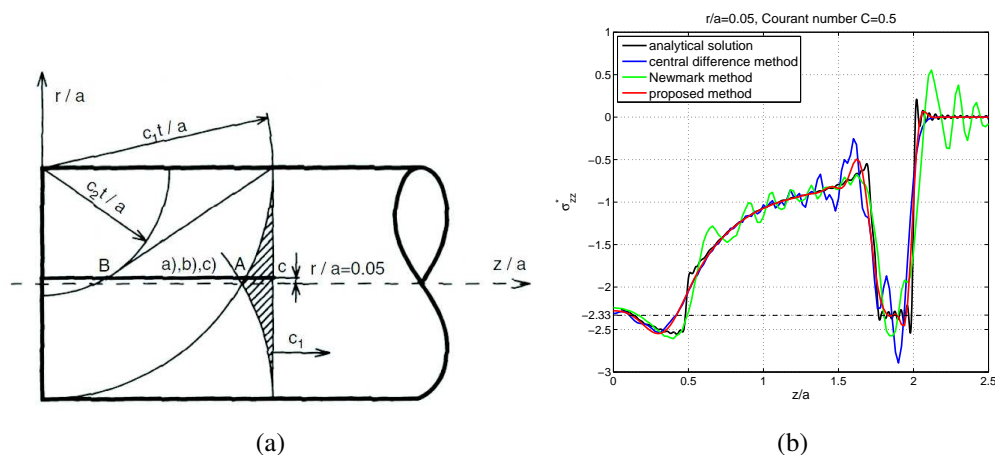


Fig. 1. Impact of elastic cylinders [2, 6]. (a) Theoretical position of wave fronts at the time $t = 2a/c_L$, where c_L is the speed of longitudinal wave and a is the cylinder radius. (b) Dimensionless distribution of axial stress $\sigma_{zz}^* = \sigma_{zz} c_L / (\Lambda v_0)$ along the line $r/a = 0.05$ in comparison with analytical data [6]. Λ marks the Lamé constant and v_0 denotes the impact velocity.

The algorithm has been successfully implemented in the predictor-corrector form [3] into an open source research code *Tahoe* [5]. As a numerical example, we show wave propagation in impact problem of elastic cylinders [6], for scheme see Fig. 1a. Stress distributions σ_{zz} along

the line $r/a = 0.05$ obtained by the central difference method, the Newmark method and the proposed method compared with the analytical results [6] are presented in Fig. 1b. One can see in Fig. 2. that the proposed scheme gives the stress distributions without spurious oscillations unlike the central difference method and the Newmark method.

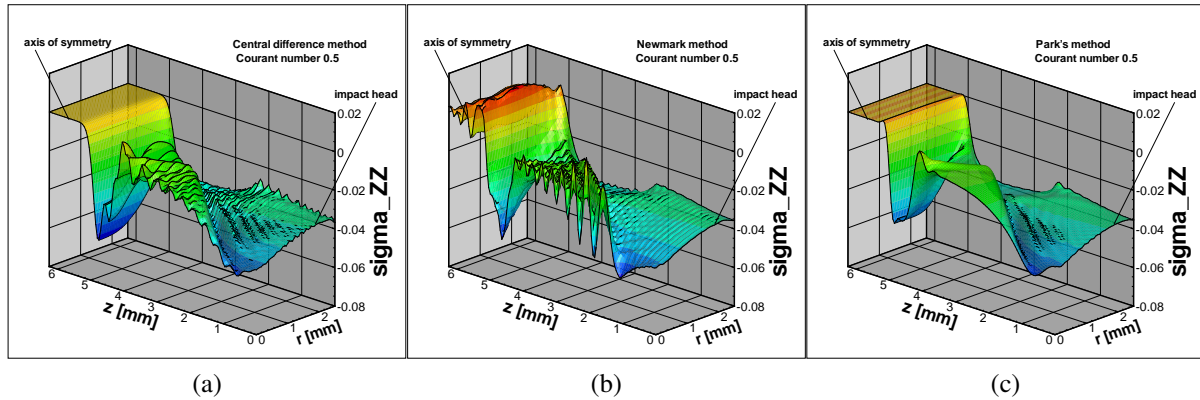


Fig. 2. Distributions of axial stress σ_{zz} (in GPa) in impact problem of elastic cylinders at the time $t = 2a/c_L$: (a) the central difference method, (b) the Newmark method (c) the proposed method. The cylinder is made of steel, the radius $a = 2.5$ mm, the length $L = 6.25$ mm, the impact velocity $v_0 = 1$ m/s.

Acknowledgments

The work has been supported by the Czech Science Foundation (GACR) (No. GAP101/12/2315, GAP101/11/0288) within the institutional support RVO: 61388998. The presented study has been partially supported by WCU (World Class University) Program through the Korea Science and Engineering Foundation (Grant Number R31-2008-000-10045-0), the National Research Foundation of Korea (MSIP, 2012M2A8A4026290) and the Radioactive Waste Management Technology Development Project (MOTIE, 20111710200011) by the Republic of Korea.

References

- [1] Cho, S.S., Park, K.C., Huh, H., A method for multi-dimensional wave propagation analysis via component-wise partition of longitudinal and shear waves, *International Journal for Numerical Methods in Engineering* 95 (2013) 212–237.
- [2] Gabriel, D., Plešek, J., Kolman, R., Valeš, F., Dispersion of elastic waves in the contact-impact problem of a long cylinder, *Journal of Computational and Applied Mathematics* 234(6) (2010) 1930–1936.
- [3] Kolman, R., Cho, S.S., Park, K.C., A method for multidimensional wave propagation analysis via component-wise partition of longitudinal and shear waves: Predictor-corrector form, implementation, and performance, *International Journal for Numerical Methods in Engineering* (2014). (to appear)
- [4] Park, K.C., Lim, S.J., Huh, H., A method for computation of discontinuous wave propagation in heterogeneous solids: basic algorithm description and application to one-dimensional problems, *International Journal for Numerical Methods in Engineering* 91 (2012) 622–643.
- [5] Tahoe, 2012, <http://tahoe.sourceforge.net>.
- [6] Valeš, F., Morávka, Š., Brepta, R., Červ, J., Wave propagation in a thick cylindrical bar due to longitudinal impact, *JSME International Journal Series A* 39(1) (1996) 60–70.

Isogeometric analysis in free vibration problems

R. Kolman^a, S. Sorokin^b, B. Bastl^c, J. Kopačka^a, J. Plešek^a

^aInstitute of Thermomechanics, v.v.i., Academy of Sciences of the Czech Republic, Dolejškova 5, Prague 8, Czech Republic

^bFaculty of Engineering and Science, Aalborg University, Fibigerstræde 16, 9220 Aalborg, Denmark

^cFaculty of Applied Science, NTIS, University of West Bohemia, Univerzitní 8, 301 00 Pilsen, Czech Republic

The paper is devoted to numerical solution of free vibration problems for elastic bodies [6] by means of a spline based finite element method (FEM), called Isogeometric Analysis (IGA) [1]. It has an advantage that the geometry is described exactly and the approximation of unknown quantities in the Galerkin approximation framework is smooth due to higher-order continuous shape functions. IGA exhibits very convenient convergence rates, small frequency errors for higher frequency spectrum and small dispersive pollution [3].

In this paper, the IGA strategy is used in computation of eigen-frequencies of a block and cylinder as benchmark tests [2, 4]. Results are compared with the standard FEM, the Rayleigh-Ritz method and available experimental data. The attention is also paid to the comparison of convergence rates, accuracy, and time-consuming of IGA against FEM.

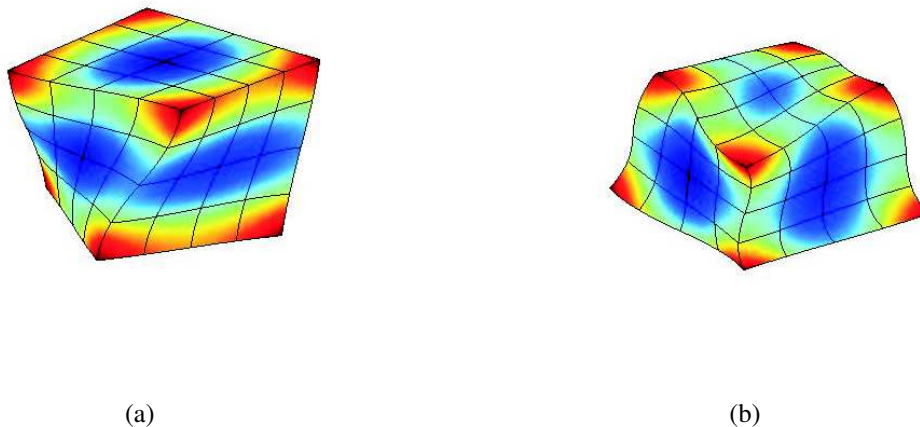


Fig. 1. Examples of (a) the first and (b) the sixth non-zero eigen-modes of a glass block [2]

The potential of isogeometric analysis in resonant ultrasound spectroscopy measurements [5] of elastic properties of general anisotropic solids and modelling of free vibration of functionally graded structures and heterogeneous solids are discussed.

Acknowledgments

The work has been supported by the Czech Science Foundation (GACR) (No. GAP101/12/2315, GAP101/11/0288) within the institutional support RVO: 61388998.

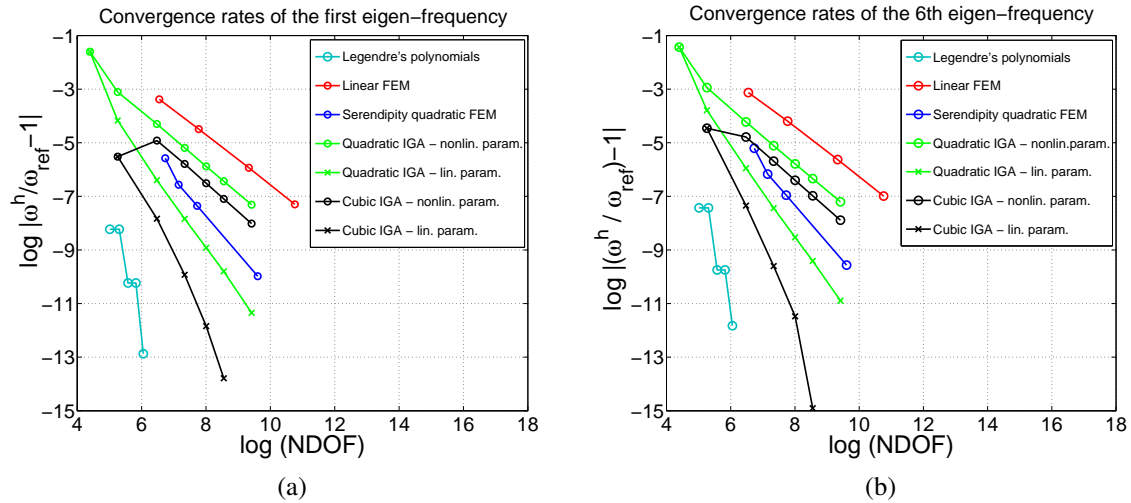


Fig. 2. Convergence rates of IGA, FEM and the Rayleigh-Ritz method in free vibration of an elastic block [2, 4]: (a) the first eigenmode, (b) the sixth eigenmode

References

- [1] Cottrell J.A., Hughes, T.J.R., Bazilevs, Y., Isogeometric analysis: Toward integration of CAD and FEA, John Wiley & Sons, New York, 2009.
- [2] Kolman, R., Isogeometric free vibration of an elastic block, *Engineering Mechanics* 19 (4) (2012) 279–291.
- [3] Kolman, R., Plešek, J., Okrouhlík, M., Complex wavenumber Fourier analysis of the B-spline based finite element method, *Wave Motion* 51 (2) (2014) 348–359.
- [4] Kolman, R. Sorokin, S., Bastl, B., Kapačka, J., Plešek, J., Isogeometric analysis of free vibration of simple shaped elastic samples, *Journal of the Acoustical Society of America* (2014). (submitted)
- [5] Plešek, J., Kolman, R., Landa, M., Using finite element method for the determination of elastic moduli by resonant ultrasound spectroscopy, *Journal of the Acoustical Society of America* 116 (2004) 282–287.
- [6] Timoshenko, S., *Vibration problems in engineering*, 3rd edition, McGraw Hill, 1961.

Analytical solution of the film flow on the inner surface of the pipe driven by the flow of the wet steam

M. Kořista ^a

^a Siemens, s.r.o., odštěpný závod Industrial Turbomachinery, Olomoucká 7/9, 618 00 Brno, Czech Republic

Flow of wet steam in pipes is a very common case in every power plant utilizing Rankine–Clausius cycle. The fluid entering the pipe is a two phase single component substance with homogeneous distribution of the moisture content in form of small droplets of the liquid phase with a wide spectrum of the droplet radii. Generally the pipe wall is non adiabatic with a wettable inner surface. The interaction of the pipe wall with the fluid results in splitting of the homogeneous entering flow. The equilibrium state of the fluid interacting with the wall is different than that of the entering state. The flow is split into two flows of different moisture content. Liquid film flow occurs on the pipe wall. In this study high quality of the pipe insulation is expected and the pipe wall is treated as adiabatic. This assumption is acceptable for large, well insulated pipes. Due to the adiabatic wall condition the film created on the wall has to be part of the liquid phase of the entering moisture content. (For non–adiabatic case the heat flux of the wall has to be considered and the film mass flow rate is increased by the condensation contribution.) In either case the liquid separation from the homogeneous flow entering into the film decreases the moisture content in the core flow which remains two phase. Subject of this study is the adiabatic wall. From the technical praxis it is known that the liquid film is spread around the whole pipe circumference independently if the pipe is vertical or horizontal. That fact supports the adopted assumption that the gravity effect can be neglected from the investigation as negligible. Focusing on the straight circular pipes as the most common case the surface tension effect can be avoided too since the film surface under the above specified conditions has to be cylindrical and concentric with the inner pipe surface since it is experimentally known the pipe radii is much greater than the film thickness. The film surface is cylindrical because of the existence of equilibrium i.e. the film thickness is constant for a constant given mass flow. Under the above specified conditions the mass flow split of the two phase pipe flow is governed by the principles of incompressible viscous flow if the Mach number is low. The common mathematical model of the film and core flow is obtained when the equations for incompressible viscous flow are applied separately on film and core regions and the equations for coexistence of both regions are added. The film surface is mathematically treated as an infinitely thin solid wall dragged on the inner side by the shear stress of the core flow while it is sliding on the liquid film. On the outer surface of this abstract wall acts drag in the opposite direction caused by the film between this wall and physical inner surface of the pipe. The equilibrium of the abstract wall occurs when the wall moves with constant velocity. The first equation of the coexistence of both regions implies from this equilibrium in form of the shear stress equilibrium of the film and core on the abstract wall. The second equation of the coexistence is implied from the fact that the streamlines of both regions in the meridian section are parallel for the stationary case (developed velocity profile). This condition implies a constant pressure drop in both regions at the finite pipe length. Mathematically this can be expressed as the equality of the first

derivative of the pressure along the pipe length for both regions. Complexity of the problem is reduced to the laminar film flow and turbulent core flow. Analytical models of both flows are used. The laminar flow is integrated for film flow with inner moving wall in the concentric gap and the power law of 1/7 is used for turbulent core. The complete set of equations is treated by software for symbolic algebra calculation "Maxima". The complete mathematical model consists of nonlinear equations for equality of the shear stress on the film surface, film thickness, velocity of the film surface and equality of the pressure derivatives in the film and core. Any analytical solution in Maxima is impossible. The practical guide for quick estimation of the film thickness provides the following formula solved for mean steam velocity calculated for the wet steam.

$$\begin{aligned}
 & \text{(30118)} \quad \frac{v_{wg1}^{1/4} w_{wg1} c_B \left(x_0 m_{wg0} (\rho_{V0} - \rho_{L0}) + \pi w_{wg1} \rho_{L0} (R - \delta)^2 \rho_{V0} \right)}{2^{13/4} \pi (w_{wg1} - w_f)^{1/4} (R - \delta)^{9/4} \rho_{V0}} + \mu_f \\
 & \left(\frac{2 \delta dp_x R - \delta^2 dp_x - 4 \mu_f w_f}{(R - \delta) (4 \mu_f \log(R) - 4 \mu_f \log(R - \delta))} - \frac{dp_x (R - \delta)}{2 \mu_f} \right) = 0
 \end{aligned}$$

In this equation, $w_{wg1}, v_{g,1}$ are the mean velocity and kinematic viscosity of the wet steam in the core flow, $\rho_{L0}, \rho_{V0}, x_0$ the density of the saturated liquid and vapor and moisture content of the core flow w_f, μ_f, δ are the surface film velocity, dynamic viscosity and thickness of the film, R is pipe radius, $c_B = 0,3164$ is Blasius constant [1] and dp_x is pressure drop per one meter of the pipe.

Reference

- [1] Fleischner, P., Hydromechanics, VUT, Brno, 1990. (in Czech)

Fracture mechanics of composite materials – determination and representation of stress coefficient terms

M. Kotoul^a

^aFaculty of Mechanical Engineering, Brno University of Technology, Technická 2, 61669 Brno, Czech Republic

The increasing use of fibre reinforced composites has brought a renewed interest in the analysis of cracks, notches and multi-material corners in anisotropic materials. In the case of anisotropic materials, a number of elastic constants must be handled during calculations. To this end, Lekhnitskii –Stroh formalism of plane strain elasticity [1] is a very efficient tool. Existence of the material interface in composite materials, especially in laminated structures and/or layered structures brings a specific problem in the crack analysis. As an example, a problem of cracks terminating at the interface of two generally anisotropic (most often orthotropic) materials, or problem of cracks lying on the interface could be mentioned. A similar situation can be encountered in the technology of protective surface layers. The assessment of the behaviour of the mentioned general stress concentrators requires a good knowledge of the stress field in the vicinity of the singular point. The problem complexity can be further increased due to presence of the bridging fibres which can significantly influence the stress field. Understanding of the competition between the crack penetration and delamination is essential to correctly assess the reliability of given structure. Apparently, an effective technique needs to be worked up to handle these problems.

In most of the geometrical and material configurations of a bi-material corner (special case is a crack impinging at a bi-material interface), there are two singular terms in the stress distribution at its tip. Contrary to a crack in a homogenous material or a crack at a bi-material interface, the stress singularity exponents differ from 1/2 and the corresponding generalized stress intensity factors belong to both the normal and shear modes of loading. Anisotropy usually lifts a degeneracy of the singularity exponents and strongly influences the direction of crack penetration across the interface. Because the elastic T-stress and other coefficients of the higher-order terms play an important role in fracture mechanics such as the stability of crack kinking, crack path, and two-parameter characterization of elastic-plastic crack tip fields, determination of all the coefficients in the crack tip field expansion is crucial. Since the standard computational procedures such as singularity elements with nodes moved to the quarter points or the path independent J integral do not apply, conservation laws of elasticity and Betti's reciprocal theorem, together with selected auxiliary fields are more convenient for the determination of stress coefficient terms. The reciprocal theorem of elastostatics states that in the absence of body forces and residual stresses the following integral is path independent

$$\Psi(\mathbf{U}, \mathbf{V}) = \int_{\Gamma} [\sigma_{ij}(\mathbf{U}) \cdot n_i \cdot V_j - \sigma_{ij}(\mathbf{V}) \cdot n_j \cdot U_i] ds, \quad (1)$$

where Γ is any contour surrounding the crack tip and \mathbf{U} , \mathbf{V} are two admissible displacement fields and $\sigma_{ij}(\mathbf{U})$ and $\sigma_{ij}(\mathbf{V})$ are the corresponding stress fields. The asymptotic expansion of displacements $\mathbf{U}(x)$ is possible to write in the following form [2]

$$\mathbf{U}(x) = \mathbf{U}(0) + H_1 r^{\delta_1} \mathbf{u}_1(\theta) + H_2 r^{\delta_2} \mathbf{u}_2(\theta) + T r^{\delta_3} \mathbf{u}_3(\theta) + \dots = \sum_{i=0}^{\infty} k_i r^{\delta_i} \mathbf{u}_i(\theta), \quad \delta_3 = 1, \quad (2)$$

where H_1, H_2 are the generalized stress intensity factors, $\mathbf{u}_i(\theta), i=1,2$ are angular distributions of displacements in the corresponding leading terms of the asymptotic expansion, and $\mathbf{u}_3(\theta)$ is the angular distribution of displacements corresponding to the T-stress. If the displacement fields $\mathbf{U} = U_i(x) = r^{\delta_i} \mathbf{u}_i(\theta), \mathbf{V} = U_j(x) = r^{\delta_j} \mathbf{u}_j(\theta)$ obtained by solving the eigenvalue problem are considered, it can be proved that the contour integral Ψ is equal to zero for $-\delta_i \neq \delta_j$ and non-zero if $-\delta_i = \delta_j$. Since the basis function corresponding to the coefficients $k_1=H_1, k_2=H_2, k_3=T$ in the asymptotic expansion for \mathbf{U} are $r^{\delta_1} \mathbf{u}_1(\theta), r^{\delta_2} \mathbf{u}_2(\theta), r^{\delta_3} \mathbf{u}_3(\theta)$, it holds

$$\begin{aligned} \Psi(\mathbf{U}, r^{-\delta_1} \mathbf{u}_{-1}) &= \sum_{i=1}^{\infty} k_i \Psi(r^{\delta_i} \mathbf{u}_i, r^{-\delta_1} \mathbf{u}_{-1}) = k_1 \Psi(r^{\delta_1} \mathbf{u}_1, r^{-\delta_1} \mathbf{u}_{-1}), \\ \Psi(\mathbf{U}, r^{-\delta_2} \mathbf{u}_{-2}) &= \sum_{i=1}^{\infty} k_i \Psi(r^{\delta_i} \mathbf{u}_i, r^{-\delta_2} \mathbf{u}_{-2}) = k_2 \Psi(r^{\delta_2} \mathbf{u}_2, r^{-\delta_2} \mathbf{u}_{-2}), \\ \Psi(\mathbf{U}, r^{-\delta_3} \mathbf{u}_{-3}) &= \sum_{i=1}^{\infty} k_i \Psi(r^{\delta_i} \mathbf{u}_i, r^{-\delta_3} \mathbf{u}_{-3}) = k_3 \Psi(r^{\delta_3} \mathbf{u}_3, r^{-\delta_3} \mathbf{u}_{-3}), \end{aligned} \quad (3)$$

where $\Psi(r^{\delta_1} \mathbf{u}_1, r^{-\delta_1} \mathbf{u}_{-1})$ is computed analytically along the path Γ_1 surrounding the crack tip with diameter approaching zero, while $\Psi(\mathbf{U}, r^{-\delta_1} \mathbf{u}_{-1})$ is computed along the path Γ_2 which is any remote integration path with a finite diameter. Thus, the GSIFs $H_1 = k_1, H_2 = k_2$ can be computed as follows:

$$H_1 = \frac{\Psi(\mathbf{U}, r^{-\delta_1} \mathbf{u}_{-1})}{\Psi(r^{\delta_1} \mathbf{u}_1, r^{-\delta_1} \mathbf{u}_{-1})}, \quad H_2 = \frac{\Psi(\mathbf{U}, r^{-\delta_2} \mathbf{u}_{-2})}{\Psi(r^{\delta_2} \mathbf{u}_2, r^{-\delta_2} \mathbf{u}_{-2})}. \quad (4)$$

Since the exact solution \mathbf{U} is not known, a finite element solution \mathbf{U}^h can be used as an approximation for \mathbf{U} so to obtain an approximation for GSIFs. Similar arguments which lead to Eq. (4) apply also for the T-stress calculation.

The use of a classical fracture criterion in the vicinity of an interface is questionable as already mentioned by Atkinson [3] because the singularity exponent is different from the classical value 1/2. This problem can be resolved by introducing the concept of *finite* crack extensions a instead of infinitesimal one. In the lecture, also the concept of the Finite fracture mechanics (FFM) will be presented. FFM and the matched asymptotic expansion method together with FEM are used to derive the change of the potential energy induced by the crack increment of finite length. The principles of the matched asymptotic expansion method will be introduced and then several examples of fracture mechanics problems of composite materials will be illustrated.

Acknowledgements

The work has been supported by the research project NETME CENTRE PLUS (LO1202).

References

- [1] Stroh, A. N., Dislocation and cracks in anisotropic elasticity, *Phil. Mag.* 7 (1958) 625–646.
- [2] Profant, T., Ševeček, O., Kotouš, M., Calculation of K-factor and T-stress for cracks in anisotropic bimetals, *Eng. Fract. Mechanics* 75 (2008) 3707–3726.
- [3] Atkinson, C., On stress singularities and interfaces in linear elastic fracture mechanics, *Int J Fracture* 13 (1977) 807–820.

Comparison of numerical simulation and experiment in case of bending test of composite rectangular tubes

R. Kottner^a, L. Bek^a, J. Krystek^a

^aEuropean Centre of Excellence, NTIS - New Technologies for Information Society, Faculty of Applied Sciences, UWB in Pilsen, Univerzitní 22, 306 14 Plzeň, Czech Republic

The design of a composite footbridge using a finite element method (FEM) model is the aim of the research project TA02010501. A box beam concept is used in the footbridge design [3]. To validate the FEM model, bending tests of composite rectangular tubes were done using the Zwick/Roell Z050 testing machine [2]. In this work, the bending tests were extended. A steel pad was inserted between a compressive element and a sample for more uniform distribution of loading (see Fig. 1). The aim of this work was to compare the failure of the tubes in case of the FEM model and the experiment and to determine a safety coefficient for the load capacity evaluation of the footbridge.

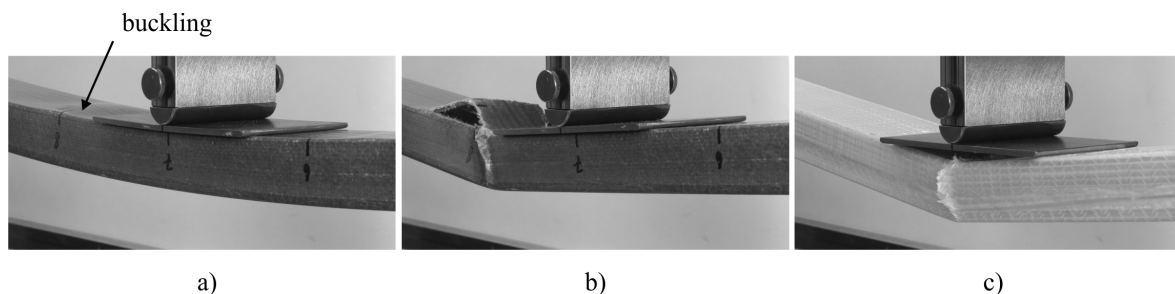


Fig. 1. Bending test: a) buckling of sample A, b) failure of sample A, c) failure of sample B

Two types of samples (tubes) were tested. Both types consisted of glass fibres and epoxy resin. Sample A consisted of two outer chopped strand mat (CSM) layers and two inner unidirectional (UD) layers. Sample B consisted of six biaxial non-crimp fabric (NCF) layers. The pultrusion technique was used for manufacturing of the samples. Elastic and strength parameters of the composites were provided by a manufacturer (5M).

Performed tests were numerically simulated using the Abaqus 6.12 finite element system. 4-node shell elements were used for the composite tubes, 8-node brick elements were used for the steel pad, the steel compressive element, and steel supports (see Fig. 3). Friction between these parts of the simulation was neglected. The maximum stress theory was used to determine failure [1]. Analyses with and without large deformation assumption were compared.

The type of the deformation assumption did not significantly influence results of the model of the sample B. However, significant differences were observed in case of the sample A. A local buckling of the sample A before its failure was the reason. The buckling of the sample A in case of the experiment and the model is obvious from Fig. 1 and Fig. 2, respectively. Critical stresses were the stress in the tube transverse direction (Sample A – see Fig. 2) and the stress in the tube longitudinal direction (Sample B – see Fig. 3).

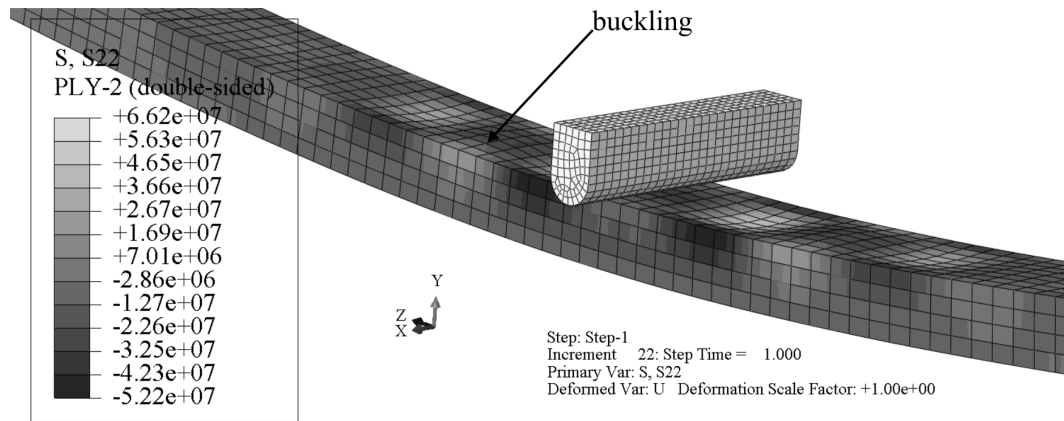


Fig. 2. Transverse stress [Pa] in inner UD layer under ultimate deflection (steel pad is hidden)

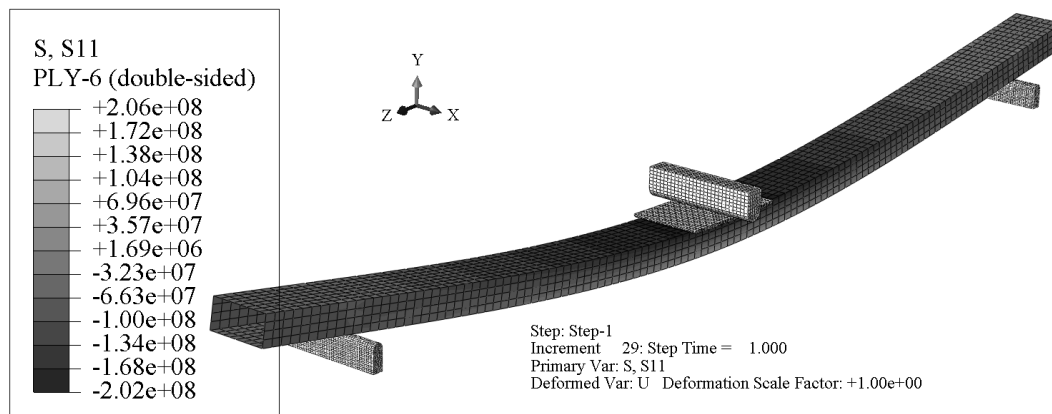


Fig. 3. Longitudinal stress [Pa] in outer NCF layer under ultimate deflection

The location of the failure determined in the numerical simulations was in sufficient agreement with experimental results (if large deformations were assumed in the model of the sample A). Based on comparison of ultimate forces in experiments and models, it was determined that the value of the safety coefficient for the load capacity evaluation of the footbridge should not be less than 3.

Acknowledgements

This work was supported by the research project TA02010501.

References

- [1] Baker, A., Dutton, S., Kelly, D., Composite materials for aircraft structures, AIAA, Reston, 2004.
- [2] Bek, L., Kottner, R., Krystek, J., Experimental investigation of critical buckle load of composite specimens, Proceedings of the 52th International Scientific Conference on Experimental Stress Analysis, Mariánské lázně, Czech Society for Mechanics, 2014, pp. 3-4.
- [3] Kottner, R., Kroupa, T., Laš, V., Design of composite footbridge, Proceedings of the Mechanics of Composite Materials and Constructions 2014, Beroun, University of West Bohemia, 2014, pp. 69-70. (in Czech)

An investigation of stochastic resonance using the Fokker-Planck equation and finite element method

R. Král^a, J. Náprstek^a, S. Pospíšil^a

^a*Institute of Theoretical and Applied Mechanics, v.v.i., Czech Academy of Sciences, Prosecká 76, 190 00 Prague, Czech Republic*

The stochastic resonance (SR) belongs to the nonlinear dynamic phenomena with a decisive role of the random noise. It has been observed and studied in a large variety of different areas of physics, e.g., in modern communication technologies, in a laser optics or in ferromagnets and ferroelectrics, see [4]. It was found even in the biological systems [1] or recently also in the problems of a wind induced vibration [5]. The physical mechanism of SR consists in the synchronization of concurrently acting additive deterministic input (such as periodic forcing) and random excitation (such as additive white noise) in the nonlinear oscillator with double-well potential. With optimal dose of noise, the periodicity of the activated hopping response between the local equilibrium states (potential minima) reaches its maximum.

The transition response of such a noise-controlled stochastic system can be investigated by various methods. Two-state theory or continuous-state theory [2] have been successfully used in the majority of studies on SR resulting in the main quantitative characteristics such as Spectral Power Amplification (SPA), the Signal-to-Noise Ratio (SNR) or the residence-time distribution density. In this paper, the Finite Element Method as a tool for the numerical solution of corresponding Fokker-Planck Equation (FPE) is introduced. By solving the periodically driven differential equation:

$$\frac{\partial p}{\partial t} = -\frac{\partial}{\partial x_1} \{x_2 p\} - \frac{\partial}{\partial x_2} \{ [x_1 - x_1^3 - x_2 + A \cos(\omega_e t + \phi)] p \} + D \frac{\partial^2 p}{\partial x_2^2}, \quad (1)$$

time-dependent Probability Density (PD) of residing $p(\mathbf{x}, t; \phi)$ can be calculated. This equation describes the stochastic temporal diffusion processes with periodically varying coefficients of drift. The system has assuming unit mass and viscous damping in a symmetric double-well potential $U(x_1) = -0.5x_1^2 + 0.25x_1^4$. The term $A \cos(\omega_e t + \phi)$ refers to the periodic excitation with amplitude A , ω_e is forcing frequency and ϕ indicates the phase shift. The variable D stands for the noise intensity being proportional to the Gaussian white noise.

The FEM efficiency when solving FPE which follows from the Duffing stochastic differential equation without external harmonic forces was already studied by the authors in [3]. With the periodic force taken into account, certain difficulties arise due to the time inhomogeneity of the corresponding stochastic process. Let us solve Eq. (1) in the Galerkin-Petrov meaning on the piecewise smoothly bounded domain $\Omega \in x_1 \times x_2$ in \mathbb{R}^d , $d = 2$. The initial and boundary conditions are $p(\Omega, 0; \phi) = p_0$ and $p(\partial\Omega, t) = 0$, respectively. After a spatial discretizing of Ω onto the rectangular finite elements using the bilinear approximation functions, the system of ordinary differential equations emerge with global matrices \mathbf{M} , $\mathbf{K}(t)$ and vector of PD values in nodes of the mesh. The matrix $\mathbf{K}(t)$ is time-dependent due to the periodic perturbation entering

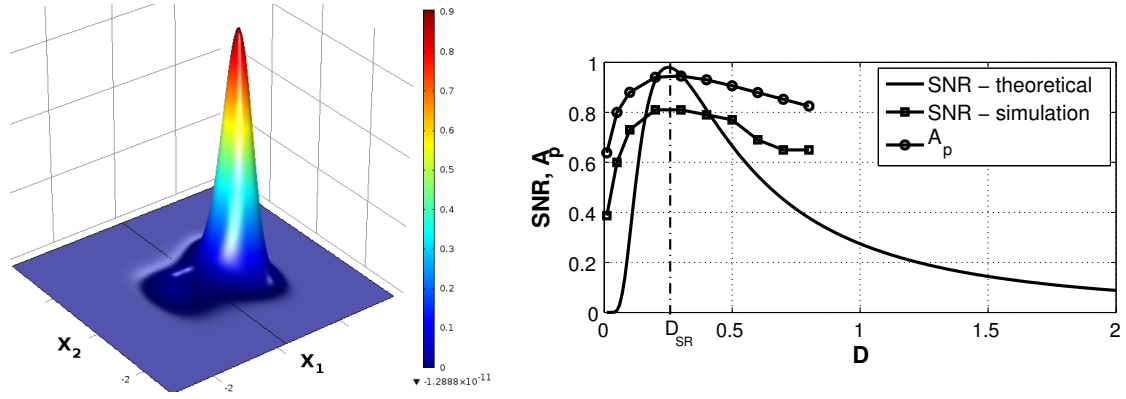


Fig. 1. Probability density distribution in SR state (*left*); Quantitative characteristics Signal-to-Noise Ratio, see [2], and amplitude A_p as a function of noise intensity D (*right*)

the drift term of FPE. The deposition of the individual matrix elements to the global matrices and the temporal numerical integration are carried out using the COMSOL MULTIPHYSICS™ software.

Since the convection indicators of SR are not applicable in this approach, other way of treating the stochastic response in SR regime is adopted. As a specific measure of optimally selected noise intensity, the integral value of PD distribution over one potential well, $x_1 \in (-\infty, 0)$, for various D is introduced as:

$$P_N(t; D) = \int_{-\infty}^{\infty} \left(\int_{-\infty}^0 p(x_1, x_2, t; \phi; D) dx_1 \right) dx_2 \quad (2)$$

that is periodic in time with the amplitude $A_p(D)$. The stochastic resonance occurs for such D for which the amplitude $A_p(D)$ assumes its maximum. Fig. 1 left shows a typical PD function as an approximation solution of Eq. (1) in the stochastic resonant state. In Fig. 1 right, the amplitude $A_p(D)$ of the periodic component of the integral value (2) vs the noise intensity D is plotted complemented with SNR characteristic based on theoretical and simulation models, see [2] for details. As evident, the peak values of all curves coincide at $D = D_{SR}$ where D_{SR} is intensity at the stochastic resonance. This point represents the highest probability that the response will jump from one basin to the other with period ω_e . The probability of switching equals to the amplitude $A_p(D_{SR}) = 0.94$.

Acknowledgments

Kind support of the Czech Scientific Foundation project No. GP14-34467P and also from project RVO68378297 are gratefully acknowledged.

References

- [1] Benzi, R., Sutera, A., Vulpiani, A., The mechanism of stochastic resonance, *Journal of Physics A: Mathematical and General* 14 (11) (1981) L453-L457.
- [2] Gammaitoni, L., Hänggi, P., Jung, P., Marchesoni, F., Stochastic resonance, *Reviews of Modern Physics* 70 (1) (1998) 223-287.
- [3] Náprstek, J., Král, R., Finite element method analysis of Fokker-Planck equation in stationary and evolutionary versions, *Advances in Engineering Software* 72 (2014) 28-38.
- [4] Néda, Z., Stochastic resonance in 3D Ising ferromagnets, *Physics Letters A* 210 (1996) 125-128.
- [5] Pospíšil, S., Náprstek, J., Investigation of stochastic resonance effects in problems of wind induced vibration, *Proceedings of the 9th Int. Conf. on Structural Dynamics, Porto, 2014*, pp. 1957-63.

Flow of non-Newtonian fluid

J. Křen^a, L. Lobovský^b, K. Vitáková^a

^a Department of Mechanics, Faculty of Applied Sciences, University of West Bohemia, Univerzitní 22, 306 14 Plzeň, Czech Republic

^b NTIS - New Technologies for the Information Society, Faculty of Applied Sciences, University of West Bohemia, Univerzitní 22, 306 14 Plzeň, Czech Republic

The paper provides an introduction to the numerical solution of non-Newtonian fluid flow. In this contribution we limit ourselves to the case of the isothermal flow of a viscous incompressible fluid. In order to incorporate the effect of the strain rate on the fluid characteristics the power-law fluid model is employed. This well-known type of the generalised Newtonian fluid is then used for a demonstration of the two-dimensional flow.

When deriving the governing equations describing the fluid flow, the standard Eulerian approach is used. If the hydraulic pressure term is separated from the fluid stress tensor and if the density is considered to be constant (incompressible material, $T_{ij} = -p\delta_{ij} + \tau_{ij}$), then the Navier-Stokes and continuity equations of the fluid motion have the form [3]:

$$\rho \frac{\partial v_i}{\partial t} + \rho v_j \frac{\partial v_i}{\partial x_j} = -\frac{\partial p}{\partial x_i} + \frac{\partial \tau_{ij}}{\partial x_j} + \rho f_i; \quad \frac{\partial v_i}{\partial x_i} = 0, \quad \text{in } \Omega,$$

where Ω is the spatial domain upon which the fluid motion is described, v_i are the components of the velocity vector of the fluid, ρ is the density, x_i are Euler's (spatial) coordinates, p is the pressure, f_i is the specific body force vector and T_{ij} is the extra stress tensor. In order to solve the flow equations, one needs to determine the initial conditions at time $t = t_0$ in the domain Ω and the boundary conditions on the boundary Γ of Ω in general. The following boundary conditions are specified: $v_i = g_i$ on Γ_U and $\sigma_i = \tau_{ij}n_j = h_i$ on Γ_σ , where σ_i is the traction, n_i is the unit outward normal vector to Γ_σ .

The constitutive equation of the power-law fluid may be written as [4]

$$\tau_{ij} = 2\mu_{app}(\dot{\gamma})V_{ij}; \quad \mu_{app}(\dot{\gamma}) = K|\sqrt{2V_{ij}V_{ij}}|^{n-1}; \quad V_{ij} = \frac{1}{2}\left(\frac{\partial v_i}{\partial x_j} + \frac{\partial v_j}{\partial x_i}\right),$$

where n is the power-law index, K is the consistency factor and $\mu(\dot{\gamma})$ is the apparent shear viscosity. Using Galerkin's method for deriving the weak solution and considering constitutive equation, the initial integral relations have a form [2]

$$\begin{aligned} \int_{\Omega} \rho \frac{\partial v_i}{\partial t} \delta v_i dx + \int_{\Omega} \rho v_j \frac{\partial v_i}{\partial x_j} \delta v_i dx - \int_{\Omega} p \frac{\partial \delta v_i}{\partial x_i} dx + \int_{\Omega} \mu_{app}(\dot{\gamma}) \frac{\partial v_i}{\partial x_j} \frac{\partial \delta v_i}{\partial x_j} dx = \\ = \int_{\Omega} \rho f_i \delta v_i dx - \int_{\Gamma_\sigma} \hat{\sigma}_i \delta v_i dx; \quad \int_{\Omega} \frac{\partial v_i}{\partial x_i} \delta p dx = 0. \end{aligned}$$

In the following, a spatial discretisation of a domain filled by a fluid using finite element method (FEM) is performed for a steady flow in a plane. Using isoparametric interpolation functions, the velocity components ($v_1 = u$, $v_2 = v$) and pressure p can be approximated as [1]

$$u(\xi, \eta, t) = \mathbf{N}^T(\xi, \eta)\mathbf{u}(t); \quad v(\xi, \eta, t) = \mathbf{N}^T(\xi, \eta)\mathbf{v}(t); \quad p(\xi, \eta, t) = \mathbf{H}^T(\xi, \eta)\mathbf{p}(t),$$

where \mathbf{N} and \mathbf{H} are vectors of interpolation functions defined locally for each element and \mathbf{u} , \mathbf{v} , \mathbf{p} are vector of nodal quantities of velocity and pressure components. From these relations we obtain three equations in matrix form

$$\begin{aligned} \mathbf{A}(\mathbf{u}, \mathbf{v})\mathbf{u} + \mathbf{B}_1(\dot{\gamma}; \mathbf{u}, \mathbf{v})\mathbf{u} + \mathbf{C}_1(\dot{\gamma}; \mathbf{u}, \mathbf{v})\mathbf{v} + \mathbf{D}_1\mathbf{p} &= \mathbf{E}_1, \\ \mathbf{A}(\mathbf{u}, \mathbf{v})\mathbf{v} + \mathbf{B}_2(\dot{\gamma}; \mathbf{u}, \mathbf{v})\mathbf{v} + \mathbf{C}_2(\dot{\gamma}; \mathbf{u}, \mathbf{v})\mathbf{u} + \mathbf{D}_2\mathbf{p} &= \mathbf{E}_2, \\ \mathbf{K}_1\mathbf{u} + \mathbf{K}_2\mathbf{v} &= \mathbf{0}. \end{aligned}$$

This matrix form represents a system of non-linear algebraic equations for unknowns \mathbf{u} , \mathbf{v} , \mathbf{p} which can be solved by an iteration method.

The solution of the above-mentioned problem was tested for a stationary isothermal laminar flow of incompressible viscous non-Newtonian fluid with power law model of viscosity. Because of clearness and good presentation of results, simple two-dimensional non-Newtonian fluid flow in horizontal channel was solved. Numerical results for $K = 8.66$ and $n = 0.585$ (pseudoplastic non-Newtonian fluid) are demonstrated in Fig. 1 (apparent viscosity distribution) and Fig. 2 (velocity and pressure distribution).

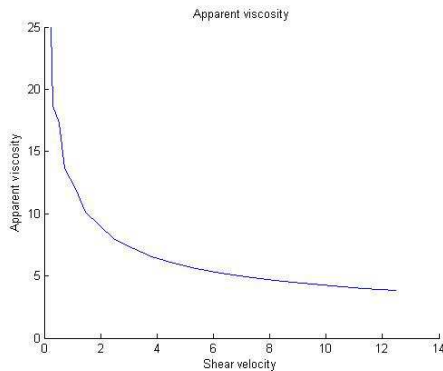


Fig. 1. Apparent viscosity distribution

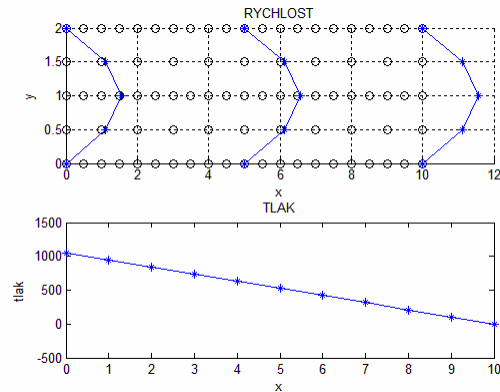


Fig. 2. Velocity and pressure distribution

Acknowledgements

This work was supported by the grant project TA ČR, no. TA03010990 and by the European Regional Development Fund (ERDF), project "NTIS - New Technologies for Information Society", European Centre of Excellence, CZ.1.05/1.1.00/02.0090.

References

- [1] Huang, H.Ch., Li, Z.H., Usmani, A.S., Finite element analysis of non-Newtonian flow, Springer-Verlag, London, 1999.
- [2] Křen, J., Rosenberg, J., Continuum mechanics, Vydavatelství ZČU, Plzeň, 2002. (in Czech)
- [3] Lai, W.M., Rubin, D., Krempl, E., Introduction to continuum mechanics, Pergamon Press Ltd., Oxford, 1993.
- [4] Pnueli, D., Gutfinger, Ch., Fluid mechanics, University Press, Cambridge, 1992.

Algorithmization issues of flat end check method according to EN 13445-3

T. Létal^a

^a Faculty of Mechanical and Engineering, Brno University of Technology, Technická 2, 616 69 Brno, Czech Republic

Design assessment procedure of flat ends with relief groove and flat ends directly welded to the shell according to EN 13445-3 [1] involves coefficient C_2 , which can be estimated either from figure 10.4-5 or using direct calculation according to paragraph 10.4.6. “Figure” method is feasible in design by hand and it is applicable for limited spectrum of input values. “Direct calculation” method is better suited for algorithmization of the whole design assessment procedure and it is applicable to broader spectrum of input values, but it sometimes yields unexpected results or even calculation errors. This may cause convergence problems in design assessment procedure. The design assessment procedure is usually iterative, because a calculation pressure is required as one of the inputs and it is also the main output. Presented paper suggests corrective measures for “direct calculation” method, which guarantee convergence of design assessment procedure, which yields conservative value of maximal allowable pressure.

According to [1] there is a formula for calculation of minimal thickness of flat end with relief groove e :

$$e = \max \left\{ \left(C_1 \cdot D_i \sqrt{\frac{P}{f}} \right); \left(C_2 \cdot D_i \sqrt{\frac{P}{f_{\min}}} \right) \right\}, \quad (1)$$

e	- minimal allowable thickness of flat end	[mm],
C_1	- coefficient (figure 10.4-4 or paragraph 10.4.3 [1])	[-],
D_i	- internal shell diameter	[mm],
P	- calculation pressure	[MPa],
f	- maximal allowable stress for flat end	[MPa],
C_2	- coefficient (figure 10.4-5 or paragraph 10.4.6 [1])	[-],
f_{\min}	- maximal allowable stress of shell and flat end	[MPa].

Since the coefficient C_2 depends on P and procedure for its calculation is rather complicated, explicit formula for P cannot be derived. Therefore, it is convenient to use an iterative procedure.

Maximum allowable pressure P is calculated for a given geometry, so the analyzed thickness e_a is known. Goal of the iterative procedure for maximum allowable pressure P will be to find such pressure P that leads to design of same value of thickness as e_a using formula (1). As an initial value of P , design pressure P_d can be used. New pressure in iteration is estimated as follows:

$$\Delta e = 2 \frac{e_i - e_a}{e_i + e_a}, \quad (2)$$

$$P_i = |P_{i-1} (1 - \Delta e \cdot 1.4)|. \quad (3)$$

Thickness e_i is calculated using formula (1) with $P = P_{i-1}$. Presented iteration procedure should be straightforward, but in tests, this procedure crashed or entered infinite loop.

To identify the cause of these problems, similar plot to the one in figure 10.4-5 in [1] was created. With the same boundaries, new plot is identical to 10.4-5 figure. However, in iteration procedure, some input values may lie out of these boundaries and functions $C_2(P/f_{\min})$ are discontinuous and sometime yield negative values of C_2 . This issue and suggested solution is shown in Fig. 1: red lines represent original function $C_2(P/f_{\min})$ for $e_s/D_i = 0.0065$ with vertical asymptote in discontinuity and blue curve represents modified function for the purposes of the iteration procedure. Grid in Fig. 1 represents the area of original plot 10.4-5 from [1].

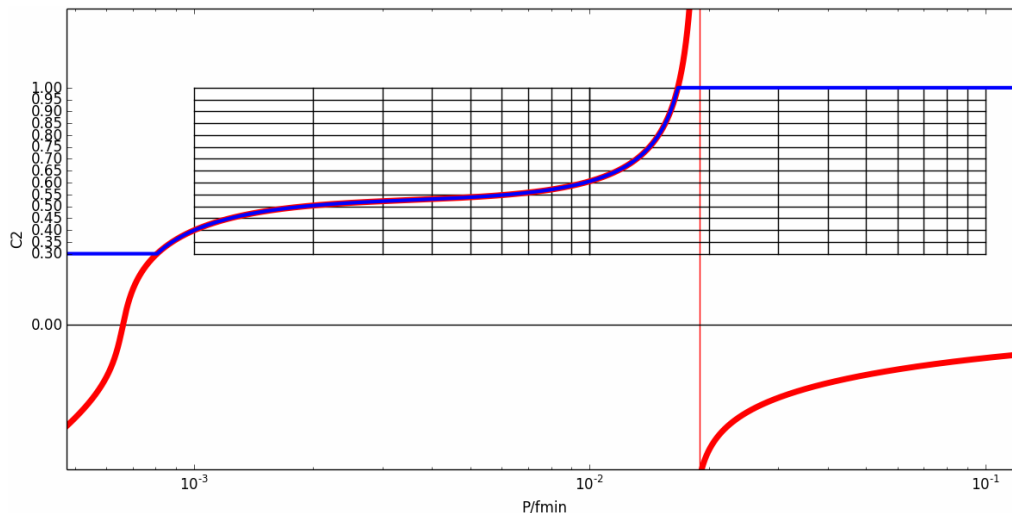


Fig. 1. $C_2(P/f_{\min})$ for $e_s/D_i = 0.0065$ (plotted using [2])

Fig. 1 suggests that the causes of the problems are negative and infinite values of C_2 at some points. Since the minimal thickness of a flat end is linearly dependent on C_2 , C_2 has to be greater than 0 and less than infinity. As one clause in the paragraph 10.4.4.1 implies, minimal value of C_2 is 0.3. According to “Figure” method, C_2 coefficient has values between 0.3 and 1.0. Suggested correction of the function $C_2(P/f_{\min})$ is using three conditions:

- For $C_2 < 0.3$: $C_2 = 0.3$,
- P/f_{\min} to the right from asymptote: $C_2 = 1.0$,
- If the calculation of C_2 crashes: $C_2 = 1.0$.

Using these corrections, a small program was written in Python language. This program can be used for estimating maximal allowable pressure for a given geometry and material of a flat end with relief groove.

Acknowledgements

The authors gratefully acknowledge financial support provided by Technology Agency of the Czech Republic within the research project No. TE02000236 “Waste-to-Energy (WtE) Competence Centre”.

References

- [1] ČSN EN 13445 Netopené tlakové nádoby, Úřad pro technickou normalizaci, metrologii a státní zkušebnictví, Praha, 2012. (in Czech)
- [2] Hunter, J.D., Matplotlib: A 2D graphics environment, Computing In Science & Engineering, 9 (3) (2007) 90-95.

Experimental investigation of deformations in human pelvis

L. Lobovský^a, J. Hartlová^b, M. Salášek^c, J. Krystek^a, R. Zemčík^a, J. Křen^b

^aNew Technologies for the Information Society, Faculty of Applied Sciences, UWB in Pilsen, Univerzitní 22, 306 14 Plzeň, Czech Republic

^bDepartment of Mechanics, Faculty of Applied Sciences, UWB in Pilsen, Univerzitní 22, 306 14 Plzeň, Czech Republic

^cClinic for Orthopaedics and Traumatology of Locomotive Organs, University Hospital, alej Svobody 80, 304 60 Plzeň, Czech Republic

Human pelvis injuries may be accompanied with fractures of pelvic bones which have to be treated surgically. In order to fix the relative position of fractured bone parts, various fixation techniques can be applied. For example, a fracture of sacral bone may be fixed using the iliosacral screws, which are screwed into sacrum through an iliac bone and attaches the two fractured parts of sacral bone together. Such a fracture can be also treated using the transiliac plate or the transiliac fixator, which do not fix sacrum directly but constraint the relative motion of both iliac bones. Even if a bone fixation is applied, a minor relative motion of fractured parts of the bone may be observed. This relative motion influences the bone healing process. Thus determining an effectiveness of various fixation techniques is of interest so that an optimal type of fixation can be selected for a given fracture. Before approaching the analysis of various fixations, a methodology for experimental investigation of deformations of pelvic ring bones has to be assessed. Within this study a non-invasive optical methods are exploited.

The orthopaedic plastic model of intact male pelvis was subjected to well defined mechanical loading and its deformations were analysed using photogrammetric approaches and techniques of digital image correlation.

The material properties of the plastic model of human pelvis resembles mechanical behaviour of real pelvic bones. The model was mounted on a dedicated metal stand that was designed and manufactured in order to provide a rigid support to pelvis in acetabula such that the position of pelvis was fixed in space and its rotations in the sagittal plane were prevented during the entire test. For fixation of the acetabula, the artificial femoral head was created as a three-dimensional negative of each acetabulum surface.

The prescribed mechanical loading was applied by the mechanical testing device at the base of the sacrum (articulation surface for the intervertebral disc L5/S1). A maximum load of 500 N was utilised, which corresponded to approximately 60 % of body weight for a 80 kg male. The deformation of pelvic bones, the displacement of selected points on their surface respectively, was studied for various states of loading.

The experimental data were analysed using two independent photogrammetric software packages, SPGM [2] and ISTR4 4D [1]. The former is capable of determining spatial three-dimensional coordinates of selected object points based on their images recorded by two separate cameras at the same instant. Thus for the SPGM analysis, it was necessary to cover the surface of pelvic bones by distinct target points, Fig. 1 (left). Furthermore, a novel software tools were developed that enabled localisation and correlation of the target points in each captured image and enabled an automated feed of data for callibration of the analysed scene.

The ISTR4 4D software package is capable of reconstructing the three-dimensional object surface based on correlation of images from multiple cameras (i.e. two and more). Such a

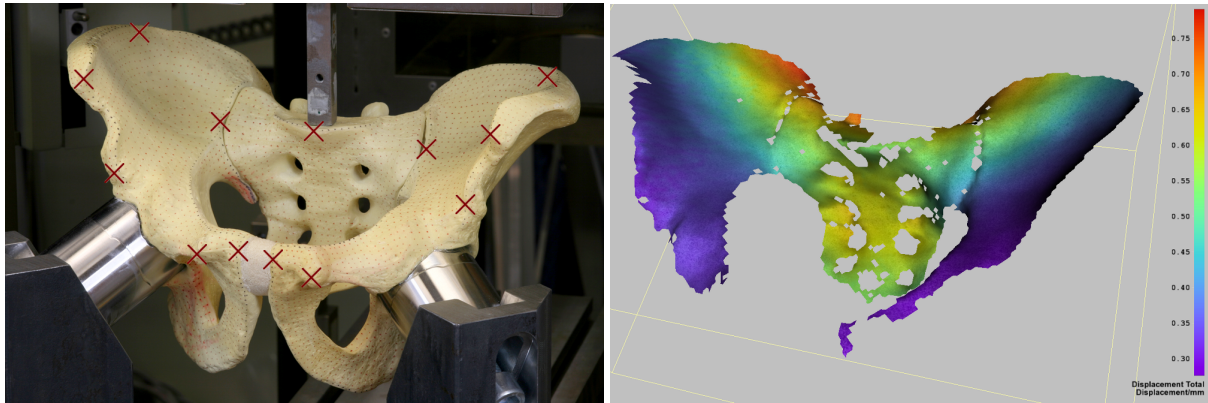


Fig. 1. The orthopaedic plastic model of male pelvis and the position of target points that were analysed by SPGM software (left), analysed displacements at the surface of the plastic model by ISTR A 4D software (right)

correlation requires a random speckle pattern which was sprayed on the pelvic surface before the images for ISTR A 4D analysis were recorded. The resulting reconstruction of the pelvic surface based on images from four camera system is shown in Fig. 1 (right). The colormap reflects the displacement between the loaded and unloaded state at various locations.

Both implemented methods, i.e. SPGM analysis as well as ISTR A 4D, were capable of resolving displacements at selected locations while maximal magnitude of the recorded displacements was in order of 1 mm. The multi-camera analysis of ISTR A 4D is superior to two-camera analysis by SPGM in reconstructing the complex three-dimensional surface of pelvic ring.

A reliable methodology for preparation of the tested specimen, its experimental testing, the optical setup and the resulting analysis process was determined. The presented data serve both as a starting point for the upcoming experimental campaign on pelvic ring fixation techniques and as a reference data for validation of the computational model used at NTIS – New Technologies for the Information Society research center.

Acknowledgements

The research leading to these results has been supported by the European Regional Development Fund (ERDF) project "NTIS – New Technologies for the Information Society", European Centre of Excellence, CZ.1.05/1.1.00/02.0090 and by the grant SVV 2014 No. 260 052.

References

- [1] ISTR A 4D, software, Dantec Dynamics. (<http://www.dantecdynamics.com/q-400-dic>)
- [2] Zemčík, R., SPGM, software, University of West Bohemia. (<http://www.kme.zcu.cz/software/spgm-14>)

Database FinLiv – focus on Manson-Coffin curves

M. Lutovinov^a, J. Papuga^a, D. Ličková^b

^a Faculty of Mechanical Engineering, Czech Technical University in Prague, Technická 4, 166 07 Praha, Czech Republic

^b Faculty of Mechanical Engineering, VŠB Technical University of Ostrava, 17.listopadu 15, 708 33 Ostrava, Czech Republic

FinLiv is a database intended to gather the information about material parameters of various static and fatigue material models. Fatigue databases are quite rare (www.matdat.com, www.practic.com/fatlim.php, www.efatigue.com), and consequently, the researchers tend to use second-hand data for their research, without any proper check that the data are of good quality and worth using [1]. Until now, now such database records also the basic input data from individual experiments and only the results of regression analyses are provided.

Such a database has to fulfill several functions – ability to input new data, list them, select between them. FinLiv is therefore prepared in two applications, which closely cooperate. The web part useful for listing or selecting the items from the database can be found on www.fadoff.cz/page/finliv. Anyhow, the direct use of the website for data input is demanding in terms of the application structure, patience of the potential user, etc. In order to simplify the way the data are entered another front-end application FinLiv.VBA was built as an MS Excel application written in Visual Basic for Applications. MS Excel is an application allowing us to program macros and make them easily accessible to a wide range of users.

VERSION	0.8		
Select test group:	<input type="button" value="FADOFF, 2011-2014"/>		
MARK	AAcheck		
ID_REF	ID 2014-015323		
ID_MAT	664	MAT_NAME	S355J0
G_COMMENT	MAT DESIGNATION of S355J0 alloy steel acc. to PN is 1802A		

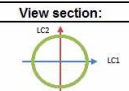
For information only:	
Curve	Type
501	1

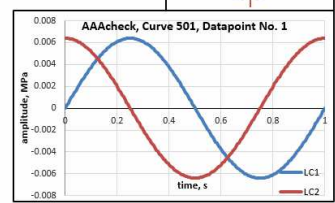
Description of load channels:				
LC	LC1 - MASTER	LC2	LC3	LC4
LC_MODE	tension-compression	torsion	no load	no load
LC_V1				
LC_V2				
LC_V3				
ID_TYPE	harmonic, constant amplitude	harmonic, constant amplitude		
LD_V1	x1	x1		
LD_V2	0	0		
LD_V3	1	1		
LD_V4	0	90		
LD_V5				
LD_V6				
LD_V7				
LD_V8				
LD_V9				

Choose a predefined load mode

Check the load path

View section:





END	not defined
END_PAR	
ROWS	60

Datapoint No.	1	2	3	4	5	6
Specimen mark						
Commentary						
Number of cycles till END	6900	2300	343	154	132	91
Master parameter [s]	0.0064	0.0071	0.0108	0.0144	0.019	0.0224
Stress amplitude LC2 [MPa]	163	184	216	233	239	240
Mean stress LC2 [MPa]						
Stress amplitude LC3 [MPa]						
Mean stress LC3 [MPa]						
Stress amplitude LC4 [MPa]						
Mean stress LC4 [MPa]						

Fig. 1. Sheet form of FinLiv with sample data

With the help of the application the user can easily input data via the main interface, which is represented by the “form” sheet. The data are set by selecting predefined options from the lists in the various list boxes, as well as by entering values into appropriate cells directly. Any additional data that cannot be assigned to the categories listed in the “form” sheet can be entered into cells reserved for comments. The input data are stored in one of the data sheets appended to the FinLiv workbook, where it can be later corrected manually. More experienced users can efficiently input the data directly to those data sheets and use the copy and paste function, which increases the speed of data input.

In addition to the previous functionality of FinLiv to gather and process the data of S-N curves, the new version [2] allows the users to work with data obtained from strain-controlled fatigue experiments. The data table in the “form” sheet is designed for entering experiment data such as master parameter (strain), mean and stress amplitudes for different load channels, etc. Ability to process the multiaxial loads is an important feature of FinLiv. The settings of each channel are set in the table “Description of load channels”. There the user can choose a load channel mode such as tension-compression, torsion, and plane bending, and choose a load history type.

With the help of the application the user can prepare input from experimental data for regression analysis and then get the regression parameters. The input for regression analysis is created automatically upon clicking the button “Input For Regression”. The application validates input data and then creates a txt-file that represents input for regression analysis. The regression analysis is performed in an external MATLAB application that prints out a txt-file with regression parameters from Manson-Coffin and Ramberg-Osgood models, as well as measures of statistical correlation of the regression curves with experimental data. The user can load the regression parameters from the output file to a corresponding datasheet with the help of the “Get regression data” button.

The application allows the user to display the data in a predefined form in order to compare different material sets, different load setups, etc. – both in terms of charts and graphs. Upon clicking the button “Show” the user can select the desired sets. After the fatigue curves are selected, a new workbook is created. The new workbook contains sheets with separate curves where the user can find basic information about the material, regression parameters and regression graphs. A summary sheet, where the user can compare different curves is prepared automatically.

The paper introduced in short a new useful application for cataloguing fatigue material parameters and data. It guided the user through the basic functionality of that application and presented new features for processing Manson-Coffin curves and their base data.

Acknowledgements

The work, results of which are presented here, was supported by TA01011274 grant project of TAČR and by SGS14/181/OHK2/3T/12 CTU grant. The authors thank for this support.

References

- [1] Papuga, J., Quest for fatigue limit prediction under multiaxial loading. *Procedia Engineering* 66 (2013) 587-597.
- [2] Papuga, J., Lutovinov, M., Help for FinLiv.VBA Excel database [ver. C], FME CTU in Prague & Evektor, spol. s r.o., Prague, 2014.

Dynamic response prediction of building loaded by traffic vibration, propagated through subsoil

D. Makovička^a, D. Makovička, Jr.^b

^a Czech Technical University in Prague, Klokner Institute, Šolínova 7, 166 08 Praha 6, Czech Republic

^b Static and Dynamic Consulting, Šultysova 170, 284 01 Kutná Hora, Czech Republic

Vibrations caused by road or railway vehicles running on surface or underground roads or rail tracks spread through the subsoil into surrounding building structures. These vibrations propagate into the surroundings of the traffic line through the geological environment and act as technical seismicity, which loads the buildings in the vicinity. Vibrations produced by traffic sources usually do not threaten the safety of structures, but their undesirable impacts can significantly lower the quality of life and the working conditions of people living or working in residential or office parts of the building.

The histories of measured vibrations (Fig. 1) were used as loads applied to a modelled building structure at the foundation base. The nature and magnitude of the vibrations caused by technical seismicity depend not only on the proximity and the nature of the source of the vibrations, but also on the local geological conditions and on the structure of the affected building. Due to its tuning, the building structure usually amplifies or, in better cases, reduces the effects of technical seismicity.

Vibro-base isolation is an effective method for reducing the vibration level of the protected structure as a whole with reference to its foundation types (plate, piles, strips, etc.). Base isolation is one of the most powerful passive structural vibration control technologies in earthquake engineering. It is meant to enable a building or some other structure to survive a potentially devastating seismic (or in our case technical seismic) impact through suitable initial design or subsequent modifications. In some cases, the application of base isolation can considerably raise both the seismic performance and the lifetime of a structure.

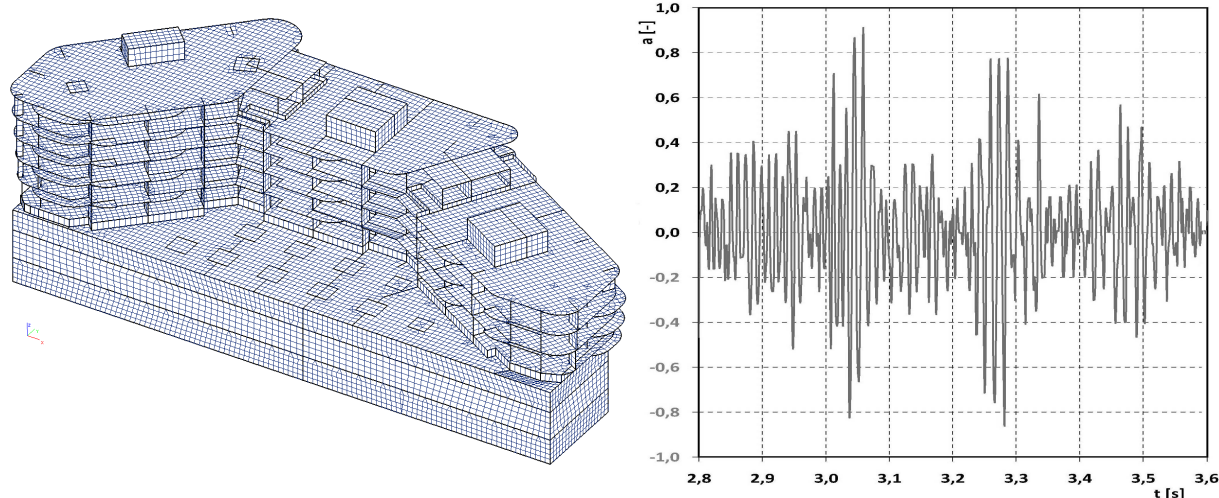


Fig. 1. Dynamic vertical response one of buildings and its normalized excitation

The calculation 3D model takes into account the individual storeys, broken down into the floor, foundation and roof slabs, columns, load-bearing walls and peripheral and interior girders (Fig. 1). For the vibroisolated structure the elastic layer of rubber on the level of baseplate was used and usually considered as the elastic subsoil of the Winkler-Pasternak model below the whole area of the upper part of the foundation plate. The mass of the floor and the foundation plates includes the masses of the non-load-bearing components (thin partitions, floorings, etc.) as well as the equivalent of the live loads of floors, roof and terraces. For the dynamic response to the effects of external actions (traffic), the lowest possible tuning of the rubber-mounted structure is decisive.

The dynamic load, i.e., the vibrations, was introduced into the model independently for both directions as a normalized load and with the identical phase all over the foundation plate. The vibrations of the building produced by underground traffic were predicted by the response analysis of the whole system (Fig. 2) for selected points as normalized displacements (in relation to the base-plate vibration).

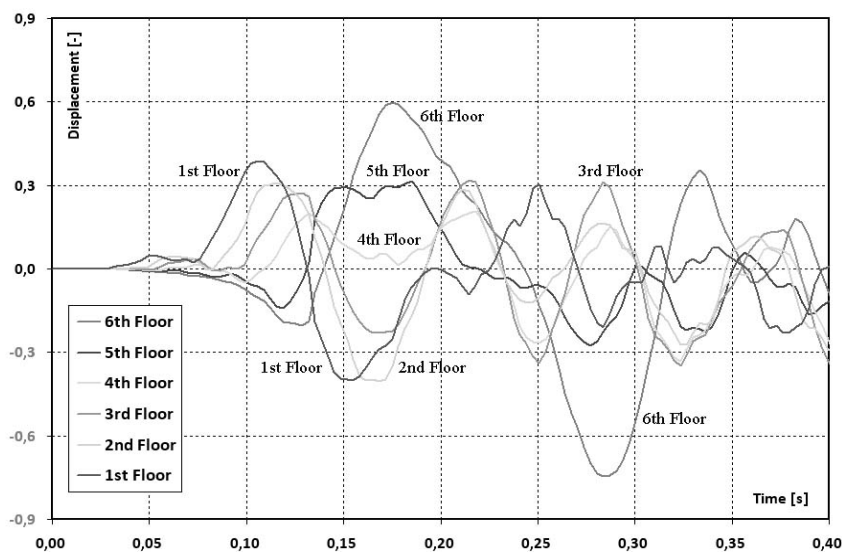


Fig. 2. Typical time histories of relative horizontal displacements for horizontal excitation

The application of vibro-isolation is, consequently, a very efficient way to reduce the transfer of vibration from the subsoil to the interior parts of the building. The floor acceleration response for each storey should be estimated in such a case, as it is the most important response parameter namely for comfort of residents, protection of contents and equipment of the building.

Acknowledgements

This research has been supported as a part of the grant project GAČR P105/11/1580, for which the authors would like to thank the Agency.

References

- [1] Makovička, D., Makovička, D., Effect of vibro-insulation on restriction of vibration transfer from subsoil into the building, *Journal of Mechanics Engineering and Automation* 2 (5) (2012) 289-293.
- [2] Makovička, D., Makovička, D., Jr., Vibro-base isolation of a building to decrease the technical seismicity effect, Brebbia, C.A., Hernández, S.: *ERES IX*, Vol 132, WIT Press, Southampton, 2013, pp. 323-331.

Direct dynamic response computation of an aircraft structure based on experimentally identified modal model

P. Malínek ^a

^a Aeronautical research and test establishment, Beranových 130, 19905 Prague, Czech Republic

Modal model contains a valuable data, joined to a specific aircraft type structure. So called Ground vibration test as a standard milestone of a prototype testing provides experimentally identified modal model suitable to enter in to the fine tuning process of structure numerical model. Finally tuned numerical model serves as a base for flutter clearance and other simulation of aircraft structural dynamics related phenomena: gust response, excitation due to failure of a rotating part.

The paper presents a technique of dynamic response computation of an aircraft structure using modal model directly, without any need of FEM model and its costly tuning. The basis of the technique is a numerical solution of convolution integral in n-dimensional space. Excitation forces are supposed arbitrary waveforms. In the special case of periodic forces the responses are calculated via transfer functions. The technique gives possibility to compute time domain responses at any spatial point of the structure.

Modal model and excitation forces presuppositions: Only complex (oscillatory) eigenvalues are considered. Modal model should be of highest quality, level 4, see [2], p. 164. Spatial resolution of original experimental modal model enables correct interpolation and extrapolation of mode shapes. Modal model may be non complete. Frequency content of excitation forces fit to modal model frequency limits. Forces are acting at nodal points only.

We begin a brief theoretical review with standard mathematical model of linear structure in physical space or in the state space:

$$M\ddot{q}(t) + B\dot{q}(t) + Kq(t) = F(t), \quad \begin{bmatrix} 0 & M \\ M & B \end{bmatrix} \begin{bmatrix} \ddot{q} \\ \dot{q} \end{bmatrix} + \begin{bmatrix} -M & 0 \\ 0 & K \end{bmatrix} \begin{bmatrix} \dot{q} \\ q \end{bmatrix} = \begin{bmatrix} 0 \\ F \end{bmatrix}.$$

Corresponding modal model consists of right side and left side modal matrices $U_{(m \times n)}$ and $W_{(m \times n)}$ and of spectral matrix $A_{n \times n}$, $n < m$.

$$U = \begin{bmatrix} u\lambda & u^* \lambda^* \\ u & u^* \end{bmatrix}, \quad W = \begin{bmatrix} w\lambda & w^* \lambda^* \\ w & w^* \end{bmatrix}, \quad A = \text{diag} \begin{bmatrix} \lambda \\ \lambda^* \end{bmatrix}.$$

This description of linear structure can handle non conservative and gyroscopic systems [1]. Using modal decoupling we obtain response function H in frequency domain

$$u(t, \omega) = U(i\omega I - A)^{-1} W^T f(t, \omega), \quad q(\omega, t) = (UDW^T + U^* D^* W^{*T}) F = H(\omega) F(\omega, t).$$

$$H_{rs} = \sum_n \left(\frac{u_{rn} w_{ns}}{i\omega - \lambda_n} + \frac{u_{rn}^* w_{ns}^*}{i\omega - \lambda_n^*} \right) = \sum_n \frac{A_{rsn}}{i\omega - \lambda_n} + \sum_n \frac{A_{rsn}^*}{i\omega - \lambda_n^*}.$$

An application of Laplace transforms to the decoupled system of differential equations finally provides time domain general solution of original state space model. For $t = 0$, $u = 0^T$.

$$x(t) = \int_0^t W^T f(\tau) e^{A(t-\tau)} d\tau, \quad u(t) = U \int_0^t W^T f(\tau) e^{A(t-\tau)} d\tau, \quad \text{where } u(t) = [\dot{q}(t)^T, q(t)^T]^T.$$

We assume time series of equidistant discrete samples as a model of forces vector. The description by Fourier series is appropriate in the special case of periodic forces.

$$F_j = \sum_{k=0}^{\infty} F_{kj}(t) = \frac{1}{2} \sum_{k=0}^{\infty} (F_{ckj} - iF_{skj}) e^{\frac{i2k\pi t}{T_j}},$$

$$F_{skj} = \frac{2}{T_j} \int_0^{T_j} F_j(t) \sin\left(\frac{2k\pi t}{T_j}\right) dt, \quad F_{ckj} = \frac{2}{T_j} \int_0^{T_j} F_j(t) \cos\left(\frac{2k\pi t}{T_j}\right) dt.$$

Let we have modal matrix $\mathbf{u} = \mathbf{w}$ and corresponding spectral matrix λ as a result of modal test. Its meaningful application in the method of direct response calculation is possible with only proper scaling of modes. It is necessary to use an orthogonality condition for the state space formulation $\mathbf{W}^T \mathbf{N} \mathbf{U} = \mathbf{I}$ and $\mathbf{W}^T \mathbf{P} \mathbf{U} = -\mathbf{A}$ instead of $\mathbf{u}^T \mathbf{M} \mathbf{u} = \mathbf{I}$, $\mathbf{u}^T \mathbf{K} \mathbf{u} = \lambda$. If we have experimentally determined modal masses μ_j for corresponding modes j , next formula provides normalization factor $c_j = (i2\mu_j \lambda_j)^{-1/2}$. Other steps are response model calibration and validation, which means fine adjustment of normalization factors so that calculated responses fit to experimental results if they are at disposal.

The numerical procedure solving convolution integral exploits trapezoidal scheme of numerical integration in n-dimensional extension. Complex arithmetic is used in the procedure. Effectiveness of the procedure is given by minimising of arithmetic operations per one integration step by reducing the number of coordinates into forces inputs and required responses only. The state space formulation doubles the dimension of the problem, yet it gives information on velocities directly. Accelerations are computed immediately by numeric derivation of velocities responses.

Validation of the procedure has involved responses computation of a 3 DOF discrete system. In the first step the responses of the system to a rectangle force impulse were calculated by Newmark's numerical integration of original differential equations. In the second step differential equations were solved through an algebraic eigenvalue problem. Resulting modal model then enters to the procedure solving convolution integral. Responses calculated via completely different procedures match well, Fig. 1. Other verification included responses calculation using experimentally derived modal model of the demonstrator Noll-Wing consisting of 8 modes of a system with 27 DOF.

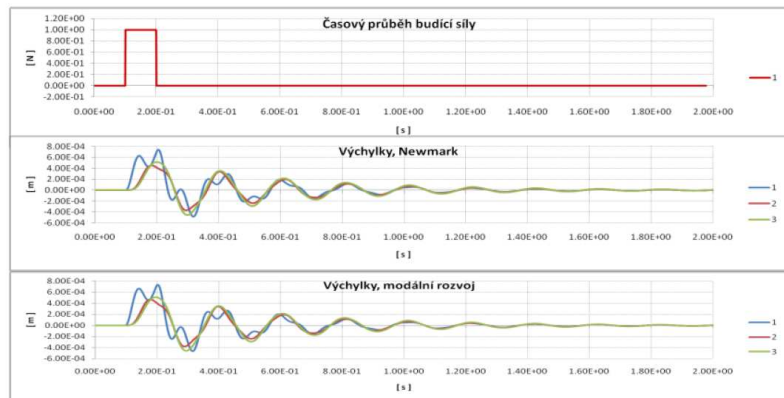


Fig. 1. Responses of 3 DOF - system to rectangular force impulse, comparison of Newmark's integration method and convolution integral solution procedure

Acknowledgements

The work has been supported by the research project STRATEX granted by The Ministry of Industry and Trade of Czech Republic.

References

- [1] Byrtus, M., Hajžman, M., Zeman, V., Dynamics of rotating systems, ZČU v Plzni, Plzeň, 2010. (in Czech)
- [2] Ewins, D.J., Modal testing: Theory, practice and application, RSP, 2000.
- [3] Malinek, P., Modal model application in dynamic response calculation of a structure excited by forces of arbitrary waveform, Report VZLÚ, R-5786, Praha, 2013. (in Czech)

Can Laplace law replace more sophisticated analyses of aortic aneurysms?

V. Man^a, K. Novák^a, S. Polzer^a, J. Burša^a

^a *Institute of Solid Mechanics, Mechatronics and Biomechanics, Brno University of Technology, Technická 2896/2, 616 69 Czech Republic*

In the recent studies it was shown that for credible calculation of stresses in the wall of abdominal aortic aneurysm (AAA) patient-specific (PS) geometry with inclusion of the unloaded geometry should be taken into account, as well as residual stresses which results in rather complex models giving nearly constant stress distribution throughout the wall thickness. These features makes the computational analysis rather complex and time-consuming while the stress distribution resembles membrane stress state being independent of material if the deformed radii of curvature are taken into consideration. In the paper stress distributions calculated on the basis of different finite element (FE) models of AAAs are compared in between and with Laplace law results to assess the acceptable simplifications.

Stresses in a shell can be calculated on the basis of Laplace law under assumption of their constant magnitude through the shell thickness. This is the case for thin shells made of linear elastic materials, while the stress gradient throughout the wall increases with the wall thickness and nonlinearity of the stress-strain dependence [1]. Recently FE models of AAAs have confirmed their credibility if unloaded PS geometry is used (obtained e.g. by backward incremental method) and residual stresses (RS) are introduced on the basis of volumetric growth applied to achieve a homogeneous stress distribution through the wall thickness [2]. Here this model is denoted as model A when Vande Geest-like (VG) constitutive model is applied and as model B when quasi-linear 2nd order Yeoh (QL) constitutive model with high stiffness (corresponding to the slope of the stress-strain curve under high strains) is used. Both of these models induce membrane-like stress states in shells with regular geometric shapes (cylinder, sphere, ellipsoid). For both cylindrical and PS geometries, the results are then compared with a much simpler model C (without residual stresses, based on the loaded geometry and QL constitutive model) to test a hypothesis that this simplification could offer acceptable results. If this was true for PS models of AAAs, the comprehensive finite element models (A or B) could be replaced by the much simpler model C giving results similar to those obtained by Laplace law.

Stresses in a shell with simple geometry are illustrated with a cylinder. While without residual stresses the results are highly dependent on constitutive models, here models A, B or C give similar stress distributions corresponding to membrane stress obtained by Laplace law applied on the deformed geometry (see Fig. 1). For model C (without residual stresses) this can be explained by the high stiffness of the model causing negligible differences between the deformed and undeformed dimensions. Then models A, B and C were applied with a PS geometry (recorded under mean blood pressure). As locations of peak wall stresses (PWS) can be different for these models, the results are compared on node-to-node basis. The error rates (Fig. 2) show differences comparable with the calculated PWS for all combinations of models.

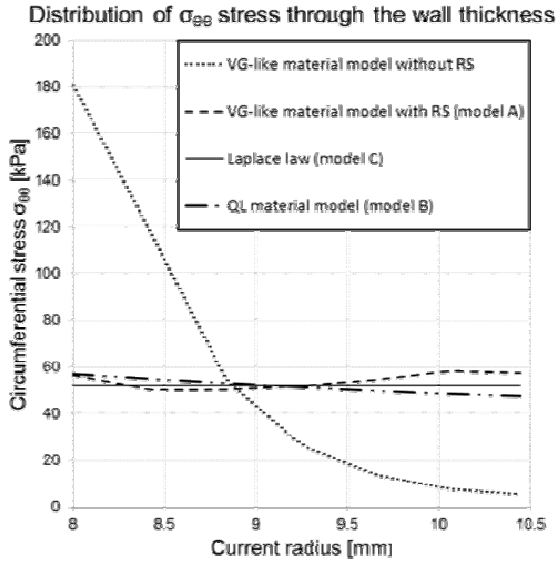


Fig. 2. Comparison of circumferential stresses for cylindric shape and different models

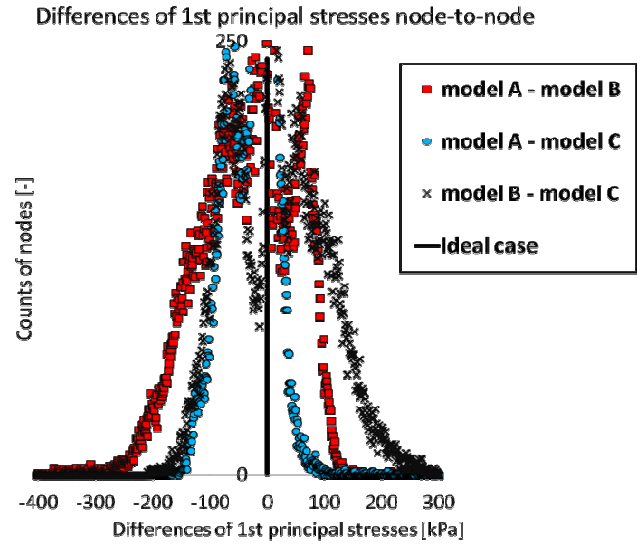


Fig. 1. Frequencies of deviations in 1st principal stress for different models pairs with PS geometries

For simple geometrical shapes the sophisticated FE models give stress distribution and consequently also PWS similar to the Laplace law. Therefore results of the simple model C are acceptable here, if radial deformations of the model are constraint sufficiently by the high stiffness of the constitutive model. However, for the PS geometry considerable differences (comparable with the magnitude of stresses) occur. This can be explained by bending of the shell caused by changes in local shell curvature between unloaded and loaded shapes. This effect is especially pronounced if the shell consists of both convex and concave parts; then the calculated stresses depend highly on the constitutive model (in contradiction to Laplace law) and the simplified model C is not acceptable.

The simple quasi-linear constitutive model without residual stresses and without taking the AAA unloaded shape into account can offer acceptable results for simple geometrical shapes but is not applicable for credible evaluation of stresses in patient specific models of AAAs.

Acknowledgements

We gratefully acknowledge the support given to this work by Czech Science Foundation, grant project No.13-16304S and faculty project No. FSI-S-14-2344.

References

- [1] Holzapfel, G.A., Gasser, T.C., Computational stress-deformation of arterial walls including high-pressure response, *International Journal of Cardiology* 116 (2007) 78–85.
- [2] Polzer, S., A numerical implementation to predict residual strains from the homogeneous stress hypothesis with application to abdominal aortic aneurysms, *Ann Biomed Eng* 41 (2013) 1516–1527.

FE implementation of directional distortional hardening model for metal plasticity

R. Marek^{a,b}, J. Plešek^b, Z. Hrubý^b, S. Parma^b

^a Czech Technical University in Prague, Faculty of Mechanical Engineering, Technická 4, 166 07, Praha 6, Czech Republic
^b Institute of Thermomechanics, Academy of Sciences of the Czech Republic, Dolejškova 1402/5, 182 00 Praha 8, Czech Republic

As seen in numerous experiments, yield surfaces change their shape and location during plastic straining. Several models of directional distortional hardening to capture such behavior have been proposed recently. Their application lies in sheet metal forming processes, in combined ratchetting, or in any application containing sequenced non-proportional plastic straining.

The presented work outlines and tests the finite element implementation of the simplest form of directional distortional hardening models proposed in [2] by Feigenbaum and Dafalias – a model derived from a more complex one in [1], which involves a fixed scalar distortional parameter. Here, the directional distortion is dictated by the scalar contraction of the backstress tensor α and the unit radial tensor \mathbf{n}_r . Therefore, possible shapes of predicted subsequent yield surfaces are limited to certain size, position and elongation of the shape with orientation always facing from the origin, as demonstrated in Fig. 1. The evolution equations are based on the Armstrong-Frederick evanescent memory type hardening rule. The associative flow rule is adopted.

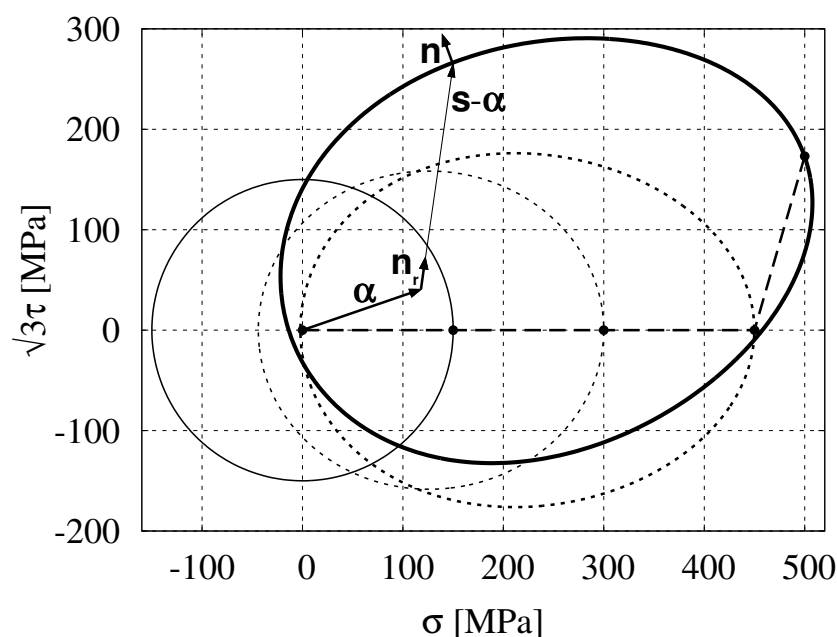


Fig. 1. Yield surface evolution – simple tension and tension-shear combined

Properties of the model are thoroughly studied in connection to convexity condition derived in [3] and later to numerical stability. The explicit integration scheme with subincrementation, the tangent stiffness-radial corrector method, is employed. Size limitations of integration increments are discussed in a series of iso-error maps. An easy to understand error map is depicted in Fig. 2. Subjecting a tensionally pre-evolved material to any combination of tension and shear strain will generate the following error for default subincrementation.

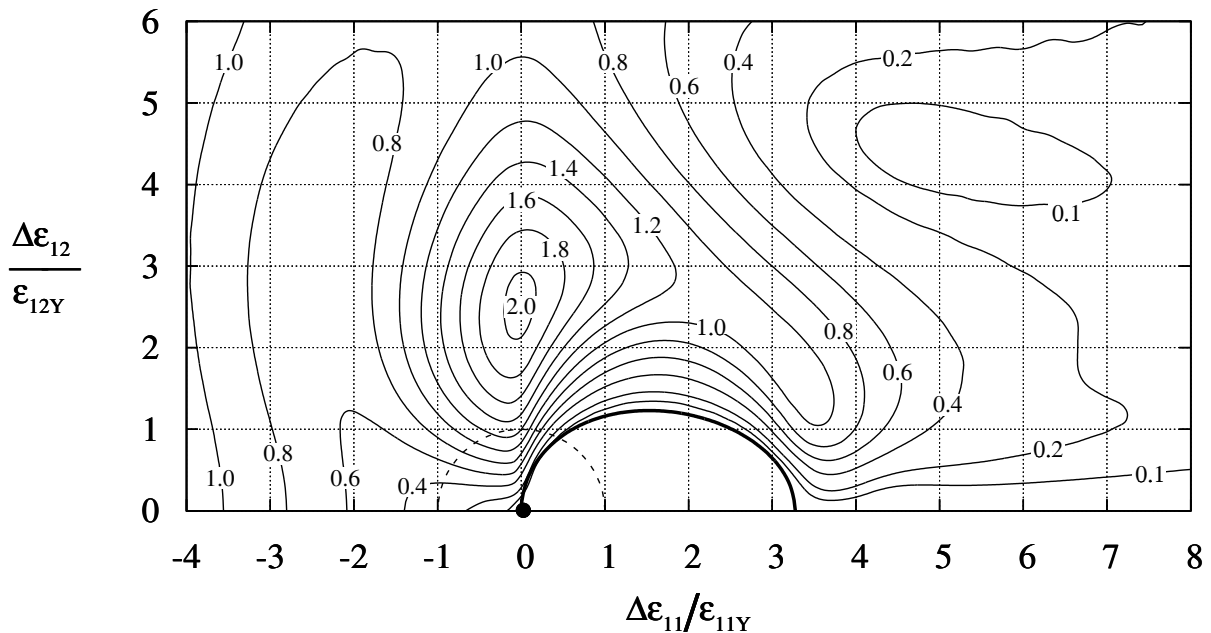


Fig. 2. Relative error [%] of the stress response, showing pre-evolved shape and initial unloaded state (black full circle) in strain space

The implementation is verified by a comparison of numerical results with analytical solutions pertinent to proportional load cases. Complex non-proportional loading paths are verified by a very fine numerical computation. Finally, the template of this implementation is presented.

This work studies phenomena in numerical implementation related to the yield surface shape distortion, therefore, it will help with other models to come.

Acknowledgements

This work was supported by GACR 101/09/1630, GACR P201/10/0357, and KONTAKT ME10024 granted projects in the framework of AV0Z20760514 research plan. R. Marek acknowledges support by the Grant Agency of the Czech Technical University in Prague, grant No. SGS12/175/OHK2/3T/12.

References

- [1] Feigenbaum, H., Dafalias, Y., Directional distortional hardening in metal plasticity within thermodynamics, *International Journal of Solids and Structures* 44 (22-23) (2007) 7526–7542.
- [2] Feigenbaum, H., Dafalias, Y., Simple model for directional distortional hardening in metal plasticity within thermodynamics, *Journal of Engineering Mechanics* 134 (9) (2008) 730–738.
- [3] Plešek, J., Feigenbaum, J., Dafalias, Y., Convexity of yield surface with directional distortional hardening rules, *Journal of Engineering Mechanics* 136 (4) (2010) 477–484.

Modelling of flexi-coil springs with rubber-metal pads in a locomotive running gear

T. Michálek^a, J. Zelenka^a

^a University of Pardubice, Jan Perner Transport Faculty, Department of Transport Means and Diagnostics – Section of Rail Vehicles, Detached Branch Česká Třebová, Slovanská 452, 560 02 Česká Třebová, Czech Republic

Nowadays, flexi-coil springs are commonly used in design of secondary suspension of rail vehicles. Besides their axial loading, these springs allow their lateral loading. Therefore, they are used to ensure the lateral suspension of the carbody as well as the elastic rotational joint carbody/bogie. It is necessary to know the lateral stiffness of these springs – knowledge of these characteristics is needed at a proposal of parameters of running gear of the vehicle and also as an input for simulations of running performance of the vehicle. The lateral stiffness of flexi-coil springs influences a moment against bogie rotation, which arises at the run of the vehicle through a curve. Because the moment against bogie rotation is related to the lateral force interaction vehicle/track in curves, which is assessed in framework of approval process of the vehicle according to the *technical specifications for interoperability* [1], it is desirable to minimize the lateral stiffness of the springs. This is the reason why the flexi-coil springs are often supplemented with various types of rubber-metal pads.

If a theoretical calculation of the lateral stiffness of a flexi-coil spring itself is a relatively difficult problem and commonly used empirical formulae (see e.g. [4]) give different results, an exact determination of the lateral stiffness of a flexi-coil spring with rubber-metal pad is very problematic. An often used type of the rubber-metal pad, which allows tilting of the end coil of the spring, is depicted in Fig. 1. In framework of research activities of the Jan Perner Transport Faculty of the University of Pardubice, a flexi-coil spring of secondary suspension of a locomotive supplemented with the tilting rubber-metal pad was put to a theoretical analysis and subsequent experimental verification of the lateral stiffness (see [2]). In the next stage, the measured lateral stiffness of the assembly spring/pad was approximated by means of a suitable function of vertical load, direction of the lateral loading and lateral deformation of the assembly. An example of the function (for a given vertical load) is presented in Fig. 2.

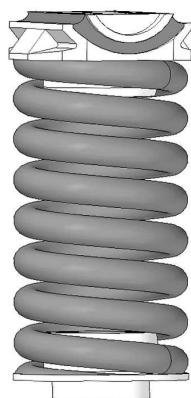


Fig. 1. Flexi-coil spring with tilting rubber-metal pad

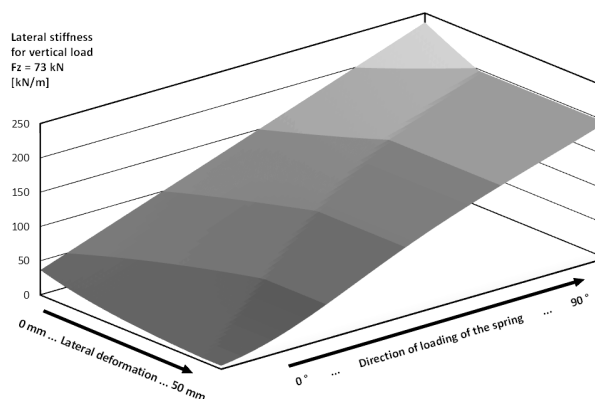


Fig. 2. Approximated characteristics of lateral stiffness of the assembly spring/pad – dependency on lateral deformation and direction of loading

Subsequently, this stiffness characteristic was implemented into a modified multi-body simulation model of a 90-ton electric locomotive created in the simulation tool *SJKV*, which has been developed at the Jan Perner Transport Faculty (see e.g. [3]). The modification of the model is based on more detailed description of joint elements (springs, dampers, etc.). Newly, these elements are modelled in such way that each element is represented by a separate joint. Especially in case of springs with a significant anisotropy of their lateral stiffness (caused by the tilting pads), this approach is necessary because the “classical” way of modelling of joints – i.e. by *reduced parameters* (lateral stiffness of suspension, resistance against bogie rotation, etc.) – seems to be insufficient for realistic description of dynamic properties of the model.

By means of the new model, a large set of simulations of run of the vehicle through curves with various radii was performed and the guiding behaviour of the locomotive was observed. The simulation results (together with results of performed theoretical analysis of properties of secondary suspension created with the springs with tilting pads) show specific properties of the *resistance against bogie rotation*. In case of the locomotive equipped with the above mentioned secondary suspension, the resistance against bogie rotation – which influences for example the safety against derailment and is assessed according to [1] by means of a quantity called *X-factor* – is dependent on the *cant deficiency*, i.e. on the speed in curve. It means that a reduction of the resistance against bogie rotation is most significant at zero cant deficiency, i.e. at a relatively low speed of run through a curve but also at the run in straight track, which is not desirable because of a negative influence of the lower resistance against bogie rotation on the *stability of vehicle run*. In the opposite case of run through a curve at high value of cant deficiency, when the softening of the resistance against bogie rotation is needed because of its positive effect on lateral force interaction between the vehicle and the track, the reduction of the resistance against bogie rotation is not as significant as it would be desirable. These properties of the resistance against bogie rotation are caused with the total deformations of individual secondary springs, which arise in relevant situations (i.e. during the run with a low or high value of the cant deficiency) and which are related with the lateral stiffness of the assemblies spring/pad under a given lateral load in given direction of lateral loading.

Knowledge of the above described behaviour of the resistance against bogie rotation of the investigated locomotive is very important at design of yaw damper characteristics and can be also used as a base for a proposal of characteristics of devices for reduction of lateral forces vehicle/track (i.e. a bogie coupling or system of active elements). Besides to that, the achieved results show that the current method of the *X-factor* calculation must not always characterize the real properties of the rotational joint carbody/bogie very well.

Acknowledgements

This work was solved in framework of the project TE01020038 “Competence Centre of Rail Vehicles” of the Technology Agency of the Czech Republic. Attendance on the conference was financially supported by the European project ESF CZ.1.07/2.3.00/20.0176 “IRICoN”.

References

- [1] 2011/291/EU. Commission Decision of 26 April 2011 concerning a technical specification for interoperability relating to the rolling stock subsystem — Locomotives and passenger rolling stock of the trans-European conventional rail system.
- [2] Michálek, T., Vágner, J., Kohout, M., Zelenka, J., Analytical calculation and experimental verification of lateral stiffness of a flexi-coil spring with tilting rubber-metal pad, *Scientific Papers of the University of Pardubice, Series B – The Jan Perner Transport Faculty* 19 (2013). (in print)
- [3] Michálek, T., Zelenka, J., Reduction of lateral forces between the railway vehicle and the track in small-radius curves by means of active elements, *Applied and Computational Mechanics* 5 (2) (2011) 187-196.
- [4] Vágner, J., Hába, A., Possibilities of assessing lateral stiffness of flexi-coil springs, *The Scientific and Technological Anthology* 30 (2010). (in Czech)

Crack propagation in welded polyolefin pipes

J. Mikula^{a,b}, P. Hutař^a, M. Ševčík^{a,b}, L. Náhlík^{a,b}

^aInstitute of Physics of Materials, Academy of Sciences of the Czech Republic, Žižková 22, 616 62 Brno, Czech Republic
^bBrno University of Technology, Technická 2896/2, 616 69 Brno, Czech Republic

A very common material used in piping industry, especially when it comes to pressure pipe applications, is the high density polyethylene (HDPE). Many advantages in compare to steel or other materials prefers it to serve mainly for water and gas transportation. Required lifetime of welded pipes is approaching 100 years, therefore lifetime prediction is one of the key issue in this field.

The most common failure of the pipes is a quasi-brittle failure which is a consequence of the slow creep crack propagation through the pipe wall. According to relevant literature the creep crack in polyethylene can be described by the stress intensity factor [2]. Therefore, in the present work the failure of butt welded pipes was modeled using a fracture mechanics approach.

Two different geometries have been considered to find the influence of the changes caused by the welding process on crack behavior. One of the geometries keeps the optimal weld bead while for the other one the weld bead was removed after the welding was finished, keeping just the material inhomogeneity caused by the welding process.

The purpose of the research was to make a more complex analysis on crack propagation, whether it is an axial or circumferential crack initiating at different places of the welded pipe.

The material inhomogeneity (also shown in the figure as a distribution of Young's modulus) was experimentally measured based on microhardness tests [3] and the results were approxi-

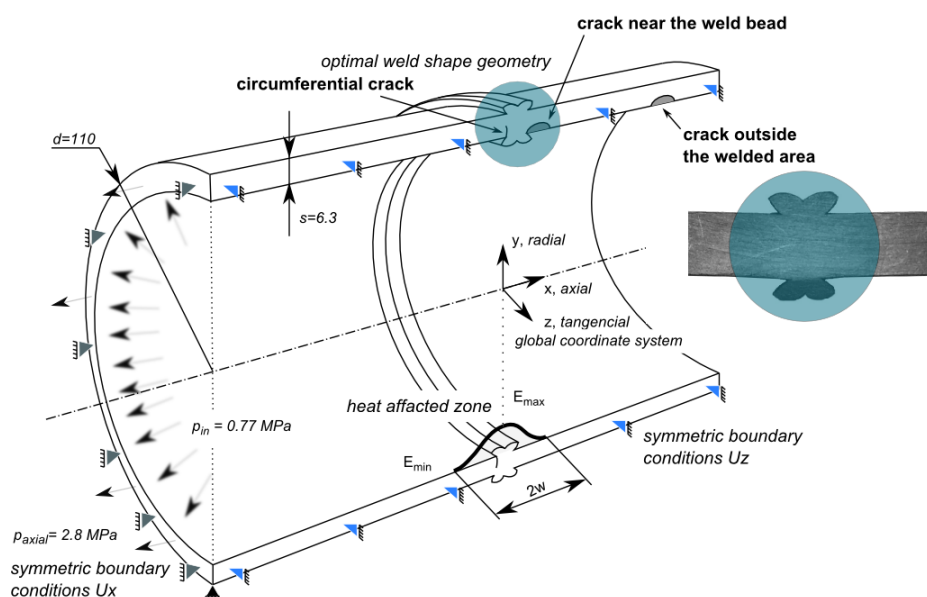


Fig. 1. Welded pipes with the optimal weld bead geometry

mated with a double power law function sketched in Fig. 1. The values of Young's modulus are highest in the centre of the weld and decrease approaching the basic material.

Finite element calculations within the commercial package ANSYS have been used to assess the fracture mechanics parameters. The kinetics of the creep crack growth may be thus described by the K_I . For the axial crack a 3D model was created whereas for the circumferential crack an axisymmetry gives the advantage for making a 2D model. For the first one the K_I was estimated based on the direct method and for the latter one the nodal displacements were used to estimate both the K_I and K_{II} , where the crack propagation was simulated by the maximal tangential stress criterion (MTS).

Knowing material parameters and the K_I the lifetime of slow crack growth can be calculated based on a power function as originally proposed by Paris and Erdogan [1]. Time to failure diagram for different axial cracks plot in Fig. 2 shows that keeping of the weld bead might have a good contribution on crack propagation because it increases the lifetime even if the axial crack propagates near the notches of the bead. Removing of the weld bead makes the area near the weld weaker and may decrease the lifetime considerably.

As for the circumferential crack, only high axial stresses and strong stress concentrations near the weld bead notches may lead to the situation when the crack would propagate. Thus in practical applications it is always more likely for an axial crack to appear.

Further, based on long-term CRB or PENT tests it may be shown that the welded area has a lower resistance to slow crack growth due to microstructural changes rather than the basic material. It can be concluded that keeping the weld bead makes the area near the weld stiffer and crack propagation in material affected region is suppressed.

The obtained results can further be used for service lifetime estimations of welded pipe systems where axial or circumferential cracks may appear.

Acknowledgement

This work was supported through the Grant No. P108/12/1560 of the Czech Science Foundation.

References

- [1] Frank, A., Hutař, P., Pinter, G., Numerical assessment of PE 80 and PE 100 pipe lifetime based on Paris-Erdogan equation, *Macromolecular Symposia* 311 (1) (2012) 112-121.
- [2] Hutař, P., Ševčík, M., Náhlík, L., Pinter, G., Frank, A., Mitev, I., A numerical methodology for lifetime estimation of HDPE pressure pipes, *Engineering Fracture Mechanics* 78 (2011) 3049-3058.
- [3] Lach, R., Hutař, P., Veselý, P., Nezbedová, E., Knésl, Z., Grellmann, W., Structural changes evolution of damage parameters and crack propagation behavior in welded plastic pipes, *Key Engineering Materials* 465 (2011) 427-430.

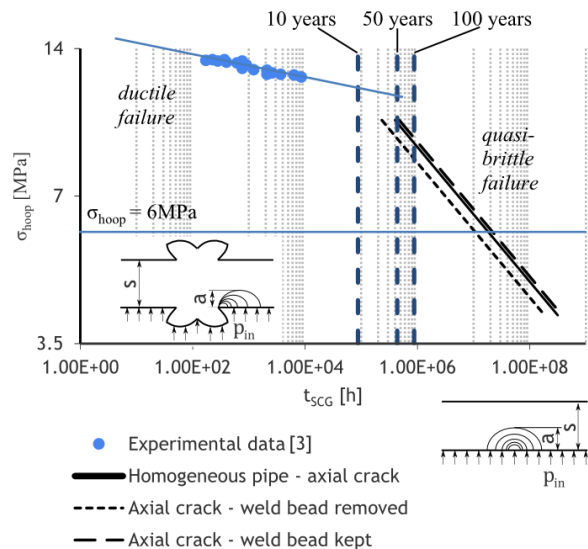


Fig. 2. Time to failure diagram of PE 100 (results for initial crack length $a_0 = 0.4$ mm)

Thermo-mechanical finite element analysis of mould for piston casting

M. Močilan^a, M. Žmindák^a

^a Faculty of Mechanical Engineering, University of Žilina, Univerzitná 1, 010 26 Žilina, Slovak Republic

The aim of this paper is the examination of the interaction of fluid and core molds for piston casting. Analysis of the core will be performed by finite element method. As a tool for FEM analysis will serve the commercial software ANSYS Workbench - Polyflow, which is often used in technical practice because of its fast and effective means of FEM model creation [1].

Computer Aided Design / Engineering (CAD / CAE) tools allow engineers to design moulds for piston casting [2]. In the last decades, together with the development of computers rose also the popularity of the finite element method (FEM) for the simulation of miscellaneous technological processes, such as welding, quenching, casting, cutting, etc. [3].

On the production line pistons for combustion engines made of aluminium alloy are cast into moulds. In the mould is the core, which is heated by flame after insertion (Fig.1). The mould and the core are subjected to extreme temperature changes. These components are made of tool steel. Cast pistons are made of aluminium alloy. Aluminium alloys are materials that are used to make the pistons because of low melting point, low weight of the piston, corrosion resistance, etc. The core is a massive forging, with nitrided surface. Core cooling is provided by a hole drilled in the bottom of the casting and water is injected into the hole. The melt is kept at a temperature of 775-785 ° C in the furnace. The mould filling time is 2-4 seconds. Opening of the bottom of the mould occurs after 60 seconds. The mould is preheated to a temperature of about 160 ° C.

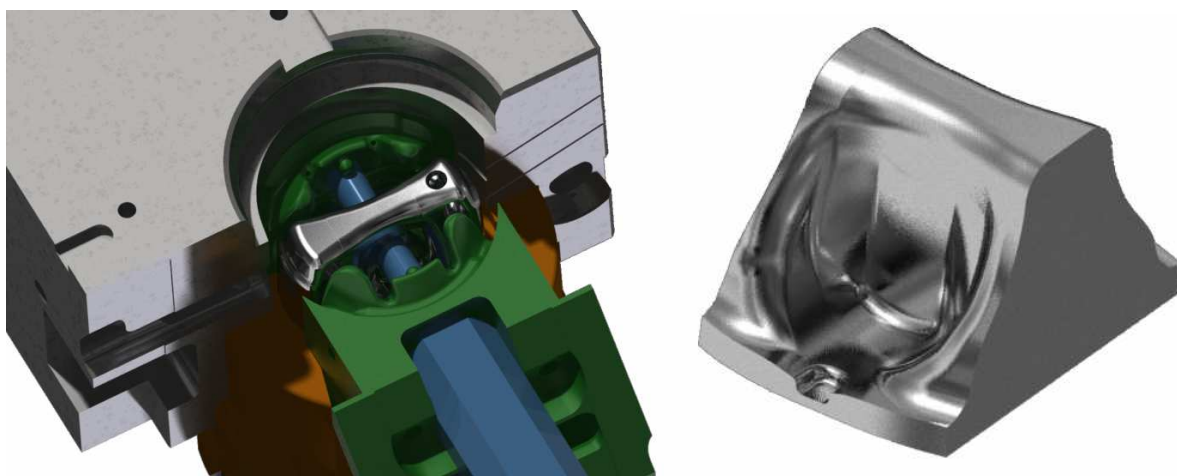


Fig. 1. CAD model of the mould (left) with the core (right)

We imported the geometry of the mould and core from the CAD software as *.stp into DesignModeler, which is integrated into the software ANSYS Workbench. We simplified the geometry of the mould to generate good mesh, reduce the number of elements and minimize errors in the simulation. We created a cut of the gating system common for the mould and the core. We eliminated the small fillets and chamfers, which were negligible in the calculation. The whole system is symmetrical, so we solved only one half. The picture shows the geometry of the core, which is the subject of our calculations. The core consists of three parts, the middle part is essential for us and we will focus on it in the simulations.

This paper is divided into two sections. The first part is a planar problem of non-isothermal Newtonian flow. It is a time-dependent simulation, where we examine the impact of fluid on the core. We want to evaluate the core temperature in contact with the liquid at different time steps. This knowledge will help us later to define boundary conditions for spatial 3D solution in the second part.

We used triangular elements, where the size of elements for the core is 2 mm and 3 mm for liquid and mould. We used adaptive mesh and re-meshing during the simulation. Fluid re-meshing was performed every 5 time steps. Zones with smaller element size have been set in the areas of interaction, for better filling of the space around the core and accurate calculation.

In the second part of the paper are shown the numerical results of the core stress field. We will not investigate the whole core, but only the central part in which cracks occur, so in this part we are mostly interested in the stress at each time step.

Acknowledgements

The work has been supported by the grant projects KEGA No.004ŽU-4/2012.

References

- [1] ANSYS 2012, ANSYS, Polyflow Users Guide [Technical guide of ANSYS], Canonsburg: ASYS, Inc, 2012.
- [2] Žmindák, M., Meško, J., Pelagić, Z., Zrak, A., Finite element analysis of crack growth in pipelines, *Manufacturing Technology* 14 (1) (2014) 116–122.
- [3] Žmindák, M., Novák, P., Meško, J., Numerical simulation of arc welding processes with metalurgical transformations, *Metalurgija* 49 (2) (2010) 595-599.

Model of robot with additional flexible deformation sensing for improved control

L. Mráz^a, J. Volech^a, Z. Šika^a, M. Valášek^a

^a Faculty of Mechanical Engineering, CTU in Prague, Technická 4, Praha 6, 166 07, Czech republic

The machining with industrial robot is nowadays an attractive area of interest for many researchers. The reason is the lower cost of robots in comparison with the traditional machines. On the other hand, the stiffness of the robots cannot compete the conventional machines. Several projects have arisen, which try to solve the low stiffness issue and thus to improve the accuracy of the position control e.g. [1, 2, 4]. The general principles are following: The precise model of the robot respecting all the flexibilities, the additional measurement of the real position of the robot and the final compensation of the errors.

The aim of this work is the development of a dynamic model of robot Mitsubishi RV-6S (Fig. 1). The model is assembled using the composite method for the flexible bodies [3]. The whole robotic structure is described using the relative coordinates in the joints expressing the movement of the arms. Their deformation is described using the modal coordinates. The deformation is considered to be a linear combination of the modal shapes and modal coordinates are the coefficients of this combination, which is time dependent. The modal shapes have been obtained using FEM analysis of the particular parts. Their geometry is obvious from the CAD model and the parameters of mass and stiffness have been estimated based on the material of them.

The deformation of the gearboxes is described by the relative coordinates of the motor rotors, which are connected by flexible gearboxes with the links. Based on [3] the final system of equations of motion (EOM) is obtained and the dynamic model of the robot is assembled in Matlab-Simulink environment.

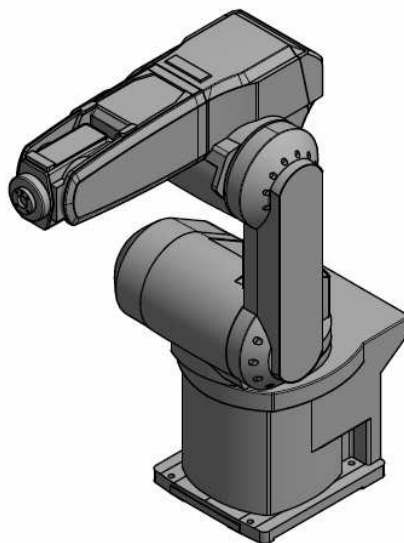


Fig. 1. Robot Mitsubishi RV-6S

Moreover, the cascade PID control have been designed and tuned for the robot model. The control block is used for the placement of the structure in desired position. The basic position is depicted in Fig. 1. In the first case, the end-point of the robot have been loaded in this static position and thus the structure deformed.

Using this model the behaviour of the flexible structure is observed. The model is virtually equipped with the sensors of deformations.

The measurement of the arms deformation is performed by the virtual laser-photodiode system [5]. The deformation sensing is following: The flexible arms are virtually equipped by the laser emitter on one side and by the photodiode on the other one (Fig. 2).

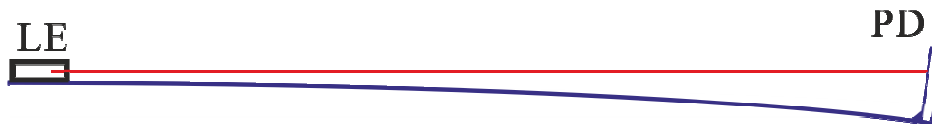


Fig. 2. Scheme of the flexible link equipped by laser emitter (LE) and by the photodiode (PD)

In the case of no loading, the laser beam is pointing to the center of the photodiode. If the loading is applied, the structure deforms and the position of the detector is changed. According to the intensity of the light on the surface of the detector, the deformation is measured. Moreover, the flexible gearboxes are virtually equipped with the rotary sensors for the torsional deformation sensing.

Thus a model is obtained, which simulate the dynamic behavior of the robotic structure with the deformation sensing. The resulting model provides the basis for the optimization of the sensors placing and for the complex optimization of the whole sensing concept. The further tasks should be the analysis of the observability and controllability of the structure in the working space. Thus the accuracy of the tool center point position control should be enhanced at the maximal level.

Acknowledgements

The authors appreciate the kind support by the grant GA13-39057S “Position Feedback Based Stiffness Increase of Robots by Redundant Measurement” of the Czech Science Foundation.

References

- [1] Abele, E., ADVOCUT, Abschlussbericht BMBF – Verbundprojekt, Adaptive vollserielle Werkzeugmaschine mit hochintegriertem mechatronischen Fräsmodul zur HSC-Bearbeitung, PTW, TU Darmstadt, Darmstadt, 2007.
- [2] Lehmann, C., Pellicciari, M., Drust, M., Gunnink, W.J., Machining with industrial robots: the COMET project approach, *Communications in Computer and Information Science* 371 (2013) 27-36.
- [3] Vampola, T., Valášek, M., Composite rigid body formalism for flexible multibody systems, *Multibody System Dynamics* 18 (3) (2007) 413-433.
- [4] Zengxi, P., Zhang, H., Improving robotic machining accuracy by real-time compensation, *ICROS-SICE International Joint Conference, Fukuoka, 2009*, pp. 4289-4294.
- [5] Zhen, H., Zhengxun, S., Shoufeng, T., Zhao, X., Hongfei, S., Huilin, J., Modeling of fine tracking sensor for free space laser communication systems, *Photonics and Optoelectronics 2009, SOPO 2009, Symposium on, 2009*, pp. 14-16. (doi: 10.1109/SOPO.2009.5230084)

Modelling and analysis of the 3D FGM beam structures

J. Murín^a, J. Hrabovský^a, V. Kutiš^a, J. Paulech^a

^a *Department of Applied Mechanics and Mechatronics, Faculty of Electrical Engineering and Information Technology, STU in Bratislava, Ilkovičova 3, 812 19 Bratislava, Slovak Republic*

Important classes of structural components, where Functionally Graded Materials (FGM) are used, are beams and beam structures. FGM beams play an important role not only in structural applications, but we can find many applications of the beam structures in thermal, electric-thermal or electric-thermal-structural systems (e.g. MEMS sensors and actuators, and other mechatronic devices). In all these applications, using new materials like FGM can greatly improve the efficiency of a system. FGM is built as a mixture of two or more constituents which have almost the same geometry and dimensions. Plasma spraying, powder metallurgy and other technologies are used for fabrication of such materials. From a macroscopic point of view, a FGM is isotropic in each material point but the material properties can vary continuously or discontinuously in one, two or three directions. The variation of macroscopic material properties can be caused by varying the volume fraction of the constituents or with varying the constituents material properties (e.g. by a non-homogeneous temperature field). The fabrication of such materials is complicated but the development in this area has progressed significantly in recent years. In the literature, many papers deal with static and dynamic analysis of the FGM single 2D beams with only a transversal variation of material properties. The longitudinal stiffness of the beam can be influenced with both the varying cross - sectional area and with varying material properties. In [1], dynamic characteristics of a functionally graded beam with axial or transversal material gradation along the thickness on the power law have been studied with a semi-analytical method. However, the authors did not find papers which consequently deal with all the longitudinal, transversal and lateral variation of material properties concerning the dynamics of single beams or beam structures built of such FGM beams. In [2, 5, 6], we discussed the analysis of free vibration of a single 2D FGM beam with continuous planar polynomial variation (in axial and transversal direction) of material properties by a fourth-order differential equation of second order beam theory. The aim of this publication was to present a new concept for expanding the second order bending beam theory considering the shear deformation according to Timoshenko beam theory. The shear deformation effect in FGM beams with planar continuous variation of material properties is included there originally by means of the average shear correction factor that has been obtained by an integration of the shear correction function [4]. The continuous polynomial variation of the effective elasticity modulus and mass density can be caused by continuous polynomial spatial variation of both the volume fraction and material properties of the FGM constituents. The choice of a polynomial gradation of material properties enables an easier integration of the derived differential equation and allows to model practically realizable variations of material properties. The effect of inertia and rotary inertia and the effect of axial forces were taken into account as well.

The presented contribution is the continuation of our previous work dealing with the derivation of general homogenized 3D FGM beam finite element with longitudinally varying effective material properties. Homogenization of the spatial continuously varying material properties in the real FGM beam and the calculation of effective parameters are done by the layering method [3]. This method can also be used in the homogenization of multilayer beams with discontinuous variation of material properties in transversal and lateral direction (multilayer beam). Numerical experiments are performed to analyze chosen FGM beam structures. The continuous spatial variation of material properties is considered. The solution results are discussed and compared to those obtained using a very fine continuum mesh in commercial software.

Acknowledgements

This paper has been supported by Grant Agency APVV-0246-12, Grant Agency VEGA No. 1/0534/12 and Agency KEGA No. 015STU-4/2012.

References

- [1] Alshorbagy, A.E., Eltaher, M.A., Mahmoud, F.F., Free vibration characteristics of a functionally graded beam by finite element, *Applied Mathematical Modelling* 35 (2011) 412–425.
- [2] Aminbaghai, M., Murin, J., Kutis, V., Modal analysis of the FGM-beams with continuous transversal symmetric and longitudinal variation of material properties with effect of large axial force, *Engineering Structures* 34 (2012) 314–329.
- [3] Kutis, V., Murin, J., Belak, R., Paulech, J., Beam element with spatial variation of material properties for multiphysics analysis of functionally graded materials, *Computers and Structures* 89 (2011) 1192–1205.
- [4] Murin, J., Aminbaghai, M., Hrabovsky, J., Kutis, V., Kugler St. Modal analysis of the FGM beams with effect of the shear correction function, *Composites: Part B* 45 (2013) 1575–1582.
- [5] Murin, J., Aminbaghai, M., Kutis, V., Exact solution of the bending vibration problem of the FGM beam with variation of material properties, *Engineering Structures* 32 (2010) 1631–1640.
- [6] Murin, J., Aminbaghai, M., Kutis, V., Hrabovsky, J., Modal analysis of the FGM beams with effect of axial force under longitudinal variable elastic Winkler foundation, *Engineering Structures* 49 (2013) 234–247.

Modal analysis of beam structures reinforced by partially embedded reinforcing core

M. Nad^a, L. Rolník^a

^a Faculty of Materials Science and Technology in Trnava, Slovak University of Technology in Bratislava,
 Paulínska 16, 917 24 Trnava, Slovak Republic

Beam structures can be considered as the fundamental building elements in many engineering applications. In operating regimes these structures are very often loaded by the dynamical forces which cause undesirable dynamical behaviour these beam structures and system is getting into critical resonance state. It is clear that the reduction of the level of unwanted vibrations or prevention of their occurrence should be one of the important objectives in the design of machine equipment and structures. To achieve these aims the knowledge of modal properties of beam structures in relation to their internal structure is necessary. Modal properties modification of the beam structure (mode shapes, natural frequencies) is achieved by the partial insertion of reinforcing core [2]. The dependence of the modal properties of modified beam structure on the geometric parameters and material properties of the embedded reinforcing core is studied.

Considered beam structure has a uniform fundamental cross section and a certain part of the beam length is reinforced using the core with uniform cross-section which is embedded into the beam body (Fig. 1). The modal properties modification of beam structure [1, 4] is based on parameters of reinforcing core, especially on longitudinal position of reinforcing core defined by length of core l_c .

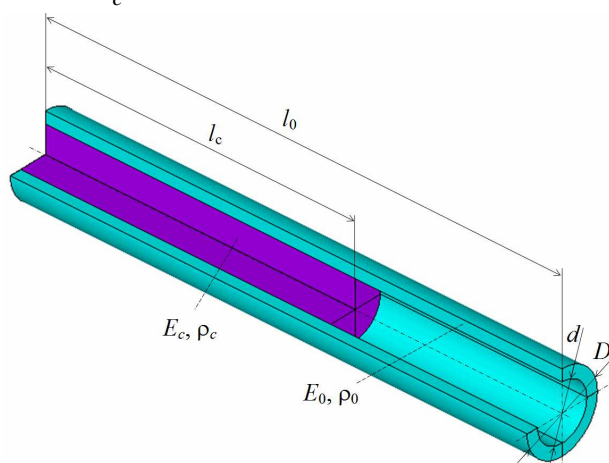


Fig. 1. Model of beam structure with partially embedded reinforcing core

The ODE's describing the free bending vibration of beam structure with reinforcing core for dimensionless variables ($\xi_k = x_k/l_0$, $\bar{W}_k(\xi_k) = w_k(x_k)/l_0$) have the form

$$\bar{W}_k^{IV}(\xi_k) - \beta_k^4 \bar{W}_k(\xi_k) = 0, \quad \text{for } k = 1, 2, \quad (1)$$

where $\xi_1 \in \langle 0; \xi_c \rangle$, $\xi_2 \in \langle \xi_c; 1 \rangle$ and $\xi_c = l_c/l_0$.

Frequency parameters β_1 and β_2 are expressed by

$$\beta_1 = \sqrt[4]{\omega_0^2 l_0^4 \frac{\rho_1 S_1}{E_1 J_1}} = \beta_2 \sqrt[4]{\frac{1+\Delta_{\rho S}}{1+\Delta_{EJ}}}, \quad \beta_2 = \sqrt[4]{\omega_0^2 l_0^4 \frac{\rho_2 S_2}{E_2 J_2}} = \sqrt[4]{\omega_0^2 l_0^4 \frac{\rho_0 S_0}{E_0 J_0}}, \quad (2)$$

where $\Delta_{\rho S} = \frac{\rho_c S_c}{\rho_0 S_0}$, $\Delta_{EJ} = \frac{E_c J_c}{E_0 J_0}$ are modification functions caused by the reinforcing core.

The solution of ODE's is

$$\bar{W}_k(\xi_k) = A_k S(\beta_k \xi_k) + B_k T(\beta_k \xi_k) + C_k U(\beta_k \xi_k) + D_k V(\beta_k \xi_k), \quad (3)$$

where $A_k \div D_k$ are integration constants and the Krylov's functions [5]

Modal analysis of clamped-free beam structure reinforced using partially embedded core is studied. To generalize the modal analysis results, the dimensionless frequency is introduced

$$\vartheta_i = \frac{f_{0m,i}}{f_{0,i}} \quad \text{for } i = 1, 2, 3, 4, \quad (4)$$

where $f_{0m,i}$ ($f_{0,i}$) - i^{th} natural frequency of modified (unmodified) beam structure for corresponding slenderness.

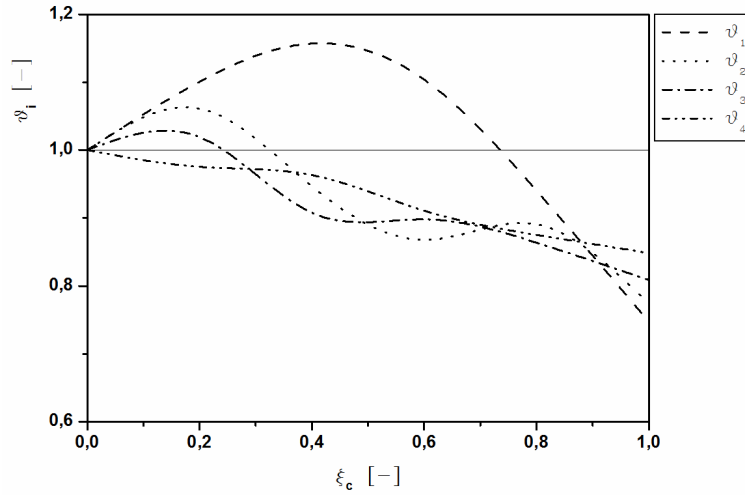


Fig. 2. Dependency of ϑ_i ($i = 1 \div 4$) on the parameter ξ_c
($\lambda_0 = D/l_0 = 0.1$; $\kappa_E = E_c/E_0 = 3.0$; $\kappa_E = \rho_c/\rho_0 = 2.89$; $\kappa_E = d/D = 0.6$)

The results of analysis confirm that this manner of beam structural modification offers a very effective tool to the modification of modal properties (Fig. 2). The approach to the structural modification presented in this paper can be considered as passive modification of the dynamic properties of beam structures.

Acknowledgements

The work has been supported by the project "Young researcher 2014 (MTF-1330) and grant projects VEGA 1/1041/11 and VEGA 1/2594/12 of Ministry of Education, Science, Research and Sport of the Slovak Republic.

References

- [1] Dekýš, V., Sága, M., Žmindák, M., Dynamics and reliability of mechanical systems, VTS ZU, Žilina, 2004.
- [2] Nađ, M., Vibration analysis of beams with reinforcing and damping cores, In: 20th Inter. Congress on Sound and Vibration-ICSV20, Bangkok, Thailand, 2013, pp.1-8.
- [3] Nánási, T., Effect of boundary conditions on vibration localization of two-span beams, In: 20th Inter. Congress on Sound and Vibration - ICSV20, Bangkok, Thailand, 2013, pp.1-8.
- [4] Thorby, D., Structural dynamics and vibration in practice-An engineering handbook, Elsevier Ltd., 2008.
- [5] Timoshenko, S.P., Young, D.H., Weaver, W., Vibration problems in engineering, John Wiley & Sons, New York, 1985.

Dynamic stability and post-critical behavior of aeroelastic systems

J. Náprstek^a

^a*Institute of Theoretical and Applied Mechanics, Academy of Sciences of the Czech Republic, Prosecká 76, 190 00 Prague, Czech Republic*

Dynamic Stability is a widely studied area that has attracted many researchers from various disciplines. Although Dynamic Stability is usually associated with mechanics, theoretical physics or other natural and technical disciplines, it is also relevant to social, economic, and philosophical areas of our lives. History of the theory of stability has been opened by L.P. Euler in 1744 by his famous work [2].

The stability of mechanical systems represents several areas that are not fully separated and that have a common theoretical basis. Although they interact very often and a sharp limit between them cannot be determined, the following fields can be outlined: (i) Dynamic Stability of multi-body systems. (ii) Problems of buckling of large deformable systems, such as frame-works, plates, and shells. (iii) Stability of flow.

Regarding Dynamic Stability of multi-body systems a wide range of literature of various types exists. It deals very theoretical or rather pure mathematical aspects of stability as far as very practical engineering approaches and hints for designers. A certain overview of the above three fields can be found for instance in [1, 3, 4, 5] where hundreds additional references of general and specialized monographs and problem related papers are given.

Four main Dynamic Stability definitions should be discussed, although a significant overlap is present among them. From the viewpoint of mechanics, the most important one is Lyapunov stability and the related Lyapunov second method (LSM). This is suitable for non-linear systems. It can be employed for the investigation of the most general theorems as well as for the investigation of particular systems. As the second definition should be stated stability of the linear systems, where Routh-Hurwitz (RH) or Sylvester determinants are the most popular approaches. Both of these definitions have a number of reduced variants that are suitable for special classes of problems.

While Lyapunov and linear stability definitions can be considered to be local stability principles, the third definition (orbital stability) is related to global stability. This deals with cases where the orbit as a whole should be observed as the local properties are not sufficient to consider overall stability. The fourth definition concerns Stochastic Stability. Stochastic stability involves working with the probability density function (PDF) of the system response. In this case, Probability Density Function (PDF) and possibly stochastic moments are analogous quantities similar to system response components in the deterministic domain. Usually Fokker-Planck (FP) operator applied onto the relevant Ito system is used as a basic tool of stability testing. FP operator is a counterpart of the Lyapunov function total time derivative in the stochastic domain.

A couple of case-related Dynamic Stability loss testing should be noticed. Their principles are diverse, but all of them are related with "enormous or infinite" increase of the system response at least in some coordinates. Enumerating some of them, we can observe their relation

to the procedures based on the LSM or RH determinants. Nevertheless, they are simple and transparent and therefore usable for a very wide variety of researchers.

Many structures in civil, mechanical, naval or aerospace engineering can get in a state of the dynamic stability loss due to interaction with streaming air. Overstepping a certain limit of an air velocity or other parameters specifying external action, the system response exhibits a dramatic increase, either approaching a certain stabilized nonlinear shape (limit cycle, homoclinic/heteroclinic orbit, etc.) or leading to final collapse following a non-periodical trajectory. Especially limit cycles (LC) are very often a general characteristic of the post-critical system behavior. Stable and unstable LC classify attractive and repulsive response areas, while homoclinic orbits including additional singular points represent singular cases.

These phenomena are related either with self-excited or auto-parametric systems as a rule. The limit separating them is not sharply defined, and many systems exhibiting such phenomena can fall into both categories. A couple of them can be mentioned: (i) SDOF and more complicated systems where the damping parameter (or parameters) are dependent on the response velocity being maximal at a standstill. (ii) Self-exciting effects within 2DOF and more complicated systems due to the special structure of stiffness and damping terms. In the case of linear systems, non-conservative and gyroscopic terms can lead to the overstepping of stability limits and a post-critical self-excited response then emerges. Nevertheless, a non-linear approach has to be adopted very often, because only post-critical non-linear forces can possibly stabilize the response. (iii) Vortex shedding. These phenomena can occur due to stability loss in a local area of a dynamic pressure field in a fluid when interacting with stiff or deformable bodies. Vortex shedding can be observed on the micro-, macro-, and giga-scales. For instance, vortex shedding has been observed in a streaming sea behind a circle-shaped island.

Linear and nonlinear approaches are introduced. While the former one provides basic stability limits, initiation of Hopf bifurcation and emerging of known types of stability loss (divergence, flutter, buffeting, etc.), the latter one shows forms of stable regimes in the post-critical domain, if any. Other types of local or global bifurcations can also emerge in post-critical regime indicating a number of special cases (Poincare-Andronov, Neimark-Sacker, etc.). Chaotic processes can occur as well. Deterministic as well as stochastic approaches are presented combining for instance influence of the vortex shedding together with the natural and generated turbulence of ambient streaming producing some times effect of the stochastic resonance, which can be observed as the aeroelastic divergence either theoretically or experimentally in a wind tunnel.

Acknowledgements

The kind support of the Czech Science Foundation Project No. GC13-34405J and of the RVO 68378297 institutional support are gratefully acknowledged.

References

- [1] Bažant, Z.P., Cedolin, L., *Stability of structures*, World Scientific Publishing, Singapore, 2010.
- [2] Euler, L.P., *Methodus inveniendi lineas curvas maximi minimive proprietate gaudentes, sive solutio problematis isoperimetrici latissimo sensu accepti*. Addamentum 1: de curvis elasticis, Laussanae et Genevae, Apud Marcum-Michaelem, Bousquet et Socios (1744) 245–310.
- [3] Náprstek, J., Combined analytical and numerical approaches in Dynamic Stability analyses of engineering systems, *Journal of Sound and Vibration* (2014) 1–40. (in press)
- [4] Païdoussis, M.P., *Fluid-structure interactions: Slender structures and axial flow*, Academic Press, San Diego, London, 1998.
- [5] Tondl, A., Ruijgrok, T., Verhulst, F., Nabergoj, R., *Autoparametric resonance in mechanical systems*, Cambridge University Press, Cambridge, 2000.

Stability limits of the pre-stressed lightweight material model

Z. Neusser^a, T. Vampola^a, M. Valášek^a

^aFaculty of Mechanical Engineering, CTU in Prague, Technická 4, 166 07 Praha, Czech Republic

Current industrial robots and manipulators are designed with relatively stiff and heavy members especially for the structures of the open kinematic chain type. During the motion of these structures act high inertial forces that negatively influence the economic parameters of the production cycle. There are ways how to remove this disadvantage. The idea using pressurized membrane together with a beam to prevent its bending is presented in [1]. The pressure doesn't significantly influence eigenfrequencies of such structure and it needs more space than using just a respective beam. In this article is designed concept of the new lightweight material based on the pre-stressed membrane structure filled with the circular particles. The parameters of the static stability of the designed material model are investigated on the basic cell. The more complex structures like robotic arms can be assembled from this cell.

The idea is to replace beams and rods in the construction by the hybrid structure consisting of the elastic membrane and hollow balls. The membrane envelopes the balls in such structure to replace the beam and keeping its main properties by keeping underpressure in the structure. The main advantages are lighter construction and some parameterization for the stiffness value of the new structure. Possible disadvantages authors see in the membrane durability, discrepancies in the ball radius and underpressure level uncertainty.

It is assumed problem only in the plane without friction. Model consists of the circular elements with the same radii and elastic membrane, which envelopes the elements. The circular element has contact stiffness to interact between each other. Inside the structure (which is covered by the membrane) is underpressure and it is controlled.

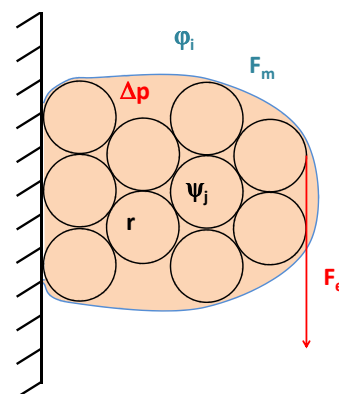


Fig. 1. Scheme of the system

Model overview and its parameters are shown on the Fig. 1. The parameters are: the radius of the elements r [m], the angles ψ_j [rad] describing the inner shape of the structure, underpres-

sure Δp [Pa], membrane stiffness k [N/m] and membrane angles φ_i [rad]. Force F_e [N] represents external forces.

Membrane is modelled as an elastic rope and when not using passive resistances, there is just one force along whole membrane length. It is necessary to calculate its prolongation to evaluate the force

$$F_m = k(l - l_0 + \xi), \quad (1)$$

where k is membrane stiffness, l_0 represents free length of the membrane, l is actual membrane length and ξ is the pretension of the membrane.

There are structure forces acting on the elements. Firstly, there must be contact forces between elements in the contact, second ones are forces due to the membrane prolongation and third loading is from the underpressure through membrane been in contact with the elements.

Using principle of virtual work it is obtained the set of nonlinear equilibrium equations:

$$(F_m + \Delta p \cdot r) \begin{bmatrix} f(\psi_j, \varphi_i) \\ F_1(\psi_j, \varphi_i) \end{bmatrix} + F_e \begin{bmatrix} 0 \\ F_2(\psi_j, \varphi_i) \end{bmatrix} = 0, \quad (2)$$

where the functions f , F_1 and F_2 are structural functions of the system. The membrane flexibility is covered within the angles φ_i and the set of equations (2) is nonlinear. It could be shown, that membrane force is dependent on the underpressure Δp and virtual radius R which represents the curvature of free membrane in the gaps between elements:

$$F_m = \Delta p \cdot R. \quad (3)$$

Using the equations (2) and (3) and eliminating the external force F_e it is obtained the final set of equations:

$$\Delta p (R + r) \begin{bmatrix} f_1(\psi_j, \varphi_i) \\ f_2(\psi_j, \varphi_i) \end{bmatrix} = 0, \quad (4)$$

where the functions f_1 and f_2 describes the structure of the system including the membrane. In such structure contact between elements could be approximated by the beam connections and it is used for evaluation of the stability limits of such the pre-stressed lightweight material.

Without loss of generality it was shown, that forces acting on the elements could be written in the form (4). Elements are represented as mass points. The preliminary results show that such structures exist, have equilibrium unloaded and are stable under some axial and tangential load. The stiffness of the structure is dependent on the underpressure inside the structure.

Acknowledgements

This publication was supported by the European social fund within the framework of realizing the project Support of inter-sectorial mobility and quality enhancement of research teams at Czech Technical University in Prague, CZ.1.07/2.3.00/30.0034.

References

- [1] Breuer, J., Ockels, W., Luchsinger, L.H., An inflatable wing using the principle of Tensairity, Proceedings of the 48th AIAA Structures, Structural Dynamics and Materials Conference, Waikiki, Hawaii, USA, 2007.

Fourier and dispersion

M. Okrouhlík^a

^a*Institute of Thermomechanics, Academy of Sciences of the Czech Republic, Dolejškova 5, Prague 8, Czech Republic*

Author intends to show the dispersion phenomena from a historical perspective, to inform about significant contributions of our famous forefathers, as Newton, Johan and Daniel Bernoulli's, Fourier and many others, and to remind the contemporary role of Fourier's tools.

Dispersion is a property of a medium in which the velocity of wave propagation depends on its frequency. It plays important role in optics, in wave propagation, in vibration of mechanical and electrical engineering, in atomic theory of solids, in experiment evaluation, etc. Dispersion effects could be analyzed, treated and explained by Fourier series and Fourier integral and by FFT. We will devote our attention to dispersion phenomena in computational mechanics and to numerous Fourier tools helping to describe and explain dispersion effects.

History goes back to Brillouin, Kolsky, Brepta, Bažant, etc. In computational mechanics today, substantial contributions of Radek Kolman and K.C. Park are being published. It all, however, started with one-dimensional lattice, consisting of sequentially assembled particles of equal mass connected by identical massless springs.

It was Isaac Newton, who used the lattice model for estimation of the velocity of sound in air. Later, Johann Bernoulli (1667 - 1748) in Basel and his son Daniel Bernoulli (1700 - 1782) in St. Petersburg independently showed that the lattice system having n degrees of freedom has n independent eigenvectors and eigenfrequencies. Laterally vibrating string is formally described by the same type of partial differential equation as longitudinally vibrating lattice. Afterwards, in 1753, Daniel Bernoulli formulated (for the string) the principle of superposition that can be considered as a special case of Fourier theorem.

The chief contribution of Fourier was the idea that any periodic function can be represented by a series of sine and cosine functions. Euler (in 1748) stated that the displacement of a vibrating string can be described by an arbitrary function provided that certain continuity conditions are met. To Euler mind the Fourier theorem was almost an absurdity. Consequently, Euler refused to accept the principle of superposition. Also Lagrange followed Euler in refusing the principle of superposition. It was Dirichlet who gave the first rigorous proof of the convergence of Fourier series.

It is known that the spatial and temporal discretizations always accompany the finite element modelling of transient problems. The topic is of academic interest but has important practical consequences as well. It appears that the dispersion topic is still alive.

In the contribution the Fourier tools are shown to play important role in validity assessments of Newmark (NM) and central differences (CD) operators, thin tube frequency approximation, approximation of the largest eigenfrequency, etc.

Dispersion phenomena also play important role in correct time step determination when integration operators in time are employed. A few procedures, accompanied by many examples, for solving this task are presented.

In the contribution we have tried to show how a role of a few historical personalities is related to contemporary tools of modern computational mechanics.

References

- [1] Boyer, C.B., A history of mathematics, John Wiley, 1968.
- [2] Brillouin, L., Wave propagation in periodic structures, McGraw-Hill, 1946.
- [3] Fried, I., Discretization and round-off errors in the finite element analysis of the elliptic boundary value problems and eigenproblems, PhD Thesis, MIT, 1971.
- [4] Kolman, R., Plešek, J., Okrouhlík, M., Complex wavenumber Fourier analysis of the B-spline based finite element method, *Wave Motion* 51 (2014) 348–359.
- [5] Kolman, R., Plešek, J., Okrouhlík, M., Gabriel, D., Grid dispersion analysis of plane square biquadratic serendipity finite elements in transient elastodynamics, *Int. J. Numer. Meth. Engng*, 96 (2013) 1–28.
- [6] Kolsky, H., *Stress waves in solids*, Clarendon Press, Oxford, 1953.
- [7] Lines, M., *On the shoulders of giants*, Institute of Physics Publishing, Bristol and Philadelphia, 1994.
- [8] Okrouhlík, M., Impact induced stress wave energy flux. Validation of numerical and experimental approaches, *International Conference on Vibration Problems 2011, Prague, 2011*. (Published in *Springer Proceedings in Physics* 139, Springer New York, 2011)
- [9] Okrouhlík, M., Dispersion and time integration schemes in finite-element analysis – a practical pictorial manual, *International Journal of Mechanical Engineering Education* 41 (1) (2013) (Manchester University Press).
- [10] Okrouhlík, M., *Matlab, numerické metody v inženýrství I a II*, Skripta UJEP, 2013 and 2014.
- [11] Okrouhlík, M., Höschl, C., A contribution to the study of dispersive properties of one-dimensional Lagrangian and Hermitian elements, *Computers and Structures* 49 (5) 1994 779–795.
- [12] Okrouhlík, M., Pták, S., FE and experimental study of axially induced shear stress waves in a tube with spiral slots, Part 1. Research of the Institute of Thermomechanics, Z 1417/2008, Prague, 2008.

Stress and strength analysis of flat samples manufactured from C/PPS pellets

Z. Padovec^a, R. Sedláček^a, M. Král^a, M. Růžička^a

^a Faculty of Mechanical Engineering, Czech Technical University in Prague, Technická 4, 166 07 Praha, Czech Republic

Presented article describes verifying tensile test based on ASTM D3039 standard [1] and its numerical simulation. Specimens were manufactured from two flat C/PPS plates randomly reinforced with pellets. These plates were cut in longitudinal and transversal directions because it is necessary to compare Young modulus in both directions. On each cut sample were bonded three strain gauges according to [1] (see Fig. 1 – where *A* stands for longitudinal direction and *B* for transversal). Specimens were tested on TIRA 2300 universal machine with head displacement rate 2 mm/min.

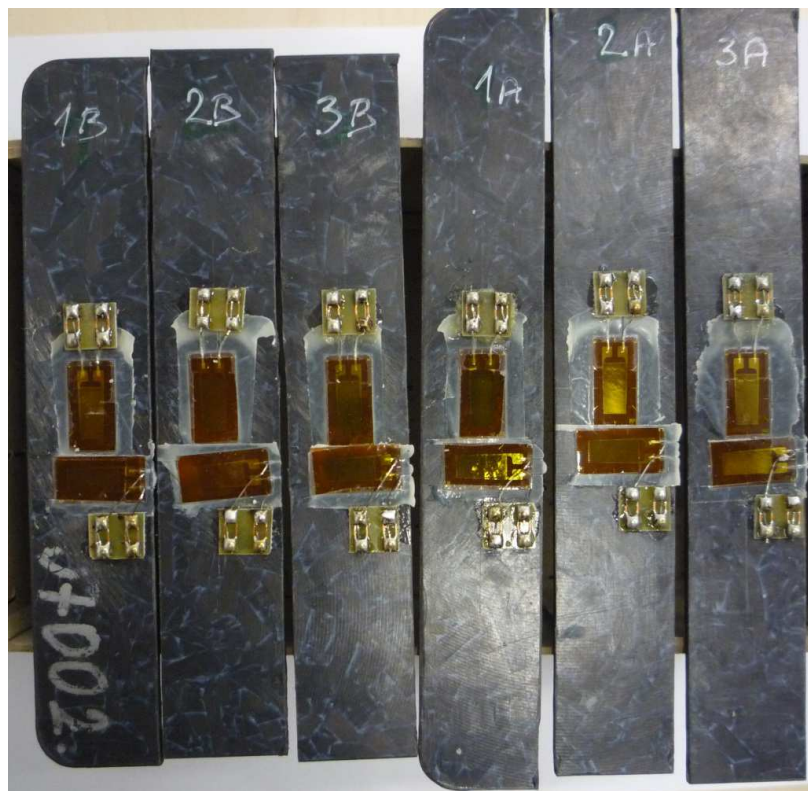


Fig. 1. Specimens with strain gauges

Obtained results were compared with FE simulation of the tensile test which was done in Abaqus software. Material data for FE simulation were based on analytical model which presumes transversally – isotropic behavior of material [2, 3]. Comparison of the results obtained by experiment and by FE simulation can be seen in Fig. 2.

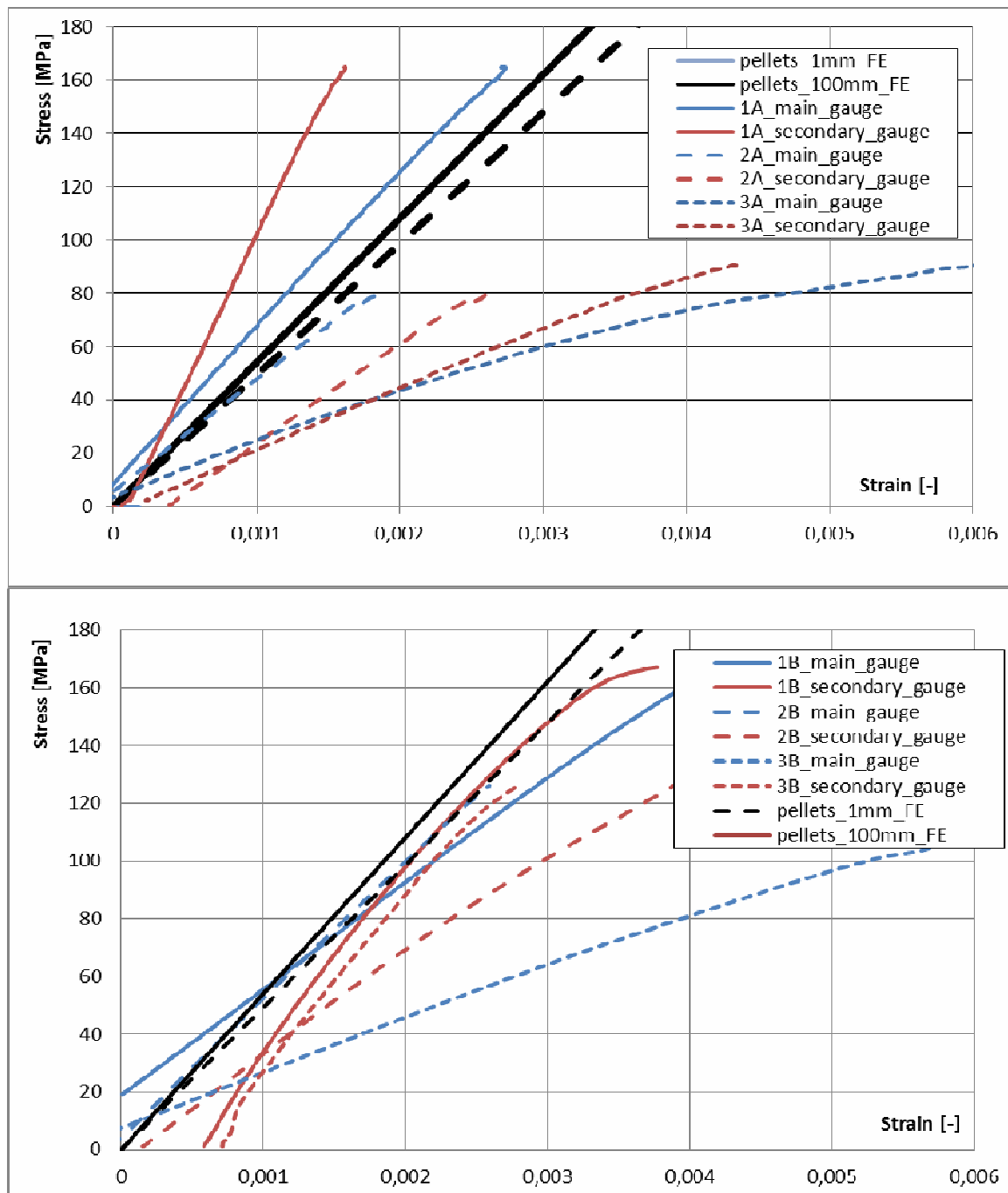


Fig. 2. Comparison of the experimental and FE results

Acknowledgements

The work has been supported by the project TA03010209 of the Technological Agency of Czech Republic and by the Grant Agency of the Czech Technical University in Prague, grant No. SGS12/176/OHK2/3T/12.

References

- [1] ASTM D3039 – Standard test method for tensile properties of polymer matrix composite materials.
- [2] Barbero, E.J., Introduction to composite materials design, Second Edition, CRC Press, Boca Raton, 2011.
- [3] Kabelka, J., Thermoelastic characteristics of polymer composites with reinforcement in the form of mats, Research Report Z935/85, Institute of Thermomechanics, ČSAV, 1985. (in Czech)

Identification of the directional distortional hardening model on the basis of hysteresis loop

S. Parma^a, Z. Hrubý^a, R. Marek^a, J. Plešek^a

^a*Institute of Thermomechanics, Academy of Sciences of the Czech Republic, Dolejškova 1402/5, 182 00 Praha 8, Czech Republic*

Distortion of yield surface can be observed during plastic deformation of metals. This phenomenon known as the directional distortional hardening has been experimentally approved by many authors who investigated various types of metals [1, 5]. Modeling of such a behaviour has been widely performed as well [3, 4].

Feigenbaum and Dafalias [2] developed a model generalizing classical concept of isotropic and kinematic hardening using only one additional parameter to model the yield surface distortion. The model forms a system of algebro-differential equations and includes six independent material parameters needed to be identified. Despite its complexity, analytical solution of this system for proportional loading modes was found, extending possibilities of identification.

Although there was a procedure developed for identification based on experimental data on monotonic loading, a method suitable for identification from cyclic loading experiments was still missing. In order to provide such a method, stress response of the model to more complex loading paths was investigated. Finally, the closed form equation of hysteresis loop has been derived, being expressed as

$$\sigma_{11} = \text{sgn} \cdot \frac{1/\kappa_2}{\sqrt{1 - \sqrt{\frac{3}{2}} c \alpha_{11} \text{sgn}}} + \frac{3}{2} \alpha_{11}, \quad (1)$$

where the kinematic hardening internal variable (backstress) is given by

$$\alpha_{11} = \sqrt{\frac{2}{3}} \frac{1}{a_2 \text{sgn}} \left[1 - \left(1 - \sqrt{\frac{3}{2}} a_2 \alpha_{11,a} \text{sgn} \right) \cdot \exp \left(-\sqrt{\frac{3}{2}} a_1 a_2 (\varepsilon_{11}^p - \varepsilon_{11,a}^p) \text{sgn} \right) \right] \quad (2)$$

and where the amplitude of backstress is given by

$$\alpha_{11,a} = \sqrt{\frac{2}{3}} \frac{1}{a_2} \tanh \left(\sqrt{\frac{3}{2}} a_1 a_2 \varepsilon_{11,a}^p \right) \quad (3)$$

with $\varepsilon_{11,a}^p$ as the plastic deformation amplitude, $\text{sgn} = 1$ for the case of tensile loading and $\text{sgn} = -1$ for the case of compressive loading. κ_2 , a_1 , a_2 and c are the internal parameters of the model. In case of cyclic loading, the other two material parameters can be expressed as $k_0 = 1/\kappa_2$ and $\kappa_1 = 0$. Finally, the dependent variable σ_{11} denotes the stress and the independent variable ε_{11}^p denotes the plastic strain.

Similarly, equation of cyclic deformation curve in $\sigma_{11,a} - \varepsilon_{11,a}^p$ can be expressed by

$$\sigma_{11,a} = \frac{1/\kappa_2}{\sqrt{1 - \sqrt{\frac{3}{2}} c \alpha_{11}}} + \frac{3}{2} \alpha_{11} \quad (4)$$

with the same meaning of parameters and variables as stated previously.

Thus, identification of parameters can be done by fitting any of the Eqs. (1) or (4) on appropriate experimental data. Particularly, the *nonlinear least squares method* was used.

Acknowledgements

This research was supported by GAP101/12/2315 and KONTAKT ME10024 granted projects.

References

- [1] Boucher, M., Cayla, P., Cordebois, J.-P., Experimental studies of yield surfaces of aluminum alloy and low carbon steel under complex biaxial loadings, *European Journal of Mechanics, A/Solids* 14 (1995) 1–17.
- [2] Feigenbaum, H. P., Dafalias, H., Simple model for directional distortional hardening in metal plasticity within thermodynamics, *Journal of Engineering Mechanics* 134 (9) (2008) 730–738.
- [3] François, M., A plasticity model with yield surface distortion for non proportional loading, *International Journal of Plasticity* 17 (5) (2001) 703–717.
- [4] Ortiz, M., Popov, E. P., Distortional hardening rules for metal plasticity, *Journal of Engineering Mechanics* 109 (4) (1983) 1042–1057.
- [5] Wu, H.C., Yeh, W., On the experimental determination of yield surfaces and some results of annealed 304 stainless steel, *International Journal of Plasticity* 7 (8) (1991) 803–826.

Identifying parameters of Kohout-Věchet fatigue curve model

S. Parma^{a,b}, J. Papuga^a

^a Faculty of Mechanical Engineering, CTU in Prague, Technická 4, 166 07 Praha, Czech Republic

^b Evector, spol. s r. o., Letecká 1008, 686 04 Kunovice, Czech Republic

Fatigue curve models have a crucial importance for fatigue life prediction and evaluation. Consequently, the analytical approximation of fatigue experimental data has been addressed by many authors, and resulted in several classical models, e.g., Wöhler (1870) [5] or Weibull (1949) [4].

Kohout and Věchet (2001) [2] developed a fatigue curve model suitable for the use in both low-cycle and high-cycle fatigue domains. Its applicability there is allowed thanks to additional parameters (total 4 in comparison to common Basquin formula of 2 parameters), which get useful in a quasi-static domain and in a region of the fatigue limit. In general form, model can be expressed by

$$\sigma = a \left(C \frac{N + B}{N + C} \right)^b, \quad (1)$$

where a , b , B and C are the independent parameters, σ is the stress level, and N is the number of cycles. For the parameters specified, the curve of discussed model is plotted in Fig. 1. Practical application of model can be found in [1, 3].

A detailed analysis of the model was realized and published in [2]. Since the model was selected as one of the main tools in the prepared FinLiv database, the model was identified on several tens of experimental data sets. During that time some difficulties were observed enforcing a new analysis of the model. It was found out that some assumptions adopted in [2], e.g., that one supposing $B \ll C$, are not fulfilled in general. In addition to it, some

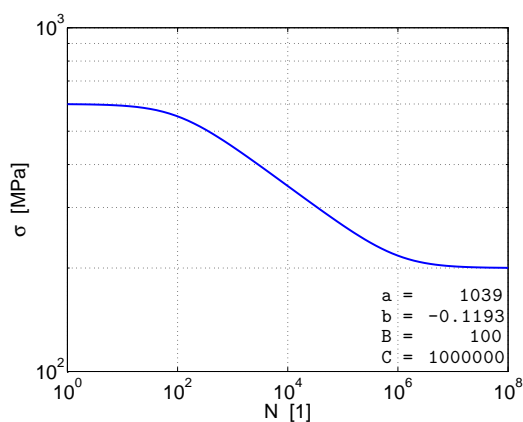


Fig. 1. Kohout-Věchet fatigue curve model for specified parameters

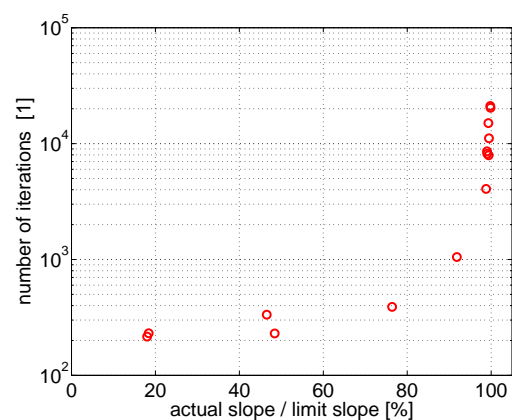


Fig. 2. Number of iterations increasing as the slope reaches the limit value

subsequent formulae derived from Eq. (1), e.g., the one providing the slope of the model, need to be generalized. While using these generalized formulae, it was shown that the limit slope of the model (1) is constrained by its other characteristics:

$$s_{\text{lim}} = \frac{1}{4} \ln \frac{\sigma_{+\infty}}{\sigma_1}, \quad (2)$$

where s_{lim} is the limit slope of model, σ_1 is the strength of material, and $\sigma_{+\infty}$ is the fatigue limit.

The *nonlinear least squares* formulation solved by *Levenberg-Marquardt algorithm* was used for identifying the parameters. Since there were problems with convergence of the algorithm in some cases, these problematic sets were evaluated with respect to Eq. (2). In Fig. 2, relation between the number of iterations to convergence and the ratio of actual and limit slope of the model (1) is shown. It can be seen that problematic convergence occurs when the actual slope of the Kohout-Věchet model reaches its limit value.

These findings are essential for any practical application of model. Thus, problematic convergence of the model can be further analysed, and possibly result in the application of new algorithms. As regards the constraints expressed by Eq. (2), it is an inherent property of the model itself. It shows the limitation of the model for some experimental data.

Acknowledgements

The research was supported by TA01011274 grant project of TAČR and by SGS14/181/OHK2/3T/12 CTU grant.

References

- [1] Chaminda, S. S., Ohga, M., Dissanayake, R., Taniwaki, K., Different approaches for remaining fatigue life estimation of critical members in railway bridges, *International Journal of Steel Structures* 7 (4) (2007) 263–276.
- [2] Kohout, J., Věchet, S., A new function for fatigue curves characterization and its multiple merits, *International Journal of Fatigue* 23 (2) (2001) 175–183.
- [3] Parma, S., Papuga, J., Identification of Kohout-Věchet model of fatigue curve, Technical Report FAD/13/001, Fadoff (<http://fadoff.eu/>), Prague, 2013. (in Czech)
- [4] Weibull, W., A statistical report of fatigue failure in solids, *Transactions Of The Royal Institute Of Technology No. 27*, Royal Institute of Technology of Sweden, Stockholm, 1949.
- [5] Wöhler, A., On strength tests of iron and steel, *Zeitschrift für Bauwesen* 20 (1870) 73–106. (in German)

Parametric excitation on the fuel assembly TVSA-T

L. Pečínka^a, M. Švrček^a

^a ÚJV Řež a.s., Hlavní 130, 250 68 Husinec Řež, Czech Republic

As the part of NPP Volgodonsk (VVER 1000 MW) initial start up tests, the pressure pulsations in coolant in hot leg were measured. At the power level related to coolant temperature 314°C, the new frequencies 2.7 Hz and 5.4 Hz were observed with very high power spectral densities with increasing temperature this frequency peaks vanished. This phenomenon is possible to explain on the basis of electromechanical analogy and under supposition of the radiolysis of the coolant. As the result, limited amount of steam is generated which significantly decreases speed of sound and finally generates those too new acoustic frequencies. In the paper the theory is derived and numeric assessment performed.

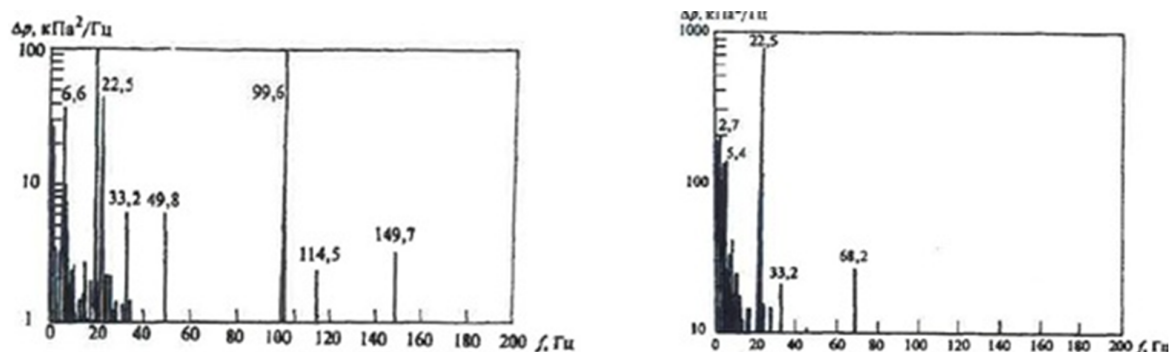


Fig. 1. PSDs of the acoustic frequencies for $P = 16$ MPa, $T_{\text{inlet}} = 284^\circ\text{C}$, $T_{\text{outlet}} = 301^\circ\text{C}$ (left) and $P = 16$ MPa, $T_{\text{inlet}} = 285^\circ\text{C}$, $T_{\text{outlet}} = 314^\circ\text{C}$ (right)

As the part of NPP Volgodonsk (VVER 1000 MW) initial start up tests, the pressure pulsations in coolant in hot leg were measured. At the power level related to the coolant temperature 314°C the new frequencies with very high power spectred densities have been observed, see Fig. 1.

For the speed of sound in two- phase flow, the following equation is recommended to use according to [1]

$$a_{df} = \sqrt{\frac{nP}{x\bar{\rho}}} \left[\left(1 + \frac{1-x}{x} \frac{c_2}{c_1} \right) \right]^{-\frac{1}{2}}, \quad (1)$$

where c_1 is the speed of sound in water and c_2 is the speed of sound in steam.

Basic equations of the parametric excitation are the equation for capacity $C(t)$, which takes the form

$$C(t) = c_0 + C_m \sin 2\omega_0 t, \quad (2)$$

and the velocity of chase of $C(t)$ given as

$$\frac{dC(t)}{dt} = 2m_c\omega_0 \cos 2\omega_0 t = \frac{2m_L}{x_c} \cos 2\omega_0 t, \quad m_c = \frac{c_m}{c_0}, \quad x_c = \frac{1}{\omega_0 C_0}. \quad (3)$$

Changes of the capacity $C(t)$ in time influence:

- Acoustic mass

$$E_k = \frac{1}{2}mv^2,$$

- Capacity of the primary circuit

$$E_p = \frac{1}{2}C(t)p_c^2.$$

Let us assume the acoustic pressure in the form

$$P_c = P_{cm} \cos \omega_0 t. \quad (4)$$

As the result we obtain

$$\frac{dE_p}{dt} = \frac{P_{cm}^2 m_c}{2x_c} \cos 2\omega_0 t + \frac{P_{cm}^2 m_c}{4x_c} + \frac{P_{cm}^2 m_c}{2x_c} \cos 4\omega_0 t. \quad (5)$$

The mean value of E_p after integration in time interval $\langle 0; T \rangle$ takes the form $E_+ = P_{cm}^2 m_c / (4x_c)$. This energy must compensate losses induced by the active resistance of the circuit $E_- = P_{cm}^2 r / (2x_c^2)$. Condition of the self-excited vibrations of the parametric resonant vibrations takes the form $E_+ \geq E_-$.

There are two conditions of the parametric excitation existence: $\omega = 2\omega_0$ and $m_c = 2r/x_c = 2d$. If $\omega = \omega_0, \frac{2}{3}\omega_0, \frac{1}{2}\omega_0$, then resonant vibrations exist but vibrations are not intensive.

Application to NPP Temelín (2x VVER 1000) – two acoustic systems shall be established:

- #1: core and part of the block of protective tubes between lower and middle plates,
- #2: hot leg including steam generator hot collector.

For $P = 16$ MPa, $t = 314^\circ\text{C}$, $n = 1.3$, $x = 10^{-4}$, $\bar{\rho} = 700$ kg/m³, $c_1 = 970$ m/s, $c_2 = 475$ m/s and $a_{tw} = 251$ m/s. As the result, we obtain for #1 and #2: $f_1 = 5.14$ Hz and $f_2 = 2.75$ Hz, respectively. These values are very close to experimentally obtained results in Volgodon NPP.

The sudden increase of pressure pulsations in hot leg of the NPP Volgodon during start up tests was explained using hypothesis of parametric excitation. Resonance vibrations are not met. It is possible to assume that this phenomenon is common in all VVER 1000 NPPs. Theory is known, experimental verification is needed.

References

- [1] Deich, M.E., Filippov, G.A., The gas dynamics of two-phase media, Energoizdat, Moscow, 1981. (in Russian)
- [2] Pečínka, L., Krupa, V., Assessment of acoustic resonances in complicated Pipiny systems by using of electromechanical analogy, Proceedings of the conference Dynamics of Machines 2001, Prague, Institute of Thermomechanics AS CR, 2001.

Comparison study of algorithms based on fully stress design method for discrete optimization of truss, beam and thin shell finite elements

P. Pecháč^a, M. Sága^a

^a Faculty of Mechanical engineering, University of Žilina, Univerzitná 1, 010 26 Žilina, Slovak Republic

This paper deals with comparison of speed and stability of modifications of the fully stress design (FSD) method for structural optimization of truss, beam and thin shell finite element models.

As the name “fully stress design” suggests, the principle of the FSD method is optimization of structures to full stress state, i.e. stresses in the structure should approach the stress limit. The FSD method is a popular approach in optimization of truss structures, mainly due to its simplicity and effectiveness [2]. Its main advantage against other methods, like Nelder-Mead method, gradient methods, Monte-Carlo or genetic algorithms, is in consumption of relatively small number of finite element analyses. The FSD method requires just one finite-element analysis per iteration step, disregarding the number of optimization variables, while for the other mentioned methods the number of analyses rises with number of optimization variables. On the other hand, the use of the presented FSD algorithms is limited only for optimization of structures from the aspect of stress state, without consideration of other limit states including buckling, excessive deformations or fatigue. Nevertheless, the general principles of this method can be used for other problems, as this method and its modifications can be considered as root finding algorithms from the mathematical point of view.

The presented algorithms are based on two root finding numerical methods i.e. Regula Falsi and Newton’s method. The Regula Falsi or false position method is based on similarity of triangles, the common vertex of these triangles is called “false point”, in this case it will be point [0, 0]. The Newton’s method is based on a presumption that the evaluated function has continuous first derivation. Derivation of the evaluated function will be calculated numerically using similarity of triangles [3]. In case of Newton’s method, the calculation of derivation requires results from $k-1$ iteration step, so for the first iteration step all algorithms based on Newton’s method have to use one of the other methods. All presented algorithms realize uni-dimensional optimization individually for each optimization variable.

This paper does not contain the description for all tested algorithms, instead only 2 algorithms for every type of structure were chosen, algorithm no. 1 “classical” FSD for the purpose of comparison and the best performing algorithm from the remaining algorithms. For truss structures were tested six algorithms: 1. “classical” FSD, 2. “squared” FSD, 3. Newton’s method, 4. linear approximation of axial forces, 5. Newton’s method for prediction of axial forces and 6. “squared” approximation of axial forces. This paper contains description of algorithm no. 1 – “classical” FSD and algorithm no. 5 Newton’s method for prediction of axial forces. For beam structures were tested five algorithms: 1. “classical” FSD, 2. linear approximation of internal forces and moments, 3. Newton’s method for prediction of internal

forces and moments, 4. “squared” approximation of internal forces and moments and 5. “mixed” approximation of internal forces and moments. This paper contains description of algorithm no. 1 – “classical” FSD and algorithm no. 2 linear approximation of internal forces and moments. For thin shell structures were tested seven algorithms: 1. “classical” FSD, 2. “squared” FSD, 3. Newton’s method, 4. linear approximation of internal forces and moments, 5. Newton’s method for prediction of internal forces and moments, 6. “squared” approximation of internal forces and moments and 7. “mixed” approximation of internal forces and moments. This paper contains description of algorithm no. 1 – “classical” FSD and algorithm no. 2 “squared” FSD.

FSD based optimization algorithms were programmed in a programming language Matlab. Truss and beam finite element models were modeled and calculated in FEA software created by authors in Matlab. Models and calculations of thin shell structures were realized in a commercial FEA software ADINA and a cross-connection between Matlab and ADINA made by authors provided data transfer between ADINA and Matlab [1]. Data transfer from ADINA to Matlab was parallelized using Matlab Parallel Toolbox. Further parallelization of optimization programs allowed us to test several algorithms simultaneously and thus significantly reduce time needed for testing and debugging.

The paper contains theoretical basics of finite element method, analysis of stress state and description of chosen optimization algorithms for truss, beam and thin shell structures. The core of the paper is numerical testing and comparison of proposed algorithms. The conclusion is dedicated to evaluation of performance of the proposed algorithms and recommendations in the choice of algorithm for particular type of structure.

Acknowledgements

The work has been supported by the grant projects VEGA No.1/0234/13 and KEGA No.004ŽU-4/2012.

References

- [1] Sága, M., Pecháč, P., Vaško, M., FSD and its modifications for shell finite elements, *American Journal of Mechanical Engineering* 7 (2013) 427-433.
- [2] Sága, M., Dudinský, M., Pecháč, P., Implementation of discrete fully stressing into structural optimization, *Zeszyty Naukowe Politechniki Śląskiej* 76 (2012) 105-112.
- [3] Sága, M., Dudinský, M., Pecháč, P., Optimization Of Thin Shell Structures Using FSD Algorithms, *Communications* 14 (3) (2012) 32-38.

Residual stress distribution in polyolefin pipes

J. Poduška^{a,b}, M. Ševčík^a, J. Kučera^c, P. Hutař^a, J. Sadílek^c, L. Náhlík^a

^a Institute of physics of materials, Czech Academy of Sciences, Žitkova 22, 616 62, Brno, Czech Republic

^b Faculty of Mechanical Engineering, Brno University of Technology, Technická 2, 616 69 Brno, Czech Republic

^c Polymer Institute Brno, Tkalcovská 36/2, 656 49, Brno, Czech Republic

The most frequent failure mechanism of a polyolefin (i.e. polypropylene or polyethylene) pipe in pressure applications is so called slow crack growth – SCG. The time to failure by this mechanism is usually estimated by standard extrapolation method from the results of the hydrostatic pressure test. However, with increasing quality of plastic piping materials, these tests take very long time to produce satisfactory results. The lifetime is then estimated by different methods that are based on the results of PENT, FNCT or CRB tests and linear elastic fracture mechanics [1].

Circumferential and axial residual stresses originate in the pipe wall during the uneven cooling in the process of manufacture [2]. Especially circumferential residual stress has a significant effect on the lifetime of the pipe, because it adds to the hoop stress invoked by hydrostatic pressure inside the pipe and thus helps cracks grow. It is important to know correct distribution and magnitude of it, so it can be included into mentioned lifetime calculations [3].

In order to assess the distribution of circumferential residual stress, an experiment was carried out using a quite old method – pipe is cut into a number of thin rings, the wall of these rings is divided into several layers and, using a lathe, some of the layers are removed. Then, the rings are slit axially and allowed to deform, while the change in diameter ΔD is measured (Fig. 1), [4].

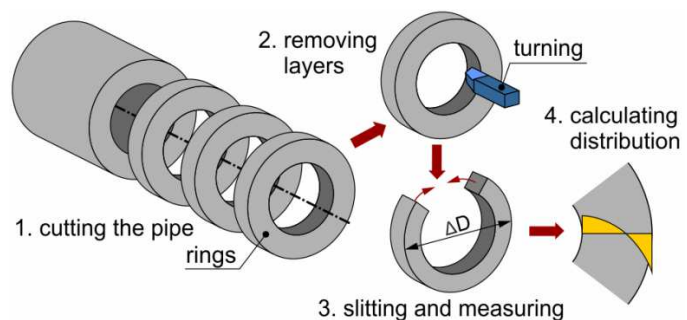


Fig. 1. Schema of the experiment

A set of 8 polypropylene (PP-R Vestolen P9426) pipes of different dimensions was used for the experiment, the dimensions being (diameter/wall thickness): 32/4.4, 40/3.7, 40/5.5, 40/6.7, 63/5.8, 63/8.6, 63/10.5 and 110/15.1. Measuring took place after one and again after four weeks after the slitting. For all of the pipes a residual hoop stress distribution was obtained by evaluating the measured ΔD by a method based on a theory of a curved beam. The residual stress distributions were obtained in the form of 10 discrete values across the pipe wall, because every pipe wall was divided into ten layers and the stress in each layer was considered constant. These values were then fitted with an exponential equation in the form of $\sigma_{RES}(x) = c_1 + c_2 e^{tx}$, where c_1 , c_2 and t are constants and x is the relative position in the pipe wall.

FEM simulation was used to test the behavior of the rings under the influence of the residual hoop stress and to verify that the method of evaluation was correct.

Although the pipe dimensions were different, the resultant residual stress distributions were all similar in shape and magnitude. If the pipes are manufactured in a similar manner, the residual stress should indeed be similar and they could be estimated by one general equation independent on pipe dimensions. This equation was proposed (see Fig. 2) for polypropylene. It was obtained as exponential fit of the average residual hoop stress values.

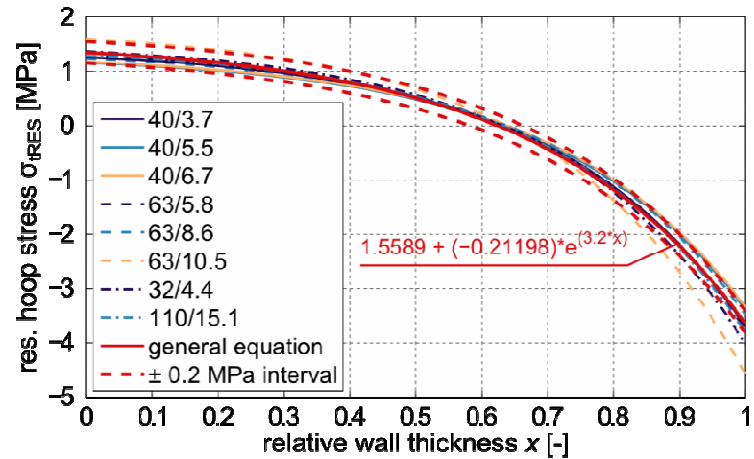


Fig. 2. The residual hoop stress distribution in polypropylene

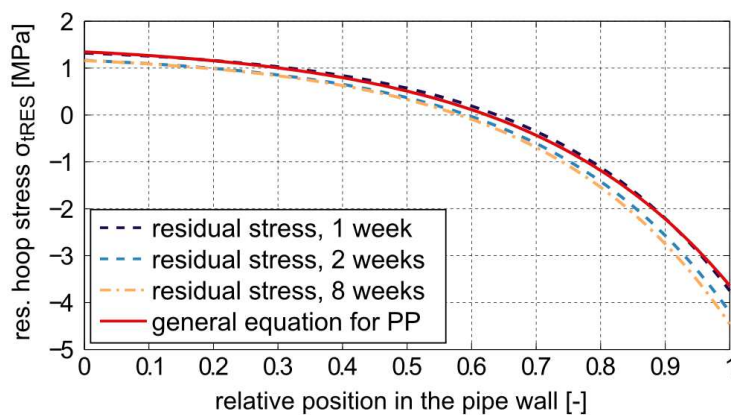


Fig. 3. The residual hoop stress distribution in polyethylene pipe compared to general equation for polypropylene

The described experiment was also carried out on one polyethylene pipe (dimensions 160/14.6). When the results for polyethylene are compared to the general equation that was set up for polypropylene, it can be seen that the distributions are again similar (Fig. 3).

However, these distributions were obtained by measuring and evaluating deflection of thin rings. Longer pieces deflect more because of the presence of the axial residual stress which does not affect the thin rings. The effective hoop stress in an actual long pipe is then higher [5].

The presented research dealt with assessing the residual hoop stress in the wall of polyolefin pipe. A general equation for residual stress distribution in polypropylene pipe was proposed. It was found that it estimates correctly also the distribution in polyethylene pipe.

The presented research dealt with assessing the residual hoop stress in the wall of polyolefin pipe. A general equation for residual stress distribution in polypropylene pipe was proposed. It was found that it estimates correctly also the distribution in polyethylene pipe.

Acknowledgements

The research was supported through the grant P108/12/1560 of the Czech Science Foundation and a grant No. CZ.1.07/2.3.00/20.0214 of the Ministry of Education, Youth and Sports of the Czech Republic.

References

- [1] Hutar, P., Sevcik, M., Nahlik, L., Pinter, G., Frank, A., Mitev, I., A numerical methodology for lifetime estimation of HDPE pressure pipes, *Engineering Fracture Mechanics* 78 (17) (2011) 3049-305.
- [2] Janson, L.E., *Plastics pipes for water supply and sewage disposal: 3rd edition*, Borealis, Stockholm, 1999.
- [3] Hutar, P., Sevcik, M., Frank, A., Nahlik, L., Kucera, J., Pinter, G., The effect of residual stress on polymer pipe lifetime, *Engineering Fracture Mechanics* 108 (2013) 98-108.
- [4] Williams, J.G., Hodgkinson, J.M., Gray, A., The determination of residual stresses in plastic pipe and their role in fracture, *Polymer Engineering and Science* 21 (13) (1981) 822-828.
- [5] Poduska, J., Kucera, J., Hutar, P., Sevcik, M., Krivanek, J., Sadilek, J., Nahlik, L., Residual stress distribution in extruded polypropylene pipes, *Polymer Testing* 40 (2014) 88-98.

Fatigue crack propagation in railway axles

P. Pokorný^{a,b}, L. Náhlík^a, P. Hutař^a

^a Institute of Physics of Materials of the Academy of Sciences of the Czech Republic, Žitkova 22, 616 62 Brno, Czech Republic

^b Faculty of Mechanical Engineering, Brno University of Technology, Technická 2, 616 69 Brno, Czech Republic

According to the latest released report of the European Railway Agency (ERA) from 2014 [1] the number of train accidents caused by failure of the railway axles was 52 cases in 2010, 33 cases in 2011 and 62 cases in 2012 (failures of the railway axles in European Union). Because of possible serious consequences of such failure the estimation of residual fatigue lifetime of the railway axles could be useful for safer operation of the trains. In many cases the failure is associated with fatigue of material [2]. The cracks dangerous for fatigue failure could be present in the railway axle already from manufacturing process of the railway axle or from assembly of the railway wheelset, where two wheels are press-fitted on the railway axle and some cracks could initiate. The dangerous crack could also initiate during train operation where e.g. flying ballast impacts could cause scratch (deeper than 1 mm), which could contribute to fatigue crack initiation. In many cases there is a contribution of corrosion [3]. The possibility of detection of such cracks is of probabilistic nature. The greater crack is, the more likely detection of crack is. For estimation of the residual fatigue lifetime of the railway axle the crack with certain size which might not be detected by non-destructive testing method should be assumed. The most important point is that the railway axle with crack has to be removed from operation before the fatigue crack reaches the critical size. This work deals with estimation of the residual fatigue lifetime of the railway axle. The methodology used can be divided into two main parts: numerical part based on finite element method (FEM) simulations of growing crack in the railway axle and analytical part dealing with estimation of the residual fatigue lifetime based on the knowledge of fracture parameters of growing crack in the axle. The numerical model considers the railway axle with initial crack. According to experimental observations the crack has semi-elliptical shape of the crack front. One of semi-axes of ellipse is crack length a .

The contribution is focused mainly on the second part, i.e. on the procedure of analytical estimation of the residual fatigue lifetime of the railway axle. The behaviour of such crack is described by stress intensity factor K . The maximal stress intensity factor in one load cycle could be expressed as:

$$K_{\max} = \sigma_{\max} \sqrt{\pi a} Y_I(a) + K_{I,PF}(a), \quad (1)$$

where σ_{\max} is the maximum of remote loading stress in one load cycle, $Y_I(a)$ is shape function obtained by K -calibration procedure based on FEM modelling and $K_{I,PF}(a)$ is stress intensity factor performed by residual stresses caused by press-fitted wheel. The contribution of press-fitted wheel to K_{\max} value is similarly obtained by FEM calculations.

For establishment of the residual fatigue lifetime of the railway axle is necessary to carry out an experiment focused on fatigue crack propagation rate determination of particular railway axle material. In this work the standard steels EA1N and EA4T for manufacturing of

railway axles are considered. The most common model of ν - K dependence is described by Paris-Erdogan law:

$$\frac{da}{dN} \cong \frac{\Delta a}{\Delta N} = C(K_{\max})^m \rightarrow \Delta a = C(K_{\max})^m \Delta N \quad \text{for } K_{\max} \geq K_{th}, \quad (2)$$

by discretization of this model it is possible to numerically express fatigue crack length increment Δa for one load cycle. However, the trains are subjected to variable amplitude loading. This variability is caused by different service regimes of train (train goes to curved tracks, over crossovers, switches or different load conditions of train: full load train, unloaded train, etc.). Therefore, the maximum of remote loading stress σ_{\max} is not constant. Such type of loading is associated with interaction effects, where fatigue crack increment is not the same as in the case of constant amplitude loading [4]. The most important interaction effect is retardation of propagating fatigue crack due to overload cycles. For inclusion of retardation in this work the generalized Willenborg model was used [5]. This model uses effective value of the stress intensity factor K_{eff} instead of the maximal stress intensity factor K_{\max} . K_{eff} is influenced by plastic material properties and by history sequence of loading. This approach provides more accurate estimation of residual fatigue life time than approach which does not take into account existence of the retardation effects. This paper also shows the impacts of several different ν - K curve descriptions on estimated residual fatigue lifetimes of the railway axles. Besides the Paris-Erdogan law, the NASGRO relationship and multi-linear model of ν - K curve are used. The Paris-Erdogan relationship is not able to describe typical bending of ν - K curve near to threshold value and thus residual fatigue lifetime obtained by Paris-Erdogan relationship gives to much conservative results. The next two considered models take into account this bending of ν - K curve near threshold value and their estimation of the residual fatigue lifetime is more accurate. The important part of this work deals with sensitivity of threshold value on the residual fatigue lifetime of the railway axles. It is shown that little change of threshold value has substantial impact on the residual fatigue lifetime of the railway axles.

Acknowledgements

This work was supported through the specific academic research grant No. FSI-S-14-2311 provided to Brno University of Technology, Faculty of Mechanical Engineering and grant No. CZ.1.07/2.3.00/20.0214 of the Ministry of Education, Youth and Sports of the Czech Republic.

References

- [1] European Railway Agency (ERA). Railway safety performance in the European Union, 2014. <<http://www.era.europa.eu/Document-Register/Documents/SPR2014.pdf>>
- [2] Zerbst, U., Safe life and damage tolerance aspects of railway axles – A review, *Engng Fract Mech* 98 (2012) 214-271.
- [3] Beretta, S., Corrosion–fatigue of A1N railway axle steel exposed to rainwater, *International Journal of Fatigue* 32 (2010) 952-961.
- [4] Schijve, J., *Fatigue of structures and materials*, Springer, New York, 2008.
- [5] Harter, J.A., *AFGROW users guide and technical manual*, 1999.

Influence of the fibre stiffness model in a weight-fibre-pulley-drive mechanical system on the coincidence with the experimental measurement results

P. Polach^a, M. Hajžman^a, Z. Šika^b, P. Svatoš^b

^a Section of Materials and Mechanical Engineering Research, Výzkumný a zkušební ústav Plzeň s.r.o., Tylova 1581/46, 301 00 Plzeň, Czech Republic

^b Department of Mechanics, Biomechanics and Mechatronics, Faculty of Mechanical Engineering, Czech Technical University in Prague, Technická 4, 166 07 Praha, Czech Republic

Experimental measurements focused on the investigation of a fibre behaviour are performed on an assembled weigh-fibre-pulley-drive mechanical system (see Fig. 1). The carbon fibre (of the length 1.82 meters), which is driven by one drive, is led over a pulley. On its other end there is a prism-shaped steel weight (of the weight 3.096 kg), which moves in a prismatic linkage on an inclined plane (angle of inclination α could be changed – in presented case $\alpha = 30^\circ$). In presented case the position of the weight is symmetric with respect to the plane of a drive-pulley symmetry [1]. Drive excitation signals can be of different shapes with the possibility of variation of a signal rate (e.g. [1]). The influence of the fibre stiffness in the computational model on the coincidence of the simulation results and the experimental measurement results are evaluated. Time histories of the weight position and of the force acting in the fibre are measured.

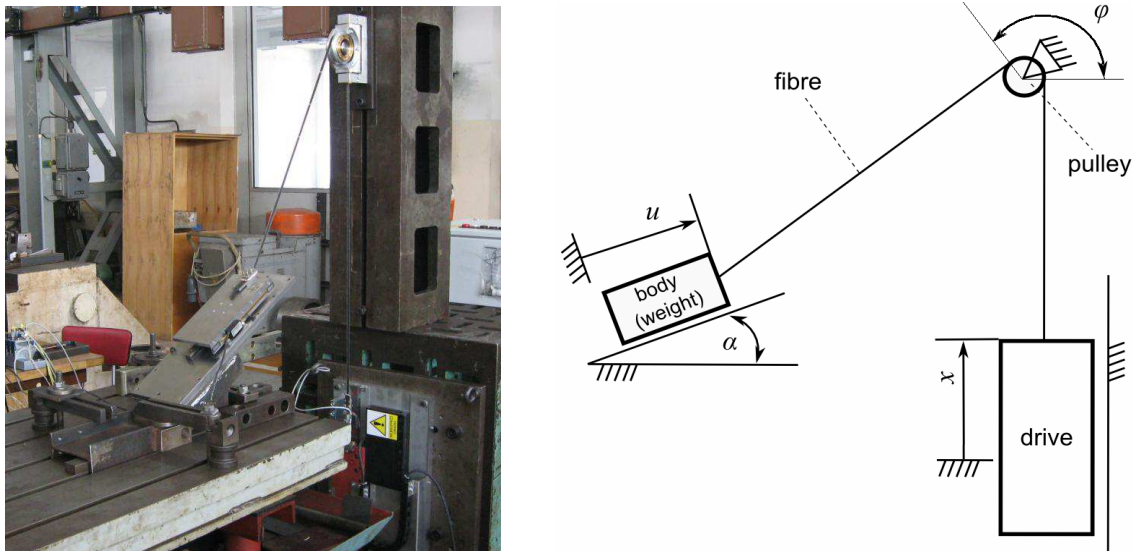


Fig. 1. A real weight-fibre-pulley-drive mechanical system and its scheme

A massless fibre model is used in the model of the investigated system. The weight, the pulley and the drive are considered to be rigid bodies. Motion of the drive is kinematically prescribed. Investigation of the fibre properties eliminating the influence of the drive and the pulley (weight-fibre mechanical system only) [2] was an intermediate stage before the

measurement on the weigh-fibre-pulley-drive mechanical system. A phenomenological model (comprises e.g. influences of fibre transversal vibration etc.) was the result of this investigation, but the general phenomenological model of the fibre was not determined. The fibre damping coefficient, the fibre stiffness and the friction force acting between the weight and the prismatic linkage were considered to be system parameters of the phenomenological model. The parameters determined at investigating the weight-fibre system [2] were applied in the fibre model of the weight-fibre-pulley-drive system.

At simulating the experimental measurements for “quicker” drive motion (e.g. [1]; see Fig. 2) the local extremes of the monitored time histories of the weight displacement and of the force acting in the fibre are dependent on all the phenomenological model parameters. From the obtained results it is evident that parameters of the fibre phenomenological model must be, in addition, considered dependent on velocity of the weight motion. That is why the influence of considering the velocity-dependent stiffness in the fibre model on dynamic response of the system is topically investigated.

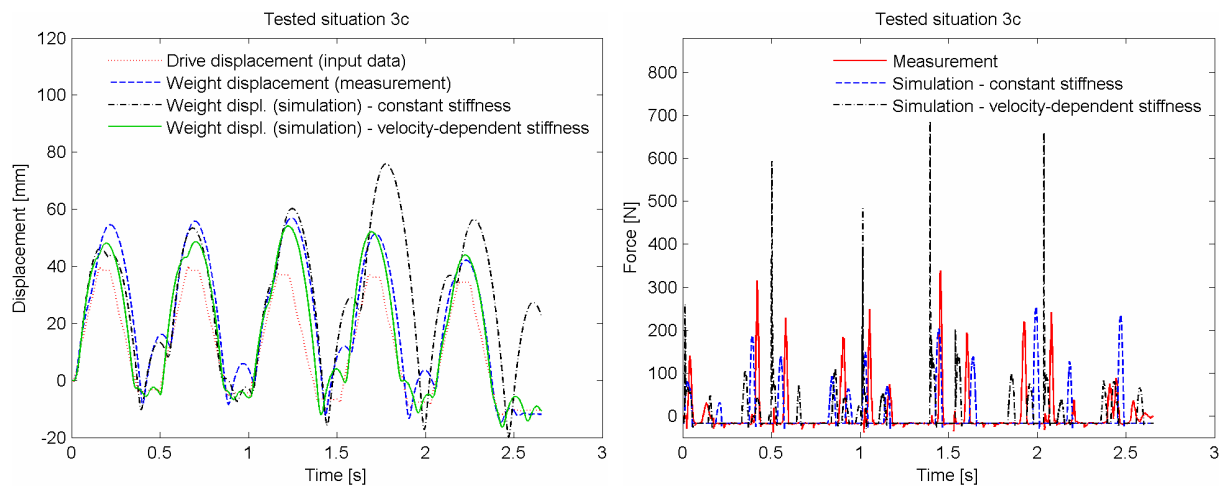


Fig. 2. Time histories of the weight displacement (left) and force acting in the fibre (right)

The velocity-dependent stiffness of the fibre is supposed in the form

$$c = \begin{cases} c_c, & \text{if } v \leq v_{tr} \\ c_c + (v - v_{tr}) \cdot c_2, & \text{if } v > v_{tr} \end{cases} \quad (1)$$

where c is fibre stiffness, c_c is constant fibre stiffness (taken from [1]), c_2 is constant, v is instantaneous velocity of the weight and v_{tr} is threshold value of the velocity of the weight. The optimal (constant) values of constant c_2 and threshold value of weight velocity v_{tr} were found.

Development of the fibre phenomenological model continues. It can be supposed that in a more sophisticated phenomenological model of the fibre a more complicated dependency of the fibre damping coefficient (and alternatively more sophisticated fibre stiffness model) will be considered.

References

- [1] Polach, P., Hajžman, M., Václavík, J., Šika, Z., Svatoš, P., Model parameters influence of a simple mechanical system with fibre and pulley with respect to experimental measurements, Proceedings of ECCOMAS Thematic Conference Multibody Dynamics 2013, Zagreb, Faculty of Mechanical Engineering and Naval Architecture, University of Zagreb, 2013. (CD-ROM)
- [2] Polach, P., Hajžman, M., Václavík, J., Experimental and computational investigation of a simple mechanical system with fibre, Engineering Mechanics 21 (1) (2014) 19-27.

Vibrations of blades couple connected by slip-stick dry friction

L. Půst^a, L. Pešek^a, A. Radolfová^a

^a*Institute of Thermomechanics, Czech Academy of Sciences, Dolejškova 5, 18200, Czech Republic*

The reduction of enormous great resonance vibrations of turbine blades is very often realized by using dry friction contacts between vibrating elements. Many theoretical, numerical and experimental investigations of dynamic properties of turbine blades were done also in Institute of Thermomechanics ASCR particularly with the main attention on the development of means for reduction of dangerous resonance amplitudes of blades. The dynamic systems investigated in previous papers [e.g. 2-4] contain dry friction elements with “force-velocity” characteristics.

Prepared paper describes a mathematical model for analysing the dynamic characteristics of two-blades bunch with more complicated “stick-slip” damping connections among blades than previously used friction characteristics. Several types of stick-slip mathematical models with 3D force-velocity-displacement characteristics will be presented and analysed. Effects of tangential micro-deformations in contact surfaces as well as of dry friction forces and excitation amplitudes on hysteresis loops and on response curves will be shown and discussed.

Application of dry friction characteristics described by a comparatively simple 2D “force-velocity” expressions are useful in the ranges of great relative velocities and stiff contacting bodies. Application of dry friction characteristics described by comparatively simple 2D „force-velocity“ expressions is useful in the ranges of great relative velocities. Use of only one motion variable - velocity v - enables an easy calculation for the majority of engineering problems, where the vibrating bodies can be supposed as stiff and when at great amplitudes only slip in contact surfaces each against other is decisive.

However with some friction couples, where friction surfaces are placed on some relative compliant parts of moving bodies it is necessary to use more sophisticated computational model. This case is significant especially at vibrations with small amplitudes. Such a “stick-slip” contact model is shown in Fig. 1, where the spring replaces the contact tangential stiffness.

This element consists of Coulomb dry friction part consecutively connected to spring with the characteristic

$$\begin{aligned}
 f(\dot{x}_1, x - x_1) &= k(x - x_1) & \text{if } \dot{x}_1 &= 0, \\
 f(\dot{x}_1, x - x_1) &= \text{sign}(\dot{x}_1) & \text{if } |\dot{x}_1| > 0.
 \end{aligned}
 \tag{1}$$

Point A of spring and damper connection can be supposed either weightless (case a) or with a very small mass m_1 , modeling mass of elastically deformed parts of contacting bodies near the friction surface.

Hysteresis loop for simple cosine motion has rhomboid-form and contains four breaks [1]. However, if the relative motion in the contact surface is not so simple, but contains higher components, the computation is much complicated and is very inconvenient for dynamic

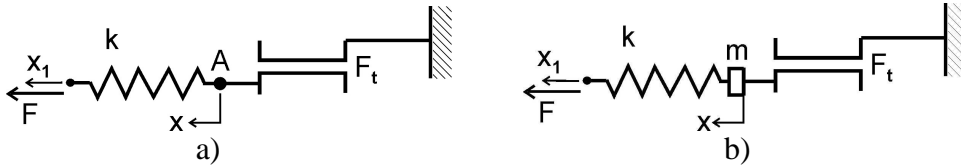


Fig. 1. Stick-slip contact model

problems solution. Direct numerical solution (e.g. ODE solvers in Matlab) of ordinary differential equation based on transformation into a set of first order equations runs in difficulties with inverting function *sign* in friction characteristic. This complication can be removed by expressing the Coulomb law by means of “arc-tangent” function, which is continuous in the whole range of velocity \dot{x} :

$$F_t = F_{t0} \frac{2}{\pi} \arctg(\alpha \dot{x}_1).$$

Examples of rhomboid hysteresis loops in Fig.2 are drawn for three amplitudes $a=2, 1.5, 1$, $\alpha=25$. and for parameters of spring and dry friction element $k=1, F_{t0}=1$.

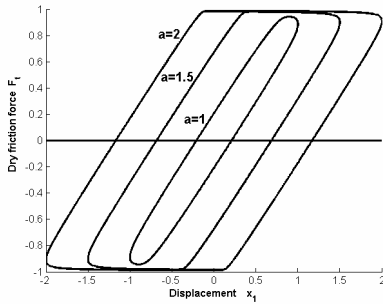


Fig. 2. Rhomboid hysteresis loops

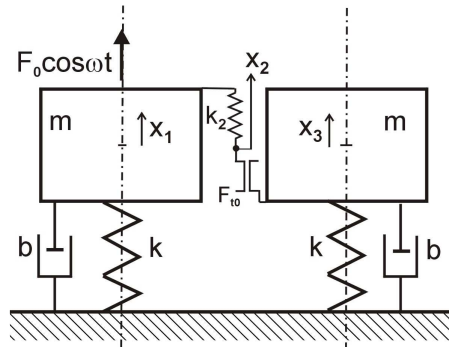


Fig. 3. Model of blades couple

Simplified mathematical model of blades couple consisting two identical 1 DOF slightly damped subsystems connected by a slip-stick friction contact is in Fig. 3. Differential equations of motion of this system excited only on the first mass are

$$\begin{aligned} m\ddot{x}_1 + b\dot{x}_1 + kx_1 + k_2(x_1 - x_2) &= F_0 \cos \omega t, \\ k_2(x_2 - x_1) + F_{t0} \frac{2}{\pi} \arctan(\alpha(\dot{x}_2 - \dot{x}_3)) &= 0, \\ m\ddot{x}_3 + b\dot{x}_3 + kx_3 - F_{t0} \frac{2}{\pi} \arctan(\alpha(\dot{x}_2 - \dot{x}_3)) &= 0. \end{aligned} \quad (2)$$

These equations contain only continuous functions and can be easy numerically solved as will be shown and discussed at presentation.

Acknowledgements

The work has been supported by the conceptual development fund RVO: 61388998 of the Institute of Thermomechanics AS CR, v.v.i.

References

- [1] Ding, Q., Chen, Y., Analyzing resonance response of a system with dry friction damper using an analytical method, *Journal of Vibration and Control* 14 (8) (2008) 1111-1123.
- [2] Pust, L., Pešek, L., Radolfova, A., Various type of dry friction characteristics for vibration damping, *Engineering Mechanics* 18 (2011) 203-224.
- [3] Pust, L., Pešek, L., Vibration damping by dry friction with micro-slips, *Proceedings of Dynamics of Machines 2013, Prague, IT AS CR, 2013*, pp. 93-102.
- [4] Püst, L., Pešek, L., Influence of delayed excitation on vibrations of turbine blades couple, *Applied and Computational Mechanics* 7 (1) (2013) 39-52.

The influence of floating ring bearing parameters on turbocharger dynamic behavior

Z. Rendlová^a

^a Faculty of Applied Sciences, UWB in Pilsen, Univerzitní 22, 306 14 Plzeň, Czech Republic

Currently the considerable attention is devoted to analyzing of dynamic behavior of turbocharger rotors that is inseparably linked to bearing system characteristics. According to [2] the rolling-element bearings or floating ring bearings are usually used in case of turbochargers. In case of automotive applications the floating ring bearings are mostly used because they do not exhibit excessive noise and reduce power losses [1].

The floating ring bearings comprise two oil films separated by a fully floating ring, see Fig. 1. According to [2], each oil film transfers the force that is specified by the bearing geometry, lubricating layer properties and angular velocities of bearing surfaces. If the journal rotates by angular velocity ω_J and the bearing bore rotates by angular velocity ω_B , then the floating ring rotates by angular velocity $\omega_R = RSR \cdot \omega_J$, where the Ring Speed Ratio (RSR) is associated with the friction power in the bearing and can be expressed using bearing parameters as

$$RSR = \frac{1}{1 + \frac{\eta(T_O)L_O c_I}{\eta(T_I)L_I c_O} \frac{\sqrt{1-\varepsilon_I^2}}{\sqrt{1-\varepsilon_O^2}} \left(\frac{D_O}{D_I}\right)^3} \quad (1)$$

Considering laminar flow of Newtonian isoviscous fluid in a radial cylindrical short bearing with no cavitation effect, the damping and stiffness coefficients of the oil film result from Reynolds equation solution. The bearing coefficients derivation is written in [3].

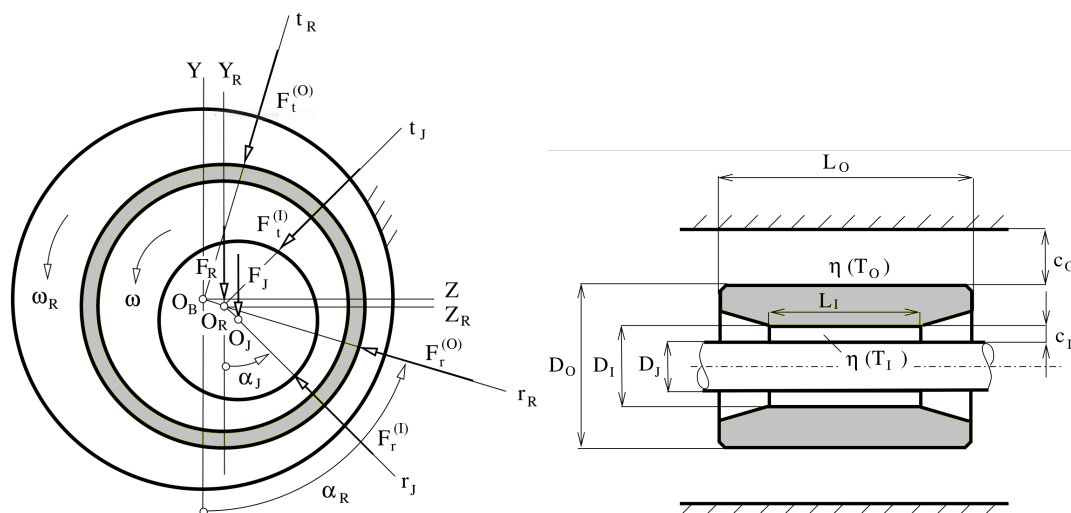


Fig. 1. Floating ring bearing scheme

Considering small displacements near the static equilibrium position, the turbocharger rotor represented by the a shaft of continuously distributed mass mounted by several wheels can be mathematically described using finite element method [3]. Then, this rotor is supported by radial floating ring bearings can be described using equations of motion that can be expressed in matrix form as

$$\begin{bmatrix} \mathbf{M}_R & \mathbf{0} \\ \mathbf{0} & \mathbf{M}_B \end{bmatrix} \begin{bmatrix} \ddot{\mathbf{q}}_R \\ \ddot{\mathbf{q}}_B \end{bmatrix} + \left(\begin{bmatrix} \mathbf{B}_R - \omega \mathbf{G}_R & \mathbf{0} \\ \mathbf{0} & \mathbf{0} \end{bmatrix} + \mathbf{B}_B(\omega) \right) \begin{bmatrix} \dot{\mathbf{q}}_R \\ \dot{\mathbf{q}}_B \end{bmatrix} + \left(\begin{bmatrix} \mathbf{K}_R - \omega \mathbf{C}_R & \mathbf{0} \\ \mathbf{0} & \mathbf{0} \end{bmatrix} + \mathbf{K}_B(\omega) \right) \begin{bmatrix} \mathbf{q}_R \\ \mathbf{q}_B \end{bmatrix} = \begin{bmatrix} \mathbf{f}_R(t) \\ \mathbf{0} \end{bmatrix}, \quad (2)$$

where \mathbf{X}_R are matrices describing the rotor and \mathbf{X}_B are matrices representing floating ring bearings.

The influence of bearing parameters is investigated on automotive turbocharger weighing about 200 g that is supported by two radial floating ring bearings. Having regard to the expression (1) determining the speed of rotation of the ring ω_R , the change of bearing parameters is realized through changes of considered operating temperatures of lubricant in both bearings, more specifically in Table 1. Recall that the change in lubricant temperature is linked to a dynamic viscosity change.

Tab. 1. Combination of lubricating layers temperatures

	Bearing a		Bearing b	
	Inner oil film	Outer oil film	Inner oil film	Outer oil film
I	20	20	20	20
II	100	80	70	70
III	180	140	130	120
IV	180	160	150	140

The aim of this work is to determine the effect of changes in lubricant temperature, and thus the parameter RSR, on the dynamic characteristics of the turbocharger rotor-bearing system. Although the floating ring bearings are more suitable in case of automotive applications [1], the presence of four layers of lubricant significantly affects the character of the system. First of all, lubricating layers are a significant source of turbocharger rotor-bearing system instability.

Acknowledgements

The work presented in this paper was supported by SGS-2013-036 project of University of West Bohemia. The usage of the AVL EXCITE software in the framework of the University Partnership Program of AVL List GmbH is greatly acknowledged.

References

- [1] San Andrés, L., Rivadeneira, J.C., Chinta, M., Gjika, K., LaRue, G., Nonlinear rotordynamics of automotive turbochargers: Predictions and comparisons to test data, *Journal of Engineering for Gas Turbines and Power* 129 (2) 488-493.
- [2] Schäfer, H. N., *Rotordynamics of automotive turbochargers*, Springer, Stuttgart, 2012.
- [3] Zeman, V., Hlaváč, Z., Rendlová, Z., *Modeling of turbocharger vibrations*, Research report, University of West Bohemia, 2013. (in Czech)

Computational modelling of cavitation in simple geometries, but complex flows

P. Rudolf^a, J. Kozák^a

^a V. Kaplan Department of Fluid Engineering, Faculty of Mechanical Engineering, Brno University of Technology, Technická 2896/2, 61669 Brno, Czech Republic

Cavitation occurs when local pressure in flowing liquid drops below saturated vapor pressure. If the resulting vapor bubbles are transported to regions of higher pressure then sudden condensation follows, which is accompanied by emission of pressure and acoustic waves [1]. Above described process leads to cavitation erosion and consequently to shorter service time of the hydraulic machines.

However cavitating flows are also characteristic by increased amount of unsteadiness. Unsteady behavior is manifested by cavitation cloud shedding and by increased pressure pulsations. These phenomena deteriorate hydraulic machine performance and are usually transmitted further to the system (pipeline, valves, etc.).

Two cases were experimentally and computationally studied: cavitating flow in converging-diverging (CD) nozzle [3] and cavitating flow around hydrofoil. Although both geometries are rather simple, the flow is very complex due to interactions of the turbulent flow and cavitation clouds. Computational simulations revealed that proper capturing of the underlying one-phase flow field is crucial to obtain correct vorticity distribution. Clouds filled with vapor are born from regions of concentrated vorticity and shed downstream. Only advanced turbulence models (Reynolds Stress Model, Scale Adaptive Simulation) are able to predict vorticity field and development of the unsteady swirling flow [3].

Increased vorticity generation in two-phase flows is caused by additional term in vorticity equation [2]. This equation is obtained by applying curl operator to Navier-Stokes equation with variable density:

$$\frac{\partial \omega_i}{\partial t} + v_j \frac{\partial \omega_i}{\partial x_j} = \omega_j \frac{\partial v_i}{\partial x_j} - \omega_i \frac{\partial v_j}{\partial x_j} + \varepsilon_{ijk} \frac{\partial a_k}{\partial x_j} + \varepsilon_{ijk} \frac{1}{\rho^2} \frac{\partial \rho}{\partial x_j} \frac{\partial p}{\partial x_k}. \quad (1)$$

The last term on the right hand side (equivalent form using differential operators is) is so called baroclinic torque. Maximum vorticity generation due to this term is when the gradients of pressure and density are mutually perpendicular. Illustration for the case of converging-diverging nozzle is depicted in Fig. 1. Resulting flow pattern is characterized by regular shedding of the vortex rings, see Figs. 2 and 3. According to numerical simulations the vortex rings are not present for the case of non-cavitating flows. Decreasing cavitation number induces generation of vorticity due to baroclinic torque term and onset of cavitated boundary layer separation, which is then rolled into vortex ring.

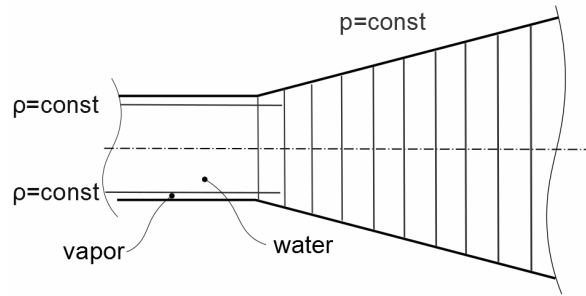


Fig. 1. Scheme of pressure and density distribution in the throat and diverging part of the CD nozzle

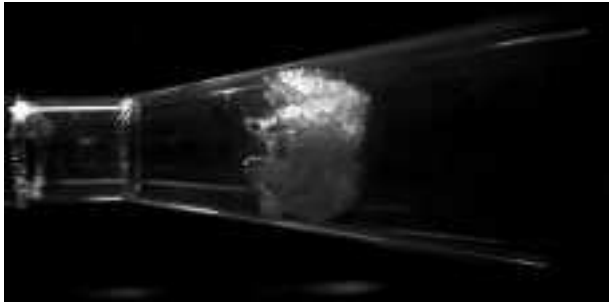


Fig. 2. Cavitating vortex ring in converging- diverging nozzle – experiment

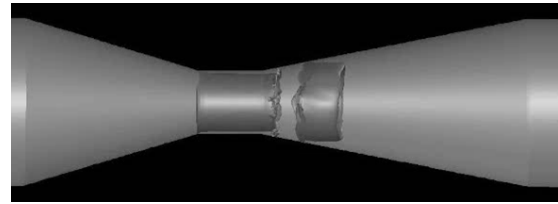


Fig. 3. Vapor region in converging-diverging nozzle – computational simulation

Shedding of the cavitation clouds was also observed in flow around NACA hydrofoil. It was confirmed that baroclinic torque is important for prediction of the vorticity in two-phase flows (or generally in flows with stratified density). Presented results stress using cavitation models based on transport equation of the volume fraction instead of barotropic models in which, by construction, the gradients of pressure and density are parallel.

Some conclusions for correct simulation of the unsteadiness and instability of cavitating flows can be drawn from present research:

- instability is connected with vorticity generation,
- proper capturing of vorticity in one-phase base flow is essential requirement,
- interplay between the phase distribution and pressure gradient has to be modeled to obtain additional vorticity generation due to baroclinic torque.

Acknowledgement

The research has been supported by project of the Czech Science Foundation No P101/13-23550S “Experimental research and mathematical modelling of unsteady phenomena induced by hydrodynamic cavitation”.

References

- [1] Franc, J.P., Michel, J.M., Fundamentals of cavitation, Series: Fluid mechanics and its applications Vol. 76, Springer, 2004.
- [2] Gopalan, S., Katz, J., Flow structure and modelling issues in the closure region of attached cavitation, Physics of Fluids 12 (2000) 895-911.
- [3] Rudolf, P., Hudec, M., Zubík, P., Štefan, D., Experimental measurement and numerical modelling of cavitating flow in converging-diverging nozzle, EPJ Web of Conf. 25, 01081 (2012).
- [4] Rudolf, P., Hudec, M., Gríger, M., Štefan, D., Characterization of the cavitating flow in converging-diverging nozzle based on experimental investigation, EPJ Web of Conf. 67, 02101 (2014).

Extended thermomechanical model for NiTi-based shape memory alloys with plasticity

V. Sháněl^{a,b}, T. Ben Zineb^c, J. Plešek^a

^a*Institute of Thermomechanics AS CR, v. v. i., Dolejškova 5, 182 00 Praha 8, Czech Republic*
^b*Faculty of Mechanical Engineering, CTU in Prague, Technická 4, 166 07 Praha 6, Czech Republic*
^c*LEMETA, UMR 7563, Université de Lorraine, Vandoeuvre-lès-Nancy 54500, France*

This work presents a thermodynamically formulated model of shape memory alloys (SMAs) extended by the element of plasticity. The model is designed to simulate the response of polycrystalline NiTi-based SMA materials. Its features include a description of the transformation between austenite, R-phase, martensite and its reorientation. This model has been improved with von Mises plasticity with linear hardening in martensite, the additional dissipative process. The model together with the extension is created within the framework of continuum thermodynamics of irreversible processes. The model was implemented into the finite element software Abaqus via UMAT subroutine. Several simulations were carried out for a description of its behavior under loading and the response of the model was compared with experimental results.

Shape memory alloys are characterized by a different response on thermo-mechanical loading than classic metals which makes them suitable for special use in technical as well as medical applications. During the past few decades, a great effort has been made to create mathematical models to describe SMA behavior.

Most of the modern SMAs models based on the principle of driving forces that are evaluated in every increment and when such driving forces reach a certain threshold, then the current

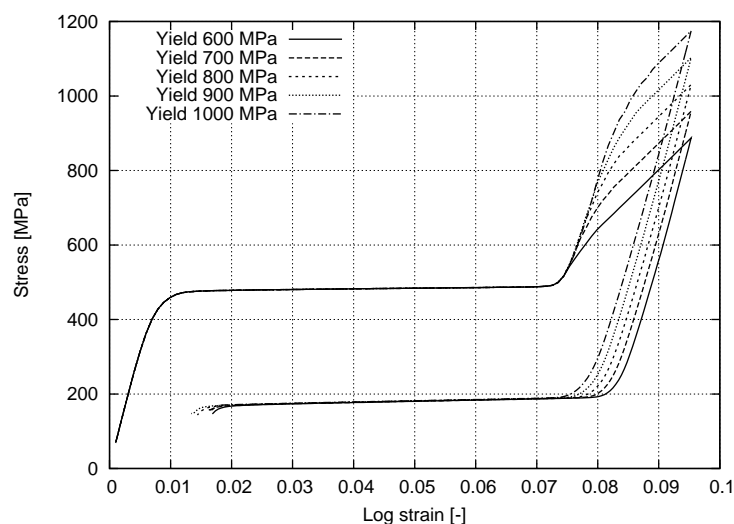


Fig. 1. Stress-strain diagram for uniaxial tensile test – loading and unloading with a five different yield stresses and a hardening parameter $H_p = 15\ 000\ \text{MPa}$

process (reorientation, phase transformations, etc...) is activated. This is one of the ways to obtain an adequate response observed in experimental results. Unfortunately these models are often quite complicated and insufficiently robust and stable.

Another possible way to describe the behavior of SMA (see Fig. 1) is to use a thermomechanical framework [2]. It is the basis for the current SMA model [4] which works due to the minimization of the Hemholtz free energy. This model is characterized by a novel form of the dissipation function coupling martensite transformation and reorientation processes, transformation between austenite and R-phase, material anisotropy and now also with plasticity in the martensitic phase. The model contains eight internal variables (martensite volume fraction, five components of a transformation strain, R-phase volume fraction and plastic multiplier) which are minimized aspect to Hemholtz free energy using the downhill simplex minimization method by Nelder and Mead. This minimization method is unconstrained so that the hyperbolic tangent transformation is used to ensure fulfilment of the physical limits.

Hemholtz free energy is now composed of three parts. Elastic energy f^{el} , chemical energy f^{chem} and plastic energy f^{pl} :

$$f = f^{el} + f^{chem} + f^{pl}. \quad (1)$$

Plastic term in the energy is active all the time and it is minimized in every increment. In relation to the aspect of plasticity, two physical parameters had to be added – Yield stress [MPa] and the Hardening coefficient [MPa]. The total plastic strain is a cumulative variable and it is composed of many small increments to capture the changes in stress so that this model can also be used for nonproportional loading.

The material model described in [4] was enhanced by the other dissipative mechanism – plasticity of the martensite through the addition of one new internal variable. The extension follows and respects all thermomechanical principles and ideas of the original model. The future development will be mainly focused on enhancing the numerical solution of the model.

Acknowledgements

This work was supported by the Grant Agency of the Czech Technical University in Prague, Grant No. SGS12/175/OHK2/3T/12.

References

- [1] Auricchio, F., Reali, A., Stefanelli, U., A three-dimensional model describing stress-induced solid phase transformation with permanent inelasticity, *International Journal of Plasticity* 23 (2007) 207-226.
- [2] Houlsby, G.T., Puzrin, A.M., A thermomechanical framework for constitutive models for rate-independent dissipative materials, *International Journal of Plasticity* 16 (2000) 1017-1047.
- [3] Lagoudas, D.C., Entchev, P.B., Modeling of transformation-induced plasticity and its effect on the behavior of porous shape memory alloys. Part 1: Constitutive model for fully dense SMAs, *Mechanics of Materials* 36 (2004) 865-892.
- [4] Sedlák, P., Frost, M., Benešová, B., Ben Zineb, T., Šittner, P., Thermomechanical model for NiTi-based shape memory alloys including R-phase and material anisotropy under multi-axial loadings, *International Journal of Plasticity* 39 (2012) 132-151.

Influence of gripping method in biaxial testing of soft biological tissues

M. Slažanský^a, J. Burša^a, S. Polzer^a

^a*Institute of Solid Mechanics, Mechatronics and Biomechanics, Brno University of Technology, Technická 2896/2, 616 69 Czech Republic*

Computational modelling has become a significant tool in many branches of biology and medicine. Accuracy of mechanical computational analyses is limited by disposal of high-quality input data on material properties of the investigated biological materials. Their specific properties require specific approaches in mechanical testing which are not standardized and consequently suffer from inaccuracies caused by varying experiment conditions. For instance, the tested specimen of soft biological tissue can be attached and loaded using clamps or hooks, see Fig. 1.

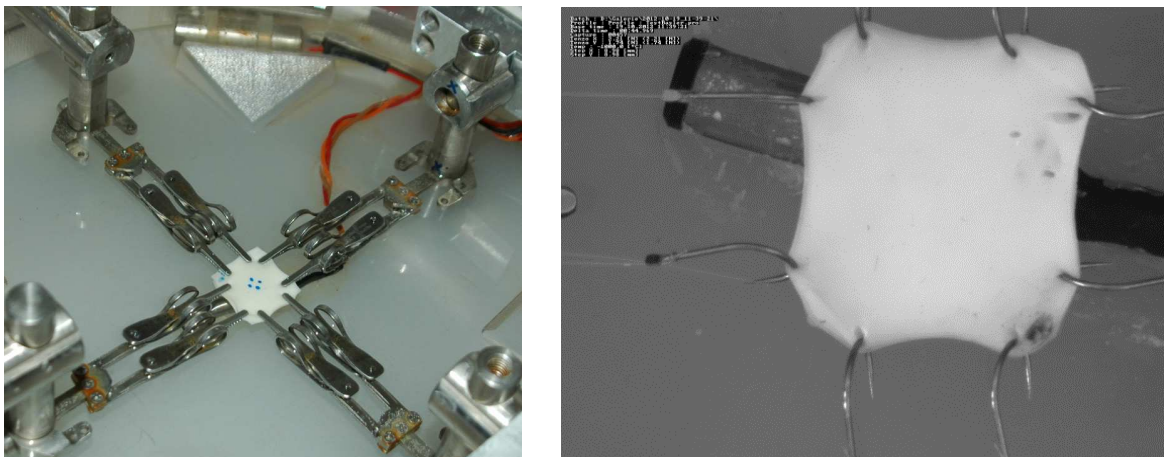


Fig. 1. Specimen gripped by means of clamps (left) and hooks (right), two pieces for each edge

The number and the size of clamps and hooks have a significant impact on the distribution of stress and strain in the centre of the specimen, where deformation is measured. These effects of different boundary conditions were analyzed in [1-3] via 2D computational models and limited variations of gripping methods. But the following questions remained unanswered adequately or at all: Are 2D models sufficient for simulation of biaxial tests of soft tissues? How can the accuracy of stress-strain dependence be influenced by range of numbers and dimensions of the loading elements (clamps or hooks)? How is the accuracy influenced by material properties and size of the sample? In short, what is the best way of realization of biaxial tension tests?

To find the answers, 3D computational models were used (see Fig. 2) to elaborate a sensitivity analysis of number and size of clamps and hooks. The number and size of clamps and hooks were optimized by computational simulations in such a way that the material parameters obtained in the biaxial tension test correspond to the utmost to the actual parameters of the investigated material.

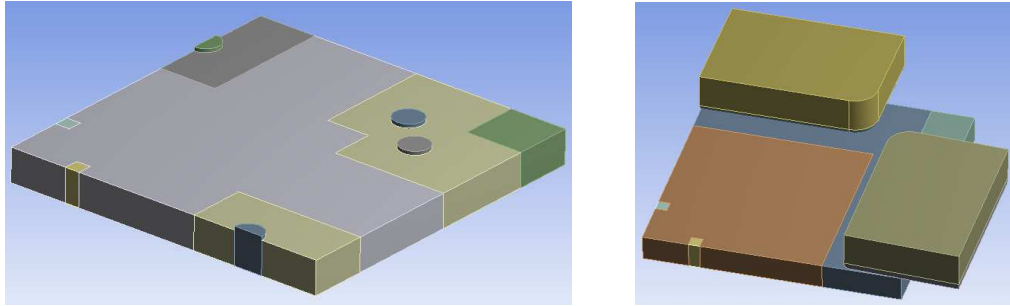


Fig. 2. Computational models of specimen gripped by hooks (left) and clamps (right)

Two isotropic hyperelastic models of material with different stiffnesses were used in both equibiaxial and proportional test protocols (displacement ratio $u_y:u_x$ 1:2, 1:4).

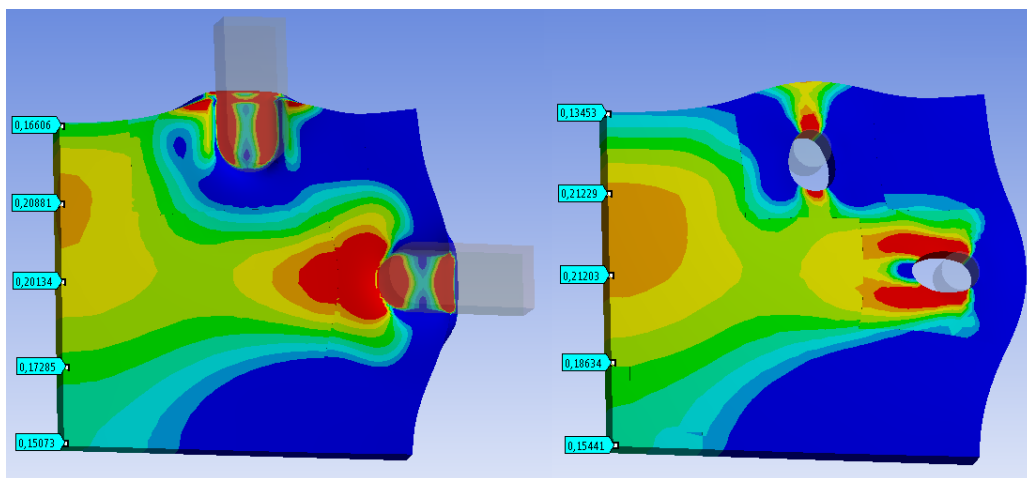


Fig. 3. Resulting normal strain in X axis in a quarter model using clamps (left) and hooks (right) in simulated proportional loading with displacement controlled protocol $u_x/u_y = 4/1$

The comparison of different influences on measured data and resulting accuracy in determination of the true material parameters showed the following conclusions: The 3D FE simulations have shown that for biaxial testing of small size specimens of soft tissues both clamps and hooks are capable to offer an acceptable accuracy of results. Two, three, or four hooks per edge can be applied independently of their diameter. Two clamps give very accurate results in a wide range of dimensions. Three clamps are applicable in a narrow range of their dimensions only and for lower loads

Acknowledgements

We gratefully acknowledge the support given to this work by Czech Science Foundation, grant project No.13-16304S and faculty project No. FSI-S-14-2344.

References

- [1] Sun, W., Sacks, M.S., Scott, M.J., Effects of boundary conditions on the estimation of the planar biaxial mechanical properties of soft tissues, *Journal of Biomechanical Engineering* 127 (4) (2005) 709-715.
- [2] Waldman, S.D., Sacks, M.S., Lee, J.M., Boundary conditions during biaxial testing of planar connective tissues. *Journal of Materials Science Letters* 21 (2002) 1215-1221.
- [3] Jacobs, N.T., Cortes, D.H., Vresilovic, E.J., Elliot, D.M., Biaxial tension of fibrous tissue: Using finite element methods to address experimental challenges arising from boundary conditions and anisotropy, *Journal of Biomechanical Engineering* 135 (2) (2013). (doi: 10.1115/1.4023503)

Numerical homogenization of fibres reinforced composite materials using representative volume

L. Smetanka^a, J. Gerlici^a, Z. Pelagič^a

^a Faculty of Mechanical Engineering, University of Žilina, Univerzitná, 010 26 Žilina, Slovak Republic

In this time we meet with trend replace steel materials with composite materials. In design practice in the selection of appropriate material puts condition that the strength, alternatively mechanical characteristics of material suits the point of maximum stress. Since steel materials have homogenous isotropic material and strength properties, the can be used from strength view only in this area. This can be considerably ineffective. Technology of composite materials allows create structure, which will suit stress state and is resistant in place of high stress, but in another place have not such characteristics. Development of new materials puts requirements not only on technology and design, but also on calculations. Today is common that before production of important construction perform numerical analysis whose aim is to design the required properties. Composite materials have be compared with steel materials significant benefits: low density, greater tenacity, resistance to chemical and weather influence, better thermal and electrical insulating properties etc. [1, 3].

In homogenization process the original heterogeneous material is replaced by homogeneous material with the same mechanical properties. In other words, homogenization and averaging of properties and micro-fields of the material are considered as a homogeneous equivalent medium at the macro-level, and the effective properties of the medium are determined on the basis of the analysis of the microstructure, micro-geometry and properties of the materials. There are various homogenization methods. Direct homogenization is based on the volume average of field variables, such as stress, strain and energy density. Effective properties can be calculated from effective properties definitions. The average and calculation of field variables can be performed numerically, for example, by finite element method (FEM) or boundary element method and geometry and microstructural properties can be generalized for real composite materials which do not have periodic structure distribution of the fibers in the matrix [4]. The composite under consideration is constituted by continuous and parallel cylindrical fibers with equal radius and centers periodically spaced in a hexagonal and a squared array, as it appears in Fig. 1. We assumed an ideal cohesion between the fiber and the matrix. A procedure of homogenization of material properties of composites using the method of representative volume element RVE was used.

Representative volume element (RVE) represents minimum volume element which the measurement can be done, to represent the properties of the whole. Its size should be large enough by compared to the size microstructural element, but small enough to allow an analysis of the available resources. The RVE dimensions are different in depending by arrangement fibers in hexagonal or square configuration, but also by the volume fraction fiber in matrix.

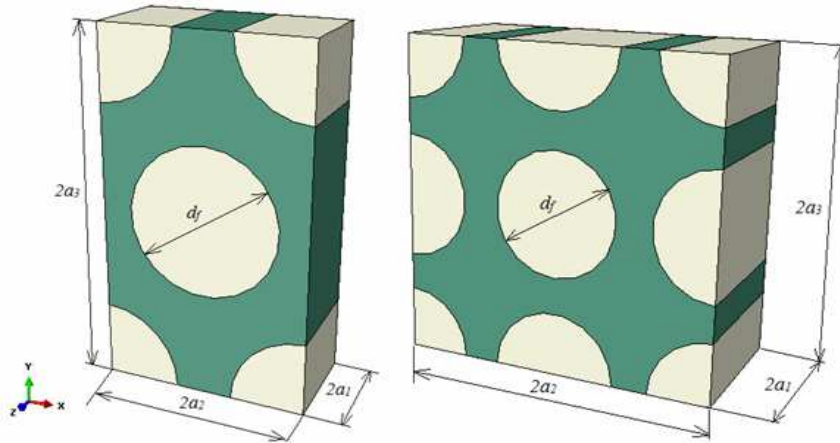


Fig. 1. Representative volume element

For the homogeneous composite material, the relationship between average stress and strain is

$$\bar{\sigma}_\alpha = C_{\alpha\beta} \bar{\epsilon}_\beta. \quad (1)$$

Once the components of the transversely isotropic tensor C are known, the five elastic properties of the homogenized material can be computed by [2]

$$\begin{aligned} E_1 &= C_{11} - 2C_{12}^2 / (C_{22} + C_{23}), \\ \nu_{12} &= C_{12} / (C_{22} + C_{23}), \\ E_2 &= (C_{11}(C_{22} + C_{23}) - 2C_{12}^2)(C_{22} - C_{23}) / (C_{11}C_{22} - C_{12}^2), \\ \nu_{23} &= (C_{11}C_{23} - C_{12}^2) / (C_{11}C_{22} - C_{12}^2), \\ G_{12} &= C_{66}, \\ G_{23} = C_{44} &= \frac{1}{2}(C_{22} - C_{23}) = \frac{E_2}{2(1 + \nu_{23})}. \end{aligned} \quad (2)$$

Acknowledgements

The work was supported by the Scientific Grant Agency of the Ministry of Education of the Slovak Republic and the Slovak Academy of Sciences in project No. 1/1098/11: “Stress Distribution in a Braked Railway Wheel”. No. 1/0347/12: “Railway wheel tread profile wear research under the rail vehicle in operation conditions simulation on the test bench”, project No. 1/0383/12: “The rail vehicle running properties research with the help of a computer simulation.” and the project No. APVV-0842-11: “Equivalent railway operation load simulator on the roller rig”.

References

- [1] Laš, V., Mechanics of composite materials, Západočeská univerzita v Plzni, Plzeň, 2007. (in Czech)
- [2] Barbero, J., Finite element analysis of composite materials using Abaqus, CRC Press, Boca Raton, 2013.
- [3] Vrbka, J., Mechanics of composite materials, Vysoké učení technické v Brně, Brno, 2008. (in Czech)
- [4] Žmindák, M., Riecky, D., Soukup, J., Failure of composites with short fibres, Communications 12 (4) (2010) 33-39.

Elastic wave propagation in nonhomogeneous media: A solution using the 2.5D meshless MLPG approach in the frequency domain

P. Staňák^a, A. Tadeu^b, J. Sládek^a, V. Sládek^a

^a *Institute of Construction and Architecture, Slovak Academy of Sciences, Dúbravská cesta 9, 845 03 Bratislava, Slovakia*

^b *ITeCons, University of Coimbra, Pólo II, Rua Pedro Hispano, 3030-289, Coimbra, Portugal*

Numerical modeling of wave propagation in solids is a subject of interest to many engineers and researchers. In recent years increased attention has been devoted to development of theoretical and numerical models that allow accurate simulation of different types of systems and structures incorporating nonhomogeneous material properties or interaction between various media. The calculation of 3D response of longitudinally invariant structures may become computationally demanding, unless more efficient techniques, such as 2.5D dimensional approach, are applied [3, 4]. In case of 2.5D approach only the cross-section of the structure is discretized and Fourier series expansion is used to retrieve the results in the longitudinal direction. A wide range of tools is currently available for the analysis of elastic wave propagation in solid media including boundary element method (BEM) or finite element method (FEM).

Even though the FEM has encountered wide acceptance and success on commercial market, it possess some drawbacks such as locking of elements, stress discontinuity across elements or costly remeshing in large problems with moving boundaries. The meshless methods, an attractive option to solve these drawbacks were developed in the last decade. Among many meshless or meshfree methods available, the meshless local Petrov-Galerkin (MLPG) method [1] has received considerable scientific attention. MLPG is a truly meshless method, thus no elements are required neither for approximation nor for integration of unknowns. This is advantageous in solving the problems with continuously nonhomogeneous material properties [2, 5].

In the present paper the MLPG is used for the analysis of elastic wave propagation in nonhomogeneous media using 2.5D approach. Nodal points are spread on the analyzed 2D domain without any restrictions. Small local circular subdomain is introduced around each nodal point. Local integral equations (LIEs) constructed from governing PDEs are defined over these circular subdomains. Moving Least-Squares (MLS) approximation scheme is used to approximate the spatial variations of the mechanical displacement field. The essential boundary conditions are satisfied by the collocation of MLS approximation expressions for prescribed displacements on boundary nodes. The analysis is performed in the frequency domain with the use of variables in the form of complex numbers.

Certain heterogeneous media can be characterized as multi-component composites with smooth variation of volume fraction of constituents. Nonhomogeneous material properties are defined through continuous variation of Young's modulus $E(\mathbf{x})$ as

$$E(\mathbf{x}) = E_0 + E_0 \frac{2y(\mathbf{x})}{r} e^{\left(-\left(\frac{2x(\mathbf{x})}{r} \right)^2 - \left(\frac{2y(\mathbf{x})}{r} \right)^2 \right)}, \quad (1)$$

where E_0 is the reference value of Young's modulus, x, y are the coordinates at the cross-sectional area and r is the radius of the cylinder.

Hollow cylinder with nonhomogeneous material properties is analysed as a numerical example to demonstrate the applicability of present method. The interior hollow part is considered rigid, while the exterior surface is subjected to non-uniform load. Fig. 1 shows resulting u_y - displacement response subjected to applied load in y -direction with frequency of 1000 Hz. The results at the cross-section of the cylinder are obtained from the nodal points while the results along longitudinal z -coordinate are computed using the Fourier series expansion. The model is applicable for various frequencies of loading and material property variations.

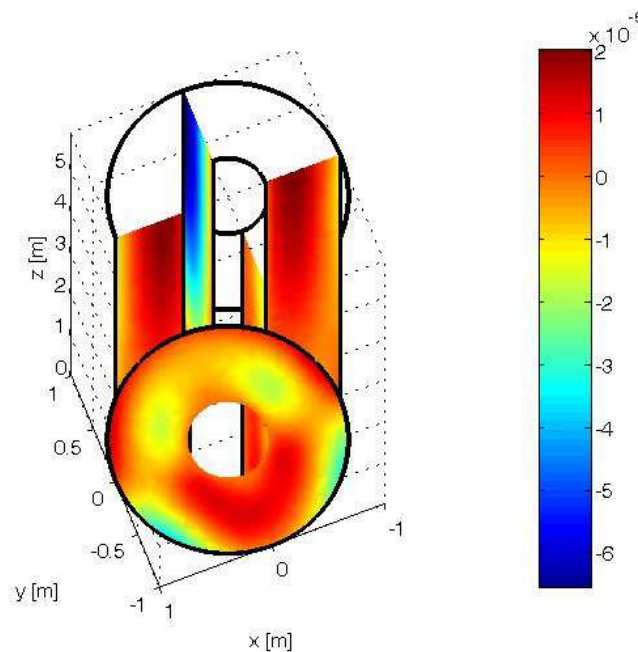


Fig. 1. Computed 3D response of displacement u_y for the nonhomogenous hollow cylinder

Acknowledgements

The authors gratefully acknowledge the financial support by the Slovak Science and Technology Assistance Agency registered under number APVV-0014-10.

References

- [1] Atluri, S.N., The Meshless Method (MLPG) for domain & BIE discretizations, Tech Science Press, Forsyth, GA, 2004.
- [2] Sladek, J., Sladek, V., Zhang Ch. Application of meshless local Petrov–Galerkin (MLPG) method to elastodynamic problems in continuously nonhomogeneous solids, CMES-Computer Modeling in Engineering and Sciences 4 (2003) 637–648.
- [3] Tadeu, A., Kausel, E., Green's functions for two-and-a-half-dimensional elastodynamic problems, ASCE J. Engrg. Mech. 126 (10) (2000) 1093–1096.
- [4] Tadeu, A., Antonio, J., 2.5D Green's functions for elastodynamic problems in layered acoustic and elastic formations, CMES- Computer Modeling in Engineering and Sciences 2 (2001) 477–495.
- [5] Tadeu, A., Stanak, P., Sladek, J., Sladek, V., Prata, J., Simões, N. A., Coupled BEM-MLPG technique for the thermal analysis of non-homogeneous media, CMES - Computer Modeling in Engineering & Sciences 93 (6) (2013) 489-516.

Model identification and control law optimization of fiber driven mechanism QuadroSphere

P. Svatoš^a, Z. Šika^a

^a Department of Mechanics, Biomechanics and Mechatronics, Faculty of Mechanical Engineering, Czech Technical University in Prague, Technická 4, 166 07 Praha, Czech Republic

The paper deals with the setup of a flexible multibody model of the fibre driven mechanism QuadroSphere. The model is completed by the combination of analytical methods for large motions and the experimental identification of the flexible eigenmodes. The complete identified flexible multibody model is used for the control law synthesis. The optimized control law is implemented to the functional model of mechanism.

Optimization and design of functional model of QuadroSphere, a spherical fibre-driven mechanism with four drives, have been presented in [1, 2]. The following Fig. 1 illustrates an experimental functional model of the QuadroSphere.

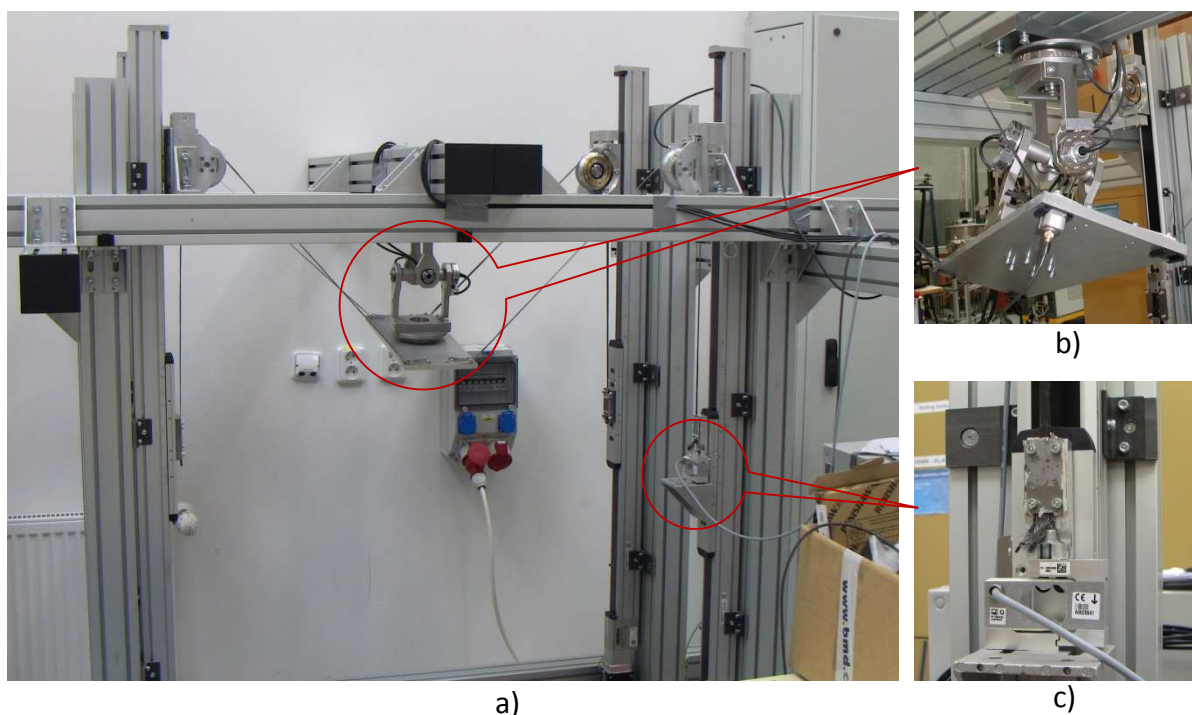


Fig. 1. Experimental functional model of the QuadroSphere

The spherical central joint is realized by the Cardan concept (universal joint) with direct measurement of three angular positions. The force sensor is placed at the end of one of four fibres. The Fig. 2 describes a basic scheme of control algorithm. The position loop is realised in the higher level controller. The controller obtains the actual spherical position of the platform based on the signals from the joint incremental sensors (Fig. 1 b)). Three of four drives are controlled directly from the inverse kinematics, the fourth drive is controlled in

order to stabilize the fibre tension measured by the force sensor (Fig. 1c). The identification measurement had been done. The measurement includes position control of the mechanism platform with reference chirp or step signal (Fig. 2). The position control accuracy is tested by several versions of platform requested motion (Fig. 3). The main target of the ongoing research is the widening of the servo bandwidth and consequently the improvement of the feedback control. There are two steps towards this aim, firstly the optimization of the regulator of the given structure and secondly the usage of additional active auxiliary structure.

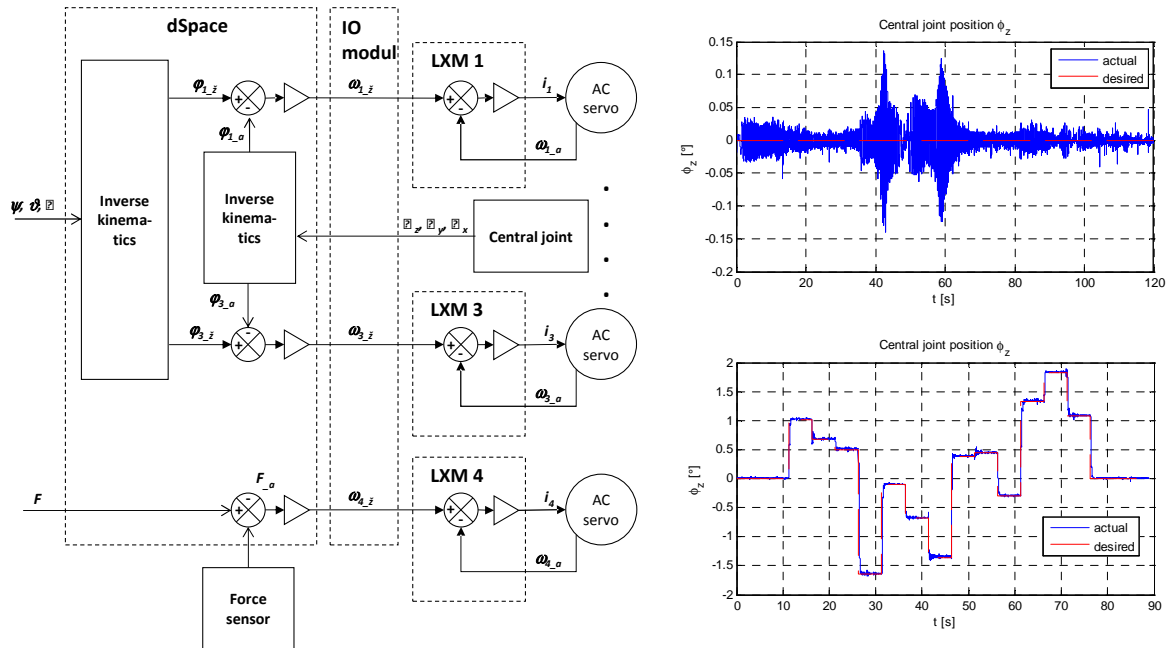


Fig. 2. Control scheme (left), identification measurement response: chirp signal (top), step (down)

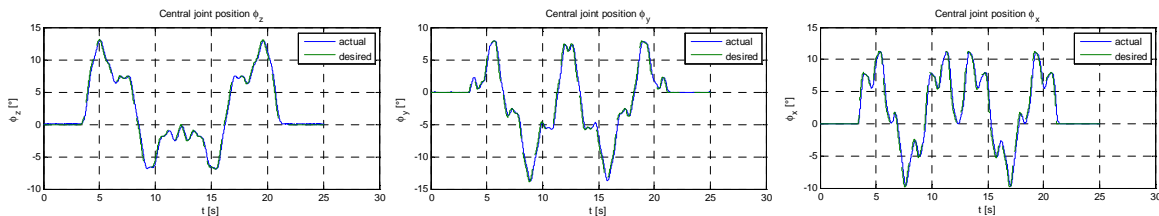


Fig. 3. Example of position control of platform

Acknowledgements

The authors appreciate the kind support by the grant GA101/11/1627 “**Tilting Mechanisms Based on Fiber Parallel Kinematical Structure with Antiblacklash Control**” of the Czech Science Foundation and project SGS13/177/OHK2/3T/12 “**Mechatronics a adaptronics 2013**” of CTU in Prague.

References

- [1] Svatoš, P., Šika, Z., Zicha, J., Valášek, M., Rada, V., Optimization and design of fibre-driven spherical mechanism, Proceedings of 29th conference with international participation Computational Mechanics 2013, Plzeň, Czech republic, 2013, pp. 123-124.
- [2] Svatoš, P., Šika, Z., Valášek, M., Bauma, V., Polach, P., Optimization of anti-backlash fibre driven parallel kinematical structures, Bulletin of Applied Mechanics 8 (31) (2012) 40-44.

Influence of soil loading on fracture behavior of multilayer polymer pipe

M. Ševčík^a, P. Hutař^a, F. Arbeiter^b, G. Pinter^b, L. Náhlík^a

^a *Institute of Physics of Materials, Academy of Sciences of the Czech Republic, Žitkova 22, 616 62, Brno, Czech Republic*
^b *Montanuniversitaet Leoben, Leoben, Austria*

Plastic pipes are attractive for non-pressure applications due to high flow rates, adequate strength for earth loads and high chemical resistance [1]. To further improve mechanical and physical properties of polymer pipes multilayer structuring are used. Multilayer pipes often consist of three different layers: inner layer (resistance against abrasion and slow crack growth), middle layer (improve stiffness of the pipe) and outer layer (resistance against external scratches and point loads). The lifetime of a modern polymer pipe is expected to reach up to 100 years in service. The long-term failure of the pipe is usually in a quasi-brittle mode in which the slow (creep) crack growth (SCG) occurs. Due to the small plastic zone in the vicinity of the crack tip in the SCG regime the linear elastic fracture mechanics can be applied. Therefore, the stress intensity factor can be used as a parameter controlling the crack growth in polymer pipes, see e.g. [1–3].

At first the pipe without a crack was numerically analysed in order to find the critical location for the crack initiation. The distribution of the tangential stress along the internal and external pipe surface is shown in Fig. 1. The nonhomogenous nature of the tangential stress is a product of nonhomogenous distribution of the external pressure from soil.

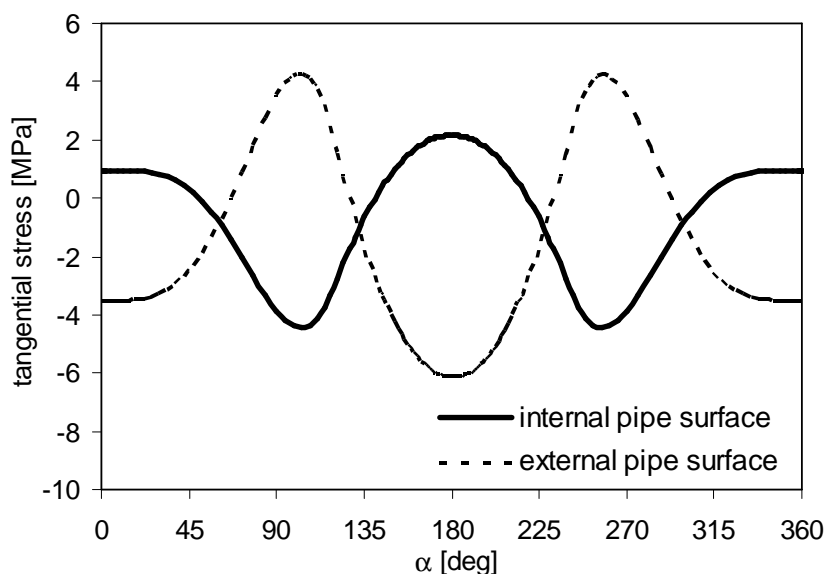


Fig. 1. Distribution of the tangential stress along the internal and external pipe surface

In the next step various geometries of the internal cracks were introduced into the numerical model. The stress intensity factors for such cracks are shown in Fig. 2.

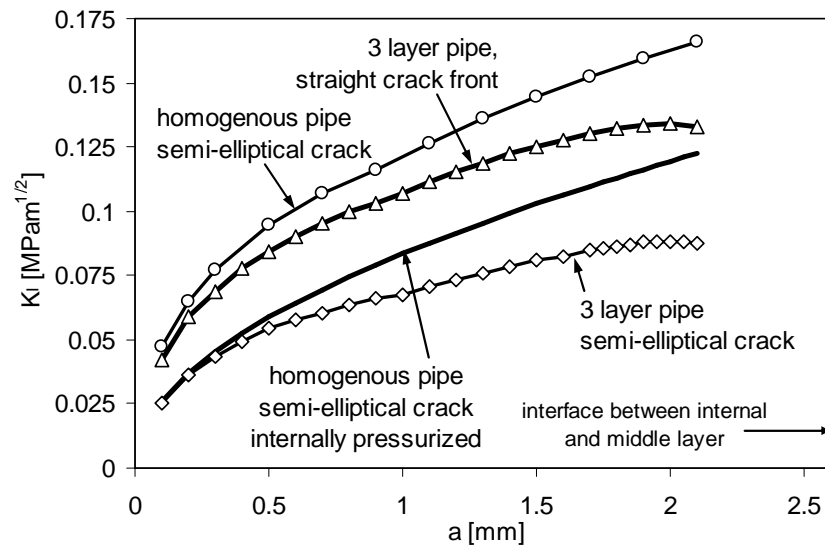


Fig. 2. Stress intensity factor for the internal crack in homogenous and three-layer pipe

In this paper it is shown that the soil loading has significant influence on the fracture behavior of buried pipes. The fracture behavior of the three layer pipe containing axially oriented semi-elliptical or straight crack was numerically studied. It was shown that the layered nature of the pipe leads to significant decrease of the stress intensity factor compared to a homogenous pipe. Furthermore, the material interface between internal and middle layer of the pipe will also contribute to the decreasing of the stress intensity factor, thereby prolonging the residual lifetime of the three-layer pipe. The results presented in this work can be useful for better prediction of the residual lifetime of the multi-layer polymer pipes subjected to complex loading.

Acknowledgements

The work was supported through the grant P108/12/1560 of the Czech Science Foundation and by the Ministry of Education, Youth and Sports of the Czech Republic throughout the Project No. CZ.1.07/2.3.00/30.0063 (Talented postdocs for scientific excellence in physics of materials). Part of research was performed at the Chair of Materials Science and Testing of Polymers (University of Leoben, Austria) within the framework of the FFG program of the Austrian Ministry of Traffic, Innovation and Technology and the Austrian Ministry of Economy, Family and Youth with contributions of the Österreichisches Forschungsinstitut für Chemie und Technik (Austria), Martin-Luther-Universität Halle-Wittenberg (Germany) and the Polymer Competence Center Leoben GmbH (Austria)

References

- [1] Watkins, R.K., Anderson, L.R., Structural mechanics of buried pipes, CRC Press, Boca Raton, FL, 1999.
- [2] Frank, A., Freimann, W., Pinter, G., Lang, R.W., Engineering fracture mechanics 76 (2009) 2780-2787.
- [3] Hutař, P., Ševčík, M., Náhlík, L., Pinter, G., Frank, A., Mitev, I., Engineering fracture mechanics 78 (2011) 3049-3058.

Foundation for heavy machines

J. Šmejkal^a, F. Plánička^a

^a Faculty of Applied Sciences, University of West Bohemia, Univerzitní 22, 306 14 Plzeň, Czech Republic

The foundations shall be designed according to EN 1990 and machine loads according to EN 1991-3. For heavy machines we usually analyse the space models of the foundation with machine. For modelling we used 3D solid elements, machine is modelled only with idealized beams with corresponding stiffness. Frame and plate models are usually not acceptable for block foundations because of spatial of all masses and forces. The main function of concrete foundations is stabilizing regularly or irregularly working of the machine. Foundation are civil structures, witch are deigned according to probability design (for example according to Euro-codes). Used materials are determined as the material with probability than 95% characteristics are better than prescribed (Fig. 1). In design we don't know really material properties. With most detailed model of the foundation we achieve behavior of the foundation with greater probability, but the really behavior of the system machine with foundation shall be achieved with modeling of the whole system with probabilistic tools.

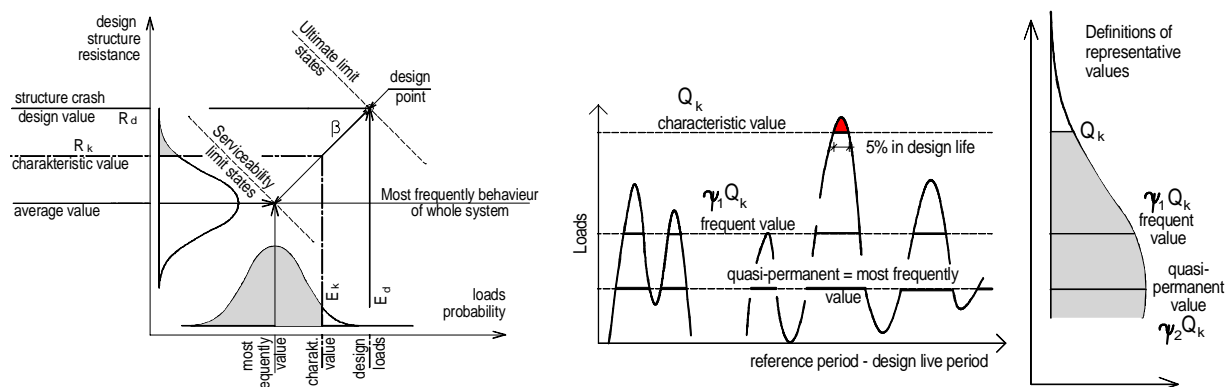


Fig. 1. Design philosophy of foundation

The Euro Standard [2] establishes principles and requirements for safety, serviceability and durability of structures, describes the basis for their design and verification and gives guidelines for greater aspects of structural reliability. EN 1991-3 Action On Structures – Part 3 Action induced by cranes and machinery [1] defined principles for the machine foundation design. A complete survey of static and dynamic forces for various design situations should be obtained from the machine manufacturer together with all other machine data such as outline drawings, weights of static and moving parts, speeds, balancing etc

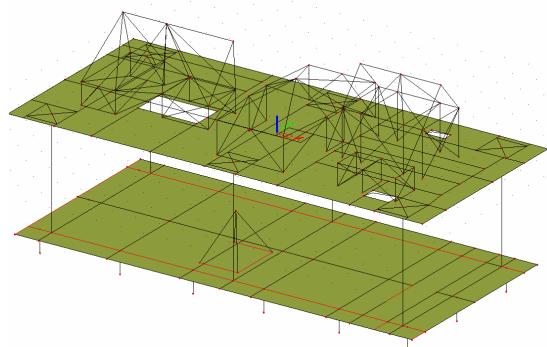
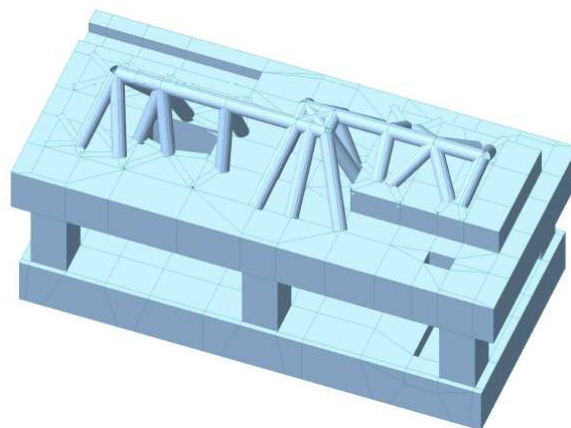


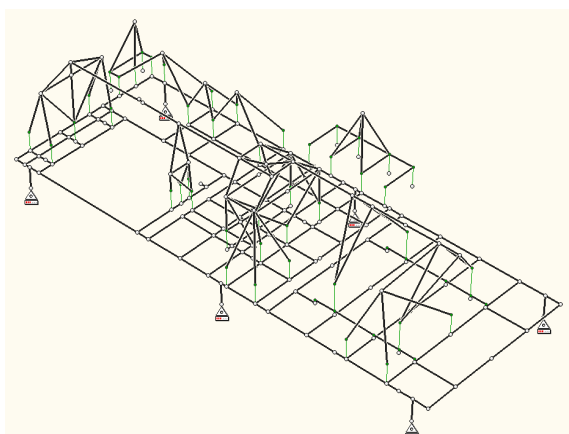
Plate model of the foundation



Solid 3D model of the foundation

Fig. 2. Various level of modeling for frame foundation for turbo - set

The most frequent material for foundations is concrete (Fig. 2). It must be concrete structure without cracks. Cracks can cause lowering of stiffness of the foundation. For normal reinforcement concrete structures all tension carry reinforcement, but for foundation for heavy machines tension must carry concrete. It is necessary to eliminate the early cracks too. Although we eliminate cracks, the non linear analyses of the foundation can be necessary caused by non linear behaviour of the bedrock.



Frame model of the foundation

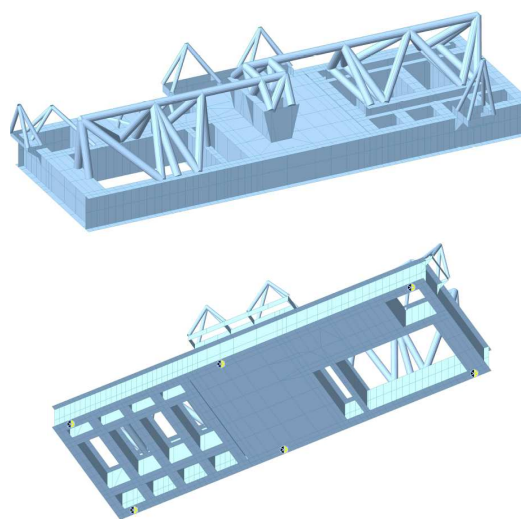


Plate-Wall model of the foundation

Fig. 3. Various models for spring supported frame foundation for turbo – set

Acknowledgements

The research work was supported by the project SGS-2013-036.

References

- [1] EN 1991-3 Action on structures – Part 3 Action induced by cranes and machinery, ČNI 2004.
- [2] ČSN EN 1990 Basis of structural design.
- [3] Program MidasGEN, version 2014 (3D solid structures, plate and wall structures).
- [4] Program 4H-Frape2, version 2014 (generally frame structures).

Multibody model of a human body

J. Špička^{a,b}, M. Hajžman^a, L. Hynčík^{a,b}

^aFaculty of Applied Sciences, UWB in Pilsen, Univerzitní 22, 306 14 Plzeň, Czech Republic

^bNew Technologies Research Centre, UWB in Pilsen, Univerzitní 22, 306 14 Plzeň, Czech Republic

Purpose of this paper is to build a 2-dimension model of a human body based on multibody dynamics approaches. A system of articulated rigid bodies is linked by rotational joints and constrained in open kinematic tree structure, to approximate external shape of a humanoid. The model contains 17 rigid bodies, namely Pelvis, Abdomen, Thorax, Neck, Head, Left and Right Arms, Left and Right Forearms, Left and Right Hands, Left and Right Tights, Left and Right Calves and Left and Right Feet and 16 rotational joints, representing real human's joints, namely L5/Sacrum joint, T12/L1 joint, C7/T1 joint, Atlas/T1 joint, Shoulder joints, Elbow joints, Wrist joints, Hip joints, Knee joints and Ankle joints, as is shown in Fig. 1.

The simple model of the human body is created in order to capture global behaviour of the human body and particular segments, respectively. Each body holds its dimensions, mass, moments of inertia and location of a centre of gravity (COG). Kinematics of all the bodies can be fully described within position of reference point A and relative rotation of the body around this particular point [1, 2], as

$$\mathbf{X} = \mathbf{r}_A + \mathbf{S}(\varphi)\mathbf{x}, \quad (1)$$

where \mathbf{X} are coordinates of any point with respect to the global coordinate system, \mathbf{r}_A are coordinates of the reference point A with respect to global coordinate system, $\mathbf{S}(\varphi)$ is transformation (rotational) matrix of relative rotation given by angle φ and \mathbf{x} are coordinates of the particular point in the local (body-fixed) coordinate system of the body.

Authors use Lagrange's equations of a mixed type with multipliers to derive equations of motion [1]. Firstly, energy balance method is introduced, namely the kinetic and the potential energy for most general case (centre of gravity does not coincide with origin of local body-fixed coordinate system). Kinetic energy of the system in a general 3D case can be expressed in the following form [4]

$$E_k = \sum_{i=1}^{17} \left[\frac{1}{2}(\dot{\mathbf{r}}_A^i)^2 m^i + \frac{1}{2}(\boldsymbol{\omega}^i)^T \mathbf{I}_A^i \boldsymbol{\omega}^i + \dot{\mathbf{r}}_A^i (\boldsymbol{\omega}^i \times \mathbf{d}^i) m^i \right], \quad (2)$$

or in a 2D case

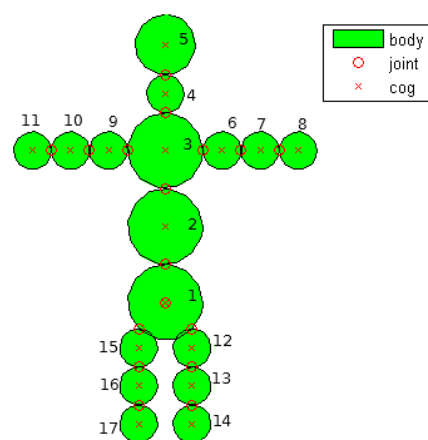


Fig. 1. MBS model of human body

$$E_k = \sum_{i=1}^{17} \left[\frac{1}{2} (\dot{\mathbf{r}}_A^i)^2 m^i + \frac{1}{2} I_A^i (\omega^i)^2 - m^i \omega^i (\hat{y}_{cog}^i v_{A_x}^i - \hat{x}_{cog}^i v_{A_y}^i) \right], \quad (3)$$

where $\dot{\mathbf{r}}_A = [v_{A_x}, v_{A_y}]^T$ is velocity vector of reference point A, m is the mass of the body, I_A is the moment of inertia with respect to point A, ω is angular velocity of the body around the point A, \hat{x}_{cog} , \hat{y}_{cog} are coordinates of the centre of gravity with respect to the local coordinate system.

Potential energy is given by the generalized forces loading the system. In this case, only gravity force is acting on all the bodies at their centre of gravity, thus the potential energy can be expressed as

$$E_p = \sum_{i=1}^{17} m^i g y_{cog}^i, \quad (4)$$

where y_{cog}^i is coordinate of the centre of gravity with respect to the global (inertia) coordinate system. Equations of motion of the human body model is derived using Lagrange's equation of a mixed type with multipliers [1, 2] as

$$\begin{bmatrix} \mathbf{M} & \Phi_q^T \\ \Phi_q & \mathbf{0} \end{bmatrix} \begin{bmatrix} \ddot{\mathbf{q}} \\ -\lambda \end{bmatrix} = \begin{bmatrix} \mathbf{Q}_e + \mathbf{Q}_v \\ \mathbf{Q}_d \end{bmatrix}, \quad (5)$$

in which \mathbf{M} is mass matrix, Φ_q is Jacobian matrix of constraints, $\ddot{\mathbf{q}}$ is vector of generalized accelerations, λ is vector of Lagrange's multipliers, \mathbf{Q}_e is vector of generalized applied forces, \mathbf{Q}_v is a vector of inertia forces, that absorbs terms that are quadratic in the velocities and \mathbf{Q}_d is a vector that absorbs terms that are quadratic in the velocities and bodies i and j are constrained by the rotational joint, that eliminates relative translation between these two bodies, and allows only one degree of freedom of relative rotation. This kinematic constraint requires two points, P^i and P^j on bodies i and j , respectively, that coincide through the motion. The constraint equation can be written [2] as

$$\Phi(\mathbf{q}^i, \mathbf{q}^j) = \mathbf{r}_A^i + \mathbf{S}^i \mathbf{x}_P^i - \mathbf{r}_A^j - \mathbf{S}^j \mathbf{x}_P^j = \mathbf{0}. \quad (6)$$

Equations of motion (5) lead to index one differential-algebraic equation, that can be numerically solved. MATLAB software is used for numerical solution, simulation and graphical visualization. Possible contacts between the model of human and some infrastructure or possible self-impact between bodies, are going to be add to the system and solve using a continuous contact force model, regarding Hertz's theory [3]. For the future improvement, the model will be expanded into 3-dimensional model respecting the contact scenario [3].

Acknowledgement

This work was supported by internal grant project SGS-2014-017.

References

- [1] Brát, V., Matrix methods for analysis and synthesis of spatial flexible multibody systems, Academia, Prague, 1981. (in Czech)
- [2] Shabana, A.A., Computational dynamics, University of Illinois at Chicago, Chicago, 2011.
- [3] Špička, J., Double pendulum contact problem, Master thesis, University of West Bohemia, Plzeň, 2013.
- [4] Equation Sheet for Engineering Mechanics 12-Dynamics, available from: <http://www.esm.psu.edu/courses/emch12/intdyn/course-docs/Equation-Sheet.pdf>

Crack initiation from sharp V-notch tip in the case of out of plane bended specimen

K. Štegnerová^{a,b}, L. Náhlík^{a,b}, P. Hutař^a

^a CEITEC IPM, Institute of Physics of Materials, Academy of Science of the Czech Republic, Žitkova 22, 616 62 Brno, Czech Republic

^b Institute of Solid Mechanics, Mechatronics and Biomechanics, Faculty of Mechanical Engineering, Brno University of Technology, Technická 2896/2, 616 69 Brno, Czech Republic

This contribution is focused on the estimation of the critical applied stress values for the crack initiation from sharp V-notch tip in the case of out of plane bended specimens. The generalized approach of the linear elastic fracture mechanics (GLEFM) was used because the stress singularity exponent differs from 0.5 in studied case.

The stability criterion based on the generalized strain energy density factor was applied [1, 2]. Analytical solution of the stress singularity exponent depends only on the value of the V-notch opening angle. In the case of out of plane bending it is also influenced by the free surface and existence of so-called vertex singularity. An analytical solution of this stress singularity is not known, therefore it has to be estimated numerically from the stress distribution around the V-notch tip [3]. The critical stress values are estimated using finite element method and analytical methods. Finally, results obtained were compared with experimental data published in the literature [4].

The numerical model of the out of plane bended specimen was created according to literature [4]. The geometry is shown in the Fig. 1. The dimensions of the specimen were: lengths $L_1 = 103.12\text{mm}$ and $L_2 = 50.8\text{mm}$, width $w = 40.64\text{mm}$, notch depth $a = \{5.08, 6.34, 7.64, 8.90, 10.16\}\text{mm}$, thickness $t = 2.921\text{mm}$ and V-notch opening angle $\alpha = 45^\circ$. Material corresponds to PMMA: Young's modulus $E = 2.3\text{GPa}$, Poisson's ratio $\nu = 0.36$, fracture toughness $K_{IC} = 1.8625\text{MPa}\cdot\text{m}^{1/2}$ and tensile strength of the material $\sigma_c = 70\text{MPa}$. Material was considered as homogenous, linear elastic and isotropic.

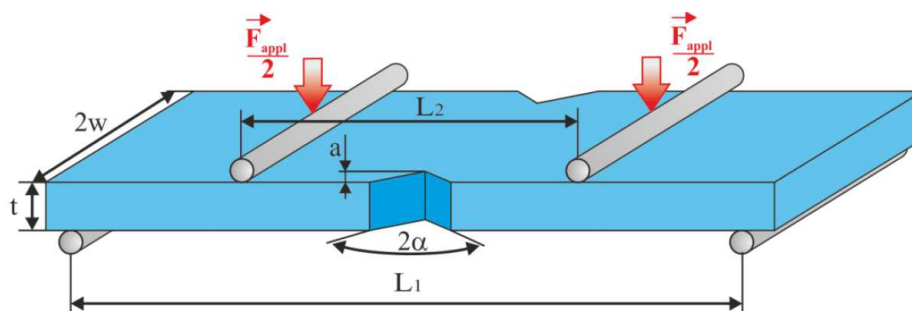


Fig. 1. Geometry and boundary conditions of the specimen [4]

According to [5] let us suppose that the stress distribution around the notch tip in each single plane perpendicular to the crack front can be generally approximated as 2D solution in the form:

$$\sigma_{ij} \approx \frac{H_I}{r^p} \cdot f_{ij}(p, \theta), \quad (1)$$

where H_I is a generalized stress intensity factor [MPa·m ^{p}], p is a stress singularity exponent and $f_{ij}(p, \theta)$ are known functions, p, θ are local polar coordinates with origin at the V-notch tip.

The used stability criterion was originally derived by Sih [6] for cracks. Subsequently it was extended by Knésl [2] for sharp V-notches. Finally it is expressed by:

$$H_{IC} = K_{IC} d^{p-\frac{1}{2}} \sqrt{\frac{4k_n}{k_n U_1(\theta = 0) + V_1(\theta = 0)}}, \quad (2)$$

where K_{IC} is fracture toughness, p is stress singularity exponent, k_n is function of the Poissons ratio ν , U_1, V_1 are known functions of the stress singularity exponent p , d is a critical distance.

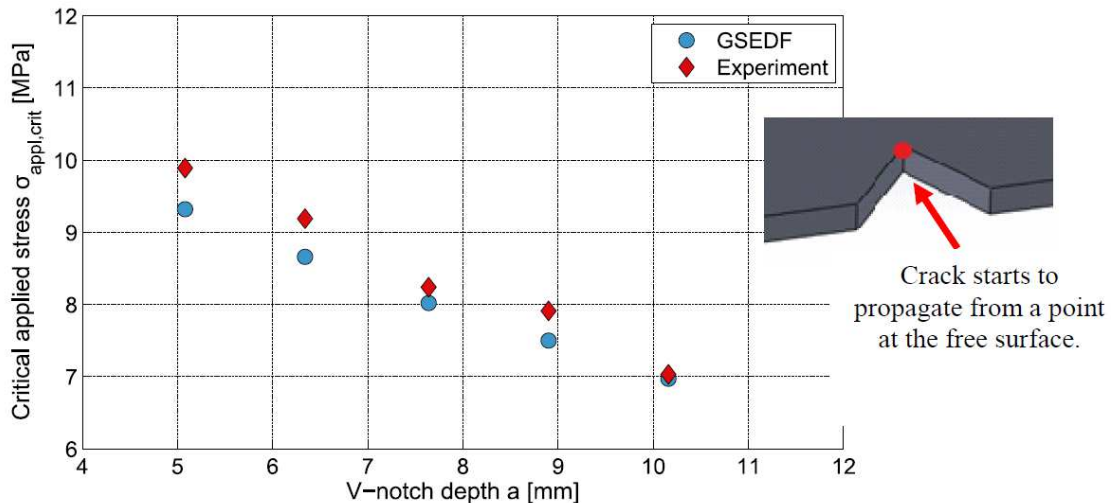


Fig. 2. Comparison of the estimated critical applied stresses with the experimental data taken from [4]

The boundary conditions and the influence of the free surface and vertex singularity were taken into account, therefore the stress singularity exponent p along the crack front must be estimated numerically by using log-log regression analysis [3]. It is caused by the different fracture behavior due to fact that the crack starts to propagate from the point at the free surface, see detail in Fig. 2.

Critical value of the applied stress for crack initiation from the sharp V-notch was estimated by using criterion based on the generalized strain energy factor. The comparison between results obtained and experimental data taken from literature is shown in the Fig. 2.

There was shown the practical applicability of the stability criteria based on GLEFM to estimate the crack propagation from the sharp V-notch, even when the area of the crack propagation is significantly influenced by the vertex singularity.

Acknowledgements

This work was supported through the grant No. CZ.1.07/2.3.00/30.0063 and No. FSI-S-14-2311 of the Ministry of Education, Youth and Sports of the Czech Republic.

References

- [1] Knésl, Z., International Journal of Fracture 48 (1991) 79-83.
- [2] Knésl Z., Acta Technica ČSAV 38 (1993) 221-234.
- [3] Awaji, A., Toshimitsu Y., Computers & Structures 22 (1986) 25-30.
- [4] Huang, C-S., Labossiere, P., Damage and Fracture Mechanics 8 (2003).
- [5] Hutař, P., Náhlík, L., Knésl, Z., International Journal of Fatigue 32 (8) (2010) 1265-1269.
- [6] Sih, G.C., A special theory of crack propagation, Mech. of Fracture, Noordhoff Inter. Publ., Leyden, 1997.

String meters for testing of mechanical functionality of bridges

P. Štemberk^a, J. Záruba^a, S. Řeháček^a, D. Čítek^a

^a Klokner Institute, CTU in Prague, Solinova 7, 166 08, Prague, Czech Republic

Basic information: String tensometric method is converting measured values into modified prestress of prestressed steel string or into the change of the own frequency of lateral oscillation of the string. Metered own frequency in case of static metering is not distorted due to long-distance transmission of frequency signal of the nominal string. It is therefore a mechanical measuring method allowing simple electrical metering and transfer of output information through similar electronic equipment as is being used by telecommunication devices for transmission of acoustic records.

General advantages of string tensometric method are:

- High stability of „zero entry“ measured with use of strings produced for musical instruments.
- As the thermal expansivity of the string is almost identical with concrete and structural steel the applications in the construction industry provide for high rate of self-compensation of thermal impacts.
- Frequency can be in fact considered as a digital information, in other words frequency information can be simply and clearly transformed into classical form of digital information.
- From the aspect of long-term observations the important advantage in order to keep the maximum continuity of measuring is full separability of the mechanical part of string meter from its electronic equipment. Mechanical part of tensometer can become a permanent part of the building structure as its case can be perfectly watertight sealed with soldering.

History of the method development in the Klokner Institute: Beginning of the string method development is close to the date of restoration of KI function after the WW II and relate mainly to need of verification of transportation buildings functionality damaged and neglected during the war. The most remarkable impulse however was the need of control of development of temperatures and internal strains in concrete works of dams of Slapská and Orlická reservoirs.

From the metrological aspect already in 50s the availability of industrially produced string meters for tensometric measurements was secured with metrological quality close to theoretical maximum of these measurement tools fully complying with real needs of the construction industry. The worldwide primacy of this achievement was awarded with gold medal during the world expo in Brussels 1958.

Further development therefore tended rather to extension of application scope of this string methodology, innovations for the purpose of production simplification of produced gauges.

The most significant act of this path was most probably the changeover to full separability of mechanical and electronic parts of string meters at the turn of 60s and 70s.

Fields of application: Orientation to issues as are control of mechanical function of transportation buildings, control of function of water works (internal strain, pore water pressures, levels, leakages etc.), construction geology (load on soils, shifting, landslips, compression, pore pressures and also states of stress and deformation of underground buildings etc.), geotechnical underground probes, scales and weighing, equipment of meteorological stations and systems of timely notification of local flood danger, controls of changes and increase of weight in livestock production, control of stock level of loose materials, experimental static dynamics, area-type flowmeters etc.

Readiness status: namely after 1968 the relation between research of measuring technologies and its production had low effectiveness and often rather sabotage defects, the condition lasting in various forms on certain level till now. It became therefore customary that the applied research terminated on the level of functional prototype but the last costly steps including among others structural modifications necessary for industrial production with the existing machinery were not considered by the government necessary to be funded.

The readiness status in this condition therefore does not correspond with tested functional sample.

Technical solution of equipment: Developed system consists of string deformeters (joint meters) for control of saddles compression, deflectometers with string load gauge for control of the deck deflection and external string tensometers (Fig. 1) in case of occasional request for control of change of state of stress in selected parts of the structure.

New electrical equipments consists of new electromagnetic converter for detection and excitation of undamped oscillations of the detector string, oscillator, transducer for digitalisation of frequency data, remote control circuits connected to the input of radio connector transmitter, metering apparatus with input provided with instruction side of radio connector fit for automated functions during bearing test.

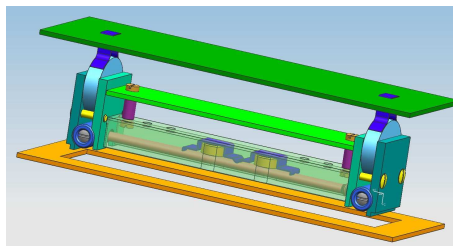


Fig. 1. External string tensometer

Acknowledgements

The work has been supported by the grant project MŠMT CZ.1.05/3.1.00/14.0301.

References

- [1] Zaruba, J., String waterproof sensor, Author's certificate No. 155445 dated 15.10.1974. (in Czech)
- [2] Zaruba, J., Equipment for measuring of deformations and mutual displacements of controlled structural parts, mainly in buildings, Patent document No. 300804 dated 19.8.2009. (in Czech)
- [3] Zaruba, J., Kostelecka, M., Universal charging tensometer, Patent No. 302834 dated 25.11.2011. (in Czech)
- [4] Zaruba, J., Stemberk, P., Bily, V., Jiroutova, D., String deformetr for control of the width of the fractures, Invention application No. 2014-41 dated 20.01.2014. (in Czech)

Thermodynamic loss of condensation in steam turbine cascade

M. Šťastný^a, M. Šejna^b

^aWest Bohemia University, NTRC, Univerzitní 8, 306 14 Plzeň, Czech Republic

^bPC-Progress, Anglická 28, 120 00 Praha, Czech Republic

The thermodynamic loss is a major part of the loss connected with steam condensation in the first wet stage of low-pressure (LP) steam turbines. The magnitude of the thermodynamic loss depends on the prevailing mode of condensation, *i.e.*, homogeneous (spontaneous) or heterogeneous. The calculations of Laali (1991) [1] indicated that, for homogeneous condensation in the first wet stage of the LP cylinder of a 900 MW nuclear steam turbine, the thermodynamic loss was 0.8 MW.

The effects of chemical impurities on nucleation and heterogeneous condensation occur mainly in the salt solution zone (SSZ). The approach used in this paper is based on the binary nucleation of the main chemical impurity NaCl and water. Physical and mathematical models are then applied to steam flow with homogeneous and heterogeneous condensation in the nozzle cascade of the first wet stage of the LP part of a 1000 MW nuclear steam turbine. These calculations help in clarifying the different thermodynamic losses related to steam flow with homogeneous or heterogeneous condensation.

The two-dimensional wet steam flow is described in the paper by the system of Euler equations. The system is linked with equations describing homogeneous or binary nucleation and with equations describing water droplet growth by condensation. The mathematical model of homogeneous and binary condensation is described in Šťastný and Šejna (2014) [2].

The nucleation numerical model was applied to the calculation of the flow with homogeneous and binary condensation in the 2D nozzle-blade cascade used in the first wet stage of the LP part of the 1000 MW steam turbine. The mid-span profile was chosen for the study and its shape can be seen in Fig. 1.

From the inlet total conditions it follows that the inlet superheat is $(T_{at} - T_s) = 0.6$ K. The Mach number downstream of the cascade assuming isentropic flow is $M_{eis} = 0.83$. The flow in the cascade is therefore subsonic and steam condensation occurs.

The distribution of the subcooling under the SSL for homogeneous condensation is shown in Fig. 1 and for heterogeneous condensation in Fig. 2. The steam saturation line lies near the leading edges of the profiles. The subcooling under the SSL gradually grows. The difference between homogeneous and heterogeneous condensation is mainly in maximum value of subcooling.

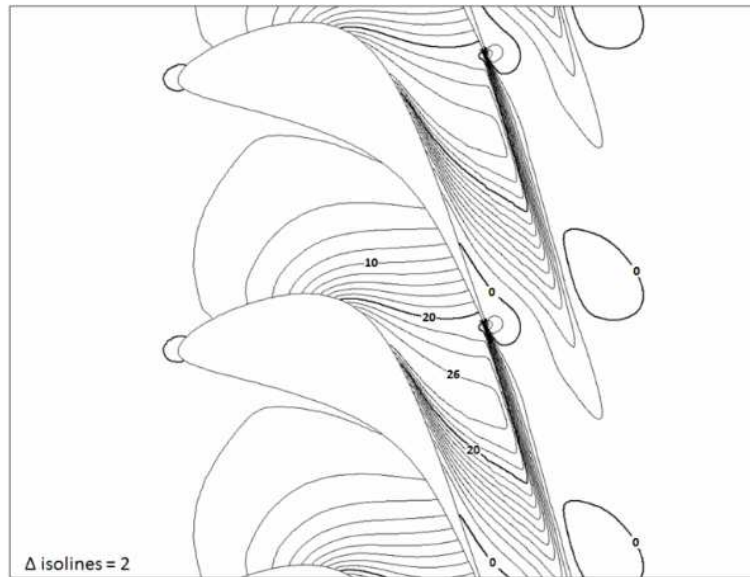


Fig. 1. Homogeneous subcooling ΔT [K] under the SSL. ΔT of isolines = 2 K

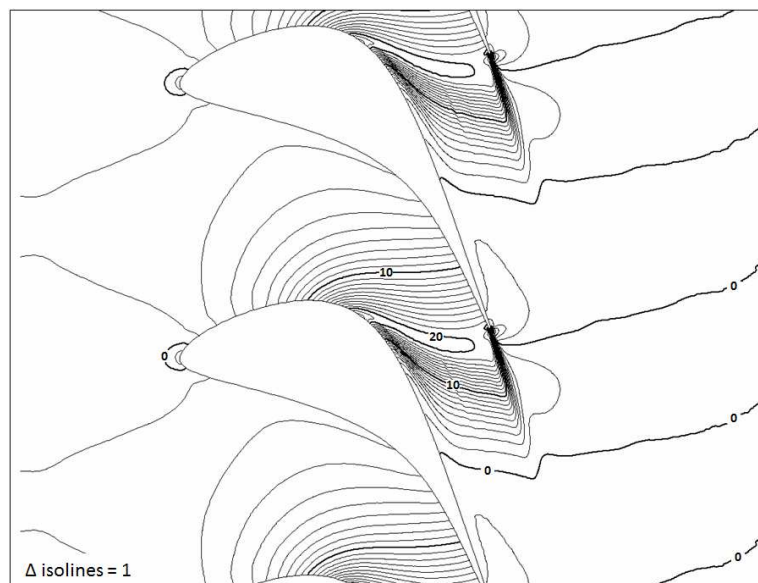


Fig. 2. Heterogeneous subcooling ΔT [K] under the SSL. ΔT of isolines = 1 K

Acknowledgement

The authors are grateful for the support given by the University of West Bohemia in Pilsen, New Technologies - Research Centre.

References

- [1] Laali, A.R., A new approach for assessment of the wetness losses in steam turbines, Proc. Instn. Mech. Engrs., C423/014, 1991, pp. 155-165.
- [2] Šťastný, M., Šejna, M., Condensation of steam with chemical impurity in a turbine cascade, Proc. Instn. Mech. Engrs. Part A: J. Power and Energy 228, 2014, pp. 194-205.

One-dimensional mathematical model of oil extraction process in a continuous screw press

J. Voldřich^a, J. Očenášek^a

^aNew Technologies - Research Centre, UWB in Pilsen, Univerzita 22, 306 14 Plzeň, Czech Republic

Oil expression within screw presses is at present the most common mechanical method to extrude oil from oleaginous seeds. The objective of this work is to present one-dimensional continuous mathematical model of the pressing and oil extruding process in an expelling screw press.

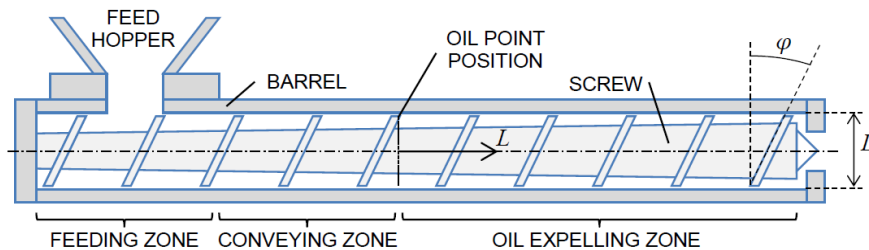


Fig. 1. Screw extruder scheme indicating main process zones

The oil-seed compression processes in a screw press undergo three main stages as marked at the Fig 1. After the feeding zone, where most of the air is pressed out, is the mass conveyed and gradually compressed until the seeds reach the oil point. Mathematical model presented within this work was design to simulate specially the processes in the oil expelling zone, where oil is being separated.

The physical model of material representing oleaginous seeds distinguishes two separate phases. First is the solid porous matrix, which represents solid parts of the seed (excluding oil). It is treated as incompressible, but its inner pores are compressible. Second phase is the oil filling the matrix pores, as well treated as incompressible. Motion of this composite in the screw press is approximated by a non-Newtonian fluid flow, whereas the drain of the oil within the porous matrix is described by the Darcy's law.

Presented one-dimensional mathematical model is based on the extruder theory [1, 2] mathematically expressed by an ordinary differential equation for pressure P distribution along the coordinate z , which is defined in transformed uncoiled slit geometry, see Fig. 2. This geometry is a good approximation for volumes with a small fraction of the slit height to width. Since the classical extruder theory describes flow of an incompressible fluid with a constant volume flow, model extension is introduced for the description of the volume flow Q related to the oil drain through the barrel mesh (Eq. (1)) and change of the porosity Φ .

$$dQ/dz = -bF\{\mathcal{K}(\Phi), \mu_{oil}, h, \Lambda\}\Phi P, \quad (1)$$

$$dP/dz = B^{-1}(\mathcal{A} - Q). \quad (2)$$

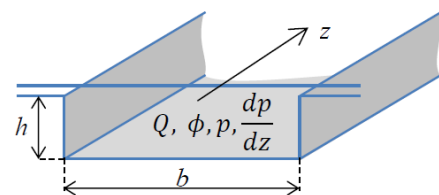


Fig. 2. Geometry of the 1D model

Here $\mathcal{K}(\Phi)$ denotes the porous matrix permeability (significantly dependent on the porosity Φ) and μ_{oil} is the oil viscosity. Function \mathcal{F} defines the oil drain out through the barrel according to Darcy's law. Parameter A characterizes throughput of the meshed barrel for the oil to leave. Terms A and B are based on the flow velocity field within a rectangular slit predicted by Newtonian fluid flow (Fig. 2)

$$\mathcal{A} = \frac{1}{2} f_1 \pi D b h N \cos(\varphi), \quad \mathcal{B} = \frac{1}{12} f_2 \frac{h^3 b}{n \mu_c}, \quad (3)$$

where parameters b , h , D , and φ define the geometry (see Fig. 1 and 2) and factors $f_{1,2}$ are correction factors incorporating the nonlinear effect of the non-Newtonian fluid flow, n is the non-Newtonian fluid exponent, μ_c is the viscosity of the compressed composite and N gives the screw rpm. Methods of material parameter identification are discussed for instance in [3].

It has been experimentally verified that the contact mode of the seed mass with the barrel and the screw is rather to be described by the Navier condition than by Coulomb friction.

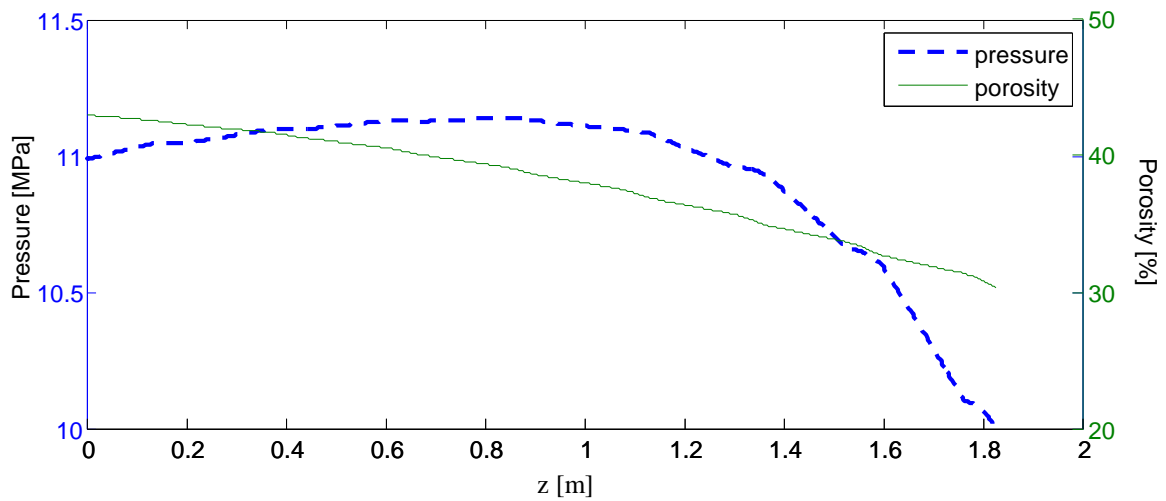


Fig. 3. Case study of a multi-segmented screw press; figure displays absolute pressure profile and decreasing porosity as a function of axial distance L

Presented model is also capable to cover partial sliding of the compressed seeds mass on the contact with the screw and the barrel, the pressure gradient along the screw press axis and the volume fraction of expressed oil. Properties of the model are demonstrated on real screw press geometry, see resulting pressure and porosity profile at Fig. 3. Details of numerical implementation are given in [4].

Acknowledgements

The work has been supported by the grant project of the Technology Agency of the Czech Republic number TA04010992.

References

- [1] Vadke, V.S., Sosulski, F.W., Shook, C.A., Mathematical simulation of an oilseed press, JAOCS 65 (10) (1988) 1610-1616.
- [2] Willems, P., Kuipers, N.J.M., de Haan, A.B., A consolidation based extruder model to explore GAME process configurations, Journal of Food Engineering 90 (2009) 238-245.
- [3] Očenášek, J., Voldřich, J., Mathematical modeling of a biogenous filter cake and identification of oilseed material parameters, Applied and Computational Mechanics 3 (2009) 339-350.
- [4] Voldřich, J., OSLO_EXTRUDER, "Oddělující šnekové lisování olejnin", Research Report NTC 01-05/2012 (NTC-VYZ-12-076), NTC ZČU v Plzni, 2012. (in Czech)

Phenomenological and physical models of automotive shock absorbers

J. Volech^a, Z. Šika^a

^a Faculty of Mechanical Engineering, CTU in Prague, Technická 4, Praha 6, 166 07, Czech republic

Shock absorbers are inconsiderable piece of engineering work that mainly contributes to the car behavior on the road. To evaluate the usefulness of automotive shock absorbers there are several steps.

The first step in this evaluation is to develop a high fidelity model for use in control design and analysis. This task is challenging because the damper is a highly nonlinear device. There are two options here.

First is phenomenological model's are used for quick simulations and control. However, the phenomenological models are black box system. The inner function of dampers isn't tractable and they can't be used for developing new shock absorbers.

Second option is that phenomenological model, in order to relate the model coefficients directly to the tunable damper components, is abandoned in favor of the so-called white box models that provide the necessary insight in the damper physics (physical model's). They are extremely versatile and can exhibit a wide variety of hysteretic behavior. For that they are used in full CAE approach to deal with tuning of dampers. However, the physical models are very sophisticated and the governing equations are extremely stiff, making them difficult to deal with numerically.

The second step is identification. Based on the given data, a simplex optimization method is employed to determine appropriate parameters for the analytical model. Comparison with the data indicates that the models presented are accurate for a wide range of operating conditions and are appropriate for use in control algorithm development and system evaluation.

This paper involves the presentation and identification of a five phenomenological damper models that predicts the damper force as a function of the damper displacement and velocity for a given set of tuning parameters. Those can be identified from dynamometer measurements only. Then three chosen models are identified on data from physical model and compared with each other Fig. 1.

The five phenomenological models are:

1	Base phenomenological model
2	Bingham model
3	Gamota and Filisko model
4	Bouc-Wen model
5	Modified Bouc-Wen model

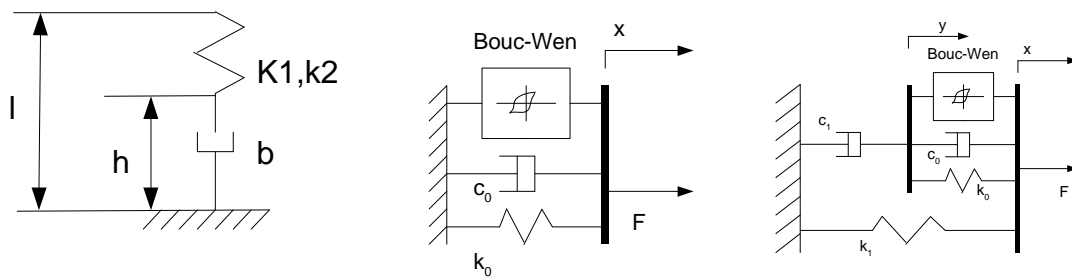


Fig. 1. (1) Base phenomenological model; (2) Bouc-Wen model; (3) Modified Bouc-Wen model

Measured data was used from physical model that predicts damper behavior with an average mean square value of RMS error is about 0,25% [1]. Three phenomenological models were chosen (Base phenomenological model, Bouc-Wen model, Modified Bouc-Wen model) the other two (Bingham model, Gamota and Filisko model) were not considered due to low prediction ability [4]. These models were identified on continuous harmonic sinusoidal displacement. And in order to quantify the validity of the present identification, the RMS value of the measured damper force and the RMS value of the residual between predicted and measured force has been computed and listed in Table 1. Quality of the predicted damper force for the three selected models.

Table 1. Quality of the predicted damper force for the three selected models

Models	RMS _{Damper force} [N]	RMS _{residual force} [N]	Relative RMS _{error}
Base phenomenological model	1093,33	84,19	7,7 %
Bouc-Wen model	1093,33	108,98	9,88 %
Modified Bouc- Wen model	1093,33	54,22	4,96 %

Acknowledgements

The author appreciates the kind support by the Josef Bozek Competence Centre for Automotive Industry TE01020020 of the Technology Agency of the Czech Republic.

References

- [1] Duym, S.WR., Simulation tools, modelling and identification for an automotive shock absorber in the context of vehicle dynamics, *Vehicle System Dynamics* 33 (4) (2000) 261-285.
- [2] Duym, S., Randy, S., Reybrouck, K., Evaluation of shock absorber models, *Vehicle System Dynamics* 27 (2) (1997) 109-127.
- [3] Lee, K., Numerical modelling for the hydraulic performance prediction of automotive monotube dampers, *Vehicle System Dynamics* 28 (1) (1997) 25-39.
- [4] Spencer, B., Dyke, S., Sain, M., Carlson, J., Phenomenological model for magnetorheological dampers, *Journal of engineering mechanics* 123 (3) (1997) 230-238.

Principles of creation of structured grids for CFD simulations

T. Zábranský^a

^a Výzkumný a zkušební ústav Plzeň s.r.o., Tylova 1581/46, 301 00 Plzeň, Czech Republic

This article deals with the creation of structured grids for CFD simulations, mainly turbine blade stages. The desired grid properties of computational grids are discussed. Trends of structured grid creation are also presented. Approach of tuning of y^+ , a parameter for first layer of cells in boundary layer, is presented, and y^+ is compared with computed results. The possibility to estimate y^+ before CFD computation is described.

In CFD simulations, mesh quality has a huge impact on both results quality and convergence speed. Experience shows that it is best for a calculation to have a fine grid with only hexagonal cells of good quality. This requirement is hard to achieve for complex geometries and impossible for some shapes. However, it is possible to mesh computation region of turbine blades according to these demands. One possibility to ensure hexagonal cells in the whole region is to create a structured grid. Most modern programs do this by dividing the computation region into large fictional hexagonal blocks, and then meshing the blocks separately with structured grids connected to each other on its sides. This approach can be achieved automatically or manually by the user.

A good example of such a program is GridPro. It requires the user to manually create the mesh blocks, which gives the user complex control over the generated mesh. This approach can be complicated and time demanding because the user has to fabricate the block grid for meshing, and to define it point by point, but the outcomes are as good as the user can think up. An example of such grid can be seen in Fig. 1. During the mesh generation, the software tries to maintain best quality for all cells within all the blocks and shapes these blocks according to this. The resulting mesh then looks like in Fig. 2. It is not necessary for the whole mesh to be strictly structured but each block is structured and all cells are hexagonal.

Another issue about mesh generation for CFD computation is so called y^+ . It is a number representing a dimensionless cell to wall distance. It is defined as $y^+ = u^* \cdot y / \nu$ where u^* is friction velocity at the nearest wall, y is the distance to the nearest wall and ν is the local kinetic viscosity of the fluid. Desired value of y^+ is below 5. Contribution of this number is in possibility to estimate whether mesh near walls is sufficiently smooth for solving the boundary layer problem or not.

There are two main problems. In time of grid generation, friction velocity near wall is unknown, and viscosity is not always known. This problem can be partially solved by guessing the properties of the flow in advance and it can be solved completely only by making one computation and making new mesh afterwards. Another problem is to generate a fine mesh on the boundaries. Resulting first cell size by the wall can be 10^3 smaller than free stream mesh, which leads to high aspect ratio or bad cells and sufficient number of cells across the boundary layer is considered to be higher than 10 (different sources state different numbers but always higher than 10), which can lead to enormous growth of cell number in the mesh.

So the question is whether it is worth it to bother with such a time consuming process in daily application. It is clear that in applications where we study flow boundary layer, it is of high importance to have very fine boundary layer.

An example of impact of the boundary layer mesh on results in ANSYS Fluent code was made on low pressure turbine stage. The grids were the same except for the boundary layer grid. Boundary layer increased cell count by about 100%. The overall flow rate, temperature and pressure drop across the stage varied less than 1% for both variants but the axial force on rotor blade varied by 55%, which is very high. This shows high importance of boundary layer and y^+ tuning for problems involving influence of the flow on walls.

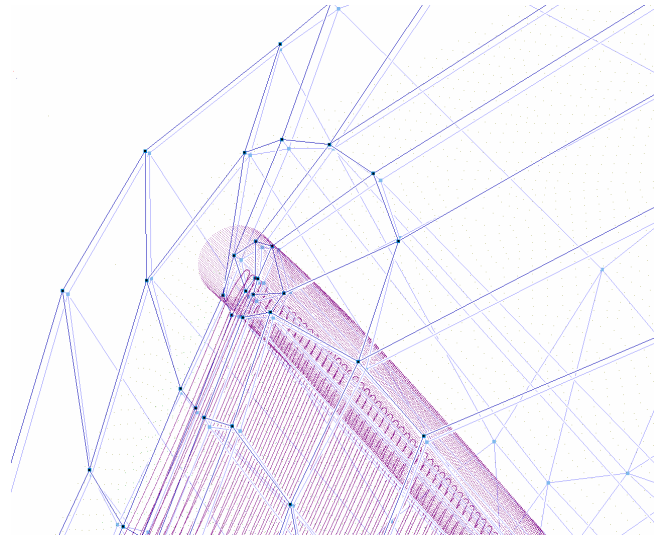


Fig. 1. Example of GridPro block generation

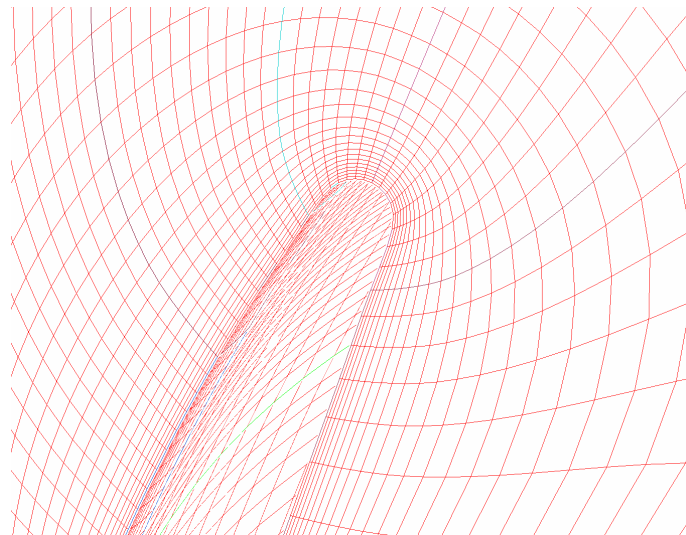


Fig. 2. Example of mesh generated in GridPro (trail edge of rotor blade)

Acknowledgements

The work has been supported by the research project with state support of Czech Ministry of Education, Youth and Sports under No. MSM 4771868401.

References

- [1] Ansys Fluent Theory Guide, Ansys Inc., 2011.

Vibration attenuation of a periodically loaded system supported by carbon composite bars

J. Zapoměl^a, V. Dekýš^b, P. Ferfecki^c, A. Sapietová^b

^a Faculty of Mechanical Engineering, VSB-TU of Ostrava, 17. listopadu 15, 708 33, Ostrava-Poruba, Czech Republic

^b Faculty of Mechanical Engineering, Žilina University, Univerzitná 1, 0101 26, Žilina, Slovak Republic

^c IT4Innovations, VSB-TU of Ostrava, 17. listopadu 15, 708 33, Ostrava-Poruba, Czech Republic

Material damping is an important factor which influences vibrations attenuation, the state of stress, the force transmission through the constraint elements and on certain conditions it can become a source of self excited oscillations. Its effect on behaviour of mechanical systems is significant especially if they work close to the resonance regions. Internal friction of metals, especially of steels, is comparatively well investigated but more studies are needed to learn about the damping of new non-metallic materials.

The system which is a subject of the following investigations (Fig. 1) consists of a rigid steel platform (80 kg mass) that is coupled with the frame by four bars made of carbon composite material (Young's modulus 120 GPa, density 1516 kg/m³). Under the platform there is placed an electric machine producing time varying magnetic field which excites the platform in the vertical direction by a force whose time history can be considered as periodic (Fig. 2). The task is to analyze amplitude of the platform oscillations in the specified frequency interval (50 - 1000 rad/s).

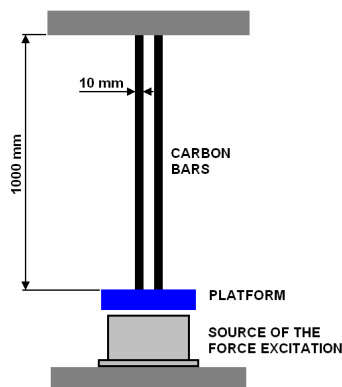


Fig. 1. Investigated mechanical system

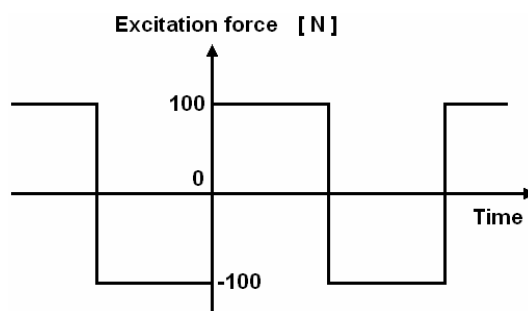


Fig. 2. Time history of the excitation force

A series of experimental measurements have been conducted to analyse material damping of a prismatic carbon composite bar. The measured parameter was the damping ratio obtained for several vibration frequencies. Consequently, it was transformed to the damping coefficient. Approximations of its dependence on frequency assuming the viscous and hysteretic damping models are evident from Figs. 3 and 4. The results show that the damping coefficient is almost frequency independent which implies that character of the damping can be considered as hysteretic with the mean value of the damping coefficient 0.017.

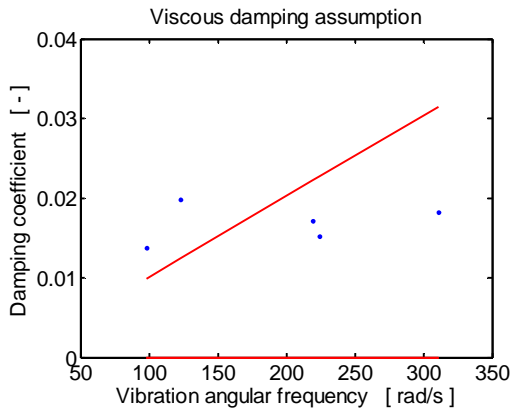


Fig. 3. Approximation assuming viscous damping

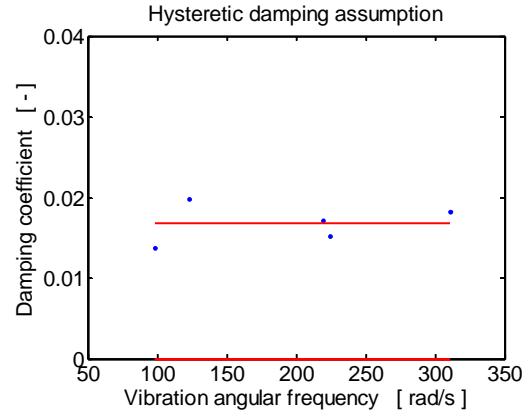


Fig. 4. Approximation assuming hysteretic damping

Because of the symmetry only one quarter of the system was analyzed (one bar and $\frac{1}{4}$ of the platform). In the computational model the bar was considered as linearly elastic and the platform as absolutely rigid. Material of the bar was represented by a Maxwell-Weichert model whose constitutive relationship takes the form

$$\sigma = E\varepsilon + \sum_{K=1}^{N_D} \int_0^t \mu_K e^{-\mu_K(t-\vartheta)} b_K \dot{\varepsilon} d\vartheta . \quad (1)$$

σ , ε are the stress and strain, E is the Young's modulus, μ_K , b_K are the damping parameters, t is the time, N_D is the number of terms used to describe the hysteretic damping and (\cdot) denotes the first derivative with respect to time. Values of the damping parameters determined by means of the procedure described in [1] ensure that the damping coefficient remains (sufficiently) constant in the required frequency interval (Fig. 5).

The bar was discretized into finite elements. Time history of the periodic excitation force was approximated by the first 11 terms of the Fourier series. The steady state response for the individual excitation frequencies was calculated by employing a trigonometric collocation method. The peak-to-peak vibration amplitude in dependence on the excitation frequency is drawn in Fig. 6 and the platform phase trajectory for the frequency of 230 rad/s in Fig. 7.

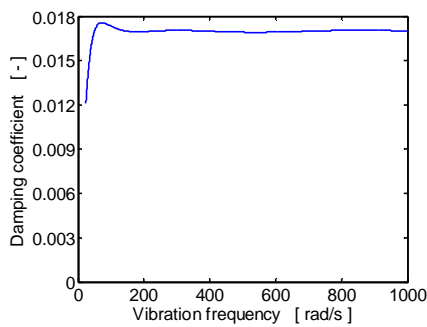


Fig. 5. Damping coefficient - frequency

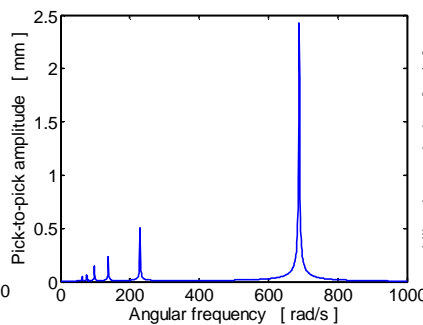


Fig. 6. Response characteristic

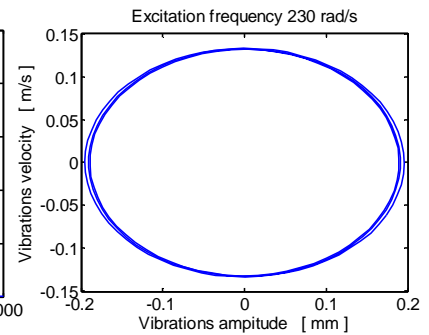


Fig. 7. Platform phase trajectory

Acknowledgements

The work has been supported by the research projects CZ.1.05/1.1.00/02.0070 and CZ.1.07/2.3.00/20.0070 which is gratefully acknowledged.

References

- [1] Genta, G., Amati, N., On the equivalent viscous damping for systems with hysteresis, Atti dell'Accademia delle Scienze di Torino, 2009.

Experimental verification of fatigue state of bridge construction using string tensometric method

J. Záruba^a, P. Štemberk^a, D. Čítek^a

^a Klokner Institute, CTU in Prague, Solinova 7, 166 08, Prague, Czech Republic

Development of the experimental method was caused by urgent need to find new diagnostic method for checking of the condition of mechanical functionality of bridges and so without need of closure of traffic for diagnostic monitoring of the building. The need was necessitated mainly by orientation of the bridge building industry on mixed and prestressed reinforced structures even in case of construction of strategic buildings as is Nuselský bridge, built in the developed area.

From the aspect of diagnostics the most serious new problem is that in mixed and prestressed reinforced structures the most serious fatigue failures do not have to originate and spread from the structure surface. Besides efforts of design engineers to secure maximum reliability and life of buildings lead to the endeavor to provide all parts of the structure with the same level of reliability and life thus causing that the point of origin of first failure is even more difficult to find. Problems of diagnostics of condition of strategic transportation buildings are methodically almost analogical with problems of diagnostics of health condition of living organisms, where the development of diagnostic methods is on much higher level so when looking for possible methods of diagnostics in construction we can come from solutions reached by health services.

Construction industry is missing mainly real operative and economical methods of assessment of the extent and importance of internal failures (inner organs). Basic difference are much larger dimensions of building structures:

- for example methods of irradiation need relatively higher larger preliminary location of the failure point,
- use of X-rays and similar emitters in open constructions proved to be too dangerous,
- in case any analogy of a magnetic resonance is found, a military embargo would be most probably laid on it,
- internal failures with traffic load lead to defective release of heat energy due to friction in failure joints. Such sources of heat energy could have been at least locally specified with use of thermovision but because of instability of the environment (in respect of temperature, wind and humidity) the reliability of such performance is low. So a successful application use has not been known so far.

As the most promising seems methods similar to EKG and similar as is for example diagnostics based on observation of changes of response to traffic load. This method is becoming more economically real with development of electronics. Currently the main problem is, which characteristic parameter of the response to follow and how to determine reliably relation of development of monitored parameter on the fatigue level towards aging of the building.

So far the most appropriate to start solution of this problem seemed orientation on monitoring of development of autocorrelative functions of response to traffic load in areas close to areas of increased hazard of failures of bridge structure occurrence. Reason for this choice is that this characteristics of static dynamics does not in advance fully eliminate any part of information obtained by monitoring and leads to simple obtaining of diagrams in the forms that can be hopefully used similarly as EKD in health services. Besides, in relation to application of KI developed string method of measuring this is method that does not necessarily need use of electronics based on use of microcomputers.

Only experimentally obtained experiences would show which observed change of mechanical characteristics of the structure is the most suitable for purposes of estimate of its residual life and in which extent would have to be extended monitoring to other mechanical features of the structure.

Main hopes are held out for monitoring of changes of the position of neutral area of the most flexurally stressed parts of the bridge, also for monitoring of changes of first three own frequencies, namely their relative differences. As a complementary information specifying causes of monitored changes would serve monitoring of exhibits of internal dumping of the structure or relation of amplitudes of oscillation excited by the traffic in three basic shapes.

Similarly to assumed target diagnostic methodology the new preliminary practical inquiry of experiences with new developed methodology must follow from mathematical model of assumed progress of life loss until full collapse of the diagnosed building. This mathematical model should be at least for typical buildings checked by an experiment on real mechanical model. Based on the estimate of the course of gradual destruction obtained by the model the diagnosed structure must be provided with installed relevant detectors (we expect string tensometers in maximum extent possible) and monitored parameters of the response to traffic load, intervals and frequency of monitoring cycles must be selected.

Subsequently or on-line it would be necessary to compare parameters obtained by monitoring with parameters estimated with mathematical model and in case of a difference to find its cause and take remedial measure (for example to postpone deadline of planned reconstruction or maintenance). In case of verification of methodology to review the mathematical model or to look for monitored parameter which would allow higher reliability and accuracy of diagnostic estimate of real life.

It is necessary to install relevant sensors on the diagnosed structure (we expect in highest extent possible string tensometers) and to select monitored parameters of the response to traffic load, interval and frequency of monitored cycles.

Conclusion: Under current condition it is therefore difficult to get a governmental support for long-term statistical applied research without any perspective that it would bring economical contribution within first three years.

Acknowledgements

The work has been supported by the grant project MŠMT CZ.1.05/3.1.00/14.0301.

References

- [1] Švanda, J., Záruba, J., Štemberk, P., Devices for long-term observation of the structures, 39th conference Experimental Stress Analysis 2001, Tábor, Czech Republic, 2001.
- [2] Záruba-Pfeffermann, J., Štemberk, P., Experimental verification of risk analysis correctness of the extraordinary and external dynamic loaded building structure, Conference Engineering Mechanics 2003, Svatka, Czech Republic, 2003.

Nonlinear vibration and modelling of fretting wear of the nuclear fuel rods

V. Zeman^a, Z. Hlaváč^a, Š. Dyk^a

^aFaculty of Applied Sciences, University of West Bohemia, Univerzitní 22, 306 14 Plzeň, Czech Republic

The fretting wear of the fuel rod cladding is a particular type of wear that is expected in nuclear fuel assemblies [1, 2]. The main components of the fuel rods (FR) are cladding in the form of thin-walled tube from zirconium (subsystem C) and fuel pellets column (subsystem P) incorporated in tube with radial clearance δ (Fig. 1). The compact form of fuel pellets column is held by means of the pressed fixation spring at the top of FR (Fig. 2). This spring generates the pressure force F_F . Each FR in the hexagonal type nuclear fuel assembly (FA) is transverse linked by three static pre-loading spacer grid cells inside the FA skeleton on several level spacings. The flexural FR vibrations are excited by the FA support plate motion in the reactor core.

The aim of this contribution is usage known motion of FA lower piece and spacer grid cell centres for a simulation of the nonlinear kinematic excited flexural vibration of the FR subsystems. Normal contact forces $F_{l,g}$, $l = 1, 2, 3$ transmitted between FR cladding and spacer

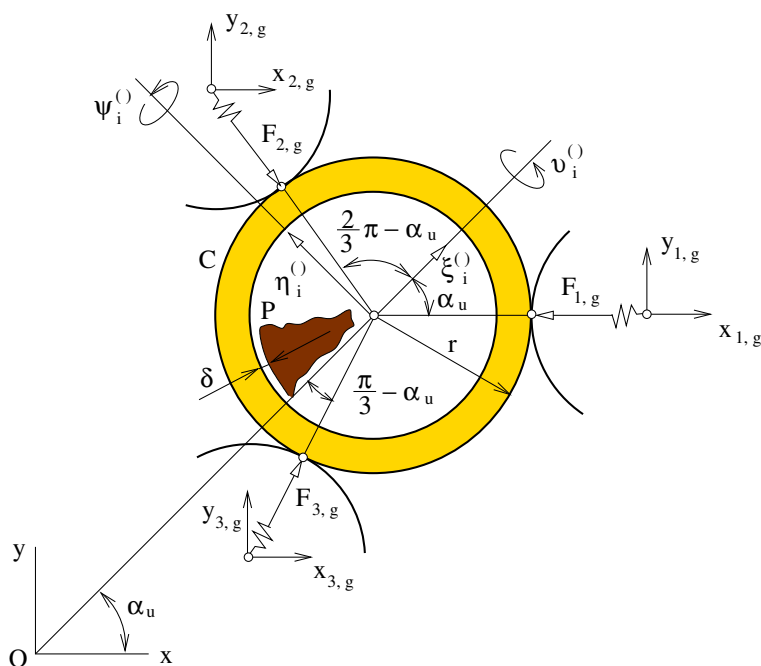


Fig. 1. Fuel rod cross-section

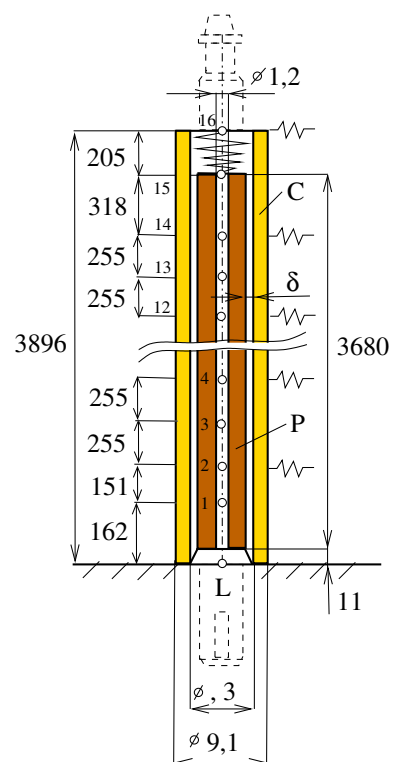


Fig. 2. Scheme of the fuel rod

grid cells (see Fig. 1) can be used for a prediction of the cladding abrasion and thinning of the Zr cladding wall thickness.

The mathematical models of FR beam subsystems are derived using FEM. An interaction between FR subsystems is expressed by impulse forces on the level of all nodal points $i = 1, \dots, 15$ (see Fig. 2). The normal contact forces $F_{l,g}$ are expressed by means of cell centres displacements $x_{l,g}, y_{l,g}$, $l = 1, 2, 3$ (see Fig. 1) and lateral displacements ξ_g, η_g of the FR cladding on the level of all spacer grid cells $g = 1, \dots, 8$ corresponding with even nodal points $2, 4, \dots, 16$.

The kinematic excitation caused by the FA support plate motion [3] generates impulse contact forces between FR components and may result in loss of contact between the FR cladding and some spacer grid cells. These nonlinear phenomena cause a change of the normal contact forces $F_{l,g}$ in comparison with till considered linear model (for $\delta = 0$ and a sufficient static pre-loading F_0 between FR cladding and spacer grid cells).

The criterion of the FR cladding fretting wear is expressed by the hourly fretting wear in grams in dependence on parameters F_0 (static contact force between FR cladding and cells), δ (radial clearance) and F_F (static spring pre-loading of the fixation spring), which are changing during the reactor operation [1]. This quantity is determined by the calculated work of friction forces in the contact surfaces between FR cladding and spacer grid cells and experimentally obtained fretting wear parameters—loss of Zr cladding mass generated by the work of friction force 1[J] at the excitation frequency and the friction coefficient at the same frequency [2].

The described methodology was applied for prediction of the FR fretting wear of the Russian TVSA-T fuel assembly in the VVER 1000/320 type reactor core in NPP Temelín.

Acknowledgements

This work was supported by the European Regional Development Fund (ERDF), project "NTIS", European Centre of Excellence, CZ.1.05/1.1.00/02.0090 and by the grant SGS-2013-036.

References

- [1] Blau, P. J., A multi-stage wear model for grid-to-rod fretting of nuclear fuel rods, *Wear* 313 (2014) 89-96.
- [2] Pečínka, L., Svoboda, J., Zeman, V., Fretting wear of the Zr fuel rod cladding, *Proceedings of the 2014 International Conference on Nuclear Engineering (ICONE22)*, Prague, ASME, 2014. (in print)
- [3] Zeman, V., Hlaváč, Z., Dynamic response of nuclear fuel assembly excited by pressure pulsations, *Applied and Computational Mechanics* 6 (2) (2012) 219-230.

Simulation of an air jet weft pick

J. Žák^a, J. Kolář^a

^aVÚTS, a.s., Svárovská 619, 460 01 Liberec XI, Czech Republic

In our work we tried to lay down some basics about an air jet weft insertion. An air jet loom compares very badly in comparison of energy consumption with other types of weft insertion, such as rapier loom or even water jet loom. It is a result of very energy demanding preparation of compressed air and from bad transfer of this energy to the weft. So a standard loom of 2 m running at normal speed of about 800 rev/min must be supplied continuously by a compressor of approximately 5 kW while the loom itself is fitted with a main drive of approximately 4 kW and this maximal power output is needed only by starting the loom, in standard regime the energy consumption of main drive is considerably lower.

Rather than attempt a further optimisation of nozzles¹ we preferred to do an analysis of exploitation of looms in a weaving factory. We soon realized that as important as an air jet optimisation is a correct setting-up of the loom. This requires careful but also time consuming manipulation of the machine and a re-setting of the control system with each change in the weaving process (e.g. change of material of the weft). This setting-up comprises a number of parameters to be entered in the control system such as the timing of valves and nozzles, setting-up of feeder and other devices, set-up of pressure regulator and many others. Their input by means of control box is subject to errors and is also time demanding. The pressure on servicing personal dictates that an universal and “robust” set-up is used. In turn, even for a well “weavable” weft material a powerful air jet is used and the consumption of air goes high.

With the previous assessment in mind, we proceeded to an optimisation of energy utilization during an air jet weft insertion. A mathematical relation between the parameters of weft insertion and the air consumption in relation to the machine parameters is needed. While the latter is relatively well known, a simple relation to describe the movement of weft is not easy to find. Moreover there are several conditions on the textile technology that should be satisfied. The description of air jet weft pick is given in this paper.

A mathematical description of movement of weft is [1, 3]

$$\int_L c_D \cdot \rho(\xi, t) \cdot (c(\xi, t) - \dot{L})^\alpha d\xi = (\lambda + f_o) \cdot ((\dot{L})^2 + \ddot{L} \cdot L), \quad \text{where } \alpha \in \langle 1, 2 \rangle$$

and c_D and f_o are parameters to be determined. λ [tex] is known fineness of the weft yarn. Some simplification, e.g. $\alpha = 2$ or assumption of constant length of weft to be acted upon, may be done to obtain:

$$k \cdot (c(t) - \dot{L})^2 = (\lambda + f_o) \cdot ((\dot{L})^2 + \ddot{L} \cdot L),$$

but the resulting function $L = f(t)$ relies essentially on knowledge of $c(\xi, t)$ and $\rho(\xi, t)$, which in itself represents a big deal of work because of very high fluctuation of c and ρ along the L and during t . With the aim on our objective we opted for a different approach.

¹The optimal shape of a nozzle is known but impractical either for fabrication and weaving.

From experience with a standard weft insertion it results some interesting points: first, after an initial acceleration the speed of weft \dot{L} stagnates; second, this ultimate weft speed $v_\infty = \dot{L}|_{t \rightarrow \infty}$ is sensibly lower than the speed of propulsing air c_∞ . Comparison of numeric solution of basic equation with experiment confirms the assumption of constant yet unknown length of weft on which the drag force is executed. Also the square of difference of speed matches well the reality. An expression of the movement equation for $t \rightarrow \infty$ may be written:

$$k \cdot (c_\infty - v_\infty)^2 \doteq (\lambda + f_o) \cdot v_\infty^2.$$

Because of $v_\infty = \text{const.}$ there must also be $k = \text{const.}$ and $c_\infty = \text{const.}$: the constant values of k and c_∞ express the integral value of propulsing forces in the steady state for $t \rightarrow \infty$.

Another aspect of our work to mention here is the fact that with each pick we get a set of values of weft position. That is to say the weft is unwound of a cylinder shaped device in the feeder and each coil is counted and the time is recorded. With these times we can well estimate the speed \dot{L} . This feature is a standard accessory of commercial feeders and the supplied values normally serve to regulate the take-up of the weft from the supply bobbin. The number of the coils usually varies between five and eight on a 2 m loom. With all the forementioned aspects in mind we selected the following approach: a fit function satisfying physical conditions was chosen in form:

$$L = v_\infty \cdot \left(t - 2.B + e^{-\frac{t}{B}} \cdot (t + 2.B) \right) \quad \text{and thus} \quad \dot{L} = v_\infty \cdot \left(1 - e^{-\frac{t}{B}} \cdot \left(1 + \frac{t}{B} \right) \right).$$

The values of v_∞ nad B should be found by means of least squares, but a good estimation may be found directly from measured values. Then the weft insertion quality for a given set of parameters is characterized by the these values.

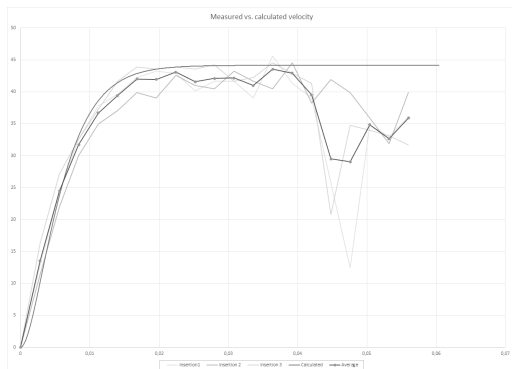


Fig. 1. Comparison of calculated speed and experiment

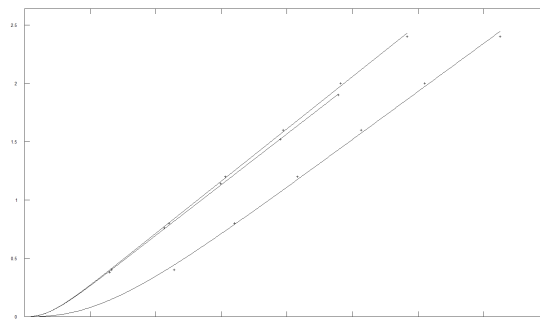


Fig. 2. Times of passage of weft and fit function for 3 different weft yarns woven on the same loom

References

- [1] Duxbury, V., Lord, R., Vaswani, T. B., A study of some factors involved in pneumatic waft propulsion, Journal of the Textile Institute, Proceedings 10/1959, Japan.
- [2] Pilipenko, V. A., Pnevmatičeskije mehanismy prokladyvanija niti, Legkaja industrija, Moscow, 1973. (in Russian)
- [3] Škop, P., Control and information systems of picking mechanisms of air-jet weaving machines, Ph.D. thesis, Technical University of Liberec, Liberec, 1985. (in Czech)

Micro-mechanical analysis of fiber reinforced composites with large aspect ratio by meshless method

M. Žmindák^a, V. Kompiš^b, Z. Murčinková^c

^a University of Žilina, Faculty of Mechanical Engineering Department of Applied Mechanics, Univerzitná 1, 010 26 Žilina, Slovakia

^b Faculty of Management Science and Informatics, University of Žilina, Univerzitna 1, 010 26 Žilina, Slovakia

^c Technical University of Košice, Štúrova 31, 08001 Prešov, Slovakia.

Fibre-reinforced composites have been widely used in engineering applications due to the superiority of their electro-thermo-mechanical properties over the single matrix. Understanding the physical behaviour of these fibre-reinforced composites is essential for structural design. The aim of this paper is to show the Method of Continuous Source Functions (MCSF) developed by the first author [1] for composite materials reinforced by finite fibres. We will give the mathematical basis of the MCSF, some results and discussion to the toughening mechanism conductivity of composite materials reinforced by straight fibres of finite length.

Due to large aspect ratio of fibres, the toughening in elasticity and increase of conductivity in heat conduction of the composite material is realized especially by corresponding effect in the fibre axis direction. Because of this, the inter-domain compatibility between fibre and matrix can be simplified and to assume that the temperature, displacement, strain, stress, etc. in all points of the cross-section are equal to each other. This property of the model is equivalent to assumption of zero bending stiffness of fibre, which is important to reduction of computational model and to correct simulation of composite materials reinforced by fibres with large aspect ratio as the nanotubes and similar fibres. The inter-domain compatibility are satisfied in discrete collocation points [3] on the fibre-matrix interface.

The interaction of fibres with matrix is simulated in the MCSF by source functions, which are 1D-continuously distributed along the fibre axis. The source functions are fundamental solution of corresponding problem (heat sources in heat conduction and forces in elasticity) and their derivatives. The forces are directed in the fibre axis direction. These source functions, however, are not able to simulate correct the interaction of fibres with the matrix. In addition the derivatives of the source functions, heat dipoles and force dipoles and force couples are included along fibre axes in order to simulate correctly the large axial stiffness of fibres to negligible bending stiffness and also the interaction of fibre with other fibres. The dipoles and couples are derivatives of the source functions. We assume that all matrix materials and fibres are homogeneous and isotropic, the dimensions of the matrix are infinite (i.e. we will deal with the infinite matrix of material with homogeneous material properties) and models are restricted to linear behaviour. Primary variables can be scalar like the temperature field in heat conduction, or vector like the displacement field in deformation of elastic bodies by forces. All fields are split into two parts, the homogeneous part corresponding to the homogeneous problem of the matrix without fibres and the local (complimentary) part simulating the influence of interactions of fibres with the matrix. We will especially investigate the local fields in the matrix of the composite material.

The paper deals with modelling of physical micro-fields, mainly thermal and mechanical, in large aspect fibrous composite materials. Interactions of matrix and reinforcing fibres involve high gradients of physical micro-fields that caused difficulties in reliable numerical simulation of composite behaviour. The developed Method of Continuous Source Functions (MCSF) eliminates disadvantages of known numerical methods and reduces the solution considerably. It uses fundamental solution and its derivatives to simulate the interaction of large aspect ratio fibres with matrix. Material properties of both matrix and fibres are assumed to be homogeneous and isotropic. The results of numerical examples and micro-fields distribution are shown in paper.

In the numerical evaluation we have to solve an integral equation, in which the intensity of source functions is approximated by 1D quadratic Non-Uniform Rational Basis Splines (NURBS) [4], which enable to define shape functions to have continuous first derivative over the whole integration path and non-equal distribution of nodal points. Basic variables are temperature in heat and displacement in elasticity problems.

The computations are performed on the homogeneous field of matrix material and boundary conditions (BC) are prescribed in collocation points along fibre boundaries. In the present models it is considered that the fibres are straight and parallel. As the BC are not known a priori, the problem is solved iteratively and is assumed that the fibres are superconductors in heat and rigid in elasticity problems in the first iteration step. This is equivalent to the assumption of constant gradient of temperature and displacement in fibre axes direction, if the fibres are straight. This corresponds to constant heat flow in heat problem and constant strain in elasticity along a fibre. Finite heat flow and temperature distribution in the heat flow problem and strain and displacements in elasticity along fibres are computed in the next steps of iteration process.

The temperature/displacement change of the centre of each fibre by the interaction is not known a priori in both the heat and elasticity problem. It is obtained by energy-balance/equilibrium condition in each fibre. This is realized by including further r.h.s. (right hand side) by prescribing temperature/displacement in corresponding fibre centre equal to one and zero for the other fibres.

See [2] more details about the computational model. Present models do not include nonlinear effects in all material behaviour of matrix and fibres, large deformations, etc. We have to realize that the micro-fibres will be often curved and the curvature can change with deformation and this will contribute to nonlinear behaviour of composite, too.

The models were programmed in MATLAB and they are suitable for parallel computing and both versions of the programs are available.

Acknowledgements

The authors gratefully acknowledge the support by the Slovak Grant Agency VEGA 1/1226/12.

References

- [1] Kompiš, V., Kompiš, M., Kaukič, M., Method of continuous dipoles for modeling of materials reinforced by short micro-fibers, *Engineering Analysis with Boundary Elements* 31 (2007) 416-424.
- [2] Kompiš, V., Murčinková, Z., Žmindák, M., Toughening mechanism for fibre of middle-large-aspect-ratio-reinforced composites. In Q. H. Qin, J. Ye, editors, *Toughening Mechanism in Composite Material*, in press Woodhead Publishing Ltd., UK.
- [3] Kompiš, V., Štiavnický, M., Kompiš, M., Murčinková, Z., Qin, Q.H., Method of continuous source functions for modeling of matrix reinforced by finite fibres, in V. Kompiš, ed.: *Composites with Micro- and Nano-Structure, Computational Modeling and Experiments*, Springer Science + Business Media B.V., Dordrecht, 2008, pp. 27-46.
- [4] Piegl, L., Tiller, W., *The NURBS book*, 2nd ed. New York, Springer-Verlag, 1997.

Workshop
Modelling and Inverse Problems
for Heterogeneous Media

Towards RVE via Wang tilings

M. Doškář^a, J. Novák^{a,b}

^aFaculty of Civil Engineering, Czech Technical University in Prague, Thákurova 7/2077, 166 29 Praha 6- Dejvice, Czech Republic

^bFaculty of Civil Engineering, Brno University of Technology, Veveří 331/95, 602 00 Brno, Czech Republic

Ubiquitous environmental tendencies along with the aftermath of lingering economic crisis emphasize need for highly optimized materials. Accurate and efficient modelling strategies are sought in order to replace expensive and time-consuming laboratory experiments with in-silico testing. The present work contributes to an ingredient of numerical analyses, the representation and reconstruction of material microstructure.

The widely applied approach to modelling of heterogeneous materials based on Statistically Equivalent Periodic Unit Cell (SEPUC) leads to long-range order spatial artefacts when used for random microstructures. These artefacts can be significantly reduced employing the recent generalization to the unit cell concept based on Wang tiles [4]. In this contribution the tiling concept is investigated from the viewpoint of the application to numerical homogenization.

The concept of tilings is based on a finite set of square dominoe-like tiles with codes assigned to the tiles edges [5]. The tiles are assembled into continuous portions of plane – tilings, such that only tiles with matching codes on congruent edges can be placed side by side.

To utilize this abstract concept in Materials Engineering a part of microstructural information has to be attributed to each tile while preserving microstructural compatibility across the corresponding edges. The tile morphology is designed such that a tiling resembles the reference medium in the sense of spatial descriptors. We limit our attention to stochastic tile sets presented in [1]. The sets correspond with intended purpose of generating random realizations of a given microstructure and can be straightforwardly extended into higher dimensions by means of Wang hypercubes.

In numerical homogenization, the central question is the representativeness of computational model. In asymptotic approach, bounds on the apparent property converge to the effective parameters as the size of the model approaches the size of Representative Volume Element (RVE) [2], see Fig. 1b. Based on the premise that an accurately compressed microstructure automatically contains information on a broad range of effective properties [3] we can investigate optimal size of RVE for various physical processes starting with the same Wang tiling compression. From the viewpoint of numerical homogenization the most appealing feature of Wang tiling concept is its ability to generate random microstructure realizations of any size in a very efficient way. Moreover, creating finite element (FE) mesh for each realization can be avoided with constructing FE mesh of each tile such that it satisfies the compatibility constraints given by the tile codes. The tiling mesh then can be synthesized in the same manner as the microstructure.

Computational cost related to the standard asymptotic homogenization can be thus reduced realizing that the reconstructed microstructure is composed of repeating instances from a limited set. Significant decrease in the number of unknowns related to a discretized RVE can be

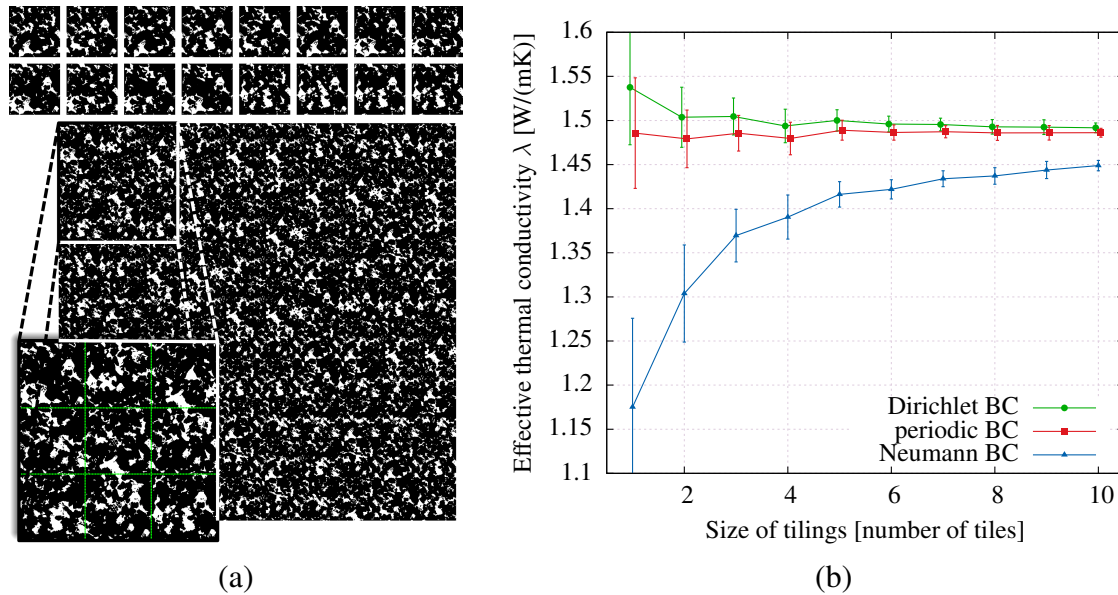


Fig. 1. (a) An example of a sandstone microstructure compressed into a tile set consisting of 16 tiles and one realization of 10×10 tiling (magnified part with highlighted tiling grid), (b) apparent thermal conductivity resulting from the asymptotic homogenization of the sandstone microstructure.

achieved taking the advantage of the repeating pattern. In particular, we eliminate internal degrees of freedom at each tile, leaving only their boundary counterparts. The global stiffness matrix of an RVE is then assembled from Schur complements of each tile (macro-element) stiffness matrix. As a result a finer resolution of FE mesh can be used while keeping the computational time feasible.

Acknowledgements

The support by the Czech Science Foundation through project No. 1324027S is gratefully acknowledged. We would also like to thank the European Social Fund endowment under Grant No. CZ.1.07/2.3.00/30.0005 of Brno University of Technology (Support for the creation of excellent interdisciplinary research teams at Brno University of Technology) and the Grant Agency of the Czech Technical University in Prague, grant No. SGS 14/072/OHK1/1T/11.

References

- [1] Cohen, M. F., Shade, J., Hiller, S., Deussen, O., Wang tiles for image and texture generation, *ACM Transactions on Graphics* 22 (3) (2011) 287–294.
- [2] Kanit, T., Forest, S., Galliet, I., Mounoury, V., Jeulin, D., Determination of the size of the representative volume element for random composites: statistical and numerical approach, *International Journal of Solids and Structures* 40 (13–14) (2003) 3647–3679.
- [3] Niezgodá, S. R., Turner, D. M., Fullwood, D. T., Kalidindi, S. R., Optimized structure based representative volume element sets reflecting the ensemble-averaged 2-point statistics, *Acta Materialia* 58 (13) (2012) 4432–4445.
- [4] Novák, J., Kučerová, A., Zeman, J., Compressing random microstructures via stochastic Wang tilings, *Physical Review E* 86 (4) (2012) 040104.
- [5] Wang, H., Proving theorems by pattern recognition-II, *Bell System Technical Journal* 40 (1) (1961) 1–42.

The additional effects of fluid in a thin gap with a heterogeneous environment

J. Krutil^a, F. Pochylý^a, S. Fialová^a

^a Brno University of Technology, Faculty of Mechanical Engineering, Technická 2896/2, 616 69 Brno, Czech Republic

The paper presents matrices of the additional effects fluid on shaft of hydraulic machine that arise from the numerical CFD modeling of turbulent mixture of water and air in the hydrodynamic sealing gap (HSG). These HSG are an integral part of hydraulic machines with impellers (pumps, turbines). Basically it is a narrow gap which is disposed between the rotor and the stator of the hydrodynamic machine, see Fig. 1.

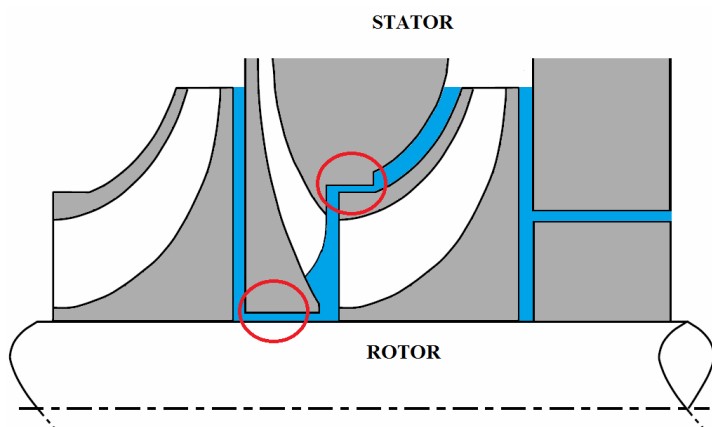


Fig. 1. Scheme of a rotor and a stator of a hydrodynamic machine (hydrodynamic sealing gaps are marked by red)

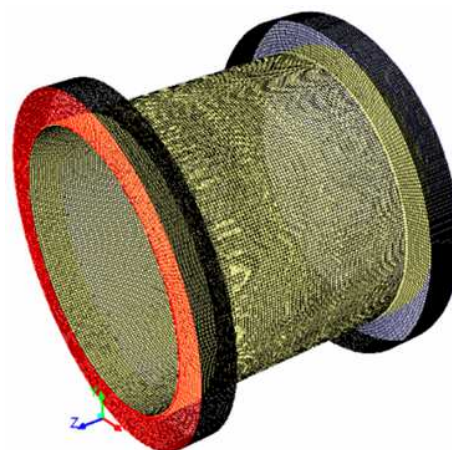


Fig. 2. Model and computational mesh of HSG

Sealing gap acts as a bearing element, which prevents mutual contact between the rotor and stator. This sealing gap combines the function of damper, spring and mass elements. Currently, the hydraulic machines are requires to work in a wide operating range. If the hydraulic machines operate outside their optimum operating point, local instabilities or cavitation may occur. Such phenomena lead to the formation of vortical structures, which may cause expelling of a certain quantity of gas or, conversely, may cause the sucking in of water with a large amount of undissolved air.

The solution is based on the method of control volumes and the used tool for the solution is numerical program ANSYS Fluent. Model and computational mesh of HSG is show in fig. 2. It is assumed unsteady movement of shaft in HSG (ie. the shaft performs precessional and the rotational movement simultaneously). The result is an assessment of the impact undissolved air on elements of matrices of mass, stiffness and damping. In Fig. 4 there are plotted the various dependences of each force components acting on the rotor of the machine from fluid (corresponds to two revolutions of the rotor).

All elements hydrodynamic sealing gap are exposed to the effects of flowing liquid. The force that acts on these elements can be symbolically expressed in the form

$$F = \begin{Bmatrix} F_r & -F_t \\ F_t & F_r \end{Bmatrix} = (-K - \Omega B \Gamma + \Omega^2 M) e, \quad (1)$$

where: mass M [Kg], damping B [kg/s] and stiffness K [N/m], for hydrodynamic sealing gap.

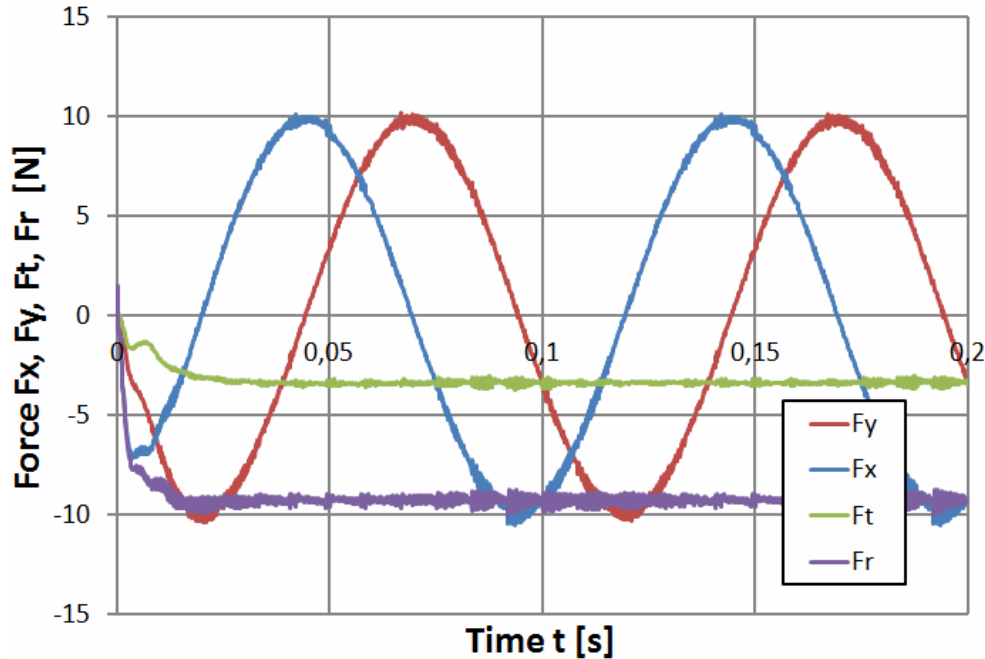


Fig. 3. Sample of progressions of forces (speed of rotation $\omega = 62.8319$ rad/s and speed of precession $\Omega = 62.8319$ rad/s)

Table 1. Sample of result of CFD simulation for speed of rotation $\omega = 62.8319$ rad/s

% of Air	K_{11}	K_{21}	B_{22}	B_{12}	M_{11}	M_{21}
0,5	60206,00	-4384,00	434,00	56,66	2,00E-01	0,00
1	60182,00	-4384,67	433,33	57,33	2,00E-01	0,00

The results from Table 1 indicate that additional effects of fluid are characteristic of anti-symmetric matrices. From this table it can be also seen that with increasing the amount of air contained in the water are affected all elements of the above mentioned matrices.

Acknowledgements

The work has been supported by the grant project GA101/13-20031S, CZ.1.07/2.3.00/30.0005.

References

- [1] Krutil, J., Pochylý, F., Fialová, S., Matrices of additional effects of the hydrophilic sealing gap of the hydrodynamic machina, Riadenie tekutinových systémov XIV. medzinárodná vedecká a odborná konferenci, Trečianske Teplice, Republic of Slovakia, 2014.
- [2] Pochylý, F., Fialová, S. Kozubková, M., Bojko, M., Tensors of added damping, stiffness and mass in a thin gap of hydrodynamic machina, IOP Conference Series: Earth and Environmental Science 15 (7) (2012) 1-8.
- [3] Pochylý, F. Krutil, J., Hydrodynamic effects of the sealing gap, Research Report number VUT-EU QR-33-13, Brno university of technology, 2013.

Homogenization using boundary element methods

D. Lukáš^{a,b}, J. Bouchala^{a,b}, M. Theuer^{a,b}

^aDepartment of Applied Mathematics, Faculty of Electrical Engineering and Computer Science, VŠB-Technical University of Ostrava,
17. listopadu 15, 708 33 Ostrava-Poruba, Czech Republic

^bIT4Innovations, VŠB-Technical University of Ostrava, 17. listopadu 15, 708 33 Ostrava-Poruba, Czech Republic

Materials with periodic microstructure, see Fig. 1, often behave as anisotropic homogeneous materials at a macroscopic level. For the sake of simplicity we consider the square or cubic periodic cell $Y := (0, 1)^d$, $d = 2, 3$, decomposed into nonoverlapping Lipschitz subdomains Y_1 (an inclusion) and Y_2 such that $\text{dist}(\Gamma, \Gamma_1) > 0$, where $\Gamma := \partial Y$, $\Gamma_1 := \partial Y_1$. We denote $\Gamma_2 := \partial Y_2 = \Gamma_1 \cup \Gamma$. The periodic material is described by a positive function $a : Y \rightarrow \mathbb{R}$ such that $a(x) = a_1$ for $x \in Y_1$ and $a(x) = a_2$ for $x \in Y_2$. It is well known [1] that the solution to a boundary value problem for the diffusion equation with the periodic material function weakly converges (in the H^1 -norm) to the solution of the same problem with a homogeneous material given by constant coefficients $A^0 \in \mathbb{R}^{d \times d}$,

$$(A^0)_{ik} := \int_Y a (\delta_{ik} - \partial_i \tilde{\chi}^k), \text{ where } \tilde{\chi}^k \in H_{\text{per}}^1(Y) : \int_Y a \nabla \tilde{\chi}^k \nabla \tilde{v} = \int_Y a \partial_k \tilde{v}$$

for all $\tilde{v} \in H_{\text{per}}^1(Y)$, where $H_{\text{per}}^1(Y)$ contains $H^1(Y)$ -functions that are periodic on Γ .

We show that the problem can be reduced to the boundary as follows:

$$(A^0)_{ik} = \delta_{ik} a_2 + (a_1 - a_2) \int_{\Gamma_1} (\delta_{ik} x_i - \chi_1^k) (n_1)_i,$$

where $(\chi_1^k, \chi^k) \in \mathcal{V} := H^{1/2}(\Gamma_1) \times H_{\text{per}}^{1/2}(\Gamma)$ solves the boundary integral formulation

$$a_1 \langle S_1(\chi_1^k), v_1 \rangle_{\Gamma_1} + a_2 \langle S_2(\chi_1^k, \chi^k), (v_1, v) \rangle_{\Gamma_2} = (a_1 - a_2) \int_{\Gamma_1} v_1 (n_1)_k$$

for all $(v_1, v) \in \mathcal{V}$, where $S_i : H^{1/2}(\Gamma_i) \rightarrow H^{-1/2}(\Gamma_i)$ denote the Steklov-Poincaré operators mapping the Dirichlet data of a Y_i -harmonic function to the Neumann data. To our best knowledge this formulation is new.

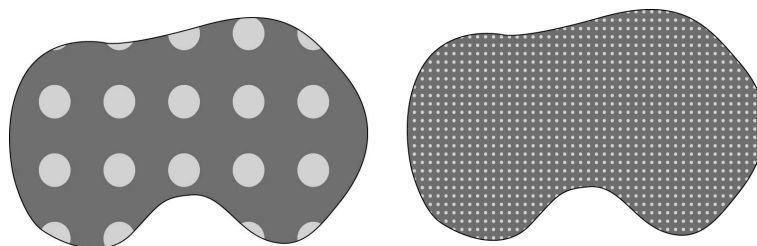


Fig. 1. Periodic materials

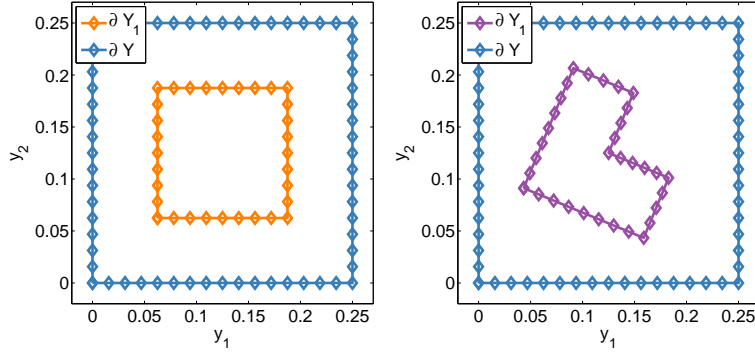


Fig. 2. Numerical examples

h	2^{-6}	2^{-7}	2^{-8}	2^{-9}	2^{-10}	2^{-11}
err(h) square	2.05e-2	7.44e-3	2.67e-3	9.36e-4	3.10e-4	8.24e-5
L-shape	4.47e-2	1.14e-2	3.73e-3	1.27e-3	4.17e-4	1.10e-4

Tab. 1. Convergence of homogenized coefficients

We add to the latter formulation the side constraint $\int_{\Gamma_1} \chi_1^k + \int_{\Gamma} \chi^k = 0$ to get a well-posed problem. This is discretized by means of a Galerkin boundary element method [3] and we arrive at the following linear system

$$\begin{pmatrix} a_1 \mathbf{S}_1 + a_2 \mathbf{S}_2^{\Gamma_1, \Gamma_1} & a_2 \mathbf{S}_2^{\Gamma_1, \Gamma} \mathbf{P} & \mathbf{e}_1 \\ a_2 \mathbf{P}^T \mathbf{S}_2^{\Gamma, \Gamma_1} & a_2 \mathbf{P}^T \mathbf{S}_2^{\Gamma, \Gamma} \mathbf{P} & \mathbf{P}^T \mathbf{e} \\ (\mathbf{e}_1)^T & \mathbf{e}^T \mathbf{P} & 0 \end{pmatrix} \begin{pmatrix} \chi_1^k \\ \widehat{\chi}^k \\ \lambda \end{pmatrix} = \begin{pmatrix} \mathbf{b}_1^k \\ \mathbf{0} \\ 0 \end{pmatrix},$$

where χ_1^k is the nodal approximation of $\chi_1^k(y)$, $\widehat{\chi}^k$ is a half of the nodal approximation of $\chi^k(y)$, \mathbf{P} preserves the Γ -periodicity of $\chi^k(y)$, \mathbf{e}_1 and \mathbf{e} realize the side constraint, and $\mathbf{S}_i^{\alpha, \beta}$ stands for the (α, β) -block of the discretized Steklov-Poincaré operator S_i .

In [2] we prove, under smoothness assumptions, that the discretized coefficients converge (in the maximum norm) to the true ones quadratically with respect to the boundary element mesh size h . We document the theory with the examples in Fig. 2, where we have chosen the material $a_1 := 1$ and $a_2 := 10$. The resulting homogenized coefficients are

$$A_{h_{\min}}^0 = \begin{pmatrix} 6.4758 & 0 \\ 0 & 6.4758 \end{pmatrix} \quad \text{and} \quad A_{h_{\min}}^0 = \begin{pmatrix} 6.8084 & -0.1882 \\ -0.1882 & 7.2662 \end{pmatrix}$$

for the square and the L-shaped inclusion, respectively, where $h_{\min} := 2^{-12}$. Table 1 documents a super-linear convergence of the error $\text{err}(h) := \max_{ik} |(A_{h_{\min}}^0 - A_h^0)_{ik}|$.

Acknowledgements

This work was supported by the project (CZ.1.05/1.1.00/02.0070), IT4Innovations Centre of Excellence, funded by the European Regional Development Fund and the national budget of the Czech Republic via the Research and Development for Innovations Operational Programme. The work was also supported by VŠB-Technical University of Ostrava under the grant SGS SP2013/191.

References

- [1] Cioranescu, D., Donato, P., An introduction to homogenization, Oxford University Press 1999.
- [2] Lukáš, D., Bouchala, J., Theuer, M., A BEM for homogenization. (in preparation)
- [3] Steinbach, O., Numerical approximation methods for elliptic boundary value problems: Finite and boundary elements, Springer, 2008.

Computational modeling of liver perfusion – towards a patient specific model

V. Lukeš^a, E. Rohan^a, A. Jonášová^a, O. Bublík^a

^aFaculty of Applied Sciences, UWB in Pilsen, Univerzitní 22, 306 14 Plzeň, Czech Republic

Using CT or MRI data, we are able to create a patient specific computational model of the human liver. The 1D models of the portal and hepatic veins, which are used for computation of fluxes and pressures in branches of the vascular trees, are reconstructed with the help of *LISA* (Liver Surgery Analyser) application [3]. Segmentation of the liver parenchyma from CT or MRI is done semi-automatically in *DICOM2FEM* software [6], a finite element mesh representing the liver tissue is generated using the marching cubes algorithm [5]. The quality of the surface FE mesh is improved by applying the Taubin smoothing filter that is able to preserve the total volume of the segmented organ. An example of a successfully reconstructed liver geometry is shown in Fig. 1 (left). The reconstructed vascular trees are often of a low quality, they are disconnected or with various non-physiological artifacts. To avoid problems in further simulation steps, we combine the reconstruction techniques with the generation of missing or corrupted branches using the constructive optimization method, see [2].

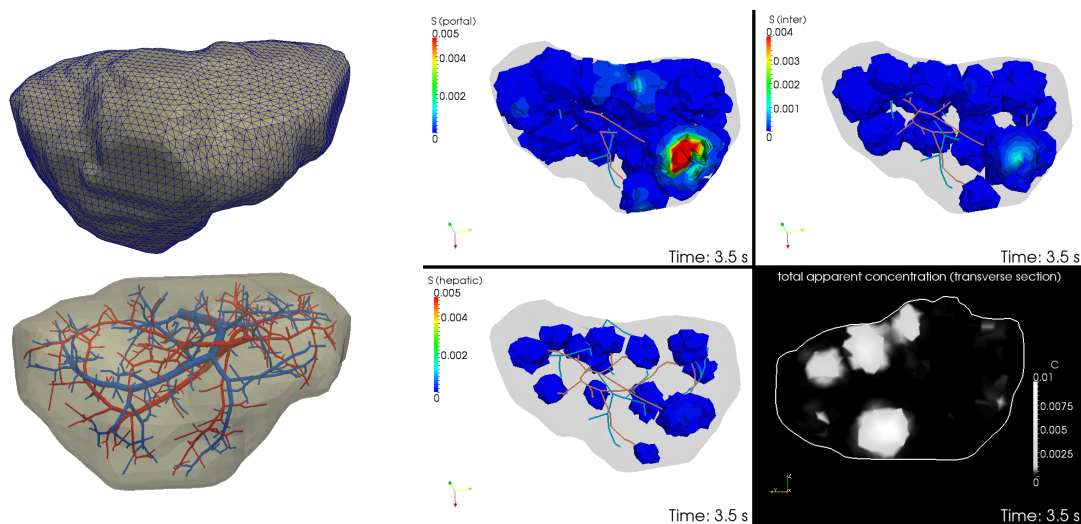


Fig. 1. Finite element model of the liver tissue and 1D model of the larger vascular structures (left); results of the numerical simulation – saturation of a contrast fluid (right)

Due to the complex hierarchical arrangement of the parenchyma and vascular structures we use different mathematical models at different spatial scales. The blood flow in larger vessels is described by a simple 1D model governed by the Bernoulli equation extended with friction loss terms. The advantage of the 1D model is the minimal computational cost compared to a full 3D flow simulation. The liver tissue including smaller vascular structures is considered

as a 3D porous medium and the blood flow is governed by the Darcy's equation. To capture the different hierarchies of the tissue vascularity, we employ the multicompartment approach, where the hierarchies are represented by spatially co-existing domains, referred to as compartments, associated with a permeability tensor that reflects the vascular structure (vessel size and orientation). The compartments communicate together and the fluid exchange between them is driven by coupling coefficients. The model of tissue parenchyma is coupled with the 1D flow through sources and sinks, see [4, 7, 8]. The computation is performed in *SfePy*, the Python based finite element solver, see [1]. Finally, the perfusion results are used for the simulation of contrast fluid propagation, Fig. 1 (right).

The crucial point of the patient oriented numerical modeling of liver perfusion is identification of perfusion parameters involved in the mathematical models. The proposed identification approach is based on the sensitivity analysis of model parameters and the optimization problem is solved in order to minimize the difference between the simulated dynamic CT perfusion test and the measured data.

Acknowledgments

This research is partially supported by the Ministry of Health of the Czech Republic, project NT 13326, and by the European Regional Development Fund (ERDF), project "NTIS - New Technologies for the Information Society", European Centre of Excellence, CZ.1.05/1.1.00/02.0090.

References

- [1] Cimrman, R., *SfePy* – Write your own FE application, Proceedings of the 6th European Conference on Python in Science – EuroSciPy 2013, 2014, pp. 65–70. (<http://arxiv.org/abs/1404.6391>)
- [2] Georg, M., Preusser, T., Hahn, H. K., Global constructive optimization of vascular systems, Technical Report, Washington University in St. Louis, 2010. (http://cse.wustl.edu/Research/Lists/Technical Reports/Attachments/910/ideavessel_1.pdf)
- [3] Jiřík, M., *LISA* – Liver Surgery Analyser, software. (<https://github.com/mjirik/lisa>)
- [4] Jonášová, A., Rohan, E., Lukeš, V., Bublík, O., Complex hierarchical modeling of the dynamic perfusion test: Application to liver, Proceedings of the 11th World Congress of Computational Mechanics, Barcelona, Spain, 2014, pp. 3438–3449.
- [5] Lorensen, W. E., Cline, H. E., Marching cubes: A high resolution 3D surface construction algorithm, *Computer Graphics* 21 (4) (1987) 163-169.
- [6] Lukeš, V., *DICOM2FEM* – application for semi-automatic generation of finite element meshes, software. (<http://sfepy.org/dicom2fem>)
- [7] Rohan, E., Lukeš, V., Jonášová, A., Bublík, O., Towards microstructure based tissue perfusion reconstruction from CT using multiscale modeling, Proceedings of the 10th World Congress on Computational Mechanics, Sao Paulo, Brasil, 2012, pp. 1–18.
- [8] Rohan, E., Lukeš, V., Modeling tissue perfusion using a homogenized model with layer-wise decomposition, Proceedings of the 7th Vienna International Conference on Mathematical Modelling – MATHMOD 2012, Vienna, Austria, 2012, pp. 1029–1034.

A model of wave propagation in homogenized Biot medium with dual porosity

E. Rohan^a, V.-H. Nguyen^b, S. Naili^b

^aEuropean Centre of Excellence, NTIS New Technologies for Information Society, Faculty of Applied Sciences, UWB in Pilsen,
Univerzitní 22, 306 14 Plzeň, Czech Republic

^bUniversité Paris-Est, Laboratoire Modélisation et Simulation Multi Echelle, MSME UMR 8208 CNRS, 61 avenue du Général de Gaulle,
94010 Créteil cedex, France

We describe a macroscopic model of waves propagating in fluid-saturated periodic media with dual porosity. At the mesoscopic level, the fluid motion in deforming elastic skeleton is governed by the Biot-Darcy model extended by inertia terms, which has been obtained by homogenization of the fluid-structure interaction, see e.g. [2, 3].

In this paper we deal with upscaling the Biot-Darcy model from the mesoscopic level, where large contrasts in the permeability and the poroelastic coefficients are considered. The two-scale homogenization method is used to obtain a macroscopic model. This model is an extension of previously studied problems with either rigid skeleton part [5], or deformable Biot medium without large contrasts in material properties [4].

Wave propagation in the Biot medium is governed by the system of three equations involving skeleton displacements \mathbf{u} , the fluid pressure p , and the fluid seepage velocity \mathbf{w} which describes the relative fluid velocity w.r.t. the solid skeleton. We consider harmonic waves with a given frequency ω , so that the complex amplitudes $(\mathbf{u}, \mathbf{w}, p)$ satisfy the momentum equation, the Darcy law extended for the inertia terms, and the fluid volume conservation:

$$\begin{aligned}
 -\omega^2 \bar{\rho} \mathbf{u} + i\omega \rho^f \mathbf{w} - \nabla \cdot (\mathbf{D} \boldsymbol{\epsilon}(\mathbf{u})) + \nabla(\boldsymbol{\alpha} p) &= \mathbf{f} , \\
 -\omega^2 \rho^f \mathbf{u} + i\omega \rho^w \mathbf{w} + \mathbf{K}^{-1} \mathbf{w} + \nabla p &= \tilde{\mathbf{f}} , \\
 i\omega \boldsymbol{\alpha} : \boldsymbol{\epsilon}(\mathbf{u}) + \operatorname{div} \mathbf{w} + i\omega \frac{1}{\mu} p &= \tilde{g} ,
 \end{aligned}$$

where $\boldsymbol{\epsilon}(\mathbf{u})$ is the small strain tensor, \mathbf{f} and $\tilde{\mathbf{f}}$ are the volume force amplitudes (acting on the mixture and on the fluid, respectively), \mathbf{D} is the skeleton elasticity tensor, ρ^f is the fluid density, density $\rho^w = \phi_0^{-1} \rho^f$ involving the fluid volume fraction ϕ_0 is relevant to the seepage acceleration, \mathbf{K} is the permeability, $\boldsymbol{\alpha}$ is the Biot effective stress coefficient (tensor), μ is the Biot modulus reflecting compressibility of the fluid and of the skeleton.

The heterogeneous porous medium occupying domain Ω consists of two distinct parts with large contrasts in magnitudes of the hydraulic permeability and poroelasticity coefficients. For a fixed scale $\varepsilon > 0$ related to the size of the mesoscopic heterogeneity, we consider the decomposition of $\Omega \subset \mathbb{R}^3$ into two parts, the matrix Ω_m^ε and the channels Ω_c^ε , whereby $\Omega_m^\varepsilon \cap \Omega_c^\varepsilon = \emptyset$ and $\Omega = \Omega_m^\varepsilon \cup \Omega_c^\varepsilon \cup \Gamma^\varepsilon$ with $\Gamma^\varepsilon = \overline{\Omega_m^\varepsilon} \cap \overline{\Omega_c^\varepsilon}$ denoting the interface. We require that both Ω_c^ε and Ω_m^ε are connected, see Fig. 1 illustrating the periodic structure with the dual porosity.

We pursue the approach of [5], accepting the classical scaling ansatz, with respect to ε , which was used first by Arbogast et al. [1] to deal with quasi-static flows in fissured rocks.

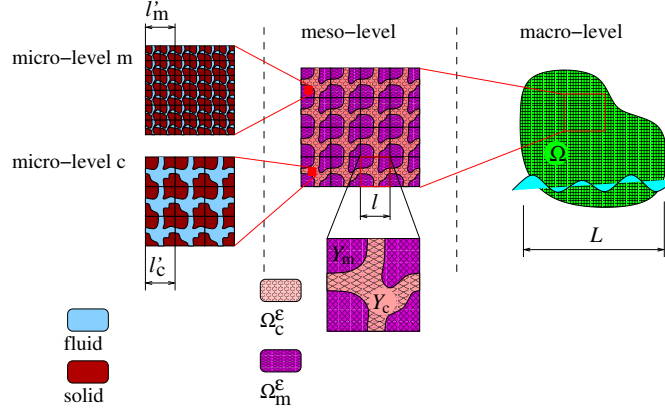


Fig. 1. The double porosity medium

Piecewise-continuous material coefficients are introduced, as follows:

$$\begin{aligned}
\rho^{w\varepsilon}(x) &= \chi_m^\varepsilon(x)\rho^{m\varepsilon}(x) + \chi_c^\varepsilon(x)\rho^{c\varepsilon}(x), \\
\mu^\varepsilon(x) &= \chi_m^\varepsilon(x)\mu^{m\varepsilon}(x) + \chi_c^\varepsilon(x)\mu^{c\varepsilon}(x), \\
\mathbf{K}^\varepsilon(x) &= \varepsilon^2\chi_m^\varepsilon(x)\widehat{\mathbf{K}}^{m\varepsilon}(x) + \chi_c^\varepsilon(x)\mathbf{K}^{c\varepsilon}(x), \\
\mathbb{D}^\varepsilon(x) &= \chi_m^\varepsilon(x)\mathbb{D}^{m,\varepsilon}(x) + \varepsilon^2\chi_c^\varepsilon(x)\widehat{\mathbb{D}}^{c,\varepsilon}(x), \\
\boldsymbol{\alpha}^\varepsilon(x) &= \chi_m^\varepsilon(x)\boldsymbol{\alpha}^{m,\varepsilon}(x) + \varepsilon\chi_c^\varepsilon(x)\widehat{\boldsymbol{\alpha}}^{c,\varepsilon}(x),
\end{aligned}$$

where χ_d^ε for $d = m, c$ is the characteristic function of domain Ω_d^ε . The wave propagation in the homogenized medium with the double porosity is given in terms of the macroscopic displacement and pressure fields \mathbf{u} and p which satisfy the following two equations:

$$\begin{aligned}
-\omega^2\mathcal{M}\mathbf{u}^0 - \nabla \cdot (\mathcal{D}\mathbf{e}(i\omega\mathbf{u}^0) - (\mathcal{B} - \omega^2\mathcal{G})i\omega p^0) + i\omega\mathcal{C}p^0 &= \mathcal{F}^f\tilde{\mathbf{f}}^f + \mathcal{F}^s\tilde{\mathbf{f}}^s - \mathcal{E}^s \cdot i\omega\nabla\bar{p}, \\
(\mathcal{B} - \omega^2(\mathcal{G})^T) : \mathbf{e}(i\omega\mathbf{u}^0) + \omega^2\mathcal{C} \cdot \mathbf{u}^0 - \mathcal{K} : \nabla(\nabla p^0) + i\omega\mathcal{H}p^0 &= \underline{\mathcal{F}}^f \cdot \tilde{\mathbf{f}}^f + \underline{\mathcal{F}}^s \cdot \tilde{\mathbf{f}}^s + i\omega\mathcal{E}^f\bar{p}.
\end{aligned}$$

All the homogenized coefficients $\mathcal{M}, \mathcal{D}, \mathcal{B}, \mathcal{G}, \mathcal{K}, \mathcal{H}$ and $\underline{\mathcal{F}}^f, \mathcal{F}^s, \mathcal{E}^f, \mathcal{E}^s$ are computed using characteristic responses of the microstructure and depend on the frequency ω of the incident wave. In the paper we explain the structure of the local problems for the characteristic responses and discuss some properties of the homogenized model.

Acknowledgements

The research was supported by project P101/12/2315 of GAČR and in part by TA02010565 of TAČR.

References

- [1] Arbogast, T., Douglas, J., Hornung, U., Derivation of the double porosity model of single phase flow via homogenization theory, *SIAM Journal on Mathematical Analysis* 21 (4) (1990) 823–836.
- [2] Auriault, J.-L., Boutin, C., Deformable porous media with double porosity III. Acoustics, *Transport in Porous Media* 14 (2) (1994) 143–162.
- [3] Ferrín, J., Mikelić, A., Homogenizing the acoustic properties of a porous matrix containing an incompressible inviscid fluid, *Mathematical Methods in the Applied Sciences* 26 (10) (2003) 831–859.
- [4] Mielke, A., Rohan, E., Homogenization of elastic waves in fluid-saturated porous media using the Biot model, *Mathematical Models and Methods in Applied Sciences* 23 (5) (2013) 873–916.
- [5] Rohan, E., Homogenization of acoustic waves in strongly heterogeneous porous structures, *Wave Motion* 50 (7) (2013) 1073–1089.

Modelling of various phase transformations in ferroic solids, in particular magnetic shape-memory materials

T. Roubíček^{a,b}

^aMathematical Institute, Charles University, Sokolovská 83, CZ-186 75 Praha 8, Czech Republic

^bInstitute of Thermomechanics of the ASCR, Dolejšková 5, CZ-182 00 Praha 8, Czech Republic

Ferroic materials is a generic name for ferromagnets, ferroelectrics, or ferroelastic materials. They exhibit various structural (in some cases called *phase-*) *transformations* (PT) of mechanical or non-mechanical character, as a martensitic PT in shape-memory materials or ferro-to-para magnetic PT, sometimes even combined with chemical transformations as e.g. metal-hydride, etc. Several ferroic phenomena may occur simultaneously and the PTs are then mutually coupled – one speaks about *multiferroics*; examples are piezoelectric or magnetostrictive materials.

Even media which are homogeneous thus typically manifest themselves as in some sense *heterogeneous* due to occurrence of (evolving) domains with very different mechanical or other properties. Often, a sophisticated microstructure is self-organized in particular single-crystals (which may further form particular grains in polycrystalline specimens). Therefore the problem

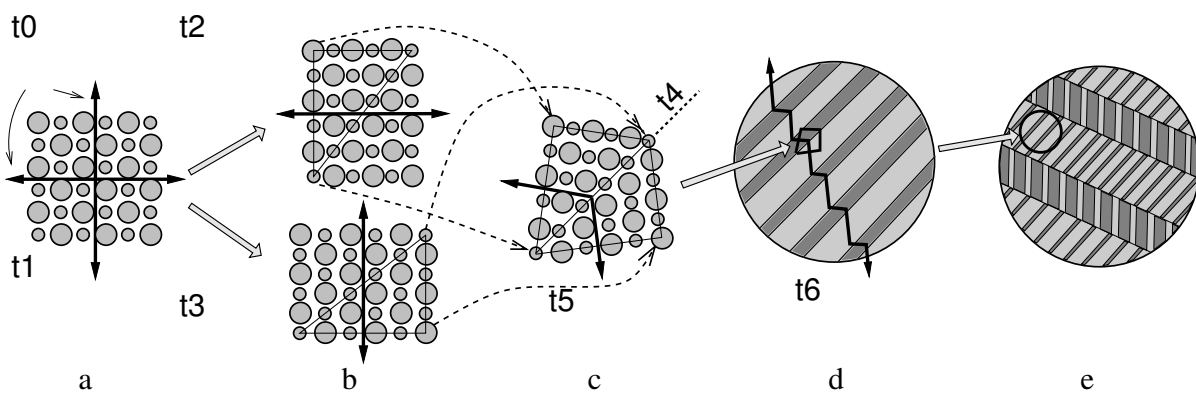


Fig. 1. Schematic explanation of microstructure formed by twinned martensite with zig-zag magnetisation as observed in single-crystals of magnetostrictive intermetallics as e.g. Ni_2MnGa :

- (a) the parent austenite (cubic): schematic atomic lattice with two sorts of atoms and two directions of easy magnetisation (out of 3 in dimension 3),
- (b) two variants of “tetragonal” martensite elongated vertically or horizontally with only 1 direction of easy magnetisation (geometrical stretch may be quite large, about 8%),
- (c) a twin occurring by matching two slightly rotated martensitic variants with an easy-magnetisation directions “bended” in a nearly 90°-angle,
- (d) 1st-order laminate (the gray levels distinguish particular variants of martensite) with a zig-zagging, easy-magnetisation,
- (e) 2nd-order laminate (layers within layers, magnetisation not depicted).

is typically truly *multi-scaled*, ranging from atomistic and microscopic (cf. Fig. 1), via mesoscopic, to macroscopic levels, to be sometimes understood in the context of particular modelling object. Beside such spatial scales, also various time scales are to be recognized.

A wide class of such materials are intermetallics (= alloys with a regular composition of atoms bonded chemically) electrically conductive, sometimes allowing diffusion of certain fluids (hydrogen, deuterium) like porous media. Together with sophisticated storage-energy mechanism, equally important is the way how such materials dissipate energy within these phase transformations. This allows typically for even much less rigorous understanding only, and thus needs even more phenomenology. And, of course, strong temperature dependence is typical and vital part of a sophisticated (sometimes called smart or intelligent) response of such materials, which makes important also the heat transfer in non-isothermal situation and the truly *thermomechanical* coupling of such *multi-physical* models.

There is a wide menagerie of mathematical and computational models which have been built many decades worldwide on various levels (micro/meso/macro) focused to various aspects (e.g. single crystals vs polycrystals, merely static vs quasi-static vs dynamic, isothermal vs anisothermal, etc.), incorporating various phenomenology and concepts (e.g. large vs small strains), and supported by some (or none) mathematical and physical rigor. For a certain survey of merely ferroelastic PTs in case of *shape-memory alloys* see [3]. Rigorous upscaling between various levels of description is usually possible at most in static problems, or sometimes in quasi-static too, cf. [4], but mostly is missing.

Following a (to some extent pioneering) work [2] which formulated the ferro-to-para-magnetic PT in ferromagnets in mathematically amenable way in particular by relaxing the Heisenberg constraint, it was possible to combine it with ferroelastic models like [1] to build a model for *magnetostrictive materials* [6], still devised for *single crystals* like in Fig. 1 only. Of course, the situation in *polycrystals* is even more complex and ultimately needs much more phenomenological models, like that in [5], which, on the other hand, are more amenable for efficient computational simulations of macroscopical specimens of engineering interest.

Moreover, diffusion of hydrogen in rare-earth- or Uranium-based intermetallics may combine ferromagnetic/ferroelastic PTs with *metal-hydride structural transformation* like in [7].

Acknowledgements

This long-lasting research has partly been supported by the Grant Agency of the Czech Rep., currently through the projects 201/10/0357 “Modern mathematical and computational models for inelastic processes in solids”, 13-18652S “Computational modeling of damage and transport processes in quasi-brittle materials”, and 14-15264S “Experimentally justified multiscale modelling of shape memory alloys”.

References

- [1] Arndt, M., Griebel, M., Novák, V., Roubíček, T., Šittner, P., Martensitic transformation in NiMnGa single crystals: Numerical simulations and experiments, *Int. J. Plasticity* 22 (2006) 1943-1961.
- [2] Podio-Guidugli, P., Roubíček, T., Tomassetti, G., A thermodynamically-consistent theory of the ferro/paramagnetic transition, *Archive Rat. Mech. Anal.* 198 (2010) 1057-1094.
- [3] Roubíček, T., Models of microstructure evolution in shape memory alloys, In: *Nonlinear Homogenization and its Appl. to Composites, Polycrystals and Smart Materials.* (Eds. P.Ponte Castaneda, J.J.Telega, B.Gambin), NATO Sci. Series II/170, Kluwer, Dordrecht, 2004, pp.269-304.
- [4] Roubíček, T., Approximation in multiscale modelling of microstructure evolution in shape-memory alloys, *Cont. Mech. Thermodynam.* 23 (2011) 491-507.
- [5] Roubíček, T., Stefanelli, U., Magnetic shape-memory alloys: Thermomechanical modeling and analysis, *Cont. Mech. Thermodynamics* (2013), doi: 10.1007/s00161-014-0339-8.
- [6] Roubíček, T., Tomassetti G., Phase transformations in electrically conductive ferromagnetic shape-memory alloys, their thermodynamics and analysis, *Arch. Rat. Mech. Anal.* 210 (2013) 1-43.
- [7] Roubíček, T., Tomassetti, G., Thermomechanics of hydrogen storage in metallic hydrides: Modeling and analysis, *Discrete Cont. Dynam. Systems - Ser. B*, 19 (2014) 2313-2333.

Hard packing for 3D Wang cubes generation

D. Šedlbauer^a

^a *Department of Mechanics, Faculty of Civil Engineering, CTU in Prague, Thákurova 7/2077, 166 29 Prague, Czech Republic*

For a representation of heterogeneous materials some approaches can be found. Most of them deal with a concept of the Representative Volume Element (RVE). The RVE can be defined as a small enough sample including the whole domain information of a reconstructed medium. Such sample has to enable efficient usage of numerical methods for modelling as well [2]. For a creation of the RVE methods based on the Periodic Unit Cell (PUC) are commonly used. However, during a reconstruction of heterogeneous materials using the PUC unwanted periodicity artefacts occur. Therefore the concept of Wang tiling [3] is utilized that can highly reduce a periodicity without increasing of computational demands. In this paper we consider modelling of a 3D heterogeneous material that consists of hard spherical particles within a matrix.

The main idea of the Wang tiling is to stack an infinite aperiodic or strictly aperiodic plane/space with a small set of Wang tiles/cubes. In general each single Wang tile in 3D is represented as a cube with codes (colours, letters etc.) on walls. In the field of 3D material modelling it is not necessary to have strictly aperiodic domains. For a stacking of such spaces via Wang cubes a stochastic tiling based on the CSHD [1] algorithm is utilized. First cube of a set is randomly chosen and placed to the grid of a material domain. The stochastic algorithm then adds cubes gradually row by row, column by column within a layer and then layer by layer. Considering three parameters as numbers of different codes for walls in x , y and z directions, we have to have at least two possible cubes for every combination of codes in mentioned directions (stochastic principle). If we have two different codes in each direction the minimal Wang tile set consists of sixteen cubes, Fig. 1.

The generation of a set of 3D Wang cubes can be seen as a highly constrained packing problem. The hard particles distribution within a matrix highly affects a considerable amount of material properties especially the mechanical ones. Concurrently particles non-overlapping has to be ensured. In order to meet these conditions a dynamic packing algorithm for the 3D Wang cubes generation is introduced. This algorithm is based on particle motions, particle growth and dynamic phenomena such as particles collisions and rebounds.

At the beginning of the dynamic algorithm each Wang cube is divided into six marginal (border) volume parts corresponding to the walls of a cube and one central part. The centres of particles with random initial velocity vectors are than semi-randomly placed into the assigned volume parts of a cube. The particles than grow during the dynamic algorithm, elastically bounce from each other and also from the walls of the volume areas until a stopping criterion is achieved. The stopping criterion can be the final particle radius, volume fraction or required value of any material property based on particle distribution. The entire process takes place simultaneously with all the cubes of set of sixteen Wang cubes.

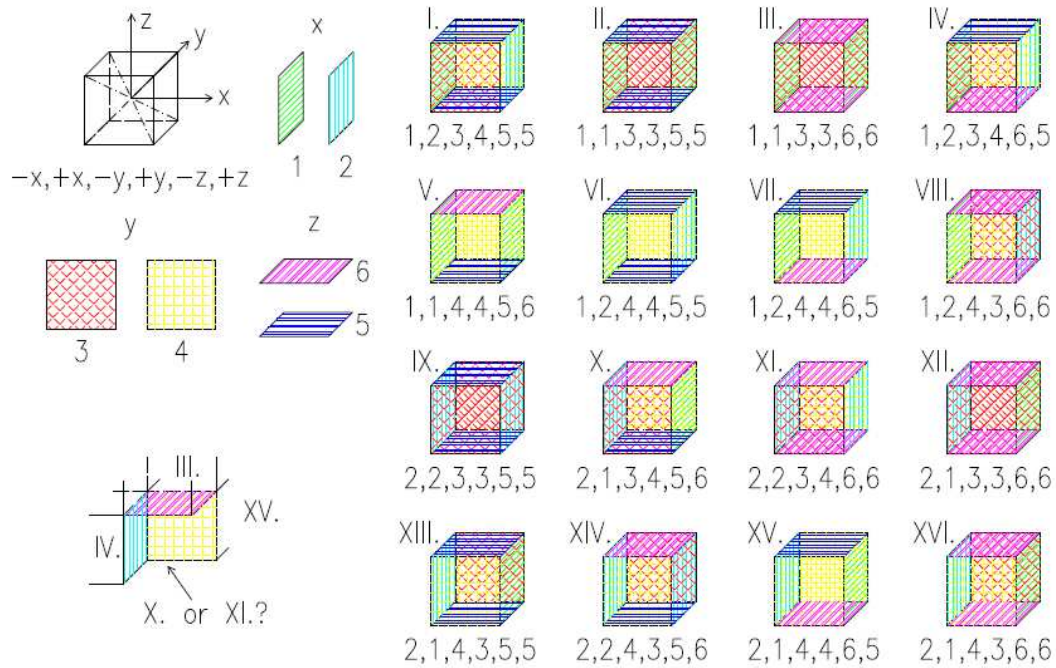


Fig. 1. The principle of stochastic Wang tiling in 3D, minimal set Wang cubes for stochastic tiling

For the task of achieving predefined or optimal particles positions there is need to update particles velocities during the process of generation. A modification of a particle velocity vector is based on principles of swarm optimization techniques where velocity of a single particle is determined in accordance with global best so far positions of all particles in terms of observed material property.

With the dynamic algorithm it is possible to generate the optimized Wang cubes. The dynamic algorithm is based on particle movements and dynamic phenomena that enable particle non-overlapping and modelling of materials with higher volume fraction. A final set of the Wang cubes meets requirements for the stochastic tiling through which we can stack aperiodic material domains. A generated set of the Wang cubes can be than used for various tasks of material engineering like homogenization or micromechanical fields.

Acknowledgements

This outcome has been achieved with the financial support of the Grant Agency of the Czech Technical University in Prague, grant No. SGS14/028/OHK1/1T/11.

References

- [1] Cohen, M. F., Shade, J., Hiller, S., Deussen, O., Wang tiles for image and texture generation, *ACM Transactions on Graphics* 22 (3) (2003) 287-294.
- [2] Kanit, T., Forest, S., Galliet, I., Mounoury, V., Jeulin, D. Determination of the size of the representative volume element for random composites: statistical and numerical approach, *International Journal of Solids and Structures* 40 (13) (2003) 3647-3679.
- [3] Wang, H., Proving theorems by pattern recognition-II, *Bell System Technical Journal* 40 (1) (1961) 1-41.

Macroscopic modeling of electro-osmosis in the porous structure of a cortical bone tissue

J. Turjanicová^a, E. Rohan^a

^aFaculty of Applied Sciences, UWB in Pilsen, Univerzitní 22, 306 14 Plzeň, Czech Republic

Porous structures are commonly found in a wide scale of biological tissues, where multiple physical phenomena may occur. In our recent work, we focus on the electro-osmosis in the cortical bone tissue, where this phenomenon participates in important physiological processes. Similar approach can be applied on other biological tissues or in geosciences, see [1].

In the previous work, see [3], we already introduced a macroscopic model of electro osmosis, where the velocity of the convective flow on the microscale was given. Our current aim is to improve the previous model with Stokes problem and compare the behavior of derived effective coefficients dependent on the convective velocity between the previous and the extended model.

We treat the cortical bone as a hierarchical structure with multiple porosities on different scale levels. Our present work is focused on the electro-osmosis at the lacuno-canalicular porosity level with characteristic scale $l \approx 10$ nm, further referred to as the microscopic level. At this scale, the solid matrix (occupying domain Ω_s) is perforated by lacunae and canaliculi filled with the bone fluid (occupying domain Ω_f). By the macroscopic level we mean the osteon matrix.

We present a dimensionless model of ionic transport in the network of small channels perforating the osteon matrix, which are saturated with an electrolyte solution with two type of monovalent ions of opposite polarizations (cations Na^+ and anions Cl^-). The solid phase Ω_s and the solid-fluid interface Γ are charged with small negative charges, thus the ions in the bone fluid are subjected to a static electric field.

The ionic transport is governed by the following system of equations involving electric potentials in the solid matrix and fluid φ , fluid convective velocity \mathbf{w} , and concentrations of positive and negative ions q^\pm , see [3]:

Electrostatics - Gauss equations:

$$\begin{aligned} -\nabla \cdot \alpha_s \nabla \varphi &= \tilde{\pi}_s & \text{in } \Omega_s, \\ -\nabla \cdot \alpha_f \nabla \varphi - 0.5 \lambda_D^{-2} (q^+ - q^-) &= 0 & \text{in } \Omega_f, \end{aligned}$$

Insulation condition:

$$\mathbf{n} \cdot \alpha \nabla \varphi = 0 \quad \text{on } \partial\Omega,$$

Jump condition on solid-fluid interface:

$$\begin{aligned} \mathbf{n} \cdot \alpha \nabla \varphi|_s &= -\frac{\alpha_\Gamma}{d_\Gamma} [\varphi]_\Gamma - \frac{\tilde{\varrho}}{2} & \text{on } \Gamma_s, \\ -\mathbf{n} \cdot \alpha \nabla \varphi|_f &= \frac{\alpha_\Gamma}{d_\Gamma} [\varphi]_\Gamma - \frac{\tilde{\varrho}}{2} & \text{on } \Gamma_f, \end{aligned}$$

Movement of the ions - two Nerst-Planc equations for positive and negative ions:

$$\partial_t q^\pm + \mathbf{w} \cdot \nabla q^\pm - \nabla \cdot \mathbb{D}^\pm \cdot (\nabla q^\pm \pm (\bar{\Phi} z F / (RT)) q^\pm \nabla \varphi) = 0 \quad \text{in } \Omega_f ,$$

Condition of no mass transfer:

$$\mathbf{n} \cdot \mathbb{D}^\pm \cdot (\nabla q^\pm \pm (\bar{\Phi} z F / (RT)) q^\pm \nabla \varphi) = 0 \quad \text{on } \Gamma ,$$

Condition of electro-neutrality:

$$q^\pm = \bar{q}^\pm \quad \text{on } \partial\Omega .$$

The model is characterized by the following physical quantities: relative permittivity α_d , volume and surface electric charge $\tilde{\pi}_d, \tilde{\rho}_d, d = s, f$, Faraday constant F , universal constant R and valence of ion particles z . Diffusion coefficients for cations and anions are in the form of second-order tensors \mathbb{D}^\pm . The electro-osmosis is characterized by Debye's length $\lambda_D = (\varepsilon_0 RT / 2 \bar{Q} (\bar{z} F)^2)^{1/2}$, where ε_0 is the permittivity of the void space.

The electro-osmosis model given above can be extended by Stokes problem in Ω_f for velocity \mathbf{w} and pressure p , where driving force is proportional to $(\Theta^+ - \Theta^-) \nabla \Phi$, see [2]:

Stokes problem:

$$\begin{aligned} \mu_f \nabla^2 \mathbf{w} - \nabla p &= z F \bar{\Phi} \bar{Q} (\Theta^+ - \Theta^-) \nabla \Phi \quad \text{in } \Omega_f, \\ \nabla \cdot \mathbf{w} &= 0 \quad \text{in } \Omega_f, \\ \mathbf{w} \cdot \mathbf{n} &= \bar{w}_n \quad \text{on } \partial\Omega_f \setminus \Gamma, \\ \mathbf{w} &= 0 \quad \text{on } \Gamma, \end{aligned}$$

where μ_f is the viscosity.

We apply the asymptotic homogenization method on the model introduced above (for more details see [2]). The derived effective coefficients describe the material properties at macroscopic level in the derived macroscopic equations. Both the homogenization procedure and the homogenized problem on the macroscale were implemented in the software *SfePy*. We consider a few different representations of microstructure. On the derived effective coefficients, a parametric study is performed.

Acknowledgments

The research of was supported in part by project NT 13326 of the Ministry of Health of the Czech Republic and by the European Regional Development Fund (ERDF), project NTIS - New Technologies for Information Society, European Centre of Excellence, CZ.1.05/1.1.00/02.0090. Jana Turjanicová is also grateful for the support of her work by project SGS-2013-026.

References

- [1] Allaire, G., Brizzi, R., Duf r che, J. F., Mikeli c, A., Piatnitski, A., Ion transport in porous media: Derivation of the macroscopic equations using upscaling and properties of effective coefficients, *Computational Geosciences* 17 (3) (2013) 479-495.
- [2] Rohan, E., Griso, G., Lemaire, T., Naili, S., Homogenization of electro-osmosis in porous solid saturated by ionized fluid, Report, 2010.
- [3] Turjanicov , J., Electro-mechanical coupling in porous bone structure – Homogenization method application, Master thesis, University of West Bohemia, Plze , 2013.

FFT-based Galerkin method for homogenization of periodic media

J. Vondřejc^a, J. Zeman^{b,c}, I. Marek^b

^a NTIS, Faculty of Applied Sciences, UWB in Pilsen, Univerzitní 22, 306 14 Plzeň, Czech Republic

^b Faculty of Civil Engineering, Czech Technical University in Prague, Thákurova 7, 166 29 Prague 6, Czech Republic

^c Centre of Excellence IT4Innovations, VŠB-TU Ostrava, 17. listopadu 15/2172, 708 33 Ostrava-Poruba, Czech Republic

An FFT-based homogenization belongs to effective numerical algorithms for the evaluation of homogenized properties, which arise from the unit cell problem for periodic media, demonstrated here for scalar linear elliptic problems defined on a periodic unit cell $\mathcal{Y} = \prod_{\alpha=1}^d (-\frac{1}{2}, \frac{1}{2}) \subset \mathbb{R}^d$ with periodic boundary conditions. The variational formulation yields the homogenized matrix $\mathbf{A}_H \in \mathbb{R}^{d \times d}$ in the primal formulation

$$(\mathbf{A}_H \mathbf{E}, \mathbf{E})_{\mathbb{R}^d} = \min_{\mathbf{e} \in \mathcal{E}} (\mathbf{A}(\mathbf{E} + \mathbf{e}), \mathbf{E} + \mathbf{e})_{L^2_{\#}(\mathcal{Y}; \mathbb{R}^d)} = (\mathbf{A}(\mathbf{E} + \mathbf{e}^{(\mathbf{E})}), \mathbf{E} + \mathbf{e}^{(\mathbf{E})})_{L^2_{\#}}$$

for arbitrary $\mathbf{E} \in \mathbb{R}^d$. The quantity \mathbf{e} from $L^2_{\#}(\mathcal{Y}; \mathbb{R}^d)$, consisting of square integrable \mathcal{Y} -periodic \mathbb{R}^d -valued functions, denotes electric current while second-order tensor $\mathbf{A} : \mathcal{Y} \rightarrow \mathbb{R}^{d \times d}$ denotes coercive and bounded material coefficients. The minimization space $\mathcal{E} = \{\mathbf{e} \in L^2_{\#}(\mathcal{Y}; \mathbb{R}^d) : \int_{\mathcal{Y}} \mathbf{e} = 0, \nabla \times \mathbf{e} = 0\}$, the subspace of the Helmholtz decomposition $L^2_{\#}(\mathcal{Y}; \mathbb{R}^d) = \mathbb{R}^d \oplus \mathcal{E} \oplus \mathcal{J}$, and consists of functions \mathbf{e} having a \mathcal{Y} -periodic potential $P \in H^1_{\#}(\mathcal{Y})$ satisfying $\nabla P = \mathbf{e}$. The formulation in the potential form is useful especially for FEM as the curl-free condition is satisfied a priori. This simplification is impossible in the dual formulation as the dual space \mathcal{J} consists of divergence-free fields.

Since the introduction of FFT-based algorithm [4] in 1994, various improvements and modifications of the original formulation have been provided, e.g., [3, 5], however rigorous theories of discretization with convergence proofs have been published only recently. The first approach by Brisard and Dormieux [1] is based on the discretization with piece-wise constant functions corresponding to pixel or voxel-based images. Our approach described in [7]–[9] builds on approximation with trigonometric polynomials with bounded frequencies

$$\mathcal{T}_N^d = \left\{ \sum_{\mathbf{k} \in \mathbb{Z}_N^d} \hat{\mathbf{v}}_N^{\mathbf{k}} \varphi_{\mathbf{k}} : \hat{\mathbf{v}}_N^{\mathbf{k}} = \overline{(\hat{\mathbf{v}}_N^{-\mathbf{k}})} \in \mathbb{C}^d \right\} \quad \text{for} \quad \mathbb{Z}_N^d = \left\{ \mathbf{k} \in \mathbb{Z}^d : -\frac{N_{\alpha}}{2} \leq k_{\alpha} < \frac{N_{\alpha}}{2} \right\}. \quad (1)$$

The main advantage of this approach is that trigonometric polynomials preserve the Helmholtz decomposition $\mathcal{T}_N^d = \mathbb{R}^d \oplus \mathcal{E}_N \oplus \mathcal{J}_N$, providing the conforming approximations to spaces \mathcal{E} and \mathcal{J} of curl-free and divergence-free fields respectively. The decomposition can be provided by orthogonal projections formed from the Green function corresponding to homogeneous problem, which is fully employed also in discrete formulations. The connection of trigonometric polynomials with their Fourier coefficients by FFT algorithm also provides the way to efficient implementation.

Two types of discretization that are based on the Galerkin (Ga) approximation and the Galerkin approximation with Numerical integration (GaNi) are stated here for the primal formulation only

$$\begin{aligned} (\mathbf{A}_{H,N}\mathbf{E}, \mathbf{E})_{\mathbb{R}^d} &= \min_{\mathbf{e}_N \in \mathcal{E}_N} (\mathbf{A}(\mathbf{E} + \mathbf{e}_N), \mathbf{E} + \mathbf{e}_N)_{L^2_{\#}} = (\mathbf{A}(\mathbf{E} + \mathbf{e}_N^{(\mathbf{E})}), \mathbf{E} + \mathbf{e}_N^{(\mathbf{E})})_{L^2_{\#}}, \\ (\tilde{\mathbf{A}}_{H,N}\mathbf{E}, \mathbf{E})_{\mathbb{R}^d} &= \min_{\mathbf{e}_N \in \mathcal{E}_N} (\mathcal{Q}[\mathbf{A}(\mathbf{E} + \mathbf{e}_N)], \mathbf{E} + \mathbf{e}_N)_{L^2_{\#}} = (\mathcal{Q}[\mathbf{A}(\mathbf{E} + \tilde{\mathbf{e}}_N^{(\mathbf{E})})], \mathbf{E} + \tilde{\mathbf{e}}_N^{(\mathbf{E})})_{L^2_{\#}}, \end{aligned}$$

with numerical integration provided by an interpolation operator $\mathcal{Q} : C^0_{\#}(\mathcal{Y}; \mathbb{R}^d) \rightarrow \mathcal{T}_N^d$. GaNi scheme corresponds to the original Moulinec and Suquet algorithm [4], while Ga scheme is innovative, possess better behavior, and thus opens new area for investigation. The convergence rates for the schemes are proven in [5, 7] and the relation between primal-dual discrete formulations are investigated in [8], where we show that the duality is transferred to the discrete setting GaNi scheme for the odd number of discretization points.

According to work by Dvořák [2], the guaranteed bounds on homogenized matrix can be obtained, cf. [6, 8], in a sense of quadratic forms, with the lower bounds obtained from the dual formulation:

$$\overline{\mathbf{B}}_{H,N}^{-1} \preceq \mathbf{B}_{H,N}^{-1} \preceq \mathbf{B}_H^{-1} = \mathbf{A}_H \preceq \mathbf{A}_{H,N} \preceq \overline{\mathbf{A}}_{H,N}.$$

Matrices $\overline{\mathbf{A}}_{H,N}, \overline{\mathbf{B}}_{H,N} \in \mathbb{R}^{d \times d}$ are obtained as a posteriori estimates from minimizers of GaNi scheme.

Acknowledgements

This work was supported from the project EXLIZ – CZ.1.07/2.3.00/30.0013, which is co-financed by the European Social Fund and the state budget of the Czech Republic, and from the Czech Science Foundation through project No. P105/12/0331.

References

- [1] Brisard, S., Dormieux, L., Combining Galerkin approximation techniques with the principle of Hashin and Shtrikman to derive a new FFT-based numerical method for the homogenization of composites, *Computer Methods in Applied Mechanics and Engineering* 217-220 (2012) 197-212.
- [2] Dvořák, J., Optimization of composite materials, Master thesis, Charles University, Prague, 1993.
- [3] Monchiet, V., Bonnet, G., A polarization-based FFT iterative scheme for computing the effective properties of elastic composites with arbitrary contrast, *International Journal for Numerical Methods in Engineering* 89 (11) (2012) 1419–1436.
- [4] Moulinec, H., Suquet, P., A fast numerical method for computing the linear and nonlinear mechanical properties of composites, *Comptes rendus de l'Académie des sciences. Série II, Mécanique, physique, chimie, astronomie* 318 (11) (1994) 1417–1423.
- [5] Schneider, M., Convergence of FFT-based homogenization for strongly heterogeneous media, *Mathematical Methods in the Applied Sciences* (2014), doi: 10.1002/mma.3259. (in press)
- [6] Vondřejc, J., An improved FFT-based homogenization of periodic media. (in preparation)
- [7] Vondřejc, J., Zeman, J., Marek, I., An FFT-based Galerkin method for homogenization of periodic media, *Computers & Mathematics with Applications* 68 (3) (2014) 156–173.
- [8] Vondřejc, J., Zeman, J., Marek, I., Guaranteed bounds on homogenized properties by FFT-based Galerkin method, 2014, arXiv:1404.3614.
- [9] Zeman, J., Vondřejc, J., Novák, J., Marek, I., Accelerating a FFT-based solver for numerical homogenization of periodic media by conjugate gradients, *Journal of Computational Physics* 229 (21) (2010) 8065–8071.